

**Synthesis and Biological Studies of
DNA-Binding Cyclic Py-Im Polyamides**

Thesis by

Benjamin Chun Yeung Li

In Partial Fulfillment of the Requirements

for the Degree of

Doctor of Philosophy

California Institute of Technology

Pasadena, California

2013

(Defended February 27, 2013)

© 2013

Benjamin Chun Yeung Li

All Rights Reserved

... for my parents, Elinor and Stephen...

Acknowledgments

As I reflect on my graduate career, I am left in awe of how quickly five years have passed while marveling at how much I have grown as a scientist and matured as an individual in this period of time. I would like to take this opportunity to acknowledge the great people who have made this a worthwhile experience, knowing full well that I cannot possibly thank everyone who has had a positive impact during my time at Caltech. To my research advisor, ***Peter Dervan***: Thank you for providing a nurturing environment for my research education. Your mentorship and advice have motivated me through tougher times, and I am grateful to you for challenging me to become a more effective communicator. I am most certain all the lessons I have learned from you will be invaluable towards my future career development. To my thesis committee, ***David Tirrell, Brian Stoltz, and Doug Rees***: Your support and insights have been helpful over the years, and it has been an honor to have scientific discussions with such brilliant minds.

Dave: Where do I even begin? I guess I'll start with thanking you for being a great co-worker in lab and an even better friend outside of lab. As the other half of the "Ben & Dave" duo, or as Megha would put it, my "life partner" for these past five years, I appreciate your help and support during the many times of need. Whether it was playing our annual trifecta of sports, enjoying the sun out at Coachella, or spending a late night in lab, I will treasure all of our shared memories dearly. To put it in short, I honestly could not have asked for a better baymate. Thank you. ***Jordan***: As not only a physical pillar, but a metaphorical one as well, you have been a great role model for us. I have always been impressed by your masterful balance between sustaining a high level of professional productivity and keeping a fruitful private life, which is something I aspire to achieve myself one day. I am indebted to your support and advice during challenging

situations, and I thank you for bringing the leadership to Room 330. **Jim**: It is not every day that I meet someone with your breadth of knowledge, and even rarer is it to find someone who is as patient and willing to share that knowledge as you. I enjoyed our intellectual discussions over coffee, and I treasure your advice and insights on my future career path. **JJ**: Thanks for being a fun yet professional labmate and for completing “the three people” trio. Good times. **Katy**: I appreciate your help in getting us acclimated to the unique culture of the Dervan lab, Group Mom. Your encouragement and advice early on has resonated throughout my graduate career.

Dervan Lab: Throughout the years, I have had the good fortune of working with a group of brilliant and motivated researchers in the Dervan group: Justin, Michelle, Christian, Dave C., Dan H., Carey, Mareike, John, Fei, Sam, Nick, Jevgenij, Thomas, Mandy, Jerzy, Tim, and Alissa. I would like to thank you all for sustaining a professional work environment and for everything I have learned from each and every one of you. **C60 Soccer Team & SNS Softball Team**: I honestly don’t think I would have made it through graduate school without relieving stress periodically by competing on the fields with you. I will always remember our 2009 soccer & 2011 softball championships! **HKSA (Heywood, Raymond, Michael & Stephen)**: For a nomad who left H.K. at the age of 15, thanks for bringing me a piece of home from time to time. **Caltech Staff**: I’d like to especially thank the support staff, including but not limited to: Vicky Brennan, Lynne Martinez, Joe Drew, Ron Koen, Paul Carrod, Steve Gould, and Agnes Tong.

DADA BABA (Kar, Kit, Hei & Vince) & Danny: While our paths have separated over time, it has been enormously comforting to know that you will all have my back through good times and bad. And finally, to **my parents**: Thank you for all the years of unconditional support. I love you.

Abstract

Pyrrole-imidazole (Py-Im) polyamides are programmable oligomers that bind to the minor groove of DNA in a sequence-specific manner at affinities comparable to natural DNA-binding proteins. Hairpin polyamides have been shown to localize within the nucleus of live cells, disrupt protein-DNA interactions, and modulate endogenous gene expression. Cyclic polyamides display further enhanced DNA binding affinities and exhibit similar gene regulatory effects, but investigations into their biological activity have been limited by the lack of effective synthetic methods. Herein, we demonstrate the efficient synthesis of a focused library of cyclic polyamide utilizing a novel microwave-assisted solid-phase technique. The orthogonal protection strategy allowed for selective turn modifications, and the mild cleavage conditions gave access to polyamide cores beginning with a C-terminal imidazole. In addition to expanding our synthetic repertoire, we further examined the cytotoxicity and cell uptake profiles of the cyclic polyamide variants, which highlighted the significant changes in biological activity resulting from minor structural modifications. Molecular recognition of the polyamide turn unit was also explored by installing heteroatom substituents at the α -position. Interestingly, while none of the fluoro, hydroxyl, or amino derivatives increased turn specificity, the (S)-fluoro turn exhibited better tolerance for binding a C•G pair. Finally, we optimized the synthesis of several biologically active hairpin polyamides on a 50-mg scale and examined their antitumor activity in mice xenograft models.

Table of Contents

Acknowledgements.	iv
Abstract.	vi
Table of Contents.	vii
List of Figures, Tables and Schemes.	x
List of Abbreviations.	xvi
List of Symbols and Nomenclature.	xix
 Chapter 1: Introduction.	 21
1.1 Deoxyribonucleic Acid (DNA).	22
1.2 Regulation of Gene Expression by Transcription Factors.	22
1.3 DNA-Binding Natural Products.	25
1.4 Recognition of the DNA Minor Groove by Py-Im Polyamides	27
1.5 Polyamide Regulation of Gene Expression in Cell Culture	29
1.6 Allosteric Modulation of Transcription Factor Driven Gene Expression.	32
1.7 Scope of this Thesis.	35
1.8 References.	36
 Chapter 2: Synthesis of Cyclic Py-Im Polyamide Libraries	 40
Abstract.	41
2.1 Introduction.	42
2.2 Results and Discussion.	45
2.3 Conclusion.	64
2.4 Materials and Methods.	65
2.5 Acknowledgements.	75
2.6 References.	76
2.7 Experimental Data.	79

Chapter 3: DNA Sequence Specificity of Hairpin Polyamide Turn Units.	95
Abstract.	96
3.1 Introduction.	97
3.2 Results and Discussion.	100
3.3 Conclusion.	109
3.4 Materials and Methods.	110
3.5 Acknowledgements	124
3.6 References.	125
3.7 Experimental Data.	127
 Chapter 4: Synthetic Advances Underpinning the Biological Studies of Hairpin Polyamides. .	130
Abstract.	131
4.1 Introduction.	132
4.2 Results and Discussion.	134
4.3 Conclusion.	145
4.4 Materials and Methods.	146
4.5 References.	154
4.6 Experimental Data.	157
 Appendix A: Alternative Approaches towards Cyclic Polyamide Precursors.	161
A.1 Introduction.	162
A.2 Results and Discussion.	163
A.3 Conclusion.	168
A.4 Materials and Methods.	169
A.5 References.	173
A.6 Experimental Data.	174

List of Figures, Tables, and Schemes

Chapter 1

Figure 1.1	X-ray crystal structure of double-stranded DNA and examination of hydrogen bonding between Watson-Crick base pairs.	23
Figure 1.2	X-ray crystal and NMR structures of transcription factor-DNA complexes. . . .	24
Figure 1.3	Chemical structures of DNA-binding natural products.	25
Figure 1.4	X-ray crystal structures displaying the molecular recognition of DNA by netropsin and distamycin.	26
Figure 1.5	Molecular recognition of the DNA minor groove by Py-Im polyamides.	28
Figure 1.6	Modulation of gene expression by Py-Im polyamides.	30
Figure 1.7	A composite model illustrating the cooperative assembly of interferon- β enhancosome	33
Figure 1.8	Polyamide perturbation of DNA structure.	34

Chapter 2

Scheme 2.1	Microwave-assisted synthesis of cyclic polyamides 1-7	44
Table 2.1	Standard Fmoc deprotection and microwave-assisted coupling times for solid-phase polyamide synthesis.	46
Table 2.2	Summary table of MALDI-TOF data and synthetic yields for cyclic polyamides 1-8 and intermediates 18-25	47
Scheme 2.2	Preparation of cyclic polyamides 9-11	48
Scheme 2.3	Preparation of cyclic polyamides 12-14	50
Scheme 2.4	Preparation of cyclic polyamide 8	52
Scheme 2.5	Preparation of hairpin polyamide 17	53
Figure 2.1	Stick and space-filling model of benzoyl substituted turn along the DNA minor groove.	56
Table 2.3	<i>T_m</i> Values for polyamide library.	57
Table 2.4	SRB cytotoxicity data on compounds 1-3 , 9 , and 15	59
Table 2.5	SRB cytotoxicity data on compounds 4-7 , 10-11 , and 16	60
Figure 2.2	Confocal microscopy of cyclic polyamide-fluorescein conjugates 12-14 in A549 cells.	61
Figure 2.3	Confocal microscopy of cyclic polyamide-fluorescein conjugates 12-14 in T47D cells.	63
Figure 2.4	HPLC spectrum of 18 and 1	79
Figure 2.5	HPLC spectrum of 19 and 2	80
Figure 2.6	HPLC spectrum of 20 and 3	81
Figure 2.7	HPLC spectrum of 21 and 4	82
Figure 2.8	HPLC spectrum of 22 and 5	83

Figure 2.9	HPLC spectrum of 23 and 6	84
Figure 2.10	HPLC spectrum of 24 and 7	85
Figure 2.11	HPLC spectrum of 25 and 8	86
Figure 2.12	HPLC spectrum of 26 and 17	87
Figure 2.13	HPLC spectrum of 9 and 12	88
Figure 2.14	HPLC spectrum of 10 and 13	89
Figure 2.15	HPLC spectrum of 11 and 14	90
Figure 2.16	HPLC spectrum of 15 and 16	91
Figure 2.17	Confocal microscopy analysis of 12–14 in A549 cells.	92
Figure 2.18	Confocal microscopy analysis of 12–14 in T47D cells.	93
Figure 2.19	Cytotoxicity of compound S1 in A549 cells.	94

Chapter 3

Figure 3.1	Schematic diagram of six-ring hairpin polyamide (ImImPy-turn-PyPyPy) targeting the DNA sequence 5'-WWGGWW-3'	97
Figure 3.2	Chemical and ball-and-stick structures of 1 , 2R , 4R , 4S , 3R , and 5R	100
Table 3.1	Melting temperatures of DNA/polyamide complexes for 1 , 2R , 4R , 4S , 3R , and 5R	101
Figure 3.3	Illustration of the EcoRI/PvuII restriction fragment derived from plasmid pCDMF6.	102
Figure 3.4	Quantitative DNase I footprinting experiments for 1 , 2R , 4R , 4S	103
Table 3.2	Binding affinities (M^{-1}) for polyamides. 1 , 2R , 4R , 4S , 3R , and 5R	103
Figure 3.5	Quantitative DNase I footprinting experiments for 3R and 5R	104
Table 3.3	Relative binding affinities for 1 , 2R , 4R , 4S , 3R , and 5R	104
Scheme 3.1	Synthesis of α -fluoro GABA turns 18 and 22	105
Scheme 3.2	Synthesis of α -hydroxyl GABA turns 23 and 26	105
Figure 3.6	Chemical and ball-and-stick structures of 6R , 7R , 6S , and 7S	106
Table 3.4	Melting temperatures of DNA/polyamide complexes for 6R , 7R , 6S , and 7S	106
Figure 3.7	Quantitative DNase I footprinting experiments for 6R , 7R , 6S , and 7S	107
Table 3.5	Binding affinities (M^{-1}) for 6R , 7R , 6S , and 7S	108
Table 3.6	Relative binding affinities for 6R , 7R , 6S , and 7S	108
Figure 3.8	Analytical chiral HPLC assays for fluoro turn derivatives 27 and 28	122
Figure 3.9	Analytical chiral HPLC assays for hydroxyl turn derivatives 29 and 30	123
Figure 3.10	Chemical and ball-and-stick structures of 8–13	127

Table 3.7	Melting temperatures of DNA/polyamide complexes for 8–13	127
Figure 3.11	Quantitative DNase I footprinting experiments for 8–10	128
Table 3.8	Relative binding affinities for 8–10	129
Table 3.9	Melting temperatures of DNA/polyamide complexes for 6R, 7R, 6S, and 7S	129

Chapter 4

Figure 4.1	Chemical structure and binding preferences of 1 and 2	133
Figure 4.2	Retrosynthetic strategy towards hairpin polyamides 1–3	135
Scheme 4.1	Synthesis of tetramer intermediate 7	135
Scheme 4.2	Solid-phase assembly of polyamide cores 15–17	136
Scheme 4.3	Synthesis of hairpin polyamides 1–5	137
Figure 4.3	Biodistribution and toxicity profile of 1 and 2 in mice.	139
Figure 4.4	Anti-tumor activity of 1 in LNCaP prostate cancer xenografts.	140
Figure 4.5	Animal weights following injection of 1	141
Figure 4.6	Chemical structure and binding preferences of 3	141
Figure 4.7	Relative mRNA levels of <i>TFF1</i> , <i>TFGB2</i> , and <i>WT1</i>	142
Figure 4.8	Activity of 3 in T47D-KBLUC breast cancer xenografts.	143
Figure 4.9	Crude HPLC spectra tracing the synthesis of 5 starting from 18	157
Figure 4.10	Crude HPLC spectra tracing the synthesis of 2 starting from 19	158
Figure 4.11	Crude HPLC spectra tracing the synthesis of 3 starting from 20	159
Table 4.1	Melting temperatures of DNA/polyamide complexes for 1 and 2	160
Table 4.2	Melting temperatures of DNA/polyamide complexes for 3	160

Appendix A

Figure A.1	Retrosynthesis of cyclic polyamide 1 from linear precursor 2	162
Scheme A.1	Direct deprotection of 3 under acidic conditions.	163
Scheme A.2	Synthesis of Boc-Py-HMFS-OH linker 6	164
Scheme A.3	Microwave-assisted synthesis of 8 on HMFS resin.	165
Scheme A.4	Microwave-assisted synthesis on HMFS resin.	166
Scheme A.5	Two-step cleavage of 11 off Kaiser oxime resin.	167
Scheme A.6	Direct deprotection of 3 with TFA at room temperature.	174
Scheme A.7	Direct deprotection of 3 with HCl at room temperature.	175
Scheme A.8	Direct deprotection of 3 with HCl at -40 °C.	176

List of Abbreviations

A	adenine
Å	angstrom
Ac	acetyl
Ac ₂ O	acetic anhydride
A ₅₉₅	absorbance maximum
AR	androgen receptor
ARE	androgen response element
A·T	adenine Watson-Crick hydrogen bonded to thymine
ATCC	American Type Culture Collection
atm	atmosphere
β	beta-amino alanine
Boc	<i>tert</i> -butyloxycarbonyl
Boc-Im-OH	(4-[(<i>tert</i> -Butoxycarbonyl)amino]-1-methylimidazole-2-carboxylic acid)
Boc ₂ O	di- <i>tert</i> -butyl dicarbonate
Boc-Py-OBt	[(1,2,3-Benzotriazol-1-yl 4-[(<i>tert</i> -Butoxycarbonyl)amino]-1-methylpyrrole-2-carboxylate)
bp	base pair
BSA	bovine serum albumin
°C degrees	Celsius
C	cytosine
C·G	cytosine Watson-Crick hydrogen bonded to guanine
calc'd	calculated
Cbz	carbobenzyloxy
ChIP	chromatin immunoprecipitation
cm	centimeter
Da	Dalton
dATP	2'-deoxyadenosine triphosphate
DABA	diaminobutyric acid
DCM	dichloromethane
dex	dexamethasone
DFO	deferoxamine
DHT	dihydrotestosterone
DIEA	N,N-diisopropylethylamine
DMF	N,N-dimethylformamide
DMSO	dimethylsulfoxide
DNA	deoxyribonucleic acid
Dp	N,N-dimethylaminopropylamine
DPPA	diphenylphosphoryl azide
DTT	dithiothreitol
EDTA	ethylenediaminetetraacetic acid
ELISA	enzyme-linked immunosorbant assay
EMSA	electrophoretic mobility shift assay
ESI	electrospray ionization
Et ₂ O	diethyl ether

List of Abbreviations

Ex	excitation
FBS	fetal bovine serum
FITC	fluorescein isothiocyanate
Fmoc	fluorenylmethyloxycarbonyl
γ -DABA	γ -2,4-diaminobutyric acid
G	guanine
G·C	guanine Watson-Crick hydrogen bonded to cytosine
GABA	γ -aminobutyric acid
h	hour(s)
HIF-1 α	hypoxia inducible factor 1 α
Hp	3-hydroxypyrrole
HPLC	high-performance liquid chromatography
HRE	hypoxic response element
Im	N-methylimidazole
IPA	isophthalic acid
k	kilo (1 x 10 ³)
K _a	association constant
K _d	dissociation constant
λ	wavelength
LN ₂	liquid nitrogen
<i>m/z</i>	mass to charge ratio
μ	micro (1 x 10 ⁻⁶)
M	molar
m	milli (1 x 10 ⁻³)
Max	Myc associated protein X
max	maximum
MALDI	matrix-assisted LASER desorption/ionization
min	minute(s)
mol	mole(s)
mRNA	messenger ribonucleic acid
MS	mass spectrometry
N	A, T, G, or C
n	nano (1 x 10 ⁻⁹)
n-BuLi	n-butyl lithium
NF- κ B	nuclear factor- κ B
OBt	hydroxytriazole ester
p	pico (1 x 10 ⁻¹²)
PCR	polymerase chain reaction
PET	Paired End diTag
PSA	prostate-specific antigen
Py-Im	pyrrole-imidazole
qPCR	quantitative polymerase chain reaction
RT	room temperature
RT-PCR	reverse transcriptase polymerase chain reaction

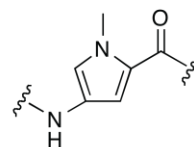
List of Abbreviations

PAGE	polyacrylamide gel electrophoresis
PBS	phosphate-buffered saline
Py	N-methylpyrrole
PyBOP	(benzotriazol-1-yloxy)tripyrrolidinophosphonium hexafluorophosphate
R	guanine or adenine
RCF	relative centrifugal force
RIPA	radio immunoprecipitation assay
RNA	ribonucleic acid
RNAi	ribonucleic acid interference
RT	reverse transcription
siRNA	small interfering ribonucleic acid
Smad	Sma and Mad-related protein
T	thymine
T·A	thymine Watson-Crick hydrogen bonded to adenine
t-BuOH	<i>tert</i> -butanol
TF	transcription factor
TFA	trifluoroacetic acid
TFO	triplex-forming oligonucleotides
THF	tetrahydrofuran
T _m	midpoint of transition temperature
TOF	time-of-flight
TFRE	transcription factor response element
tri/triamine	3,3'-diamino-N-methyldipropylamine
U	uracil
UV	ultraviolet
VEGF	vascular endothelial growth factor
Vis	visible
W	adenine or thymine

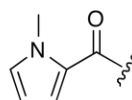
List of Symbols and Nomenclature



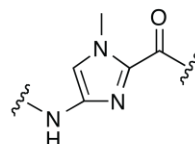
-Py-



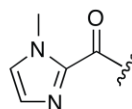
Py-



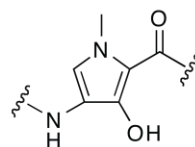
-Im-



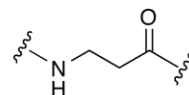
Im-




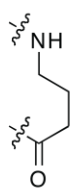

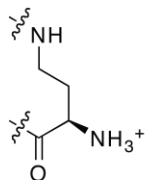
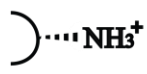
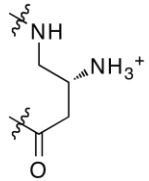
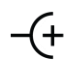
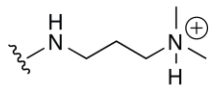

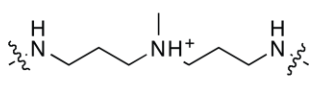
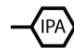
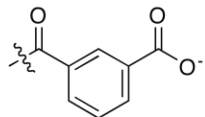
-Hp-



-β-



List of Symbols and Nomenclature

	-GABA-	
	-(R)-2,4-DABA-	
	-(R)-3,4-DABA-	
	-Dp	
	-tri-	
	-IPA	

Chapter 1

Introduction

1.1 Deoxyribonucleic Acid (DNA)

Deoxyribonucleic acid is the double helical biopolymer that encodes all heritable information necessary for the development and function of all living organisms. Each strand of DNA is composed of a phosphodiester deoxyribose sugar backbone that links together a sequence of four nucleotides - deoxythymine (T), deoxyadenine (A), deoxycytosine (C) and deoxyguanine (G) (Fig. 1.1). Two strands of DNA intertwine in an antiparallel fashion to form a double helix through hydrogen bonding between the Watson-Crick base pairs, such that T pairs with A and C pairs with G. Depending on the sequence context and physiological conditions, DNA exists in several different conformations, including A-form, B-form and Z-form. In the most commonly observed B-DNA, the right-handed helix displays ten base pairs per turn with the plane of each hydrogen-bonded base pair lying perpendicular to the helical axis.¹ The overall asymmetric DNA duplex can be further subdivided into a wide major groove and a narrow minor groove, each offering sequence-specific chemical functionalities for DNA recognition.

1.2 Regulation of Gene Expression by Transcription Factors

A human cell nucleus contains 3×10^9 base pairs of DNA that encodes 20,000 to 25,000 protein-coding genes.² The gene expression process begins with the transcription of genomic DNA into an mRNA template, which is then translated into the final protein product. Although every cell in any given organism contains the same genome, the regulation of gene expression dictates the production levels of various proteins that results in the diverse phenotypes found in different cell types. The gene expression profile within each cell is also continually modulated, depending on internal factors (e.g. cell cycle progression) as well as external stimuli (e.g. intracellular signaling, environmental stress, etc.).

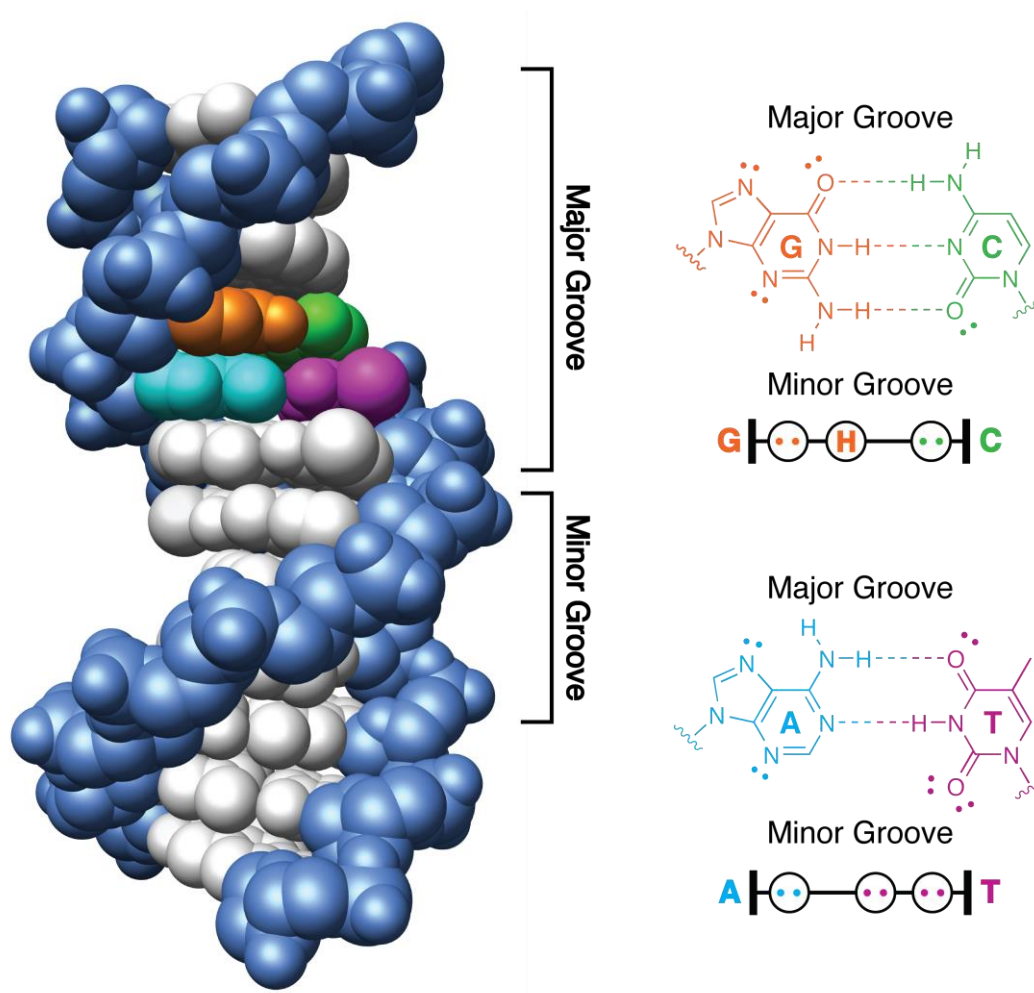


Figure 1.1 X-ray crystal structure of double-stranded DNA (PDB 1BNA) and examination of hydrogen bonding between Watson-Crick base pairs.

The regulation of gene expression at the transcriptional level can be achieved by three general modes - direct binding of a control factor to the target gene interactions between a control factor with the transcription machinery, or modifications in the tertiary DNA structure and thus accessibility of the target site. The most direct method for a protein to modulate gene expression is by directly interacting with specific binding sites (i.e. promoters, enhancers, repressors, etc.) found in the genome. The mechanism for regulating transcription through these interactions are often complex and, by recruiting or blocking RNA polymerase, either transcription activation or repression may be achieved.

Transcription factors are a class of DNA-binding proteins that participate in the transcriptional regulation of gene expression. By interacting with gene promoter or enhancer regions, which are generally upstream of the transcription start site, transcription factors modulate the occurrence of RNA polymerase binding events and thus control the level of gene transcription. Most transcription factors possess a DNA-binding domain that recognizes and interacts with either the minor groove, major groove, or both, of a specific DNA sequence. TATA-binding protein (TBP) and Lef-1 are examples of minor groove binding transcription factors,^{3,4} whereas NF- κ B, Myc/Max, AR, and Ets-1 recognize the major groove of DNA.⁵⁻⁸

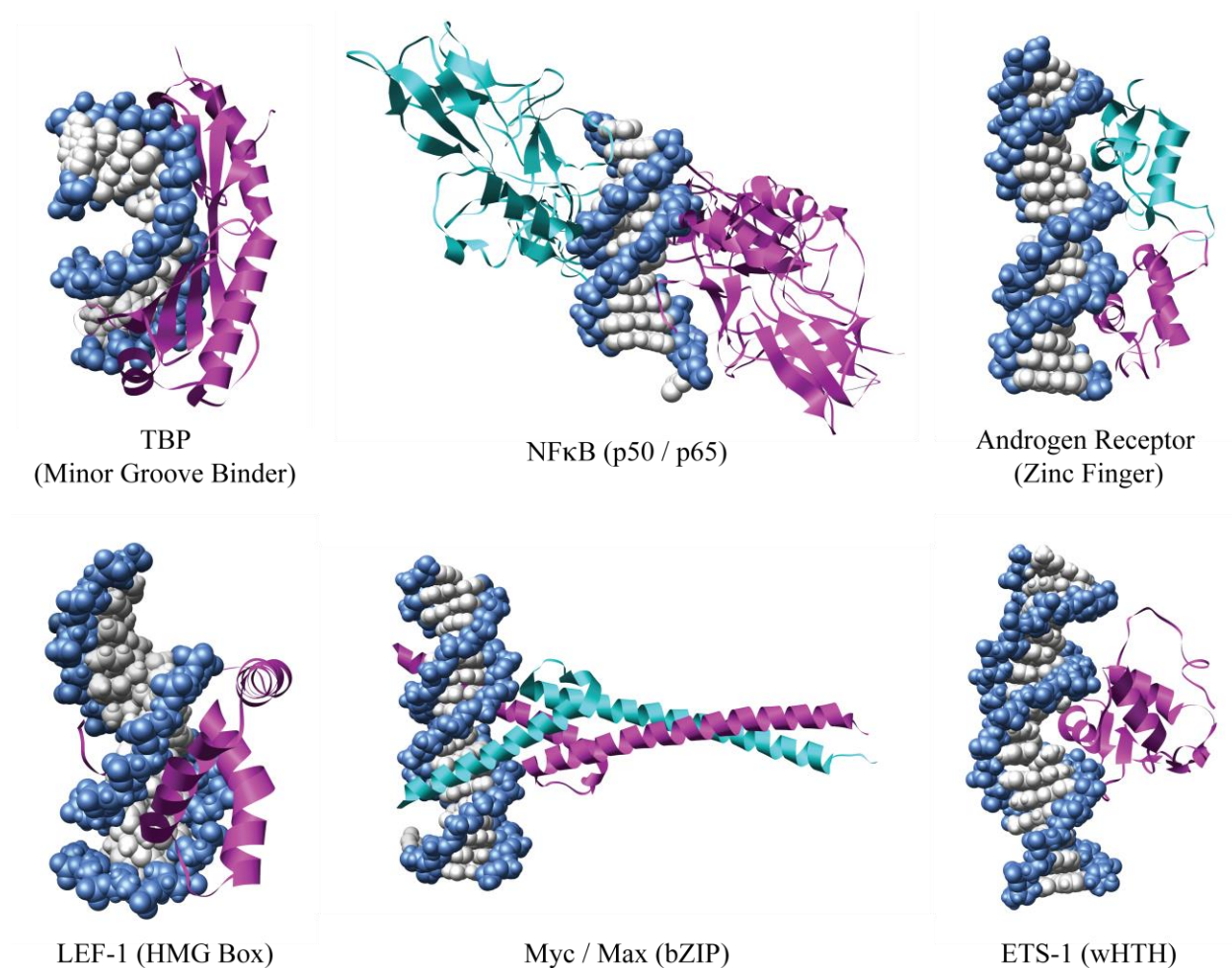


Figure 1.2 X-ray crystal and NMR structures of transcription factor-DNA complexes: TBP (PBD 1TGH), NF κ B (PBD 1VKX), AR (PBD 1R4I), LEF-1 (PBD 2LEF), Myc/Max (PBD 1NKP), and ETS-1 (PBD 2STW).

1.3 DNA-Binding Natural Products

In addition to the transcription factors described above, there are numerous small molecule natural products that recognize and bind DNA in a sequence-specific fashion. Four particular examples are given in Figure 1.3. Chromomycin A3 binds to 5'-GGCC-3' sequences in the DNA minor groove in a 2:1 ligand:DNA stoichiometry, and has exhibited biological activity by interfering with replication and transcription.⁹ Calicheamicin oligosaccharide recognizes the sequence 5'-TCCT-3' and binds to the minor groove of DNA in a monomeric fashion.¹⁰ Actinomycin D intercalates DNA specifically at 5'-GC-3' sites in a 1:1 ligand:DNA stoichiometry, and is known inhibit transcription and potentially DNA replication.^{11,12}

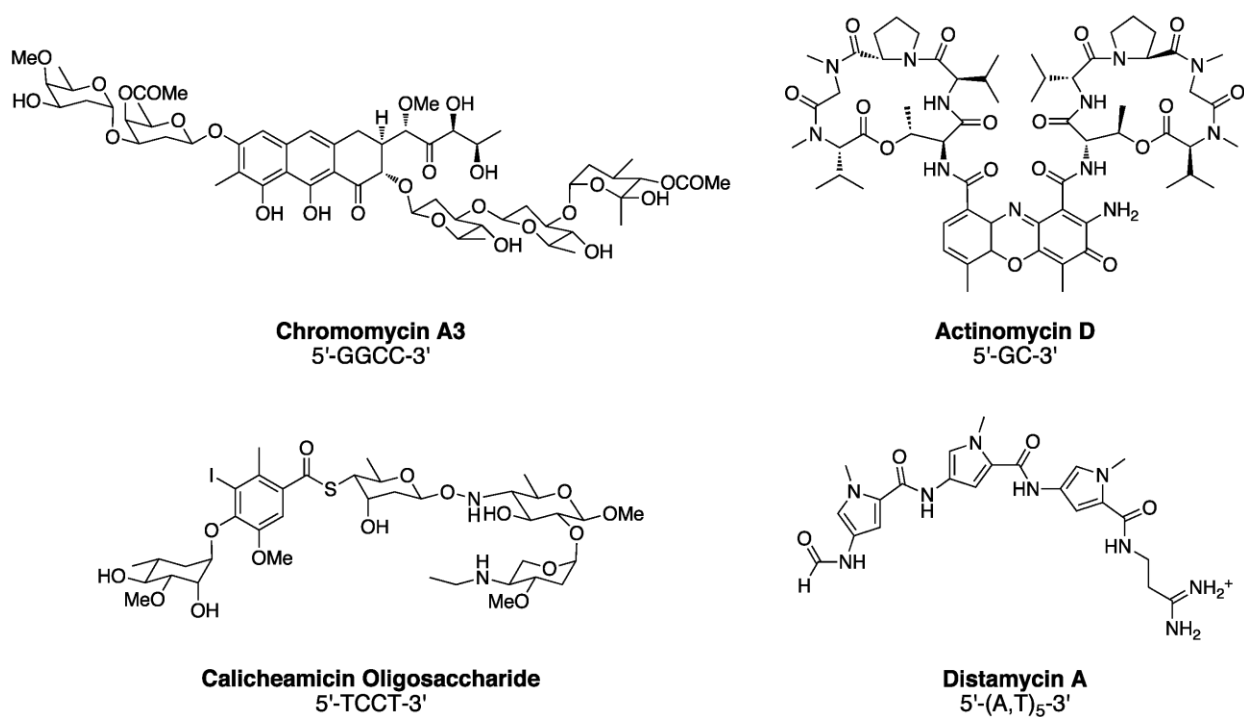


Figure 1.3 Chemical structures of DNA-binding natural products: chromomycin A3, actinomycin, calicheamicin oligosaccharide, and distamycin.

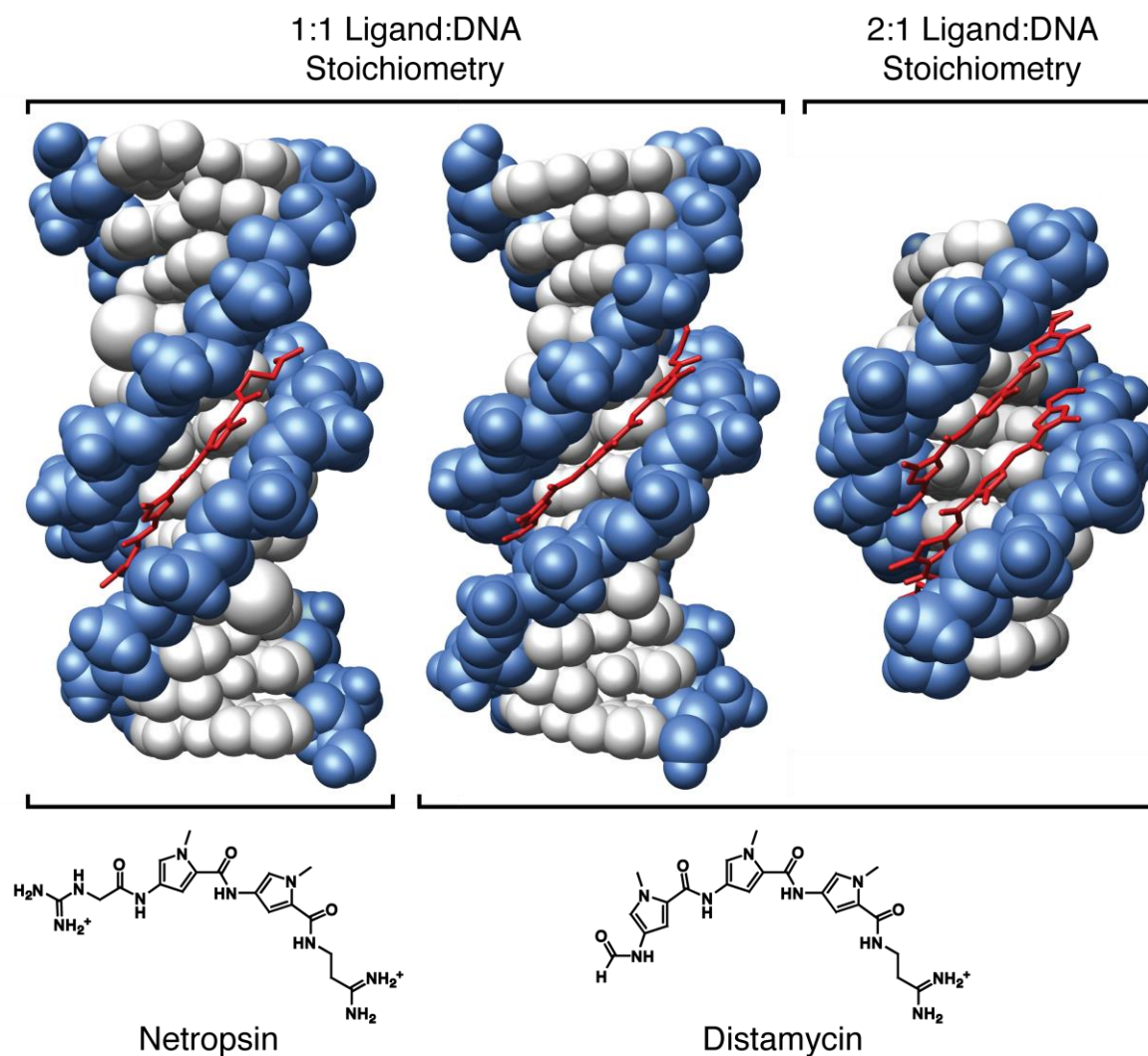


Figure 1.4 X-ray crystal structures displaying the molecular recognition of DNA by netropsin (PBD 6BNA) and distamycin (PBD 2DND in a 1:1 complex and PBD 378D in a 2:1 complex).

Distamycin and netropsin are oligopeptides that bind to AT tracts of DNA, which contain three and two *N*-methylpyrrole (Py) carboxamide units, respectively.^{13,14} While distamycin can bind to DNA in either a 1:1 or 2:1 ligand:DNA stoichiometry, netropsin is only known to form a 1:1 ligand:DNA complex (Fig. 1.4).¹⁵⁻¹⁷ The width and depth of the DNA minor groove is altered upon binding of the 1:1 and 2:1 complexes. Upon ligand binding in a 1:1 stoichiometry, the minor groove of DNA is narrowed and deepened. The 2:1 complex formed by distamycin is an antiparallel dimer that widens the minor groove.

1.4 Recognition of the DNA Minor Groove by Py-Im Polyamides

Based on the simple natural product distamycin A, a new class of programmable heterocyclic oligomers known as Py-Im polyamides has been developed to distinguish all four base pairs with high affinity and sequence specificity for the minor groove of DNA.^{18,19} In an early proof-of-principle experiment, *N*-methylimidazole (Im) was incorporated into a distamycin-like Im-Py-Py-Dp structure, which was shown to recognize the 5'-WGWCW-3' sequence in a 2:1 ligand:DNA stoichiometry.^{20,21} This not only expanded the sequence recognition capabilities of polyamides, but these side-by-side antiparallel ring pairings would also form the basis for recognition of all four DNA base pairs in the minor groove (Fig. 1.5). When Im is across from Py to form an Im / Py pair, the endocyclic secondary amine of Im presents a lone pair of electrons that can form a favorable hydrogen bonding interaction with the exocyclic amine of guanine, so binding to G•C is preferred. Conversely, Py / Im is selective for C•G, whereas Py / Py recognizes T•A or A•T. Distinction between T•A and A•T was accomplished by introducing the *N*-methyl-3-hydroxypyrrole (Hp) monomer.²² Hp projects an exocyclic OH group toward the minor groove floor that is sterically accommodated in the cleft of the T•A base pair and forms a favorable hydrogen bonding interaction with one of the thymine carbonyl lone pairs, and the Hp / Py pair therefore shows preference for T•A over A•T.²³

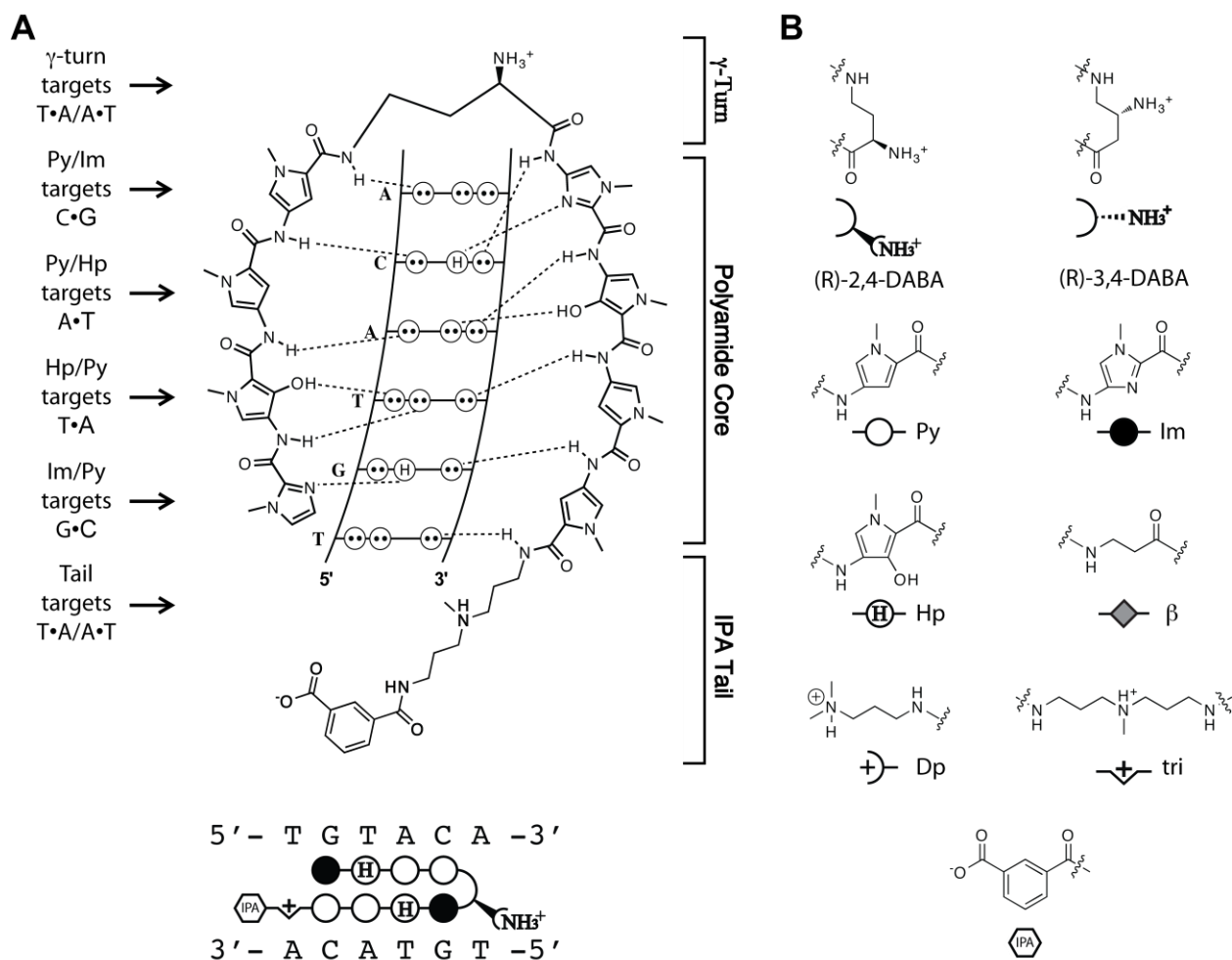


Figure 1.5 Molecular recognition of the DNA minor groove by Py-Im polyamides. (A) Schematic illustration of the polyamide ImHpPyPy-(R) $^{\alpha\text{-H}_2\text{N}}$ - γ -ImHpPyPy-(+)-IPA binding to its target sequence 5'-WGTACW-3'. Potential hydrogen binds are indicated by dashed lines. Ball-and-stick representation of the polyamide bound to DNA is shown below. (B) Ball-and-stick symbols and abbreviations listed below the corresponding chemical moieties, which will be used throughout this dissertation

In addition to completing the pairing rules for the Watson-Crick base pairs, a γ -aminobutyric acid (GABA) linker has been introduced to covalently attach the two polyamide oligomers in an antiparallel fashion to form a hairpin polyamide structure.²⁴ This hairpin “turn” unit prepaid the entropic cost for polyamide binding in a 2:1 ligand:DNA stoichiometry, and improve the DNA binding affinity by two orders of magnitude.²⁵ Since hairpin polyamides are known to occasionally align N- to C-terminus against DNA in a 3' to 5' direction, commonly

referred to as “reverse” binding, a (R)-2,4-diaminobutyric acid linker was used instead of the GABA turn, which not only increased binding affinity but also enforced the “forward” binding orientation of polyamide N- to C- terminus aligning to DNA in a 5’ to 3’ direction.^{26,27} By shifting the turn α -amine to the β -position, the (R)-3,4-diaminobutyric acid linker has also been utilized and exhibits better tolerance for turn conjugation.²⁸ Hairpin polyamides containing eight heterocycles linked by a turn unit can target six DNA base pairs, and serve as the typical substrates used in our biological studies. By fully preforming the 2:1 complex, cyclic polyamides containing a second turn unit display further enhanced binding affinities and have been recently examined for their biological activity.^{29–31}

1.5 Polyamide Regulation of Gene Expression in Cell Culture

The regulation of gene expression using programmable DNA-binding oligomers presents a promising new approach towards molecular medicine. Hairpin polyamides containing a GABA linker bind to their match DNA sequences at subnanomolar concentrations comparable to endogenous DNA-binding proteins.^{18,19} Along with the modular sequence recognition characterized by the pairing rules, polyamides can be designed to target an array of transcription factor binding sites in gene promoter sequences and thereby disrupt downstream transcriptional events (Fig. 1.6). Towards this goal, the nuclear localization of polyamide-fluorophore conjugates have been confirmed by confocal microscopy and the incorporation of a isophthalic acid (IPA) moiety at the C-terminus have yielded polyamide conjugates with high affinity and improved nuclear permeability.^{32–34}

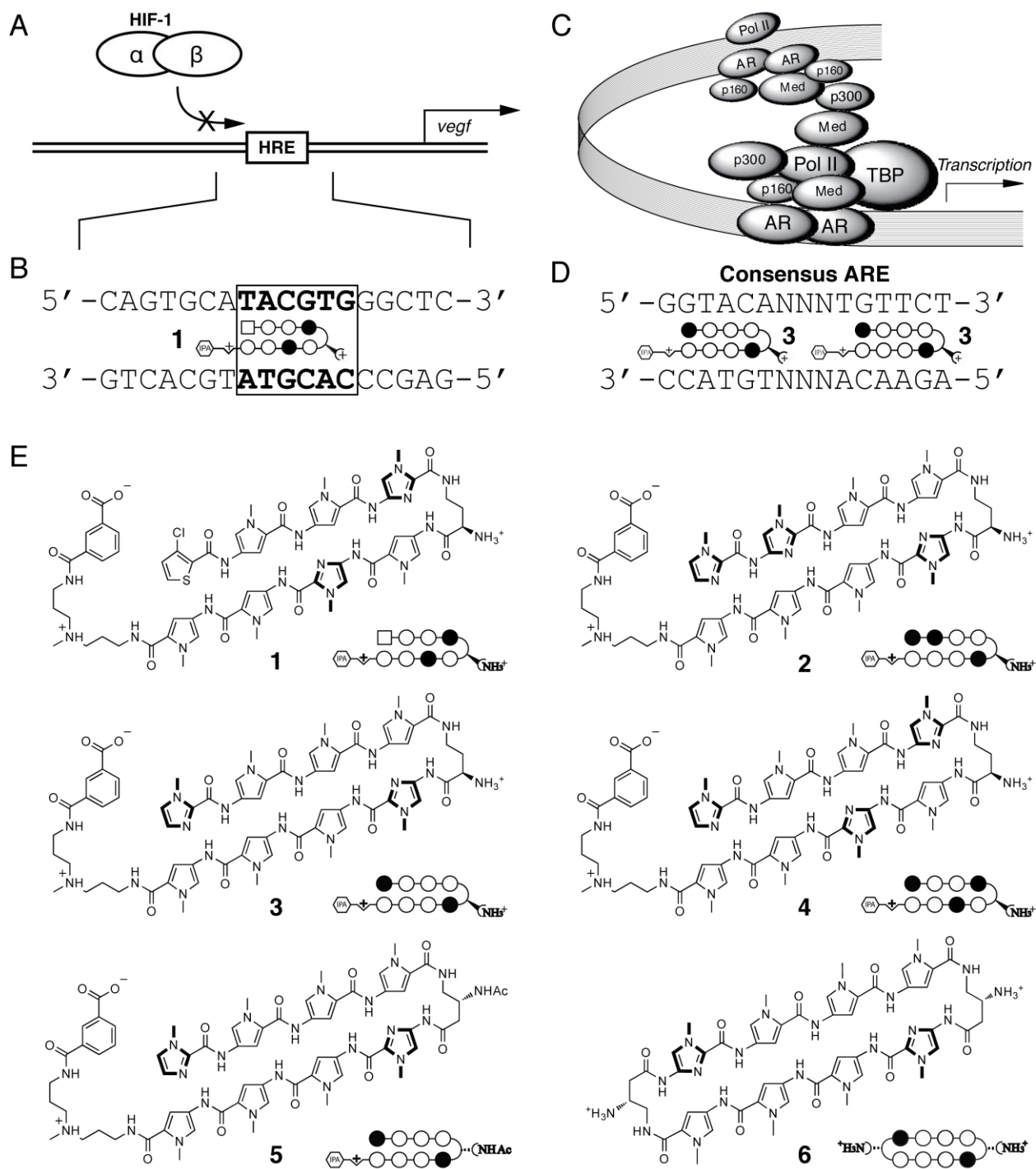


Figure 1.6 Modulation of gene expression by Py-Im polyamides. (A) Schematic diagram showing inhibition of VEGF gene transcription by disrupting HIF-1 α binding to HRE. (B) Polyamide **1** binding to 5'-ATACGT-3' sequence found in HRE enhancer. (C) Schematic illustration of the androgen receptor transcription complex. (D) Consensus ARE-targeted by match polyamide **3**. (E) Chemical structure and ball-and-stick models of polyamides **1** (VEGF match), **2** (VEGF mismatch), **3** (AR match), and **4** (AR mismatch), along with **5** and **6** that exhibit improved activity towards regulating AR-driven gene transcription.

Hypoxia inducible factor 1 α (HIF-1 α) is a transcription factor that drives gene expression in response to low oxygen environments by binding to the hypoxic response element (HRE) consensus sequence 5'-TACGTG-3'. Among these activated genes is the vascular endothelial growth factor (VEGF) responsible for tumor vascularization. HeLa and U251 cells dosed with **1**, which binds to a subset of HREs, exhibited a reduction in deferoxamine (DFO) induction of the VEGF gene.^{35,36} In contrast, treatment with polyamide **2** that does not bind the HRE did not result in a statistically significant change in VEGF expression. On a global scale, microarray analysis indicated that **1** downregulated a subset of genes activated by DFO induction. Chromatin immunoprecipitation (ChIP) experiments further demonstrated a decrease in occupancy of HIF-1 α at the VEGF HRE following treatment with **1**, supporting a sequence-dependent mechanism.

The androgen receptor (AR) transcription factor regulates gene expression in response to steroid hormones, such as testosterone, by binding to the androgen response element (ARE) consensus sequence 5'-GGTACAnnnTGTTCT-3'. AR-driven gene expression is essential to the development and progression of prostate cancer. A particularly noteworthy AR-activated gene is prostate specific antigen (PSA), which is a well-studied marker gene with high correlation to the presence of prostate cancer. In the presence of dihydrotestosterone (DHT), LNCaP prostate cancer cells treated with **3** targeted to the ARE half-site 5'-WGWWCW-3' exhibited a suppressed induction of PSA transcription.³⁷ On the other hand, mismatch polyamide **4**, which binds to the 5'-GWWCGW-3' sequence, produced a much smaller effect on PSA mRNA levels. Microarray experiments showed reduced DHT induction by **3** for a subset of DHT-induced genes, whereas ChIP assays again support the disruption of transcription factor-DNA interactions as a plausible mechanism for polyamide modulation of gene expression. In a follow-up study,

LNCaP cells were treated with hairpin polyamide **5** containing an acetylated β -amino turn and cyclic polyamide **6** under DHT induction, and both ARE-targeted compounds exhibited gene regulatory effects similar to **3** at ten-fold lower concentrations.³¹ Following these two pioneering studies, the modulation of gene expression mediated by the glucocorticoid receptor, NFkB, and estrogen receptor (to be discussed in greater detail in Chapter 4) has also been achieved.^{38,39}

1.6 Allosteric Modulation of Transcription Factor-Driven Gene Expression

Although HIF-1 α and AR both bind to the major groove of DNA, minor groove binding Py-Im polyamides may successfully perturb transcription factor-DNA interfaces and thus alter gene expression via allosteric regulation of the DNA-binding sites.⁴⁰ The process of promoter recognition involves a series of specific interactions between transcription factors and promoter sites to form stable protein-DNA complexes that allow for transcription initiation. These protein-DNA interactions are generally weak and dissociate readily, and the capacity to stabilize these otherwise weak interactions is likely crucial to transcriptional control that often requires cooperative assembly of multiple factors.⁴¹ In other words, the sequence-specific binding of a transcription factor induces perturbations to the local DNA structure, which creates the optimal shape for binding of the next transcription factor and so forth. This allosteric modulation of protein-DNA specificity on a gene enhancer site is elegantly displayed by the model structure of the interferon-beta enhancesome (Fig. 1.7).⁴² In this model, eight different transcription factors (ATF-2, c-Jun, IRF-3A, IRF-7B, IRF-3C, IRF-7D, p50, and RelA) are cooperatively assembled on the enhancer without any direct protein-protein contacts. Each transcription factor binds specifically to four to eight base pairs, and inhibiting the binding of any one of these proteins may disrupt the association of the entire complex and thereby its transcription activation activity.

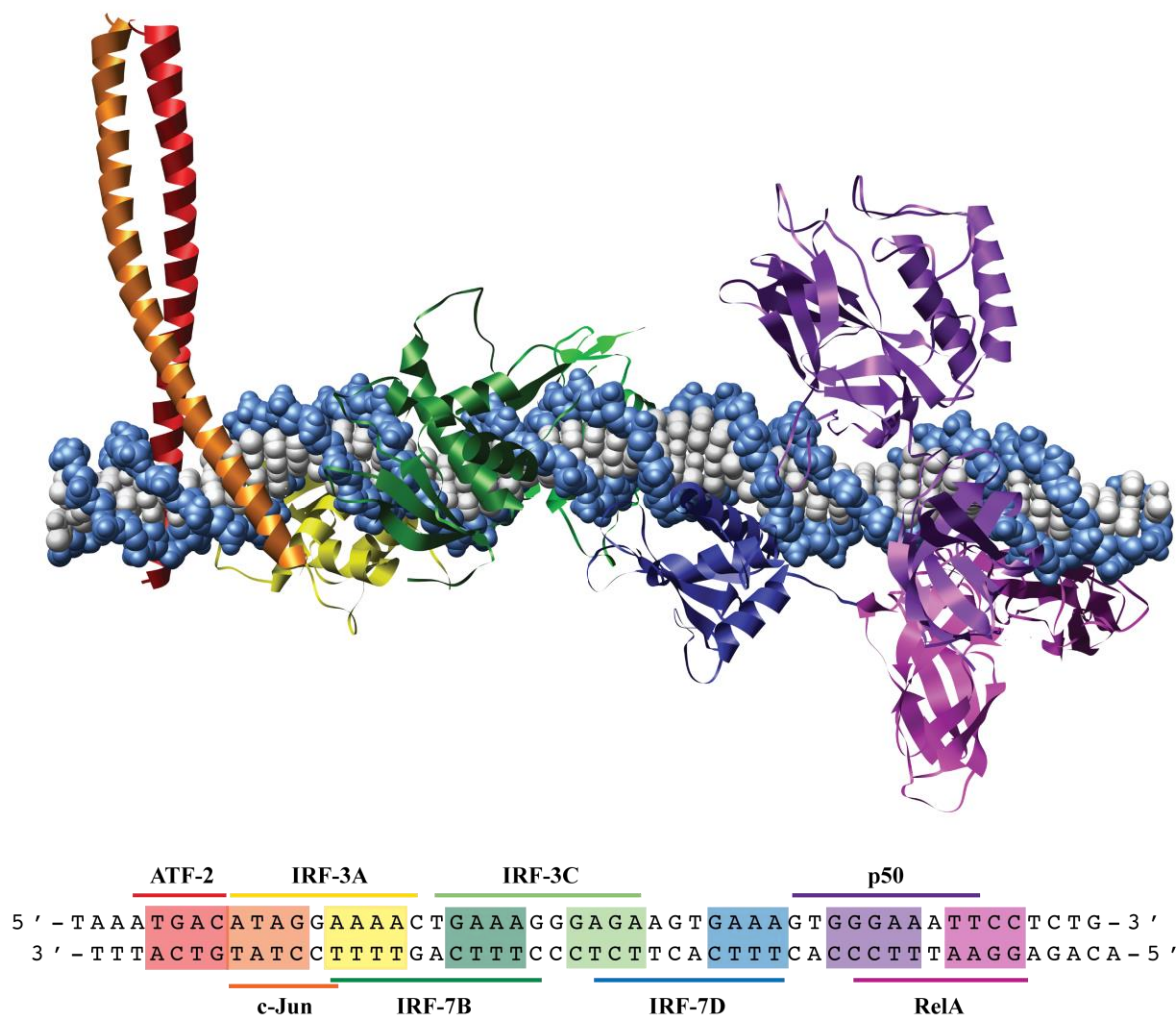


Figure 1.7 A composite model illustrating the cooperative assembly of interferon- β enhanesome, created from overlaid x-ray crystal structures (PBD 2O6G, 2O61).

A high-resolution X-ray crystal structure of cyclic polyamide **6** in complex with the DNA sequence 5'-CCAGTACTGG-3' reveals the significant alterations in DNA structure upon polyamide binding (Fig. 1.8).⁴³ Compared to unliganded B-form DNA,⁴⁴ the 10 base pair oligonucleotide bound by **6** experiences a substantial widening of the minor groove and compression of the major groove by more than 4 Å in both directions. Furthermore, the overall DNA helix in the polyamide-bound structure is bent by $> 15^\circ$ towards the major groove. This distortion in the geometry of the minor and major grooves is highlighted by a slice through the

short axis of the DNA helix in the uncomplexed and complexed structures. Polyamide binding to the minor groove of DNA, therefore, converts the normally wide and shallow major groove to a narrow and deep cleft that can no longer accommodate the association of a transcription factor. This allosteric modulation of the DNA helix offers a mechanistic model for the perturbation of transcription factor-DNA interactions by Py-Im polyamides.

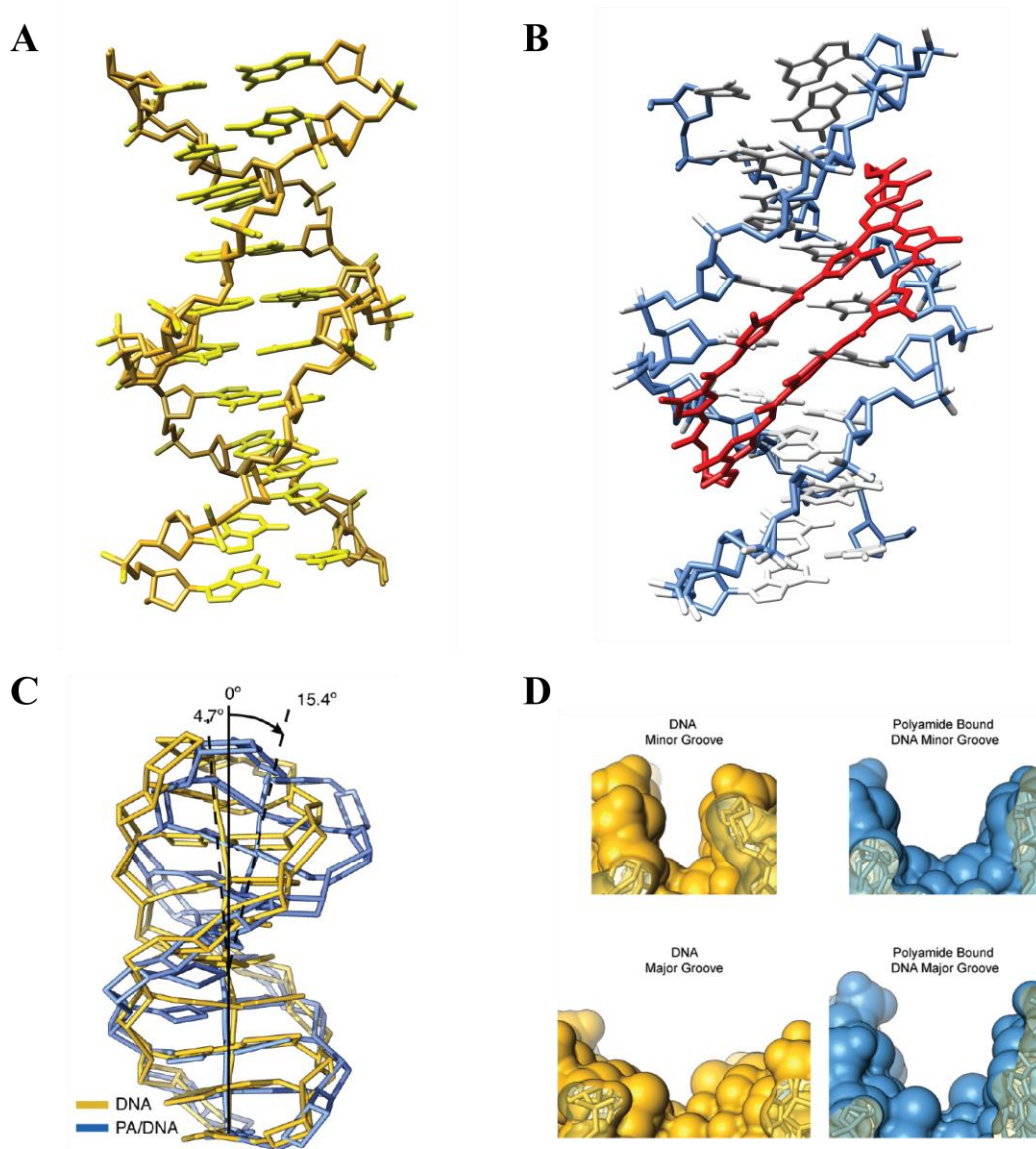


Figure 1.8 Polyamide perturbation of DNA structure. (A) X-ray -crystal structure of native DNA at 0.98 Å resolution (PDB 1D8G). (B) X-ray crystal structure of polyamide/DNA complex at 0.95 Å resolution (PDB 3OMJ). (C) DNA bending upon polyamide binding (blue) vs. unbound DNA (yellow). (D) Minor groove widening (top) and major groove narrowing (bottom) of polyamide/DNA complex (blue) relative to native DNA (yellow).

1.7 Scope of this Thesis

The work in this thesis is aimed at the further advancement in polyamide synthesis technology to gain access towards novel structural derivatives. In our ongoing efforts in studying the biological activity of Py-Im polyamides, the pronounced effects of minor structural modifications have been repeatedly observed in both cell culture and animal models. The efficient synthesis of polyamide derivatives has, therefore, proven instrumental to our continued biological investigations. In Chapter 2, we describe a newly developed method utilizing Fmoc chemistry to synthesize cyclic polyamides under microwave-assisted solid-phase conditions. The modular approach provided quick and reliable access to a focused library of macrocyclic derivatives, which were tested and compared for their cytotoxicity and uptake properties in two cancer cell lines. In Chapter 3, we explored the molecular recognition properties of the polyamide turn unit by substitution with different heteroatoms at the α -position. The fluoro, hydroxyl, and amino turn derivatives were synthesized and measured for their binding affinities and preferences by DNase I footprinting and DNA thermal denaturation assays. In Chapter 4, we describe in detail the optimized and expedited synthesis of several hairpin polyamides and examine their antitumor activity *in vivo*.

1.8 References

- (1) Drew, H. R.; Wing, R. M.; Takano, T.; Broka, C.; Tanaka, S.; Itakura, K.; Dickerson, R. E. *Proc. Natl. Acad. Sci. U. S. A.* **1981**, 78, 2179–2183.
- (2) Consortium, I. H. G. S. *Nature* **2004**, 431, 931–945.
- (3) Juo, Z. S.; Chiu, T. K.; Leiberman, P. M.; Baikarov, I.; Berk, A. J.; and Dickerson, R. E. *Journal of Molecular Biology* **1996**, 261, 239–254.
- (4) Love, J. J.; Li, X.; Case, D. A.; Giese, K.; Grosschedl, R.; Wright, P. E. *Nature* **1995**, 376, 791–795.
- (5) Chen, F. E.; Huang, D. B.; Chen, Y. Q.; Ghosh, G. *Nature* **1998**, 391, 410–413.
- (6) Nair, S. K. and Burley, S. K. *Cell* **2003**, 112, 193–205.
- (7) Shaffer, P.L.; Jivan, A.; Dollins, D.E.; Claessens, F.; Gewirth, D.T. *Proc. Natl. Acad. Sci. U.S.A* **2004**, 101, 4758–4763.
- (8) Werner, M. H.; Clore, G. M.; Fisher, C. L.; Fisher, R. J.; Trinh, L.; Shiloach, J.; Gronenborn, A. M. *J. Biomol. NMR* **1997**, 10, 317–328.
- (9) Hou, M. H.; Robinson, H.; Gao, Y. G.; Wang, A. H. *Nucleic Acids Res.* **2004**, 32, 2214–2122.
- (10) Bifulco, G.; Galeone, A.; Nicolaou, K. C.; Chazin, W. J.; Gomez-Paloma, L. *J. Am. Chem. Soc.* **1998**, 120, 7183–7191.
- (11) Kamitori, S. and Takusagawa, F. *J. Am. Chem. Soc.* **1994**, 116, 4154–4165.
- (12) Hou, M. H.; Robinson, H.; Gao, Y. G.; Wang, A. H. *Nucleic Acids Res.* **2002**, 30, 4910–4917.
- (13) Arcamone, F.; Penco, S.; Orezzi, P.; Nicoletta, V.; Pirelli, A. *Nature* **1964**, 203, 1064–1065.

- (14) Kopka, M. L.; Yoon, C.; Goodsell, D.; Pjura, P.; Dickerson, R. E. *Proc. Natl. Acad. Sci. U. S. A.* **1985**, 82, 1376–1380.
- (15) Kopka, M. L.; Yoon, C.; Goodsell, D.; Pjura, P.; Dickerson, R. E. *J. Mol. Biol.* **1985**, 183, 553–563.
- (16) Coll, M.; Frederick, C. A.; Wang, A. H.; Rich, A. *Proc. Natl. Acad. Sci. U. S. A.* **1987**, 84, 8385–8389.
- (17) Mitra, S. N.; Wahl, M. C.; Sundaralingam, M. *Acta Crystallogr.* **1999**, D55, 602–609.
- (18) Dervan, P. B. *Bioorg. Med. Chem.* **2001**, 9, 2215–2235.
- (19) Dervan, P. B. and Edelson, B. S. *Curr. Opin. Struct. Biol.* **2003**, 13, 284–299.
- (20) Mrksich, M.; Wade, W. S.; Dwyer, T. J.; Geierstanger, B. H.; Wemmer, D. E.; Dervan, P. B. *Proc. Natl. Acad. Sci. U. S. A.* **1992**, 89, 7586–7590.
- (21) Wade, W. S.; Mrksich, M.; Dervan, P. B. *J. Am. Chem. Soc.* **1992**, 114, 8783–8794.
- (22) White, S.; Szewczyk, J. W.; Turner, J. M.; Baird, E. E.; Dervan, P. B. *Nature* **1998**, 391, 468–471.
- (23) Urbach, A. R.; Szewczyk, J. W.; White, S.; Turner, J. M.; Baird, E. E.; Dervan, P. B. *J. Am. Chem. Soc.* **1999**, 121, 11621–11629.
- (24) Mrksich, M.; Parks, M. E.; Dervan, P. B. *J. Am. Chem. Soc.* **1994**, 116, 7983–7988.
- (25) Trauger, J. W.; Baird, E. E.; Dervan, P. B. *Nature* **1996**, 382, 559–561.
- (26) White, S.; Baird, E. E.; Dervan, P. B. *J. Am. Chem. Soc.* **1997**, 119, 8756–8765.
- (27) Herman, D. M.; Baird, E. E.; Dervan, P. B. *J. Am. Chem. Soc.* **1998**, 120, 1382–1391.
- (28) Dose, C.; Farkas, M.E.; Chenoweth, D.M.; Dervan, P.B. *J. Am. Chem. Soc.* **2008**, 130, 6859–6866.

- (29) Cho, J.; Parks, M. E.; Dervan, P. B. *Proc. Natl. Acad. Sci. U. S. A.* **1995**, *92*, 10389–10392.
- (30) Herman, D.M.; Turner, J.M.; Baird, E.E.; Dervan, P.B. *J. Am. Chem. Soc.*, **1999**, *121*, 1121–1129.
- (31) Chenoweth, D.M.; Harki, D.A.; Phillips, J.W.; Dose, C.; Dervan, P.B. *J. Am. Chem. Soc.*, **2009**, *131*, 7182–7188.
- (32) Best, T. P.; Edelson, B. S.; Nickols, N. G.; Dervan, P. B. *Proc. Natl. Acad. Sci. U. S. A.* **2003**, *100*, 12063–12068.
- (33) Edelson, B. S.; Best, T. P.; Olenyuk, B.; Nickols, N. G.; Doss, R. M.; Foister, S.; Heckel, A.; Dervan, P. B. *Nucleic Acids Res.* **2004**, *32*, 2802–2818.
- (34) Nickols, N. G.; Jacobs, C. S.; Farkas, M. E.; and Dervan, P. B. *Nucleic Acids Res* **2007**, *35*, 363–370.
- (35) Olenyuk, B. Z.; Zhang, G. J.; Klco, J. M.; Nickols, N. G.; Kaelin, W. G., Jr.; Dervan, P. B. *Proc. Natl. Acad. Sci. U. S. A.* **2004**, *101*, 16768–16773.
- (36) Nickols, N. G.; Jacobs, C. S.; Farkas, M. E.; Dervan, P. B. *ACS Chem. Biol.* **2007**, *2*, 561–571.
- (37) Nickols, N. G.; Dervan, P. B. *Proc. Natl. Acad. Sci. U. S. A.* **2007**, *104*, 10418–10423.
- (38) Muzikar, K.A.; Nickols, N.G.; Dervan, P.B. *Proc. Natl. Acad. Sci. U.S.A.*, **2009**, *106*, 16598–16603.
- (39) Raskatov, J.A.; Meier, J.L.; Puckett, J.W.; Yang, F.; Ramakrishnan, P.; Dervan, P.B. *Proc. Natl. Acad. Sci. USA*, **2012**, *109*, 1023–1028.
- (40) Chenoweth, D.M. and Dervan, P.B. *Proc. Natl. Acad. Sci. U.S.A.* **2009**, *106*, 13175–13179.

- (41) Darnell, J. E. and Lodish, H. F. *Molecular cell biology*; W.H. Freeman: New York, **2000**.
- (42) Panne, D.; Maniatis, T.; Harrison, S. C. *Cell* **2007**, *129*, 1111–1123.
- (43) Chenoweth, D.M. and Dervan, P.B. *J. Am. Chem. Soc.* **2010**, *132*, 14521–14529.
- (44) Kielkopf, C. L.; Ding, S.; Kuhn, P.; Rees, D. C. *J. Mol. Biol.* **2000**, *296*, 787–801.

Chapter 2

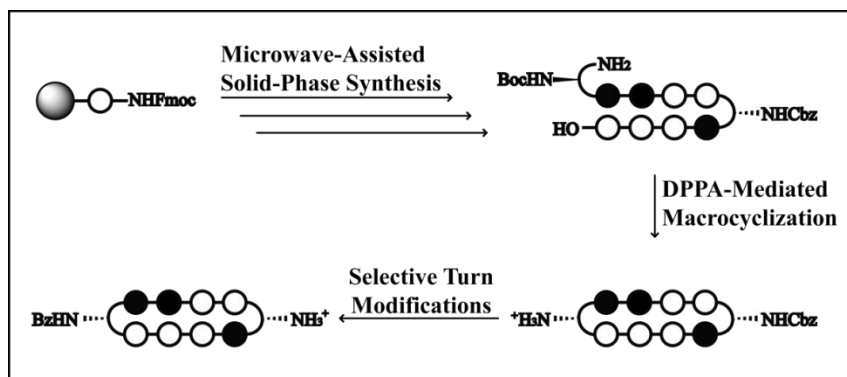
Synthesis of Cyclic Py-Im Polyamide Libraries

The text of this chapter was taken in part from a manuscript co-authored with David C. Montgomery, James W. Puckett and Peter B. Dervan (California Institute of Technology).

Li, B.C.; Montgomery, D.C.; Puckett, J.W.; Dervan, P.B. "Synthesis of Cyclic Py-Im Polyamide Libraries" *J. Org. Chem.* **2013**, 78, 124–133.

Abstract

Cyclic Py-Im polyamides containing two GABA turn units exhibit enhanced DNA binding affinity, but extensive studies of their biological properties have been hindered due to synthetic inaccessibility. A facile modular approach towards cyclic polyamides has been developed via microwave-assisted solid-phase synthesis of hairpin amino acid oligomer intermediates followed by macrocyclization. A focused library of cyclic polyamides **1–7** targeted to the androgen response element (ARE) and the estrogen response element (ERE) were synthesized in 12-17% overall yield. The Fmoc protection strategy also allows for selective modifications on the GABA turn units that have been shown to improve cellular uptake properties. The DNA binding affinities of a library of cyclic polyamides were measured by DNA thermal denaturation assays and compared to the corresponding hairpin polyamides. Fluorescein-labeled cyclic polyamides have been synthesized and imaged via confocal microscopy in A549 and T47D cell lines. The IC₅₀s of compounds **1–7** and **9–11** were determined, revealing remarkably varying levels of cytotoxicity.



2.1 Introduction

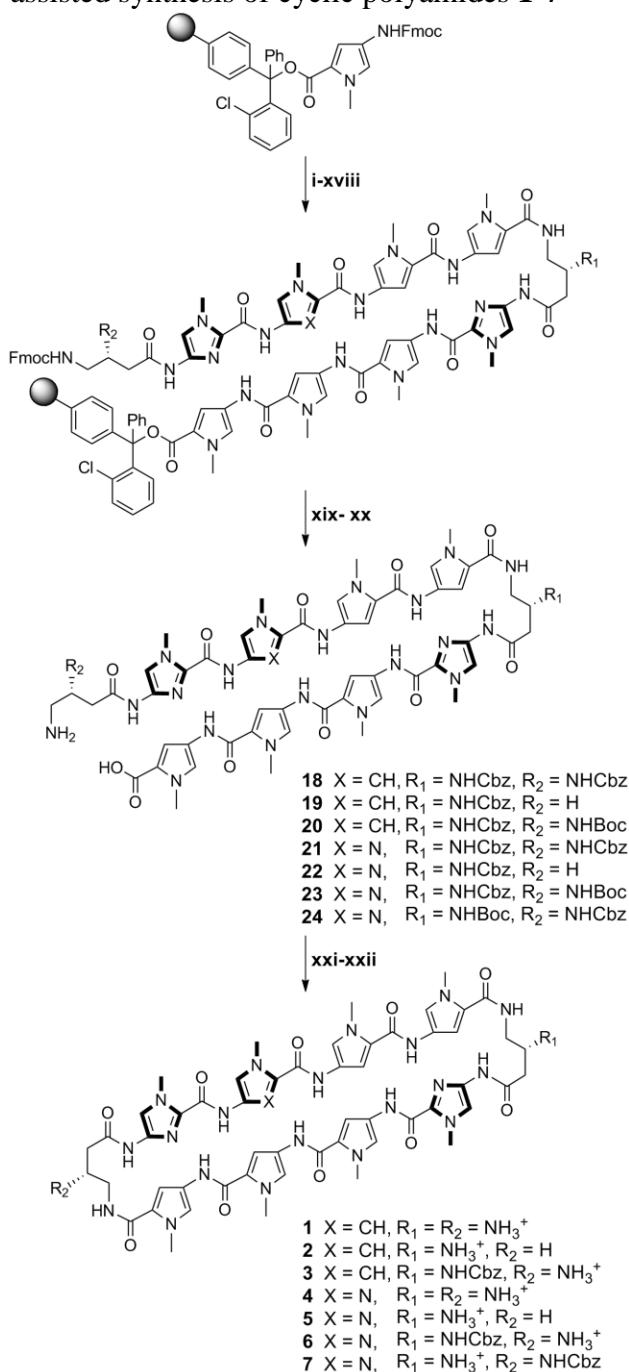
The selective modulation of eukaryotic gene expression by small molecules may have important implications in the field of chemical biology and human medicine. Pyrrole-imidazole polyamides are a class of synthetic ligands that can be programmed to bind the minor groove of specific DNA sequences.¹ Antiparallel, side-by-side N-methylpyrrole (Py) and N-methylimidazole (Im) carboxamides (Im/Py) pairs distinguish G·C from C·G base pairs, N-methyl-3-hydroxypyrrole (Hp)/Py shows specificity for T·A over A·T, whereas Py/Py pairs are specific for both T·A and A·T.²⁻⁵ By linking two strands of these heterocyclic oligomers via a γ -amino butyric acid (GABA) turn unit, hairpin Py-Im polyamides can be programmed to bind a large library of DNA sequences with affinities comparable to natural DNA-binding proteins.⁶⁻⁸ Hairpin polyamides have been shown to localize to the nuclei of living cells, and regulate endogenous gene expression by disrupting protein / DNA interfaces.⁹⁻¹⁷ Cyclic polyamides containing a second GABA turn unit exhibit further enhanced DNA binding properties.¹⁸⁻²¹ We have recently demonstrated their gene regulatory effects on AR-activated gene expression in prostate cancer models.²²

This discovery has opened a new area of research towards transcriptional regulation with small molecules, but the relative synthetic inaccessibility of cyclic polyamides has remained a bottleneck for examining libraries of structural variants that would modulate affinity, cell uptake and biological activity. Initial solid-phase methods were low yielding, and required substantial pre-modifications of the PAM resin.¹⁸⁻²⁰ While the solution-phase synthesis of cyclic polyamides remains useful in large-scale target-oriented synthesis, it has limited practicality towards libraries for screening biological activities.²² The recent report by Morinaga et al. offers a modular approach to achieve cyclic polyamides by intramolecular coupling of a cysteine and a

chloroacetyl residue, but the modification of the optimal three-carbon GABA turn into a sulphur-containing four-atom linker compromises its DNA binding affinity and may alter its biological properties.²³

We report here a solid-phase polyamide synthesis of a key hairpin amino acid oligomer intermediate, which followed by intramolecular cyclization, affords cyclic polyamides **1–8** in good yields. The polyamides were synthesized step-wise on 2-chlorotrityl resin. The modular approach led to rapid access of a focused library of cyclic polyamides **1–7** with various core sequences and turn unit modifications. The utilization of Fmoc chemistry allowed for differentially protected turn units, which were modified selectively to complement existing cellular imaging and cell uptake enhancement technologies.²⁴ We examined the DNA-binding properties and cytotoxicity profiles of compounds **1–11**, and the cellular localization of cyclic polyamides **12–14** by fluorescence microscopy.

Scheme 2.1 Microwave-assisted synthesis of cyclic polyamides **1-7**



¹All PyBOP-mediated coupling conditions were performed under microwave-assisted conditions (see Table 1).

²Reagents and conditions: (i) 50% piperidine, DMF; (ii) FmocPyOH, PyBOP, DIEA, DMF; (iii) 50% piperidine, DMF; (iv) FmocPyOH, PyBOP, DIEA, DMF; (v) 50% piperidine, DMF; (vi) FmocImOH, PyBOP, DIEA, DMF; (vii) 50% piperidine, DMF; (viii) Z-β-Dab(Fmoc)-OH (for **1-6**) or Boc-β-Dab(Fmoc)-OH (for **7**), PyBOP, DIEA, DMF; (ix) 50% piperidine, DMF; (x) FmocPyOH, PyBOP, DIEA, DMF; (xi) 50% piperidine, DMF; (xii) FmocPyOH, PyBOP, DIEA, DMF; (xiii) 50% piperidine, DMF; (xiv) FmocPyOH (for **1-3**) or FmocImOH (for **4-7**), PyBOP, DIEA, DMF; (xv) 50% piperidine, DMF; (xvi) FmocImOH, PyBOP, DIEA, DMF; (xvii) 50% piperidine, DMF; (xviii) Z-β-Dab(Fmoc)-OH (for **1 & 4 & 7**) or Fmoc-GABA-OH (for **2 & 5**) or Boc-β-Dab(Fmoc)-OH (for **3 & 6**), PyBOP, DIEA, DMF; (xix) 30% HFIP, DCM; (xx) 20% piperidine, DMF; (xxi) DPPA, DIEA, DMF; (xxii) 10% TFMSA, TFA (for **1, 2, 4 & 5**) or TFA (for **3, 6 & 7**).

2.2 Results and Discussion

I. Microwave-Assisted Solid-Phase Synthesis

Due to previously observed decomposition of the conjugated C-terminal free carboxylic acid in polyamide intermediates, 2-chlorotrityl-chloride (2-Cl-Trt-Cl) resin was chosen for its mild synthesis and cleavage conditions. Polyamide synthesis on this resin has been previously reported by Aldrich-Wright and co-workers, but a resin-bound β -alanine linker was used in both instances, and a new loading procedure was therefore needed.^{25,26} 2-Cl-Trt-Cl resin was first loaded with the Fmoc-protected Py monomer in N,N-dimethylformamide (DMF) and capped with methanol. Resin substitution levels were determined by the Fmoc test and confirmed by weighing the dry mass of the loaded resin. Fmoc deprotection was achieved using a 50% piperidine in DMF solution. In light of the recent improvements in both efficiency and yield, the couplings were performed under microwave-assisted conditions using the desired PyBOP-activated monomers.²⁷ Initial syntheses performed at 60 °C led to premature cleavage of intermediates off the 2-Cl-Trt resin, and 50 °C couplings were therefore preferable. The challenging Im to Py coupling required an FmocPyImOH dimer, which was obtained via an optimized procedure by Weltzer and Wemmer.²⁸ The deprotection and coupling conditions are detailed in Table 1. This 2-step deprotection-coupling procedure was repeated until the desired polyamide sequence was achieved. To build the small library of polyamides in a modular fashion, the resin was split into different batches at corresponding steps for further derivatization. Upon completion, the N-terminal Fmoc-protected polyamide oligomer was cleaved from the resin with 30% hexafluoroisopropanol (HFIP) in dichloromethane (DCM), concentrated *in vacuo*, and the resulting residue was subjected to a 20% piperidine solution to remove the Fmoc group. Direct cleavage of the free-amine polyamide oligomer was attempted, but found to be

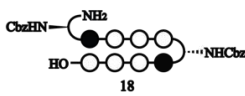
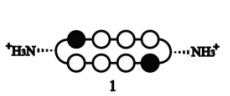
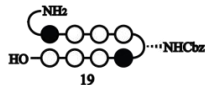
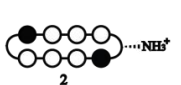
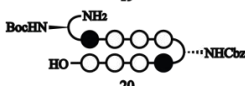
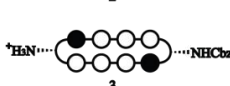
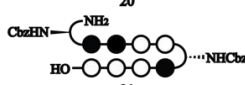
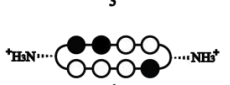
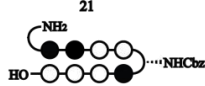

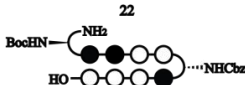
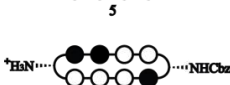
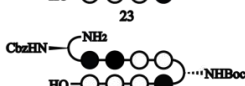
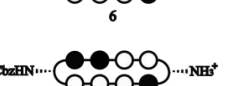

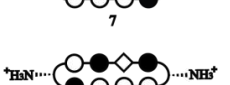
ineffective due to poor solubility of the zwitterion intermediate in the cleavage solution. After purification by high-performance liquid chromatography (HPLC), the desired polyamide intermediates **18–24** were obtained in 31–40% yields.

Table 2.1 Standard Fmoc deprotection and microwave-assisted coupling times for solid-phase polyamide synthesis.

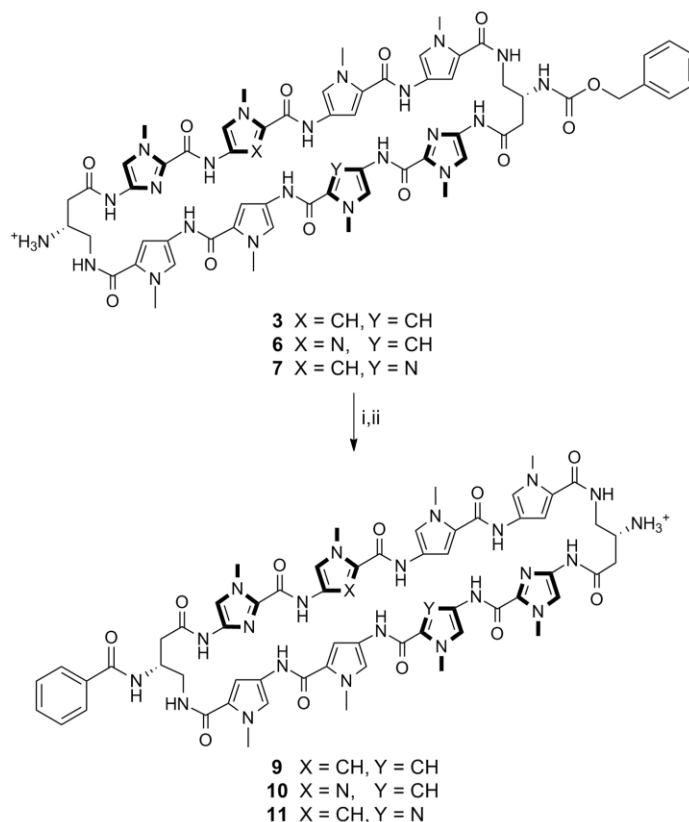
Resin-Bound Nucleophile	Deprotection Times ¹	Coupling Times ² (min)		
		Py	Im	GABA/ β -Ala
Py	3 x 10 min	20	20	20
Im	3 x 10 min	IR ³	30	30
GABA/ β -Ala	2 x 5 min	20	20	20

¹All deprotections were performed in 50% piperidine in DMF. ²All coupling reactions were conducted under microwave-assisted conditions at 50 °C with a 0.3M solution of the activated monomers (3 eq. monomer acid, 3 eq. PyBOP, 8 eq. DIEA, DMF). ³FmocPyOH coupling onto resin with N-terminal Im was incomplete even at 60 °C for up to 1h. Synthesis of polyamide sequences that require this linkage should use the FmocPyImOH dimer instead, demonstrated later in the synthesis of **8**.

Table 2.2 Summary table of MALDI-TOF data and synthetic yields for cyclic polyamides **1–8** and intermediates **18–25**.

Polyamide Precursor	[M+H] ⁺ (expected)	m/z (observed)	Solid-Phase Yield (%)	Cyclic Polyamide	[M+H] ⁺ (expected)	m/z (observed)	Cyclization Yield (%)	Overall Yield (%)
 18	1465.4	1465.9	33	 1	1179.5	1179.9	35	12
 19	1316.5	1316.9	40	 2	1164.5	1164.9	42	17
 20	1431.6	1453.9 [M+Na] ⁺	34	 3	1313.6	1314.0	47	16
 21	1466.5	1466.9	31	 4	1180.5	1180.9	39	12
 22	1317.5	1317.2	34	 5	1165.5	1165.5	48	16
 23	1432.6	1455.0 [M+Na] ⁺	32	 6	1314.5	1314.7	37	12
 24	1432.6	1454.9 [M+Na] ⁺	33	 7	1314.5	1314.8	38	13
 25	1414.6	1372.0 [M-CO ₂] ⁺	34	 8	1129.5	1130.0	39	13

Scheme 2.2 Preparation of cyclic polyamides **9–11**



¹Reagents and conditions: (i) BzOH, PyBOP, DIEA, DMF; (ii) 10% TFMSA, TFA.

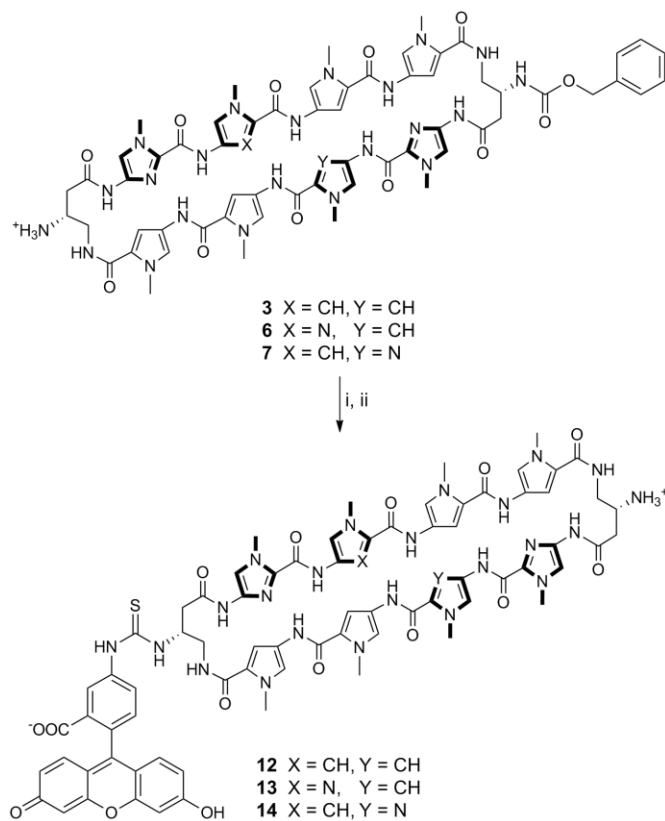
II. DPPA-Mediated Macrocyclization

The polyamide macrocyclization step was achieved by a DPPA-mediated ring-closing reaction between the N-terminal amino group and the C-terminal carboxylic acid. This method was first employed by Cho et al. in the synthesis of cyclic polyamides.^{18,29,30} In order to obtain a general work-up procedure applicable to polyamides of various lipophilicities, diisopropylethylamine (DIEA) was used as the base in place of sodium bicarbonate ($NaHCO_3$) in the original conditions.³¹ Deprotection of the turn units with trifluoromethanesulfonic acid (TFMSA) or trifluoroacetic acid (TFA), followed by HPLC purification, afforded polyamides **1–7** in **37–43%** yields over 2 steps.

III. Selective Derivatization of Cyclic Polyamide Turn Units

By taking advantage of the Fmoc protection scheme, the two GABA β -amino groups in **3** were differentially protected. This is further highlighted in **6** and **7**, which share the same asymmetric polyamide core targeted to the 5'-WGGWCW-3' sequence, and allowed for the selective conjugation of a benzoic acid moiety on a single turn unit in polyamides **9–11** that has been recently developed to enhance the cellular localization properties of hairpin polyamides.²⁴ Mono-substituted benzyl carbamate (Cbz) polyamides **3**, **6** and **7** were chosen as targets based on unpublished results indicating Cbz-functionalized polyamides are biologically active (Supp. Fig. S16). Cyclic polyamides **12–14** with a fluorescein dye were synthesized in a similar fashion, and imaged in living cells via fluorescence microscopy. Furthermore, both the solubility and the pharmacokinetic profiles of cyclic polyamides have been shown to be highly dependent on subtle structural modifications, and this method allows for the modular synthesis of these structural variants in an efficient manner.^{31–33}

Scheme 2.3 Preparation of cyclic polyamides **12–14**



¹Reagents and conditions: (i) FITC, DIEA, DMF; (ii) 10% TFMSA, TFA.

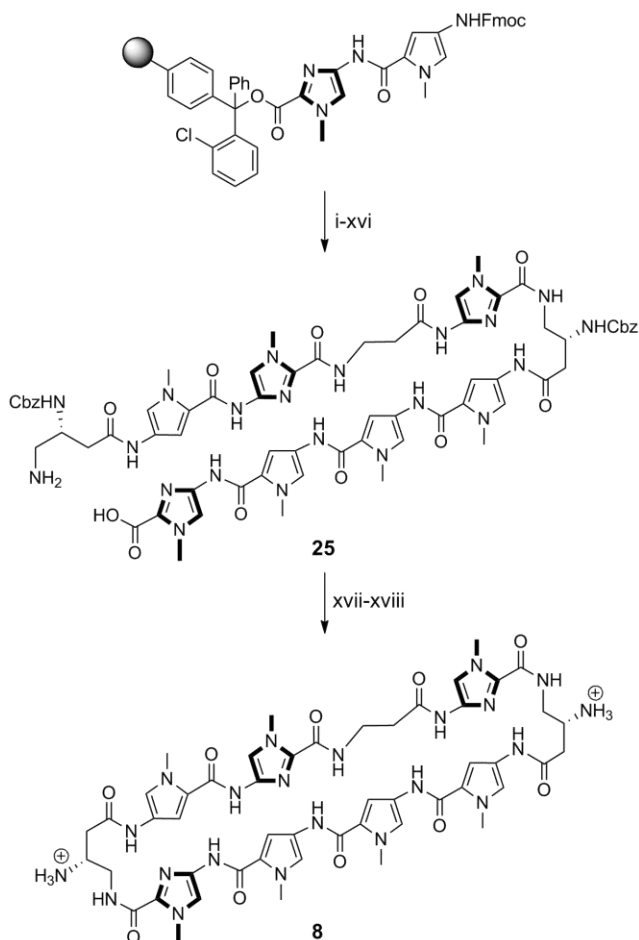
IV. Synthesis of Cyclic and Hairpin Polyamides with C-terminal Imidazole Units

Previously established solid-phase polyamide synthesis methods have been generally limited to sequences beginning with a pyrrole monomer.^{34,35} Solid-phase synthesis of polyamides starting with imidazole units on the commonly used Kaiser oxime resin have been low yielding, mainly attributed to the sensitivity of the oxime-imidazole linkage that lead to premature cleavage of resin-bound intermediates. The addition of an aliphatic linker (e.g. Boc- β -Ala-PAM resin) circumvents this issue, but previous studies on hairpin polyamides with C-terminal β -alanine motifs have shown reduced cellular uptake properties and thus diminished gene regulatory effects of these products.⁹ Using the microwave-assisted conditions reported above,

cyclic polyamide **8** targeted to the 5'-WCGWGW-3' sequence found in E-Box binding sites have been synthesized in 13% yield overall.

Initial attempts starting with FmocImOH-loaded resin resulted in undesired cleavage during subsequent steps, and so syntheses began with loading of the FmocPyImOH dimer onto 2-chlorotrityl resin. After deprotection-coupling of the corresponding monomer units, followed by resin cleavage and Fmoc removal, polyamide intermediate **25** was isolated by HPLC purification in 34% yield. DPPA-mediated cyclization of **25**, followed by Cbz deprotection afforded cyclic polyamide **8** in 39% yield over 2 steps. Hairpin polyamide **17** was synthesized in a similar stepwise manner to afford the Im-capped, C-terminal acid intermediate, which was then coupled to a 3,3'-diamino-N-methyldipropylamine linker, followed by isophthalic acid conjugation, Boc deprotection, and isolated in 24% yield over 16 steps (Scheme 2.5). This is a step forward which allows for the synthesis of both cyclic and non- β -alanine-linked hairpin polyamides with sequences beginning with an imidazole unit, further expanding the scope of targetable DNA sequences and inhibition of transcription factor-mediated gene expression by Py-Im polyamides.

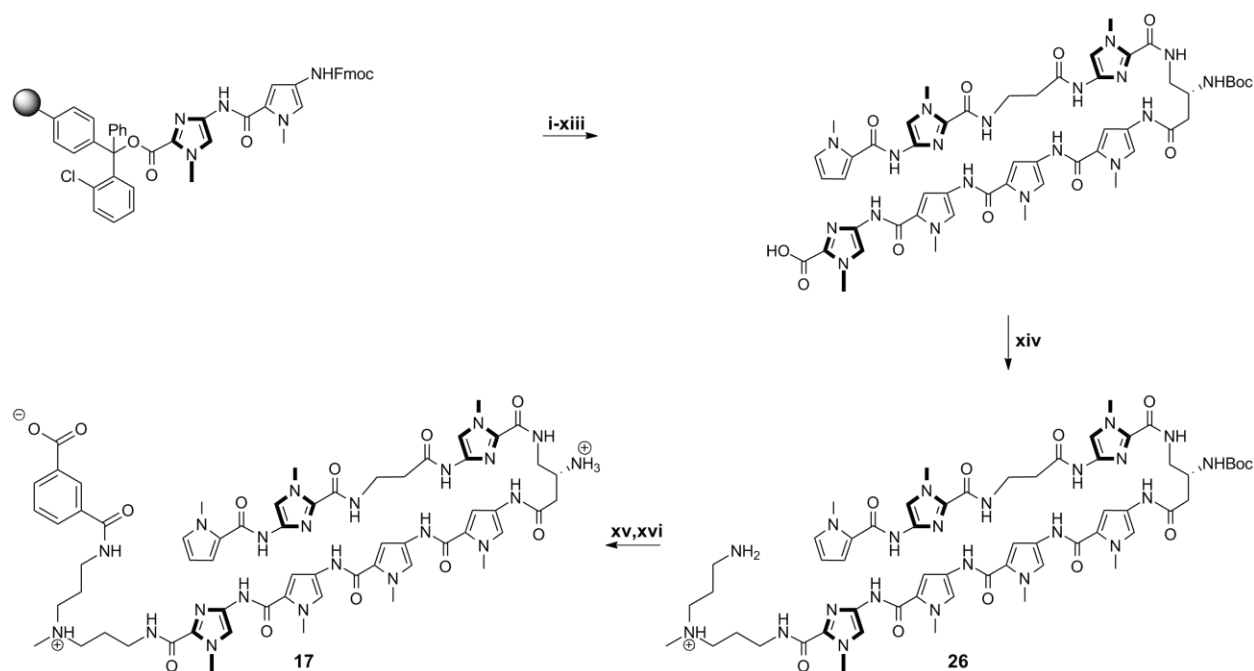
Scheme 2.4 Preparation of cyclic polyamide **8**



¹All PyBOP-mediated coupling conditions were performed under microwave-assisted conditions (see Table 1).

²Reagents and conditions: (i) 50% piperidine, DMF; (ii) FmocPyOH, PyBOP, DIEA, DMF; (iii) 50% piperidine, DMF; (iv) FmocPyOH, PyBOP, DIEA, DMF; (v) 50% piperidine, DMF; (vi) Z-β-Dab(Fmoc)-OH, PyBOP, DIEA, DMF; (vii) 50% piperidine, DMF; (viii) FmocImOH, PyBOP, DIEA, DMF; (ix) 50% piperidine, DMF; (x) Fmoc-β-Ala-OH, PyBOP, DIEA, DMF; (xi) 50% piperidine, DMF; (xii) FmocPyImOH, PyBOP, DIEA, DMF; (xiii) 50% piperidine, DMF; (xiv) Z-β-Dab(Fmoc)-OH, PyBOP, DIEA, DMF; (xv) 30% HFIP, DCM; (xvi) 20% piperidine, DMF; (xvii) DPPA, DIEA, DMF; (xviii) 10% TFMSA, TFA.

Scheme 2.5 Preparation of hairpin polyamide **17**



¹All PyBOP-mediated coupling conditions were performed under microwave-assisted conditions (see Table 1).

²Reagents and conditions: (i) 50% piperidine, DMF; (ii) FmocPyOH, PyBOP, DIEA, DMF; (iii) 50% piperidine, DMF; (iv) FmocPyOH, PyBOP, DIEA, DMF; (v) 50% piperidine, DMF; (vi) Boc- β -Dab(Fmoc)-OH, PyBOP, DIEA, DMF; (vii) 50% piperidine, DMF; (viii) FmocImOH, PyBOP, DIEA, DMF; (ix) 50% piperidine, DMF; (x) Fmoc- β -Ala-OH, PyBOP, DIEA, DMF; (xi) 50% piperidine, DMF; (xii) PyImOH, PyBOP, DIEA, DMF; (xiii) 30% HFIP, DCM; (xiv) 3,3'-diamino-N-methyldipropylamine, PyBOP, DMF; (xv) Isophthalic acid, PyBOP, DIEA, DMF; (xvi) TFA.

V. Thermal Stabilization of DNA Duplexes by Polyamides

Py-Im polyamide-DNA binding affinities and specificities have historically been measured by quantitative DNase I footprinting assays.³⁶ As previously reported, however, cyclic polyamides have exceptionally high DNA binding affinities that exceed the detection limit of this experiment (i.e. $K_a \geq 2 \times 10^{10} \text{ M}^{-1}$).^{22,37,38} The DNA binding affinities of cyclic polyamides **1–14** have been rank ordered by magnitude of DNA thermal stabilization (ΔT_m), and compared to the corresponding hairpin polyamides **14–16**. Spectroscopic measurements were performed on 12-mer DNA duplexes with sequences 5'-CGATTGTTCAAGC-3', 5'-CGATTGGTCAAGC-3', and 5'-CGATCGTGAAGC-3', each containing a match binding site for the corresponding polyamides.

Consistent with the findings of Chenoweth et al, the ΔT_m value for bis-amino cyclic polyamide **1** ($\Delta T_m = 26.1^\circ\text{C}$) was calculated to be significantly higher than that of hairpin polyamide **15** ($\Delta T_m = 22.0^\circ\text{C}$).²² So while **15** has an established binding affinity to the match androgen response element (ARE) half-site (5'-WGWWCW-3') in the subnanomolar range, cyclic polyamide **1** provides even greater stabilization to such DNA duplexes. Mono-unsubstituted cyclic polyamide **2** provides less DNA stabilization compared to **1** ($\Delta T_m = 20.4^\circ\text{C}$), which is likely due to the loss of a positive charge and thus the loss of favorable electrostatic interactions with the negatively-charged DNA backbone. Perhaps more surprising is the high ΔT_m values retained by mono-protected cyclic polyamides **3** ($\Delta T_m = 27.3^\circ\text{C}$) and **9** ($\Delta T_m = 28.0^\circ\text{C}$), each containing a lone free amino group and net +1 charge. As shown in **Fig. 1**, the benzoyl (Bz) group in **9** projects straight down the minor groove, avoiding unfavorable steric interactions with the groove wall, and may offer insight into the high degree of DNA stabilization by **3** and **9** comparable to the bis-amino cycle **1**. Fluorescein-conjugate **12** ($\Delta T_m =$

21.8°C) has a DNA binding affinity lower than **3** and **9**, perhaps due to increased steric clashes from the larger substitution group and unfavorable electrostatic interactions from the negatively-charged fluorescein group, but still binds DNA at a similar level to **15**.

The magnitude of stabilization provided by cyclic polyamides **4–7**, **10–11**, and **13–14** targeted to estrogen response element (ERE) half-sites (5'-WGGWCW-3') follows a similar pattern to the aforementioned ARE-targeting series. Mono-unsubstituted cycle **5** ($\Delta T_m = 18.6^\circ\text{C}$) stabilizes the duplex at a comparable level to hairpin polyamide **16** ($\Delta T_m = 16.7^\circ\text{C}$), whereas bis-amino compound **4** ($\Delta T_m = 23.2^\circ\text{C}$) has a higher ΔT_m value. The mono-Cbz cycles **6** ($\Delta T_m = 23.6^\circ\text{C}$) and **7** ($\Delta T_m = 24.3^\circ\text{C}$), mono-Bz substituted **10** ($\Delta T_m = 26.0^\circ\text{C}$) and **11** ($\Delta T_m = 25.1^\circ\text{C}$), and mono-fluorescein conjugates **13** ($\Delta T_m = 22.2^\circ\text{C}$) and **14** ($\Delta T_m = 21.0^\circ\text{C}$) each bind DNA similar to **4**.

Cyclic polyamide **8** ($\Delta T_m = 13.4^\circ\text{C}$) binds the match 5'-WCGWGW-3' sequence at an elevated level compared to hairpin **17** ($\Delta T_m = 6.6^\circ\text{C}$), which may prove important towards targeting oncogenic transcription factors such as c-Myc that act through binding canonical E-Box (5'-CACGTG-3') sequences.

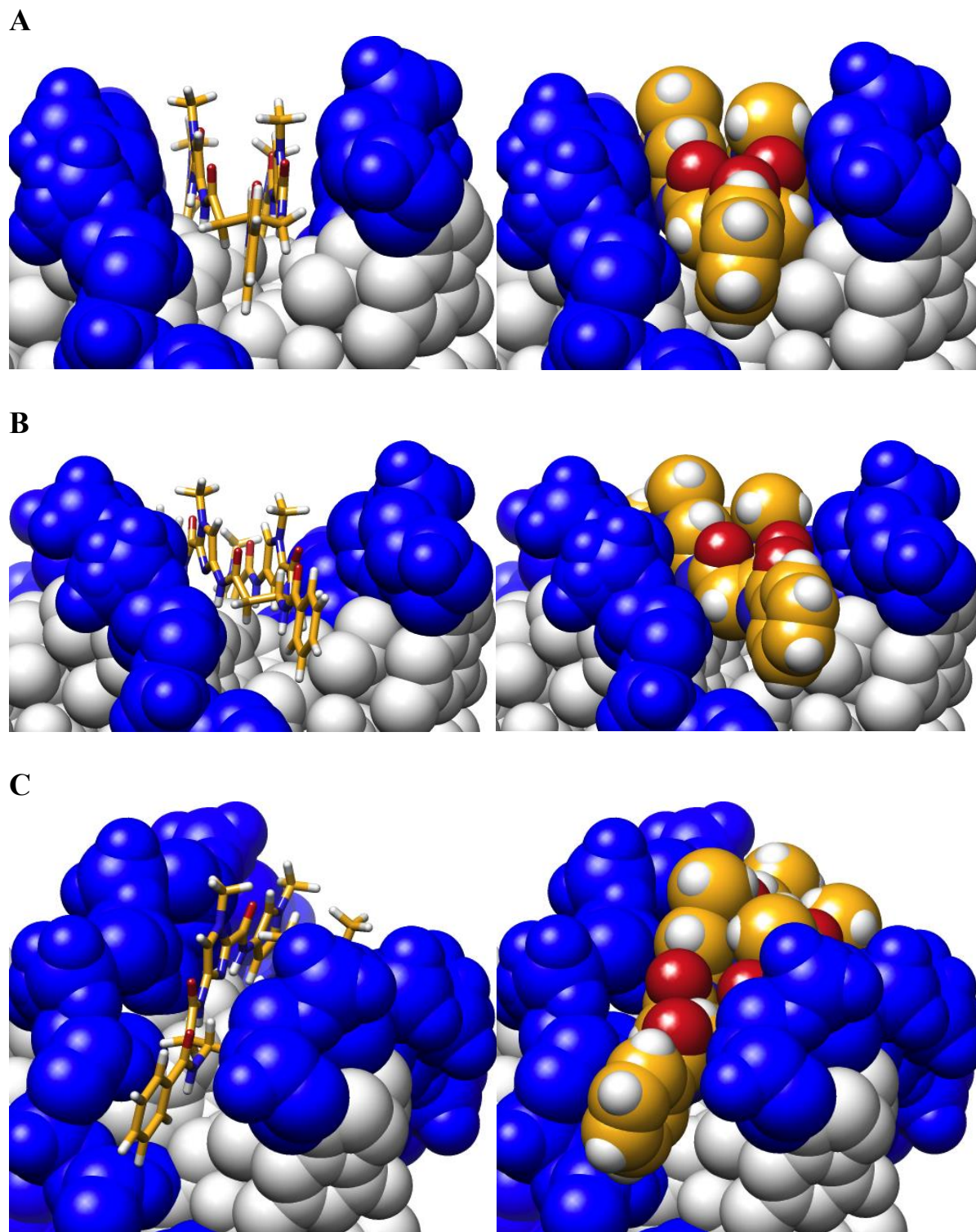
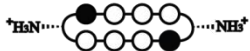

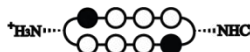
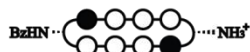

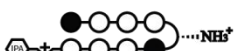







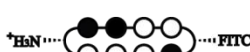
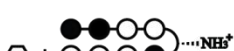




Figure 2.1 (Left) Stick model and (right) space-filling model of benzoyl substituted turn along the DNA minor groove from three different views. Based on published crystal structure by Chenoweth et al. (PDB ID: 3OMJ).

Table 2.3 T_m Values for polyamide library

Polyamides		5'- CGA TGTTCA AGC -3'	
		$T_m / ^\circ\text{C}$	$\Delta T_m / ^\circ\text{C}$
—		53.1 (± 0.2)	—
	(1)	79.2 (± 0.2)	26.1
	(2)	73.5 (± 0.2)	20.4
	(3)	80.4 (± 0.2)	27.3
	(9)	81.1 (± 0.2)	28.0
	(12)	74.9 (± 0.1)	21.8
	(15)	75.1 (± 0.1)	22.0
<hr/>			
Polyamides		5'- CGA TGGTCA AGC -3'	
		$T_m / ^\circ\text{C}$	$\Delta T_m / ^\circ\text{C}$
—		56.2 (± 0.3)	—
	(4)	79.4 (± 0.3)	23.2
	(5)	74.8 (± 0.2)	18.6
	(6)	79.8 (± 0.2)	23.6
	(7)	80.5 (± 0.3)	24.3
	(10)	82.2 (± 0.1)	26.0
	(11)	81.5 (± 0.1)	25.1
	(13)	78.4 (± 0.6)	22.2
	(14)	77.2 (± 0.1)	21.0
	(16)	72.9 (± 0.2)	16.7
<hr/>			
Polyamides		5'- CGA TCGTGA AGC -3'	
		$T_m / ^\circ\text{C}$	$\Delta T_m / ^\circ\text{C}$
—		56.7 (± 0.2)	—
	(8)	70.1 (± 0.1)	13.4
	(17)	63.3 (± 0.3)	6.6

VI. *Sulforhodamine B Cytotoxicity Assay for Compounds 1–11*

The cytotoxicity of compounds **1–11** were assessed in A549 human lung carcinoma and T47D human breast cancer cell lines (Tables 4 & 5). The cyclic polyamides targeted to the 5'-WGWWCW-3' sequence generally exhibit a higher level of cytotoxicity than the 5'-WGGWCW-3' series, which is consistent with the trends observed in the DNA thermal denaturation analysis and confocal microscopy studies. Detailed inspection of the IC₅₀ values within the series of compounds and across the cell lines, however, offers some unanticipated insights into the different biological properties of these minor structural variants.

Bis-amino cycle **1**, which has previously been shown to be biologically active, did not display any significant level of cytotoxicity in either cell line (IC₅₀ > 30 μ M). Mono-unsubstituted compound **2** (IC₅₀ = 4.9 μ M) and mono-Bz **9** (IC₅₀ = 1.0 μ M) were comparably cytotoxic to hairpin polyamide **15** (IC₅₀ = 3.1 μ M) in A549 cells, but an order of magnitude more cytotoxic (IC₅₀ = 74 nM & 79 nM, respectively) than **15** (IC₅₀ = 710 nM) in T47D cells. The mono-Cbz cycle **3** was consistently the most cytotoxic compound in both A549 (IC₅₀ = 160 nM) and T47D (IC₅₀ = 25 nM) cell lines.

For the 5'-WGGWCW-3' targeting polyamides, the only compound that exhibited an IC₅₀ value lower than 30 μ M in A549 cells was the mono-Cbz compound **6** (IC₅₀ = 1.9 μ M). In T47D cells, consistent with the 5'-WGWWCW-3' series, bis-amino cycle **4** (IC₅₀ > 30 μ M) was found to be not significantly cytotoxic and **6** (IC₅₀ = 460 nM) was the most cytotoxic compound. Mono-unsubstituted cycle **5** (IC₅₀ = 0.82 μ M) again shares a comparable level of cytotoxicity with the reference hairpin **16** (IC₅₀ = 1.1 μ M), whereas mono-Bz compounds **10** (IC₅₀ = 13.3 μ M) and **11** (IC₅₀ = 7.5 μ M) are both an order of magnitude less cytotoxic.

Perhaps most interestingly, mono-Cbz compound **7** did not exhibit observable levels of cytotoxicity ($IC_{50} > 30 \mu M$) in either A549 or T47D cells. Considering that **7** is a regioisomer of **6**, where the Cbz group is simply swapped onto the other turn, and that **7** only differs from **3** by a single $-CH$ to $-N$ substitution, it is rather surprising that **7** is more than 15- to 65- fold less cytotoxic than **6** and at least 180- to 1200- fold less cytotoxic than **3** in the two examined cell lines. Given the comparable DNA stabilization properties between **6** and **7**, and their common core sequence, we would not have predicted this vast discrepancy in cytotoxicity.

This study has demonstrated the large and somewhat unpredictable effects in biological activity induced by small structural variations of cyclic polyamides. Based on our preliminary work, the aggregation and pharmacokinetic properties of polyamides also vary greatly depending on structural modifications.^{31–33} All this combines to highlight the importance of a fast and reliable method to generate focused libraries of cyclic polyamides for future research.

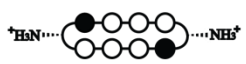

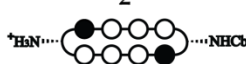
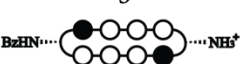

Cyclic Polyamide	A549	T47D
	$IC_{50} (\mu M)$	$IC_{50} (\mu M)$
 1	>30	>30
 2	4.9 ± 1.8	0.074 ± 0.011
 3	0.16 ± 0.05	0.025 ± 0.005
 9	1.0 ± 0.2	0.079 ± 0.003
 15	3.1 ± 0.6	0.71 ± 0.10

Table 2.4 SRB cytotoxicity data on compounds **1–3**, **9**, and **15**, in A549 and T47D cells, 72 h incubation.




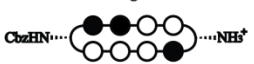



Cyclic Polyamide	A549	T47D
	IC ₅₀ (μM)	IC ₅₀ (μM)
 4	>30	>30
 5	>30	0.82 ± 0.21
 6	1.9 ± 0.2	0.46 ± 0.27
 7	>30	>30
 10	>30	13.3 ± 0.6
 11	>30	7.5 ± 0.7
 16	>30	1.1 ± 0.1

Table 2.5 SRB cytotoxicity data on compounds **4–7**, **10–11**, and **16**, in A549 and T47D cells, 72 h incubation.

VII. Confocal Microscopy of Cyclic Polyamide-Fluorescein Conjugates **12–14**

To directly examine the cellular localization of cyclic polyamides, fluorescein conjugates **12–14** were synthesized and visualized in living cells via confocal microscopy (Figs. 2 & 3). The selective conjugation of a single fluorescein molecule not only helped retain a free amino group for solubility purposes, but also allowed for the qualitative comparison of the two fluorescein conjugates **13** and **14** that share the same asymmetric polyamide core.

In each of the cases examined, cyclic polyamides **12–14** appear to permeate through the cellular membrane and localize in the cell nucleus, which was confirmed by the co-localization with Hoechst 33258 DNA stain. For ease of qualitatively assessing compound uptake, all A549 images were taken at a 660 fluorescence gain level, and all T47D images were taken at 600 fluorescence gain. Comparing Figures 2 and 3, the fluorescence levels of compounds **12–14** in

T47D cells are all significantly higher than in A549, which is only further amplified by this difference in gain levels.

Compound **12** matched to the 5'-WGWWCW-3' sequence exhibits the highest level of nuclear localization in both cell lines. Among the two 5'-WGGWCW-3' targeting cycles, polyamide **14** qualitatively appears to have a relatively higher fluorescence signal in the cell nuclei in both A549 and T47D cells. This may help explain the cytotoxicity data reported above, where compounds **6** and **11** with Cbz and Bz substitutions on the same side as the fluorescein in **14** consistently display larger biological effects than **7** and **10** that are more structurally similar to cyclic polyamide **13**.

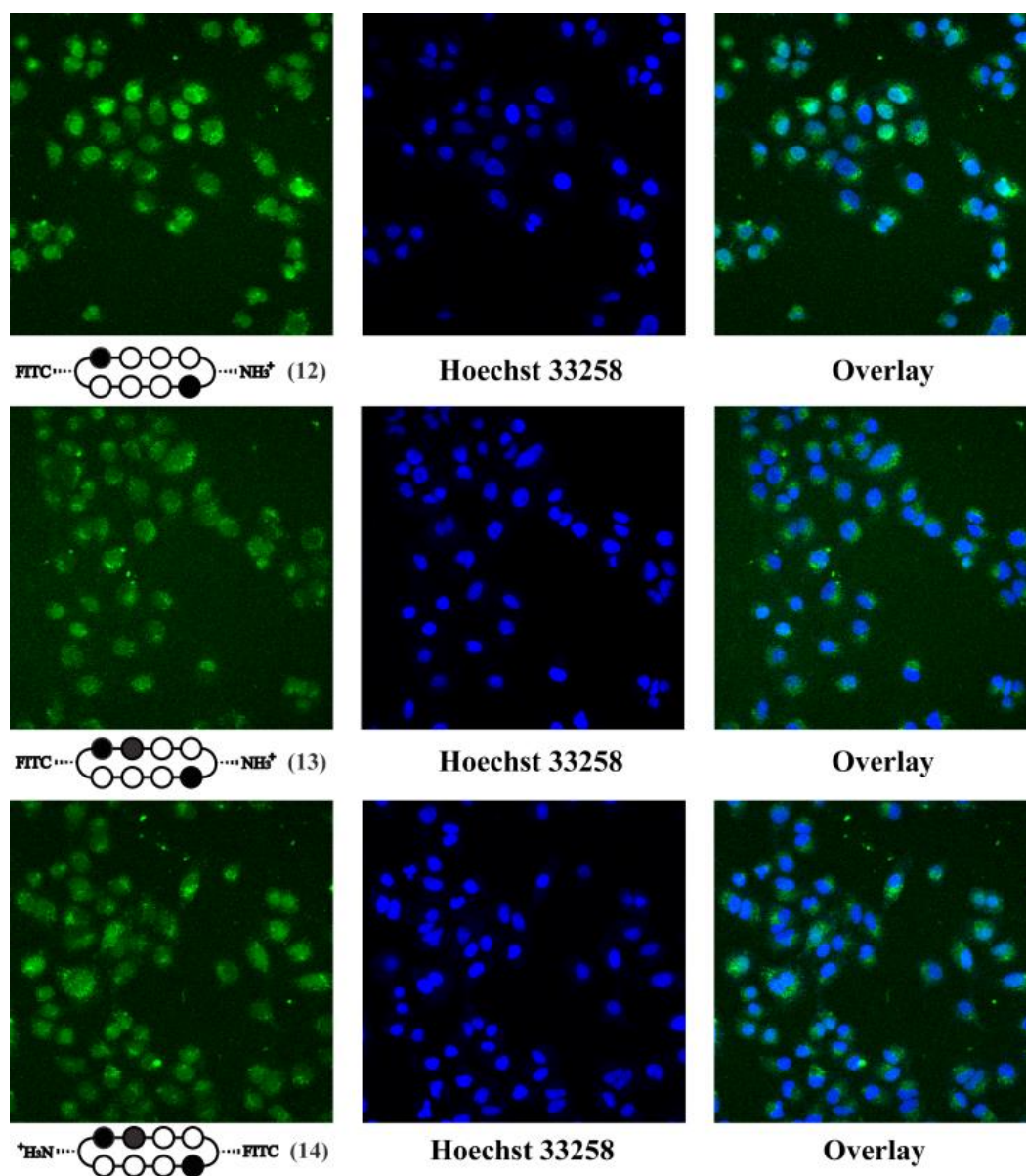


Figure 2.2 Confocal microscopy of cyclic polyamide-fluorescein conjugates **12** (top), **13** (middle), and **14** (bottom) in A549 cells. In order to confirm nuclear localization, the fluorescence panel (left) was compared with Hoechst 33258 staining (middle) and overlay (right).

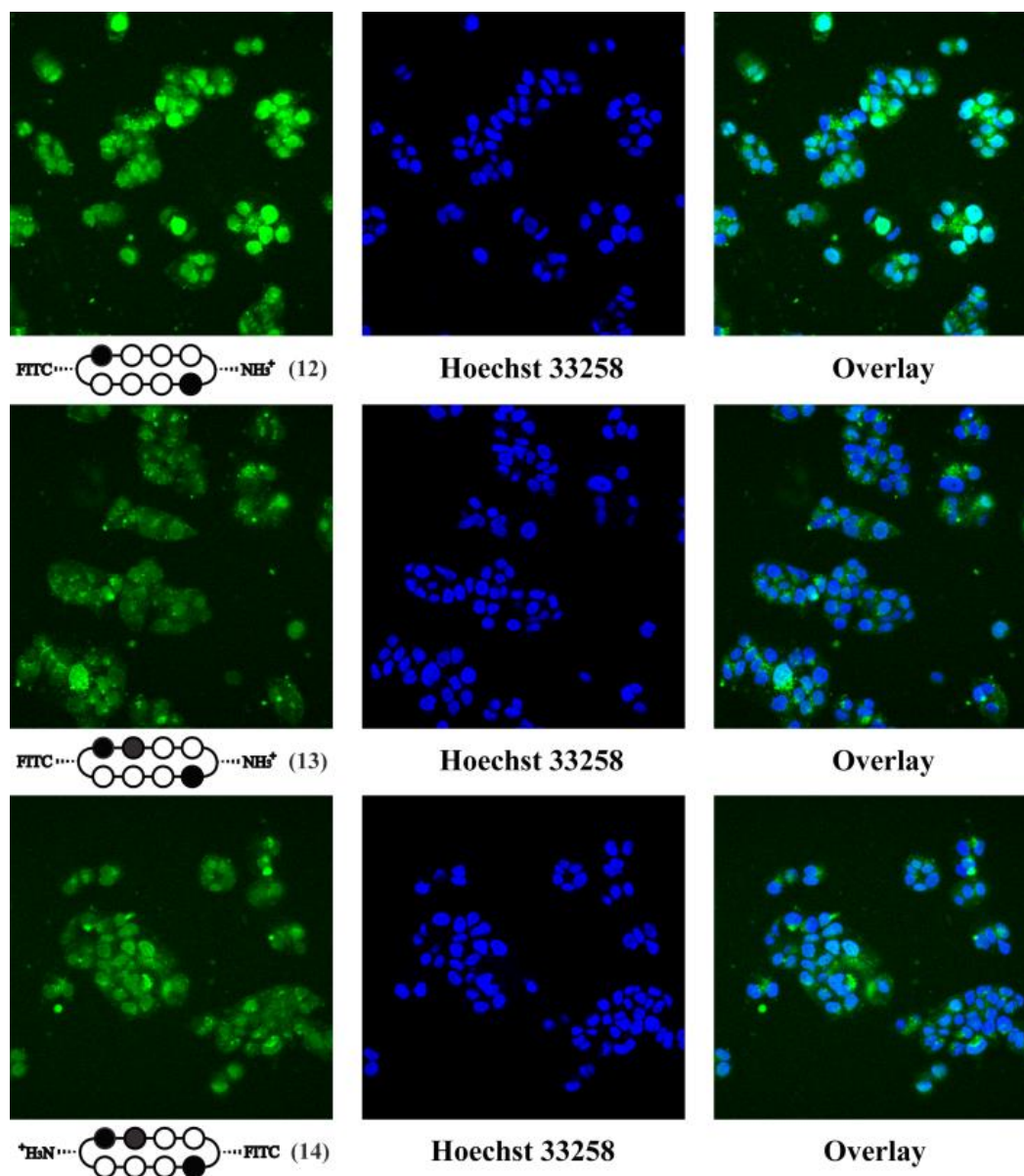


Figure 2.3 Confocal microscopy of cyclic polyamide-fluorescein conjugates **12** (top), **13** (middle), and **14** (bottom) in T47D cells. In order to confirm nuclear localization, the fluorescence panel (left) was compared with Hoechst 33258 staining (middle) and overlay (right).

2.3. Conclusion

We have described a modular solid-phase synthesis method, which, when combined with an established DPPA-mediated macrocyclization step, afforded cyclic polyamides in a high-yielding and time-efficient manner. Using this method, we have overcome previous limitations and synthesized both cyclic and hairpin polyamides that start with an imidazole unit. The binding affinities of all synthesized cycles have been assessed by DNA thermal denaturation assays and compare favorably to hairpin polyamides that bind their match DNA sequences at subnanomolar concentrations. Furthermore, the protection strategy of our method allows for selective modification of the GABA turn units, which we have used to rapidly generate a focused library of compounds. The cytotoxicity and uptake analysis of the cyclic polyamides revealed unexpected properties that further highlight the need for an efficient method to synthesize structural variants of cyclic polyamides for future studies.

2.4 Materials and Methods

Materials

2-Chlorotrityl chloride (2-Cl-Trt-Cl) resin was purchased from Bachem. FmocPyOH and FmocImOH monomers were purchased from Wako. PyBOP was purchased from NovaBioChem. Boc- β -Dab(Fmoc)-OH was purchased from Peptides International. All DNA oligomers were purchased HPLC purified from Integrated DNA Technologies. Cell culture media was purchased from Gibco. Fetal bovine serum was purchased from Omega Scientific.

Methods

Microwave-assisted coupling reactions were conducted on a Biotage Initiator Eight synthesizer. Polyamide concentrations were measured in 20% MeCN in 0.1% (v/v) aqueous TFA using an approximated extinction coefficient of $69\,200\text{ M}^{-1}\text{ cm}^{-1}$ at λ_{max} near 310 nm, unless otherwise specified.^{32, 36}

I. Monomer Loading onto 2-Cl-Trt Resin

Prior to manual microwave-assisted synthesis, 2-Cl-Trt-Cl resin (1.0 g, 1.59 mmol/g), was first loaded by mixing with 576 mg (1.59 mmol, 1 eq.) of FmocPyOH monomer, followed by addition of 6 mL dimethylformamide (DMF) and 1.38 mL diisopropylethylamine (DIEA) (7.59 mmol, 5 eq.). The suspended mixture was stirred for 18 h, then capped by addition of 1 mL methanol (MeOH) and stirred for 1 h. The orange-colored, loaded resin was then collected on a fritted peptide synthesis vessel, washed with DMF (2x), MeOH (2x), DMF (2x), MeOH (2x), and diethylether (Et₂O). [Owing to the sensitivity of the 2-Cl-Trt resin towards hydrolysis/methanolysis, this final Et₂O wash was found to be essential and all loaded resin was sealed and stored at -20 °C.] The loading efficiency was quantitated via the Fmoc test, and

confirmed by measuring the mass of the dried resin. Typical monomer loading was calculated to be 0.4–0.8 mmol/g.

II. Microwave-Assisted Solid-Phase Synthesis (18–24)

All solid-phase polyamide coupling reactions were performed manually on a Biotage Initiator Eight microwave synthesizer on a 200–500 mg scale of loaded resin. Prior to each monomer coupling reaction, the N-terminal Fmoc group was first removed in a piperidine solution. The Fmoc deprotections were performed in a fritted peptide synthesis vessel at room temperature, and the specific conditions for each N-terminal monomer are as follows:

N-Fmoc-Pyrrole / Imidazole: (a) swell resin in DCM; (b) wash with DMF; (c) add 50% piperidine in DMF; (d) shake suspension for 10 min; (e) wash with DMF; (f) repeat steps **a-e** twice.

N-Fmoc-GABA / β -Alanine: (a) swell resin in DCM; (b) wash with DMF; (c) add 50% piperidine in DMF; (d) shake suspension for 5 min; (e) wash with DMF; (f) repeat steps **a-e** once.

Following Fmoc removal, the resin was de-swelled in MeOH, washed with Et₂O, dried *in vacuo*, and transferred to a microwave synthesis vessel as a dry powder. The corresponding monomer acid (3 eq.) was activated with PyBOP (3 eq.) and DIEA (6 eq.) in DMF (0.3 M concentration of monomer), and added to the resin. The coupling reactions were then set up in the microwave reactor at 50 °C for the time durations described in **Table 1**. After the listed microwave-assisted coupling times, the reaction mixture was filtered into a peptide synthesis vessel, and the collected resin was washed with DMF (3x), MeOH (3x), Et₂O, and dried *in*

vacuo. To ensure completion of each deprotection and coupling step, analytical HPLC spectra were taken by cleaving a small resin sample in 30% hexafluoroisopropanol (HFIP) in DCM.

The polyamide core was synthesized on 2-Cl-Trt resin in an iterative manner by repeating the deprotection-coupling procedures described above using the corresponding monomeric units. Upon completion of the sequence, 100–200 mg of the resin was suspended in 1 mL 30% HFIP in DCM and stirred for 1 h to yield the crude N-terminal Fmoc-protected polyamide intermediate. The reaction mixture was then run through a cotton filter to remove the resin, and the filtrate was concentrated *in vacuo*. The residual oil was resuspended in 5 mL of a 1:1 MeOH:DCM mixture, and reconcentrated *in vacuo* to give an off-white / beige solid. To remove the N-terminal Fmoc group, the solid was redissolved in 800 μ L DMF, followed by addition of 200 μ L piperidine, and the solution was stirred for 30 min. Upon confirmation of complete deprotection by analytical HPLC, the solution was added to 4 mL 30% MeCN in 0.1% aqueous TFA. The precipitated 9-methylene fluorene side product was then removed by centrifugation, and washed twice with 2 mL 30% MeCN in 0.1% aqueous TFA. The combined aqueous solution was purified by reverse-phase HPLC and lyophilized to dryness to yield pre-cyclic polyamide intermediates **18–24**. All dried samples of **18–24** were stored at -20 °C prior to DPPA-mediated macrocyclization.

Synthetic yields and MALDI-TOF characterization data for **18–24** are summarized below:

(**18**): 12.6 μ mol recovered (38.0 μ mol theoretical, 33% yield). MALDI-TOF $[M + H]^+$ calcd for $C_{70}H_{77}N_{22}O_{15}^+ = 1465.4$, observed = 1465.9.

(**19**): 15.2 μ mol recovered (38.0 μ mol theoretical, 40% yield). MALDI-TOF $[M + H]^+$ calcd for $C_{62}H_{70}N_{21}O_{13}^+ = 1316.5$, observed = 1316.9.

(20): 12.8 μmol recovered (38 μmol theoretical, 34% yield). MALDI-TOF $[\text{M} + \text{Na}]^+$ calcd for $\text{C}_{67}\text{H}_{79}\text{N}_{22}\text{NaO}_{15}^+ = 1453.6$, observed = 1453.9.

(21): 15.1 μmol recovered (49 μmol theoretical, 31% yield). MALDI-TOF $[\text{M} + \text{H}]^+$ calcd for $\text{C}_{69}\text{H}_{76}\text{N}_{23}\text{O}_{15}^+ = 1466.5$, observed = 1466.9.

(22): 17.2 μmol recovered (51 μmol theoretical, 34% yield). MALDI-TOF $[\text{M} + \text{H}]^+$ calcd for $\text{C}_{61}\text{H}_{69}\text{N}_{22}\text{O}_{13}^+ = 1317.5$, observed = 1317.2.

(23): 16.2 μmol recovered (51 μmol theoretical, 32% yield). MALDI-TOF $[\text{M} + \text{Na}]^+$ calcd for $\text{C}_{66}\text{H}_{77}\text{N}_{23}\text{NaO}_{15}^+ = 1454.5$, observed = 1455.0.

(24): 8.2 μmol recovered (25 μmol theoretical, 33% yield). MALDI-TOF $[\text{M} + \text{Na}]^+$ calcd for $\text{C}_{66}\text{H}_{78}\text{N}_{23}\text{NaO}_{15}^+ = 1454.5$, observed = 1454.9.

III. DPPA-mediated Macrocyclization (1-7)

The macrocyclization reactions were run on a 2 μmol to 16 μmol scale. Intermediates **18-24** were first dissolved in DMF (0.25 mM) in a round-bottom flask equipped with a magnetic stir bar, followed by addition of DIEA (200 eq.), and purged with argon for 15 min. Diphenylphosphoryl azide (DPPA) (50 eq.) was then added to the reaction mixture in a dropwise manner, while rapidly stirring. Upon full addition of the DPPA, the solution was allowed to react and stirred at room temperature for 16–20 h. After confirmation of reaction completion by analytical HPLC, the reaction mixture was concentrated *in vacuo*, and the resulting oil residue was dissolved in 3 mL MeCN and transferred to a 15 mL Falcon Tube. The MeCN was then removed with air flow and 3 mL 0.1% aqueous TFA was added to the remaining oil layer to yield an off-white suspension, which was isolated via centrifugation and lyophilized to dryness.

For reactions starting with **18**, **19**, **21**, and **22**, the lyophilized residue was submitted to 1 mL 10% trifluoromethanesulfonic acid (TFMSA) in TFA, stirred for 5 min, frozen in LN2, and thawed by layering 1 mL DMF. For reactions starting with **20**, **23**, and **24**, the lyophilized residue was submitted to 1 mL neat TFA, stirred for 15 min, frozen in LN2, and thawed by layering 1 mL DMF. All the thawed solutions were then diluted with 6 mL 0.1% aqueous TFA, purified by reverse-phase HPLC and lyophilized to dryness to yield cyclic polyamides **1–7**.

Synthetic yields and MALDI-TOF characterization data for **1–7** are summarized below:

(1): 4.5 μmol recovered (12.9 μmol theoretical, 35% yield). MALDI-TOF $[\text{M} + \text{H}]^+$ calcd for $\text{C}_{54}\text{H}_{63}\text{N}_{22}\text{O}_{10}^+ = 1179.5$, observed = 1179.9.

(2): 0.84 μmol recovered (2.0 μmol theoretical, 42% yield). MALDI-TOF $[\text{M} + \text{H}]^+$ calcd for $\text{C}_{54}\text{H}_{62}\text{N}_{21}\text{O}_{10}^+ = 1164.5$, observed = 1164.6.

(3): 3.2 μmol recovered (6.7 μmol theoretical, 47% yield). MALDI-TOF $[\text{M} + \text{H}]^+$ calcd for $\text{C}_{62}\text{H}_{69}\text{N}_{22}\text{O}_{12}^+ = 1313.6$, observed = 1314.0.

(4): 3.1 μmol recovered (8.0 μmol theoretical, 39% yield). MALDI-TOF $[\text{M} + \text{H}]^+$ calcd for $\text{C}_{53}\text{H}_{62}\text{N}_{23}\text{O}_{10}^+ = 1180.5$, observed = 1180.9.

(5): 0.96 μmol recovered (2.0 μmol theoretical, 48% yield). MALDI-TOF $[\text{M} + \text{H}]^+$ calcd for $\text{C}_{53}\text{H}_{61}\text{N}_{22}\text{O}_{10}^+ = 1165.5$, observed = 1165.5.

(6): 3.7 μmol recovered (10.0 μmol theoretical, 37% yield). MALDI-TOF $[\text{M} + \text{H}]^+$ calcd for $\text{C}_{61}\text{H}_{68}\text{N}_{23}\text{O}_{12}^+ = 1314.5$, observed = 1314.5.

(7): 2.2 μmol recovered (5.7 μmol theoretical, 38% yield). MALDI-TOF $[\text{M} + \text{H}]^+$ calcd for $\text{C}_{61}\text{H}_{68}\text{N}_{23}\text{O}_{12}^+ = 1314.5$, observed = 1314.8.

IV. Selective Conjugation of Benzoic Acid Derivatives (9–11)

A solution of benzoic acid (3.0 mg, 0.025 mmol, 25 eq.) and PyBOP (13 mg, 0.025 mmol, 25 eq.) in DMF (0.5 mL) and DIEA (44 μ L, 0.25 mmol, 250 eq.) was stirred at room temperature for 10 min. The activated solution was then added to **3** (1.0 μ mol) and stirred for 3 h. After confirmation of complete reaction by analytical HPLC, 12 mL cold Et₂O was added to the reaction mixture and cooled at -20°C for 16 h. The precipitate was then isolated by centrifugation and allowed to air dry. The resulting residue was submitted to 1 mL 10% trifluoromethanesulfonic acid (TFMSA) in TFA, stirred for 5 min, frozen in LN₂, and thawed by layering 1 mL DMF. The thawed solution was then diluted with 6 mL 0.1% aqueous TFA, purified by reverse-phase HPLC and lyophilized to dryness to yield cyclic polyamides **9** (684 nmol, 68% yield). Using the same procedure described above, starting with **6** (1.60 μ mol) and **7** (750 nmol), yielded mono-benzoyl substituted cyclic polyamides **10** (1.05 μ mol, 67% yield) and **11** (367 nmol, 49% yield), respectively.

(9): MALDI-TOF $[M + H]^+$ calcd for C₆₁H₆₇N₂₂O₁₁⁺ = 1283.5, observed = 1284.1.

(10): MALDI-TOF $[M + H]^+$ calcd for C₆₀H₆₆N₂₃O₁₁⁺ = 1284.5, observed = 1284.5.

(11): MALDI-TOF $[M + H]^+$ calcd for C₆₀H₆₆N₂₃O₁₁⁺ = 1284.5, observed = 1284.9.

V. Synthesis of Cyclic Polyamide-Fluorescein Conjugates (12–14)

A solution of fluorescein isothiocyanate (FITC) (2.7 mg, 7.0 μ mol, 25 eq.) in DMF (0.2 mL) and DIEA (12 μ L, 0.07 mmol, 250 eq.) was added to **3** (0.28 μ mol) and stirred for 2 h. After confirmation of complete reaction by analytical HPLC, 12 mL cold Et₂O was added to the reaction mixture and cooled at -20 °C for 16 h. The precipitate was then isolated by centrifugation and allowed to air dry. The resulting residue was submitted to 1 mL 10%

trifluoromethanesulfonic acid (TFMSA) in TFA, stirred for 5 min, frozen in LN₂, and thawed by layering 1 mL DMF. The thawed solution was then diluted with 6 mL 0.1% aqueous TFA, purified by reverse-phase HPLC and lyophilized to dryness to yield cyclic polyamide **12** (65 nmol, 23% yield). Using the same procedure described above, starting with **6** (0.40 μ mol) and **7** (0.40 μ mol), yielded cyclic polyamide-fluorescein conjugated **13** (345 nmol, 86% yield) and **14** (118 nmol, 29% yield), respectively.

(**12**): ESI-MS $[M + H]^+$ calcd for $C_{75}H_{74}N_{23}O_{15}S^+$ = 1568.6, observed = 1568.3.

(**13**): ESI-MS $[M + H]^+$ calcd for $C_{74}H_{73}N_{24}O_{15}S^+$ = 1569.5, observed = 1569.2.

(**14**): ESI-MS $[M + H]^+$ calcd for $C_{74}H_{73}N_{24}O_{15}S^+$ = 1569.5, observed = 1569.3.

VI. Synthesis of Cyclic Polyamide Targeted to 5'-WCGWGW-3' Sequence (**8**)

2-Cl-Trt-Cl resin (200 mg, 1.59 mmol/g) was first loaded with FmocPyImOH dimer (96 mg, 0.20 mmol), which was obtained from published procedures.¹³ Experimental details were analogous to the monomer loading protocol reported above. The obtained Fmoc-Py-Im-(2-Cl-Trt) resin (265 mg, 0.59 mmol/g) was subjected to the previously described microwave-assisted solid-phase synthesis conditions to build the corresponding polyamide sequence. A *quarter* of the resin (0.15 μ mol theoretical) was then cleaved and purified by reverse-phase HPLC to yield pre-cyclic polyamide intermediate **25** as an off-white powder (13.3 μ mol, 34% yield). The isolated **25** (2.0 μ mol) was subjected to DPPA-mediated macrocyclization conditions analogous to that for compounds **1–7**, with the Cbz groups removed with 10% TFMSA in TFA, and purified by reverse-phase HPLC to afford cyclic polyamide **8** (773 nmol, 39% yield).

(**25**): MALDI-TOF $[M - CO_2 + H]^+$ calcd for $C_{65}H_{675}N_{22}O_{13}^+$ = 1371.6, observed = 1371.7.

(**8**): MALDI-TOF $[M + H]^+$ calcd for $C_{61}H_{671}N_{22}O_{11}^+$ = 1129.5, observed = 1130.0

VII. Synthesis of Hairpin Polyamide Targeted to 5'-WCGWGW-3' Sequence (17)

Fmoc-Py-Im-(2-Cl-Trt) resin, obtained via the same procedure as for **8**, was subjected to the previously described microwave-assisted solid-phase synthesis conditions to build the corresponding polyamide sequence with an N-terminal PyImOH cap. The resin (70 mg, 0.039 mmol) was then suspended in 2 mL 30% HFIP in DCM, stirred for 1 h, filtered, washed, and concentrated to afford the crude C-terminal free acid. The residue was then dissolved in DMF (1.8 mL) and added dropwise to a pre-activated solution of 3,3'-diamino-N-methyldipropylamine (252 μ L, 1.56 mmol, 40 eq.) and PyBOP (40 mg, 0.078 mmol, 2 eq.) in DMF (6.0 mL). After stirring for 1 h and confirmation of complete conjugation by HPLC, the crude product was isolated by Et₂O precipitation, air dried, redissolved in 8 mL 15% AcN : 0.1% aqueous TFA, and purified by reverse-phase HPLC to yield polyamide intermediate **26** as an off-white powder (11.8 μ mol, 30% yield).

The isolated **26** (3.1 μ mol) was dissolved in DMF (200 μ L) and added dropwise to a pre-activated solution of isophthalic acid (12 mg, 0.072 mmol) and PyBOP (5 mg, 9 μ mol) in DMF (800 μ L) and DIEA (13 μ L). After stirring for 1 h and confirmation of complete conjugation by HPLC, the reaction mixture was then precipitated in Et₂O, isolated by centrifugation, and air dried. The remaining residue was then subjected to 500 μ L neat TFA, stirred for 15 min, frozen in LN₂, thawed by addition of 1 mL DMF, diluted with 6 mL 0.1% aqueous TFA, and purified by reverse-phase HPLC to afford cyclic polyamide **8** (3.1 nmol, 86% yield). [Note: Extinction coefficient for compounds **26** and **17** were established as 40,000 M⁻¹ cm⁻¹ at λ_{max} = 302 nm.]

(**26**): MALDI-TOF [M + H]⁺ calcd for C₅₈H₇₉N₂₂O₁₁⁺ = 1259.6, observed = 1260.1.

(**17**): MALDI-TOF [M + H]⁺ calcd for C₆₁H₇₅N₂₂O₁₂⁺ = 1307.6, observed = 1307.8.

VIII. Thermal Denaturation Analysis

Melting temperature analysis was performed on a Varian Cary 100 spectrophotometer equipped with a thermo-controlled cell holder possessing a cell path length of 1 cm. A degassed aqueous solution of 10 mM sodium cacodylate, 10 mM KCl, 10 mM MgCl₂, and 5 mM CaCl₂ at pH 7.0 was used as analysis buffer. DNA duplexes and polyamides were mixed in 1:1 stoichiometry to a final concentration of 2 μ M for each experiment. Prior to analysis, samples were heated to 95 °C and cooled to a starting temperature of 25 °C with a heating rate of 5 °C / min for each ramp. Denaturation profiles were recorded at $\lambda = 260$ nm from 25 to 95 °C with a heating rate of 0.5 °C / min. The reported melting temperatures were defined as the maximum of the first derivative of the denaturation profile.

IX. Cell Culture

Cell lines were cultured at 37 °C under 5% CO₂ using standard cell culture and sterile techniques. Cell medium was supplemented with 10% fetal bovine serum. Ham's F-12K (Kaighn's) medium was used for A549 cells, and RPMI 1640 was used for T47D cells.

X. Confocal Microscopy

For each experiment, cells were plated in 200 μ L of the proper medium onto glass-bottom cell culture plates at a density of 1×10^5 (A549) cells/ mL, or 1.5×10^5 cells/ mL (T47D). Cells were grown for 24 h, and media was replaced with fresh media containing polyamide to give a final DMSO concentration of 0.1%. Next, cells were incubated for 16 h, followed by removal of media, washing, and addition of fresh media. Hoechst 33258 was added 2 h prior to imaging. Imaging was performed at the Caltech Beckman Imaging Center using a Zeiss LSM

510 Meta NLO 2-photon inverted laser scanning microscope equipped with a 40x oil-immersion objective lens. Polyamide–fluorescein conjugates **12–14** were imaged in multi-track mode using 488 nm laser excitation at 15% output with a pinhole of 375 μm and a standard fluorescein filter set. Hoechst was imaged using 800 nm two-photon excitation with an HFT KP680 dichroic and a 390- to 465-nm bandpass filter with a fully open pinhole. All images were analyzed using Zeiss LSM Zen software.

XI. Sulforhodamine B Cytotoxicity

For cytotoxicity assays, cell lines were plated in 96-well cell culture plates in 100 μL media at a density of 1×10^4 cells/mL (A549), or 5×10^4 cells/mL (T47D). IC_{50} values were determined using the sulforhodamine B (SRB) colorimetric assay as previously described.³⁹ Cells were grown for 24 h, before polyamides in 100 μL media were added in serial dilution, in quadruplicate for each concentration. After incubation for 72 h, cell media was replaced with 100 μL fresh media, and cells were allowed to recover for an additional 24 h. Cells were then fixed by adding 100 μL of 10% trichloroacetic acid directly to each well and stored at 4°C for 1 h, before being washed, dried, stained with 100 μL 0.057% SRB solution per well for 30 min, and washed and dried again as described. After solubilizing the bound dye with 200 μL of 10 mM Tris (pH 10.5) per well, absorbance at 490 nm was measured on a PerkinElmer Victor microplate reader. The data are charted as a percentage of untreated controls, corrected for background absorbance. IC_{50} is defined as the concentration that inhibits 50% of control cell growth. These values were determined by non-linear least-squares regression fit to $Y = A + (B - A)/(1 + 10^{((\text{Log EC}_{50} - X) \times H))}$, where $A = \text{max.}$, $B = \text{min.}$ and $H = \text{Hill Slope}$. All calculations were performed

using Prism 4 (GraphPad) software. Stated IC₅₀ values represent the mean and standard deviation of three independent biological replicates.

2.5 Acknowledgments

This work was supported by the National Institutes of Health (GM27681). BCL is grateful to the California Tobacco-Related Disease Research Program (18DT-0015) for a dissertation award. DCM is thankful to the National Institutes of Health for a predoctoral research training grant (5T32GM007616). The authors would like to thank Dr. Amanda E. Hargrove for helpful discussions, and Dr. Jordan L. Meier for assistance with molecular modeling.

2.6 References

- (1) Dervan, P. B. *Bioorg. Med. Chem.* **2001**, *9*, 2215–2235.
- (2) Trauger, J. W.; Baird, E. E.; Dervan, P. B. *Nature* **1996**, *382*, 559–561.
- (3) White, S.; Szewczyk, J. W.; Turner, J. M.; Baird, E. E.; Dervan, P. B. *Nature* **1998**, *391*, 468–470.
- (4) Kielkopf, C. L.; Baird, E. E.; Dervan, P. B.; Rees, D. C. *Nat. Struct. Biol.* **1998**, *5*, 104–109.
- (5) Kielkopf, C. L.; White, S.; Szewczyk, J. W.; Turner, J. M.; Baird, E. E.; Dervan, P. B.; Rees, D. C. *Science* **1998**, *282*, 111–115.
- (6) Mrksich, M.; Parks, M. E.; Dervan, P. B. *J. Am. Chem. Soc.* **1994**, *116*, 7983–7988.
- (7) Herman, D. M.; Baird, E. E.; Dervan, P. B. *J. Am. Chem. Soc.* **1998**, *120*, 1382–1391.
- (8) Hsu, C. F.; Phillips, J. W.; Trauger, J. W.; Farkas, M. E.; Belitsky, J. M.; Heckel, A.; Olenyuk, B. Z.; Puckett, J. W.; Wang, C. C. C.; Dervan, P. B. *Tetrahedron* **2007**, *63*, 6146–6151.
- (9) Best, T. B.; Edelson, B. S.; Nickols, N. G.; Dervan, P. B. *Proc. Natl. Acad. Sci. U.S.A.* **2003**, *100*, 12063–12068.
- (10) Dervan, P. B.; Edelson, B. S. *Curr. Opin. Struct. Biol.* **2003**, *13*, 284–299.
- (11) Hsu, C. F.; Dervan, P. B. *Bioorg. Med. Chem. Lett.* **2008**, *18*, 5851–5855.
- (12) Olenyuk, B. Z.; Zhang, G. J.; Klco, J. M.; Nickols, N. G.; Kaelin Jr., W. G.; Dervan, P. B. *Proc. Natl. Acad. Sci. U.S.A.* **2004**, *101*, 16768–16773.
- (13) Kageyama, Y.; Sugiyama, H.; Ayame, H.; Iwai, A.; Fujii, Y.; Huang, L. E.; Kizaka-Kondoh, S.; Hiraoka, M.; Kihara, K. *Acta Oncol.* **2006**, *45*, 317–324.

- (14) Nickols, N. G.; Jacobs, C. S.; Farkas, M. E.; Dervan, P. B. *ACS Chem. Biol.* **2007**, *2*, 561–571.
- (15) Nickols, N. G.; Dervan, P. B. *Proc. Natl. Acad. Sci. U.S.A.* **2007**, *104*, 10418–10423.
- (16) Matsuda, H.; Fukuda, N.; Ueno, T.; Tahira, Y.; Ayame, H.; Zhang, W.; Bando, T.; Sugiyama, H.; Saito, S.; Matsumoto, K.; et al. *J. Am. Soc. Nephrol.* **2006**, *17*, 422–432.
- (17) Raskatov, J. A.; Meier, J. L.; Puckett, J. W.; Yang, F.; Ramakrishnan, P.; Dervan, P. B. *Proc. Natl. Acad. Sci. U.S.A.* **2012**, *109*, 1023–1028.
- (18) Cho, J.; Parks, M. E.; Dervan, P. B. *Proc. Natl. Acad. Sci. USA* **1995**, *92*, 10389–10392.
- (19) Herman, D. M.; Turner, J. M.; Baird, E. E.; Dervan, P. B. *J. Am. Chem. Soc.* **1999**, *121*, 1121–1129.
- (20) Melander, C.; Herman, D. M.; Dervan, P. B. *Chem. Eur. J.* **2000**, *6*, 4487–4497.
- (21) Zhang, Q.; Dwyer, T. J.; Tsui, V.; Case, D. A.; Cho, J.; Dervan, P. B.; Wemmer, D. E. *J. Am. Chem. Soc.* **2004**, *126*, 7958–7966.
- (22) Chenoweth, D. M.; Harki, D. A.; Phillips, J. W.; Dose, C.; Dervan, P. B. *J. Am. Chem. Soc.* **2009**, *131*, 7182–7188.
- (23) Morinaga, H.; Bando, T.; Takagaki, T.; Yamamoto, M.; Hashiya, K.; Sugiyama, H. *J. Am. Chem. Soc.* **2011**, *133*, 18924–18930.
- (24) Meier, J. L.; Montgomery, D. C.; Dervan, P. B. *Nucleic Acids Res.* **2012**, *40*, 2345–2356.
- (25) Taleb, R. I.; Jaramillo, D.; Wheate, N. J.; Aldrich-Wright, J. R. *Chem. Eur. J.* **2007**, *13*, 3177–3186.
- (26) van Holst, M.; Le Pevelen, D.; Aldrich-Wright, J. R. *Eur. J. Inorg. Chem.* **2008**, *29*, 4608–4615.
- (27) Puckett, J. W.; Green, J. T.; Dervan, P. B. *Org. Lett.* **2012**, *14*, 2774–2777.

- (28) Weltzer, M. and Wemmer, D. E. *Org. Lett.* **2010**, *12*, 3488–3490.
- (29) Brady, S. F.; Varga, S. L.; Freidinger, R. M.; Schwenk, D. A.; Mendlowski, M.; Holly, F. W.; Veber, D. F. *J. Org. Chem.* **1979**, *44*, 3101–3105.
- (30) Boger, D. L. and Yohannes, D. *J. Org. Chem.* **1988**, *53*, 487–499.
- (31) Raskatov, J. A.; Hargrove, A. E.; So, A. Y. Dervan, P. B. *J. Am. Chem. Soc.* **2012**, *134*, 7995–7999.
- (32) Hargrove, A. E.; Raskatov, J. A.; Meier, J. L.; Montgomery, D. C.; Dervan, P. B. *J. Med. Chem.*, **2012**, *55*, 5425–5432.
- (33) Synold, T. W.; Xi, B.; Wu, J.; Yen, Y.; Li, B. C.; Yang, F.; Phillips, J. W.; Nickols, N. G.; Dervan, P. B. *Cancer Chemoth. Pharm.*, **2012**, *70*, 617–625.
- (34) Baird, E. E. and Dervan, P. B. *J. Am. Chem. Soc.* **1996**, *118*, 6141–6146.
- (35) Wurtz, N. R.; Turner, J. M.; Baird, E. E.; Dervan P. B. *Org. Lett.* **2001**, *3*, 1201–1203.
- (36) Trauger, J. W. and Dervan, P. B. *Methods Enzymol.* **2001**, *340*, 450–466.
- (37) Dose, C.; Farkas, M. E.; Chenoweth, D. M.; Dervan, P. B. *J. Am. Chem. Soc.* **2009**, *130*, 6859–6866.
- (38) Farkas, M. E.; Li, B. C.; Dose, C.; Dervan, P. B. *Bioorg. Med. Chem. Lett.* **2009**, *19*, 3919–3923.
- (39) Vichai, V. and Kirtikara, K. *Nat. Protoc.* **2006**, *1*, 1112–1116.

2.7 Experimental Data

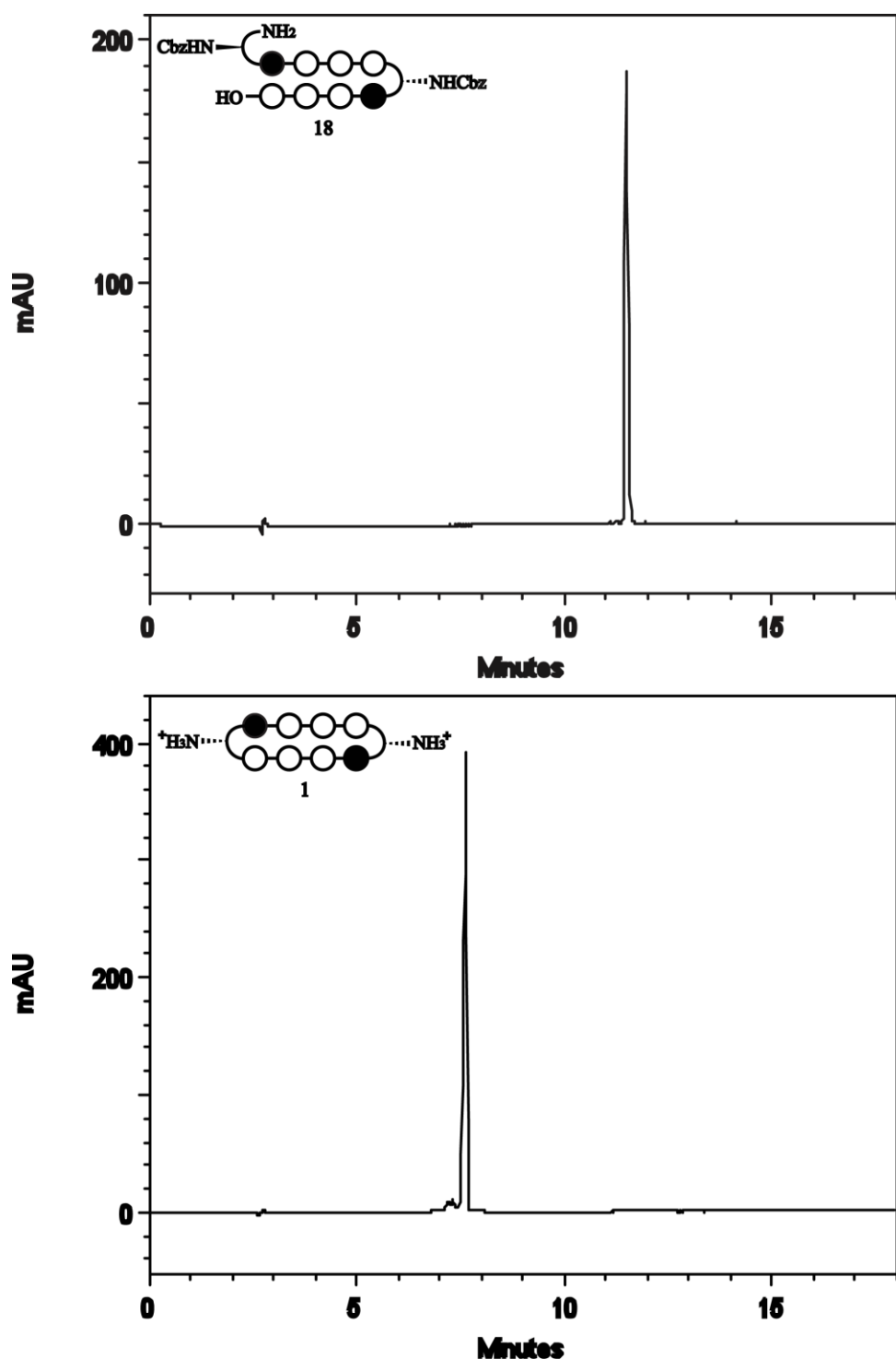


Figure 2.4 HPLC spectrum of **18** and **1**. Reverse-phase HPLC taken on Beckman Gold instrument equipped with a Phenomenex Gemini analytical column (250 × 4.6 mm, 5 μm) and a diode array detector, and the mobile phase consisted of a gradient of acetonitrile (MeCN) in 0.1% (v/v) aqueous TFA [10% MeCN, t = 0 → 30 s; 10% → 80% MeCN, t = 30 s → 18 min].

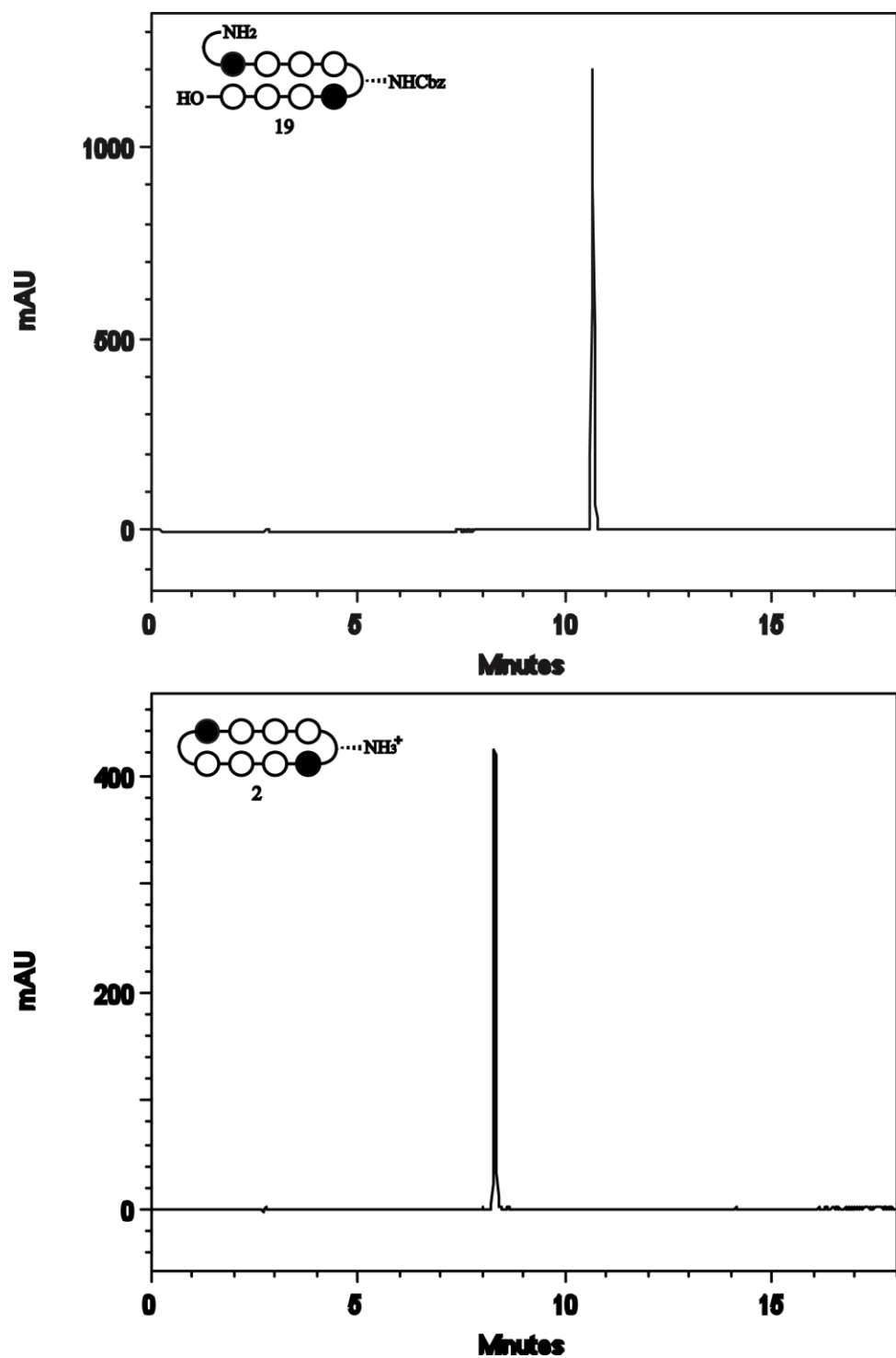


Figure 2.5 HPLC spectrum of **19** and **2**. Reverse-phase HPLC taken on Beckman Gold instrument equipped with a Phenomenex Gemini analytical column (250 × 4.6 mm, 5 μm) and a diode array detector, and the mobile phase consisted of a gradient of acetonitrile (MeCN) in 0.1% (v/v) aqueous TFA [10% MeCN, t = 0 → 30 s; 10% → 80% MeCN, t = 30 s → 18 min].

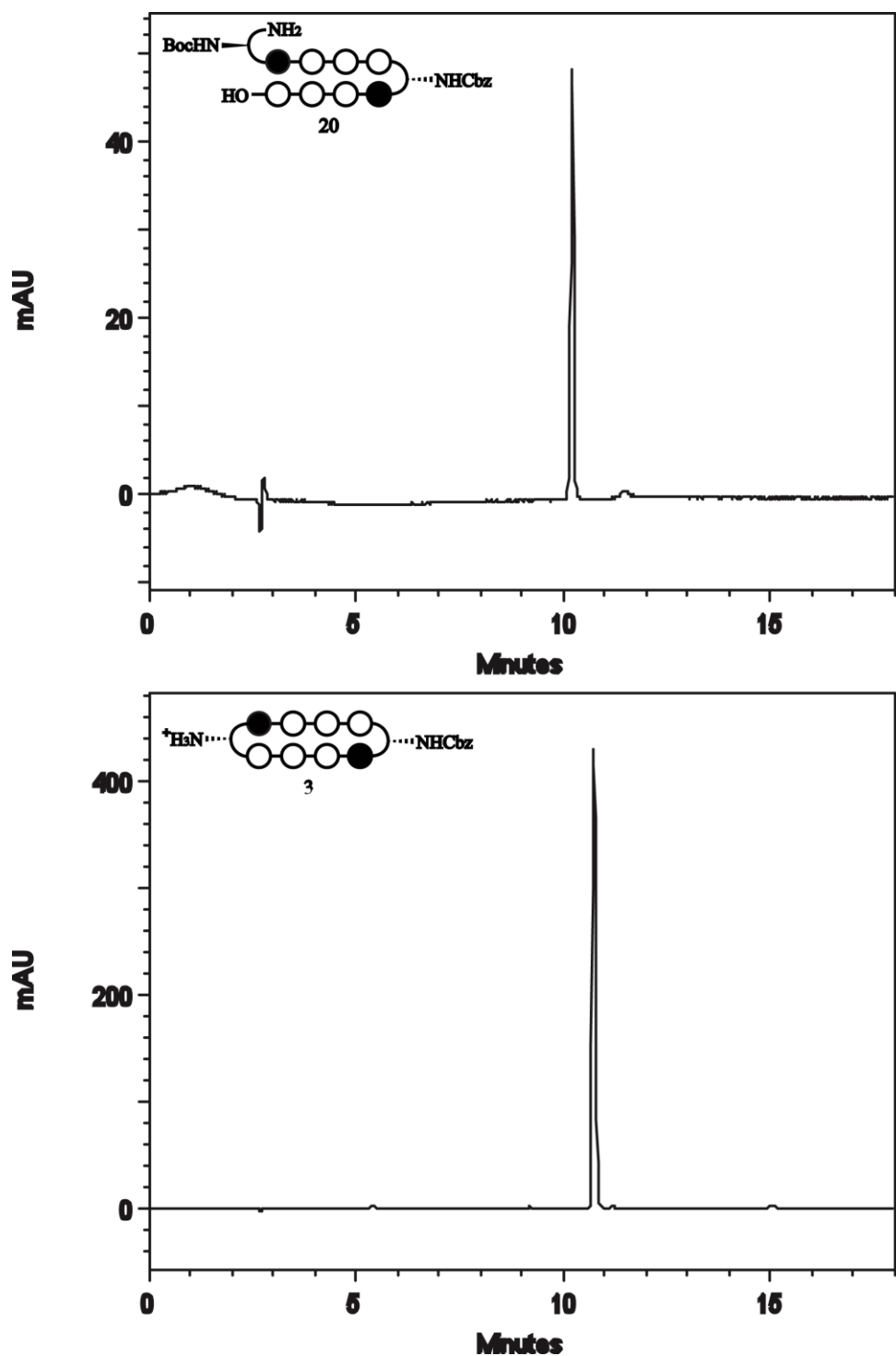


Figure 2.6 HPLC spectrum of **20** and **3**. Reverse-phase HPLC taken on Beckman Gold instrument equipped with a Phenomenex Gemini analytical column (250 × 4.6 mm, 5 μm) and a diode array detector, and the mobile phase consisted of a gradient of acetonitrile (MeCN) in 0.1% (v/v) aqueous TFA [10% MeCN, t = 0 → 30 s; 10% → 80% MeCN, t = 30 s → 18 min].

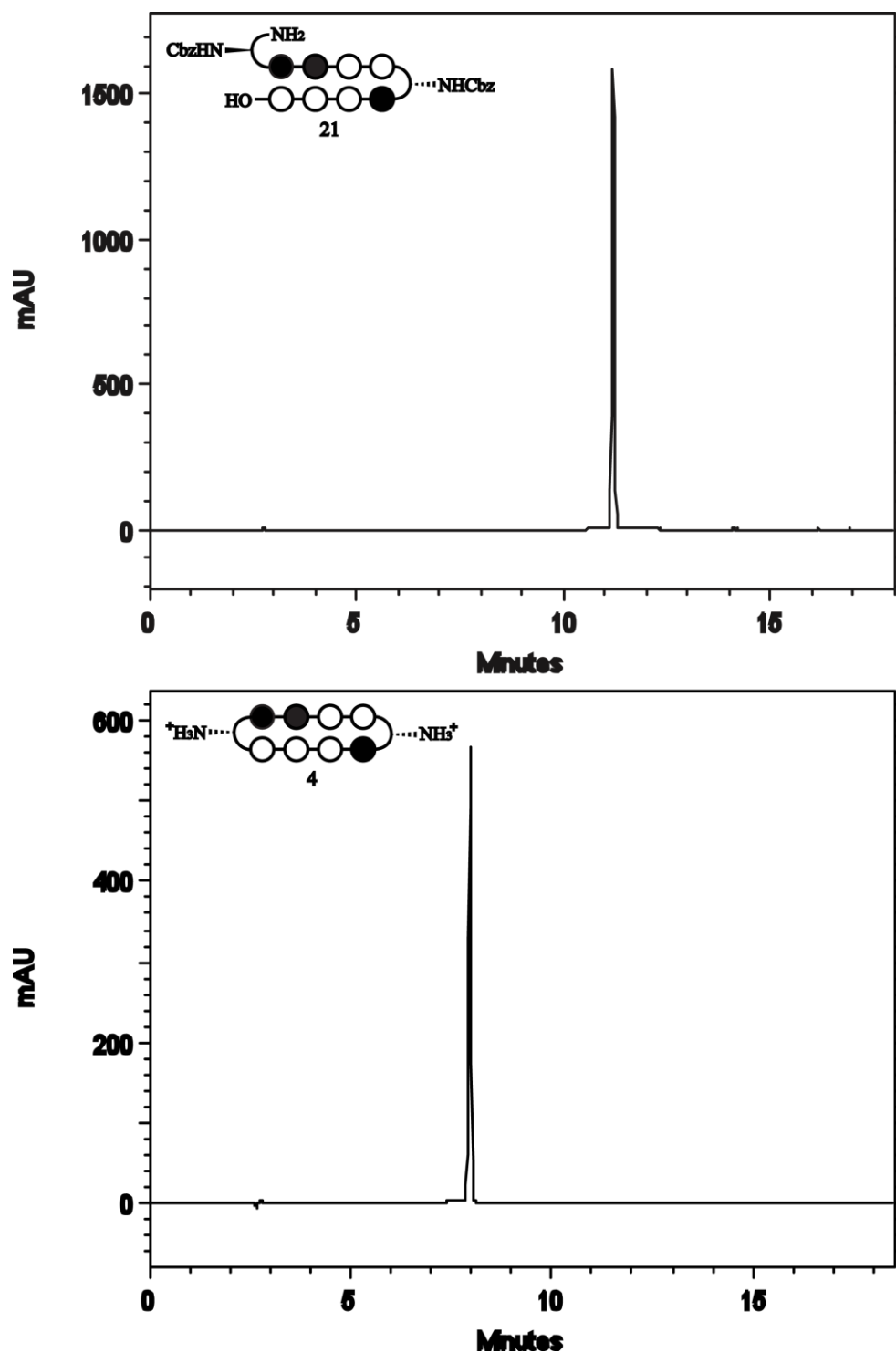


Figure 2.7 HPLC spectrum of **21** and **4**. Reverse-phase HPLC taken on Beckman Gold instrument equipped with a Phenomenex Gemini analytical column (250 × 4.6 mm, 5 μm) and a diode array detector, and the mobile phase consisted of a gradient of acetonitrile (MeCN) in 0.1% (v/v) aqueous TFA [10% MeCN, t = 0 → 30 s; 10% → 80% MeCN, t = 30 s → 18 min].

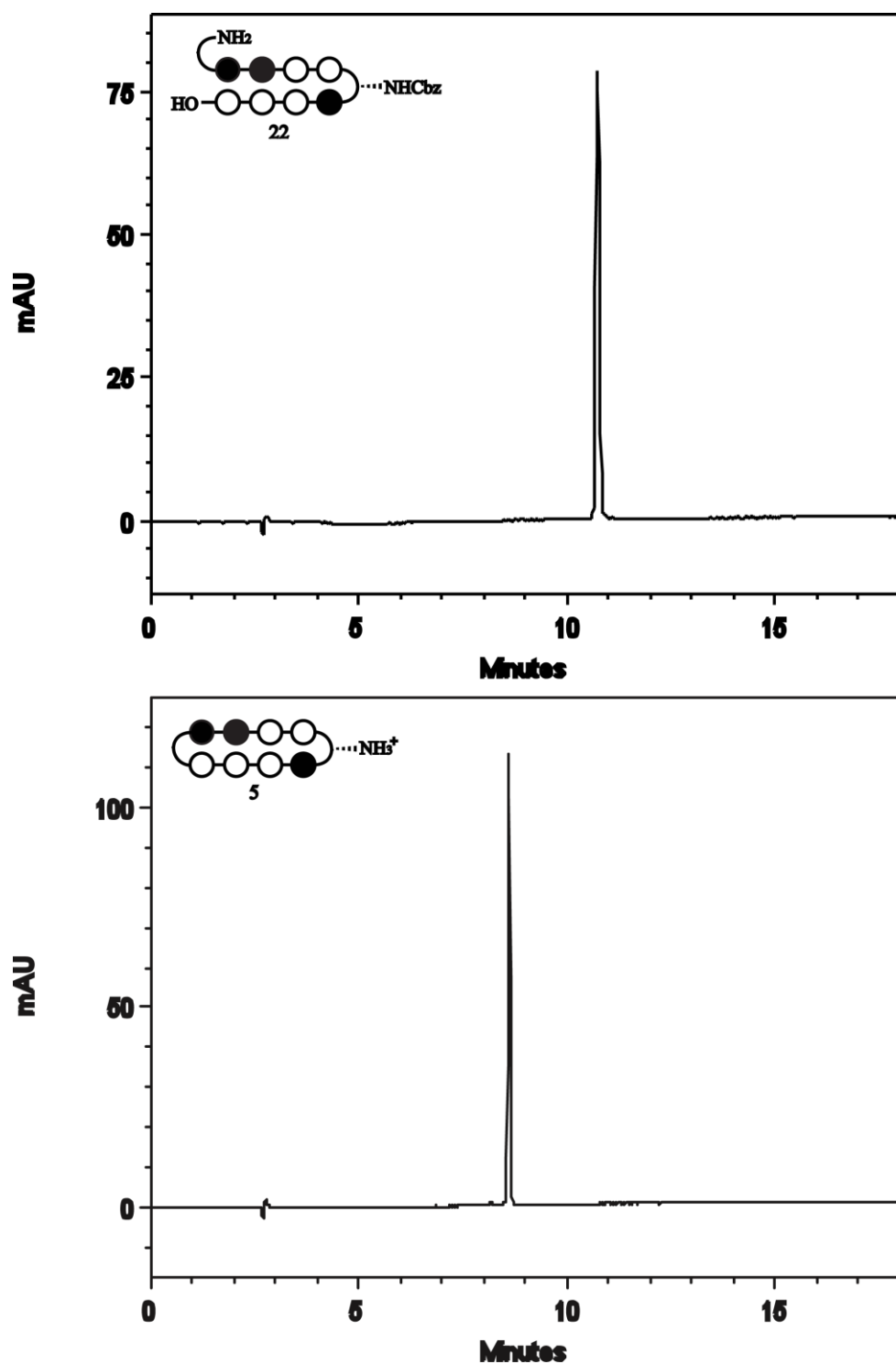


Figure 2.8 HPLC spectrum of **22** and **5**. Reverse-phase HPLC taken on Beckman Gold instrument equipped with a Phenomenex Gemini analytical column (250 × 4.6 mm, 5 μm) and a diode array detector, and the mobile phase consisted of a gradient of acetonitrile (MeCN) in 0.1% (v/v) aqueous TFA [10% MeCN, t = 0 → 30 s; 10% → 80% MeCN, t = 30 s → 18 min].

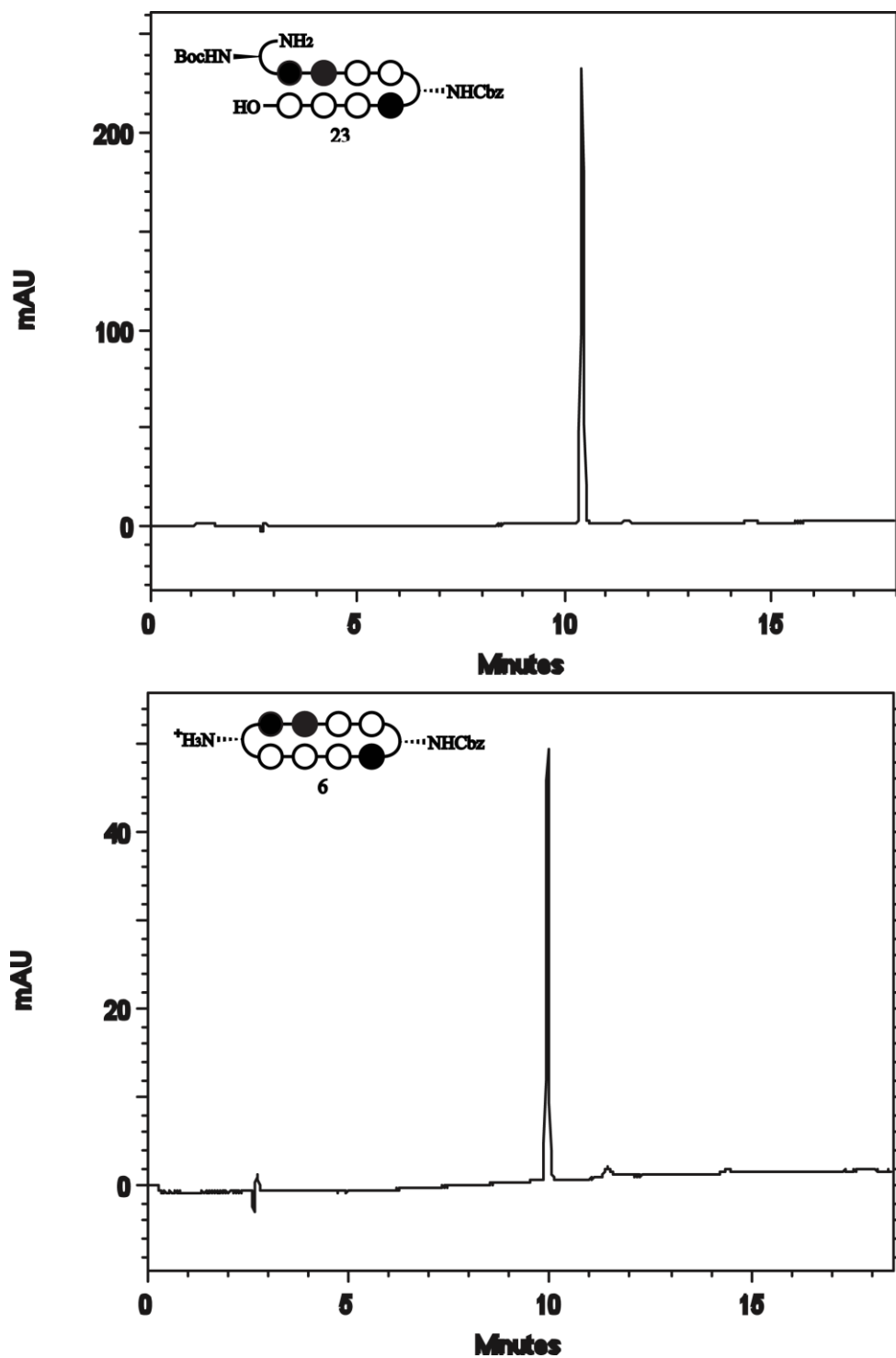


Figure 2.9 HPLC spectrum of **23** and **6**. Reverse-phase HPLC taken on Beckman Gold instrument equipped with a Phenomenex Gemini analytical column (250 × 4.6 mm, 5 μm) and a diode array detector, and the mobile phase consisted of a gradient of acetonitrile (MeCN) in 0.1% (v/v) aqueous TFA [10% MeCN, t = 0 → 30 s; 10% → 80% MeCN, t = 30 s → 18 min].

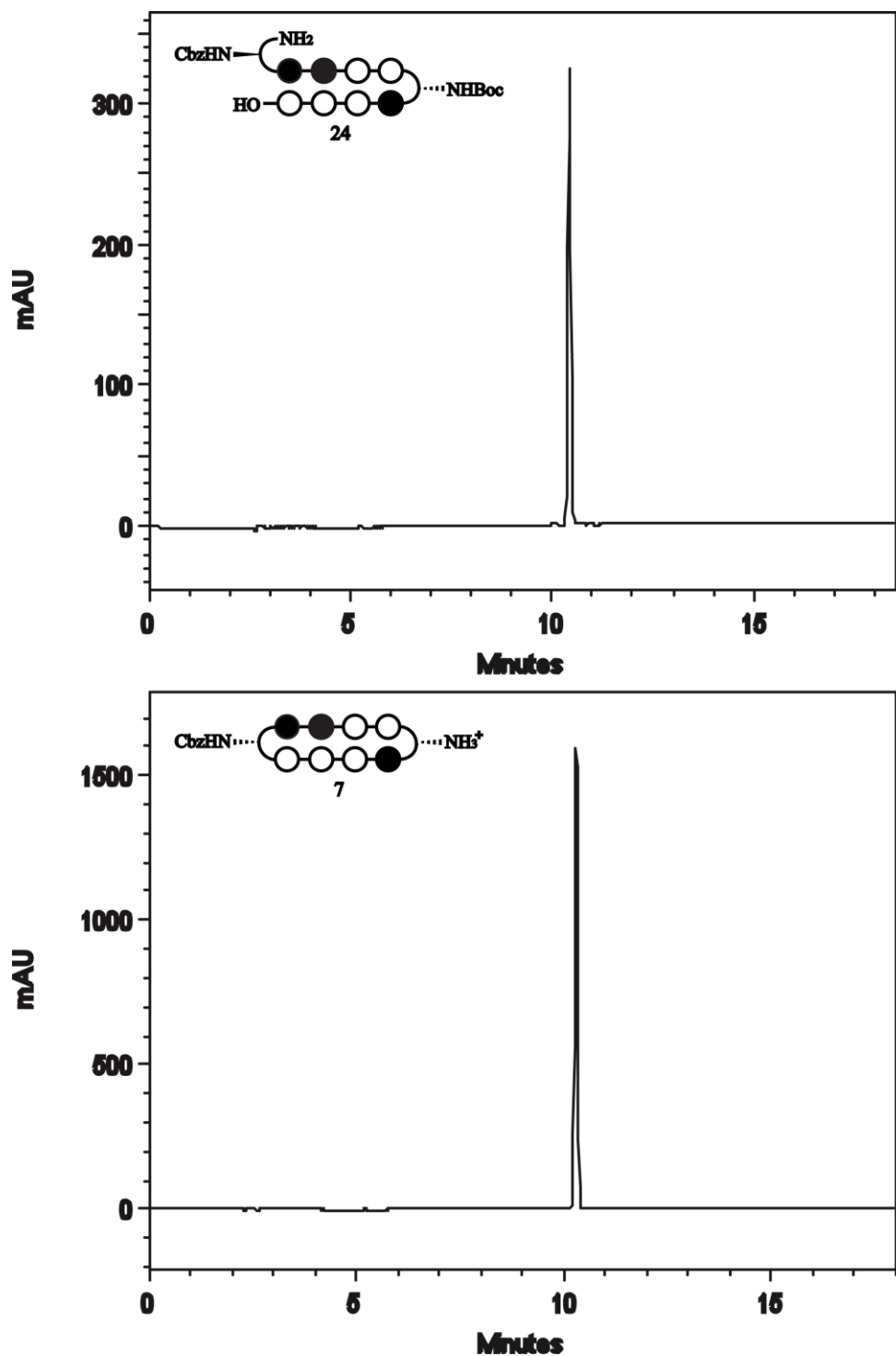


Figure 2.10 HPLC spectrum of **24** and **7**. Reverse-phase HPLC taken on Beckman Gold instrument equipped with a Phenomenex Gemini analytical column (250 × 4.6 mm, 5 μm) and a diode array detector, and the mobile phase consisted of a gradient of acetonitrile (MeCN) in 0.1% (v/v) aqueous TFA [10% MeCN, t = 0 → 30 s; 10% → 80% MeCN, t = 30 s → 18 min].

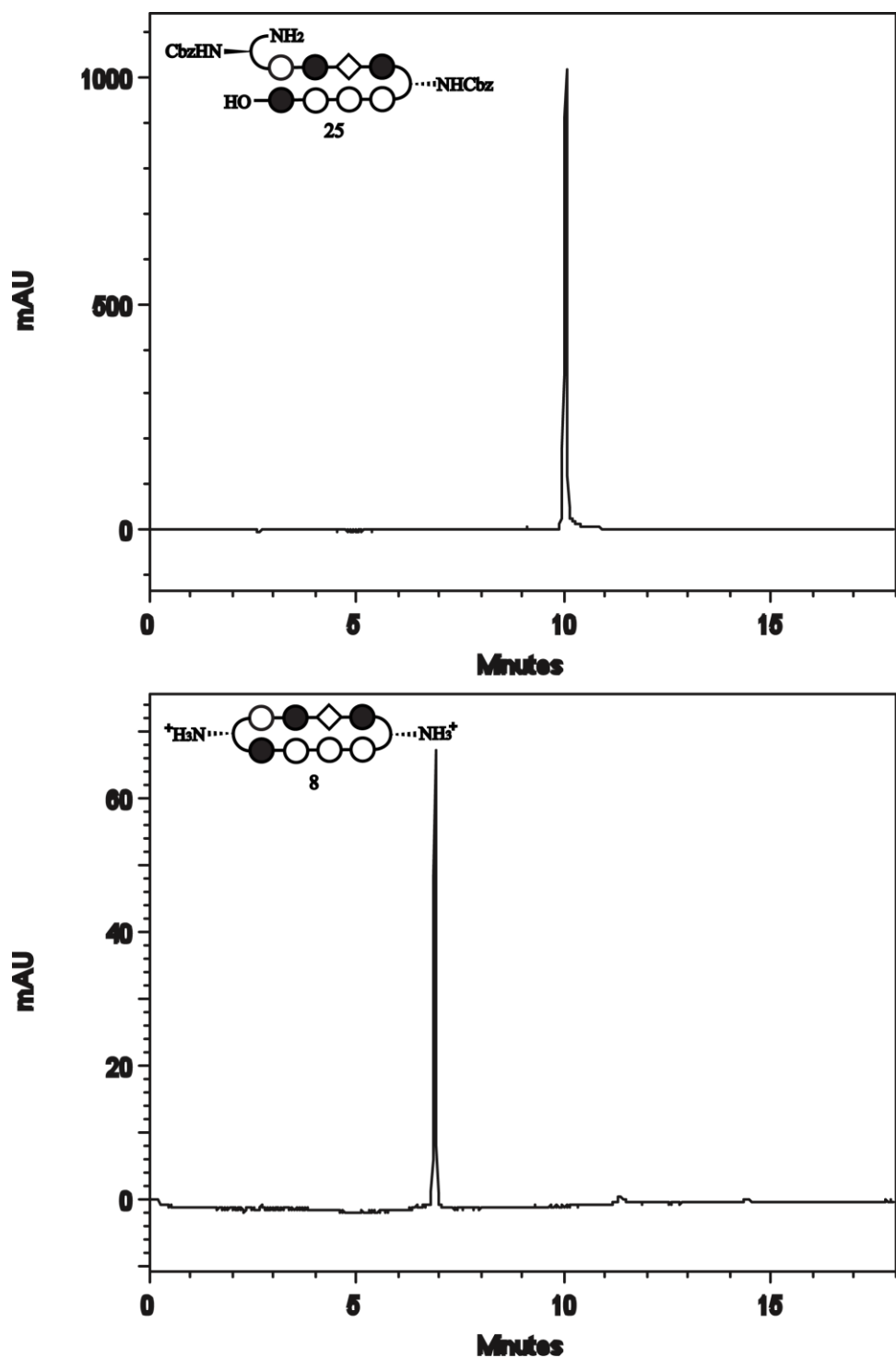


Figure 2.11 HPLC spectrum of **25** and **8**. Reverse-phase HPLC taken on Beckman Gold instrument equipped with a Phenomenex Gemini analytical column (250 × 4.6 mm, 5 μm) and a diode array detector, and the mobile phase consisted of a gradient of acetonitrile (MeCN) in 0.1% (v/v) aqueous TFA [10% MeCN, t = 0 → 30 s; 10% → 80% MeCN, t = 30 s → 18 min].

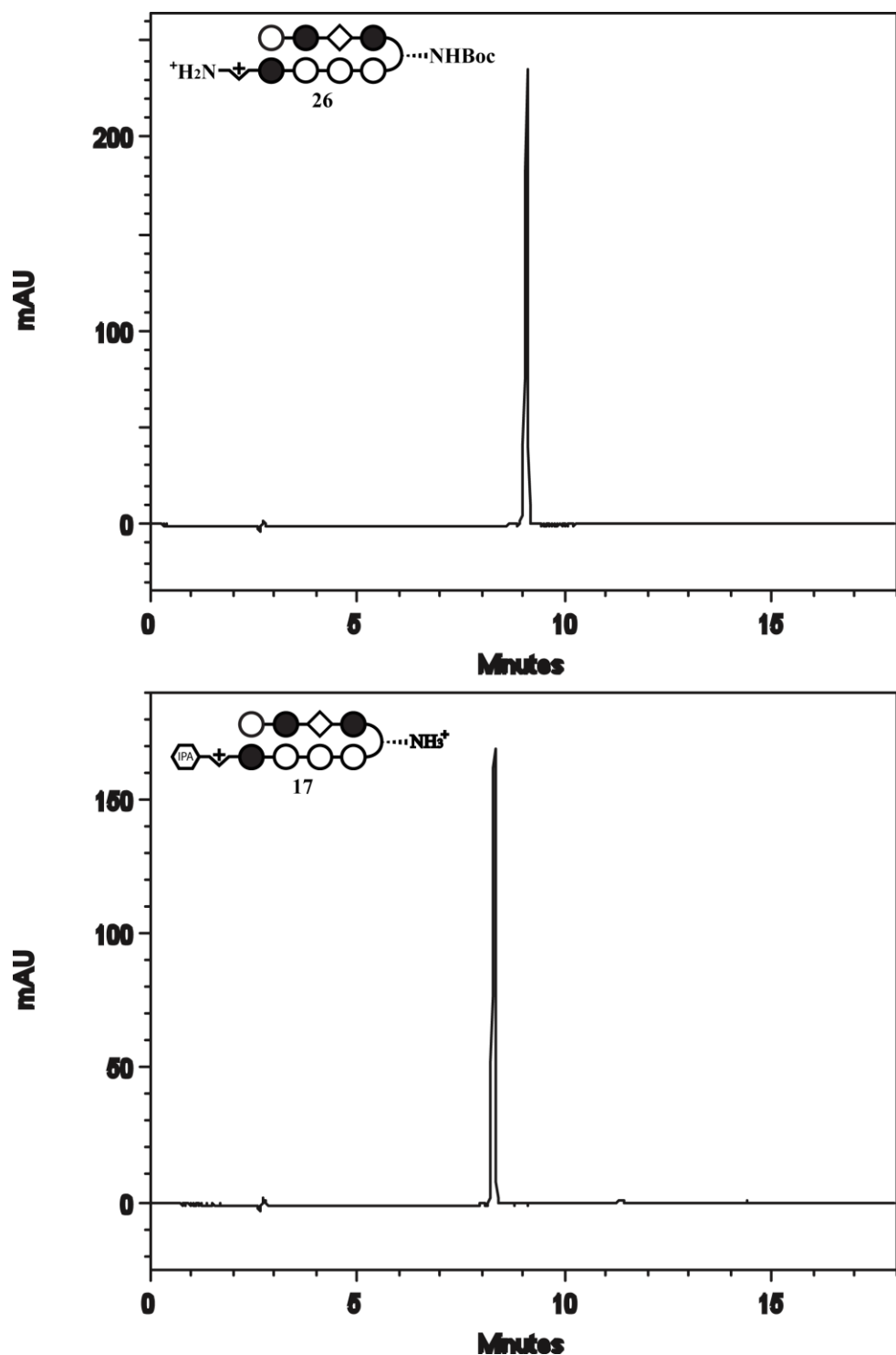


Figure 2.12 HPLC spectrum of **26** and **17**. Reverse-phase HPLC taken on Beckman Gold instrument equipped with a Phenomenex Gemini analytical column (250 × 4.6 mm, 5 μm) and a diode array detector, and the mobile phase consisted of a gradient of acetonitrile (MeCN) in 0.1% (v/v) aqueous TFA [10% MeCN, $t = 0 \rightarrow 30$ s; 10% \rightarrow 80% MeCN, $t = 30$ s \rightarrow 18 min].

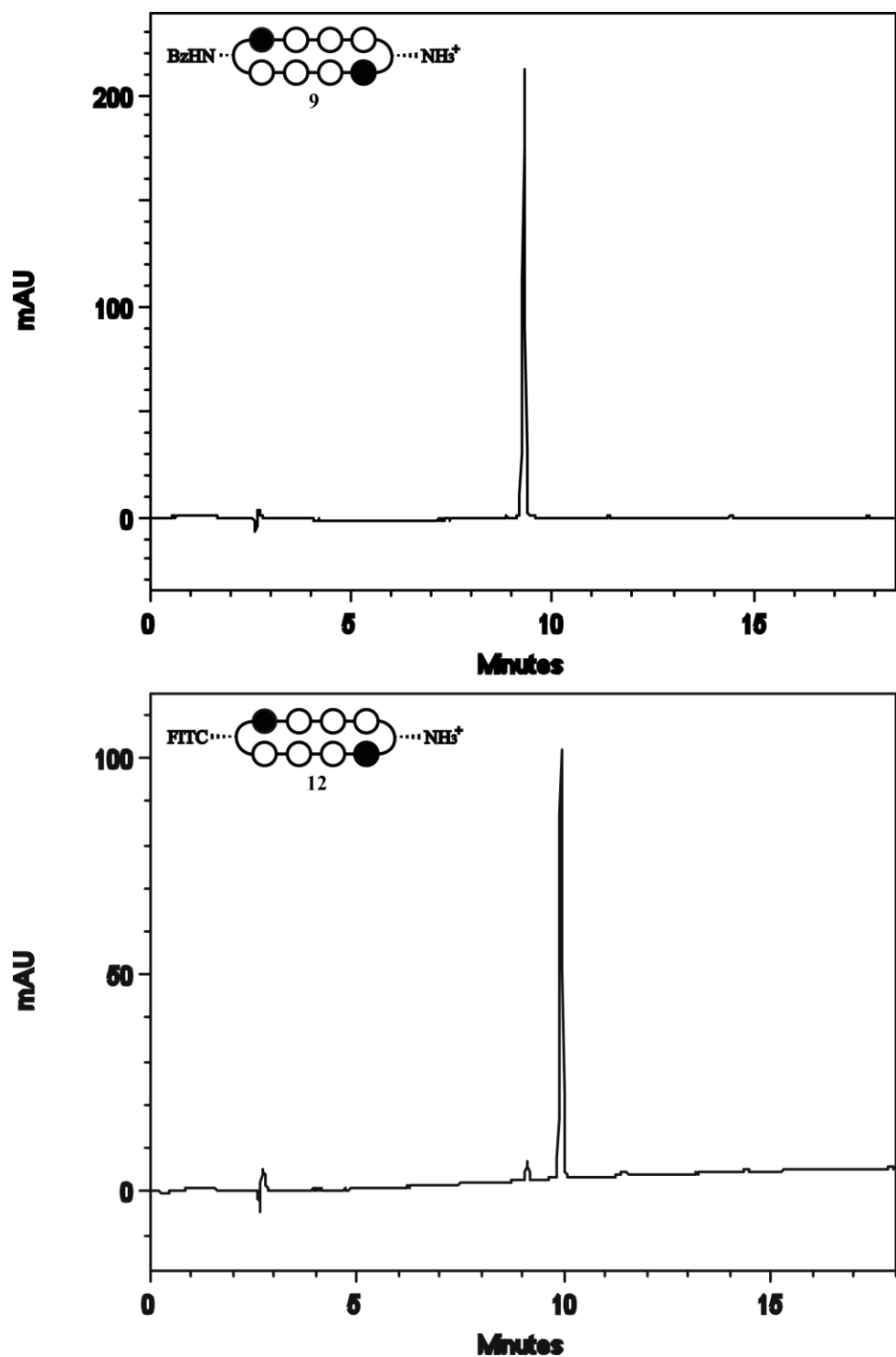


Figure 2.13 HPLC spectrum of 9 and 12. Reverse-phase HPLC taken on Beckman Gold instrument equipped with a Phenomenex Gemini analytical column (250 × 4.6 mm, 5 μm) and a diode array detector, and the mobile phase consisted of a gradient of acetonitrile (MeCN) in 0.1% (v/v) aqueous TFA [10% MeCN, t = 0 → 30 s; 10% → 80% MeCN, t = 30 s → 18 min].

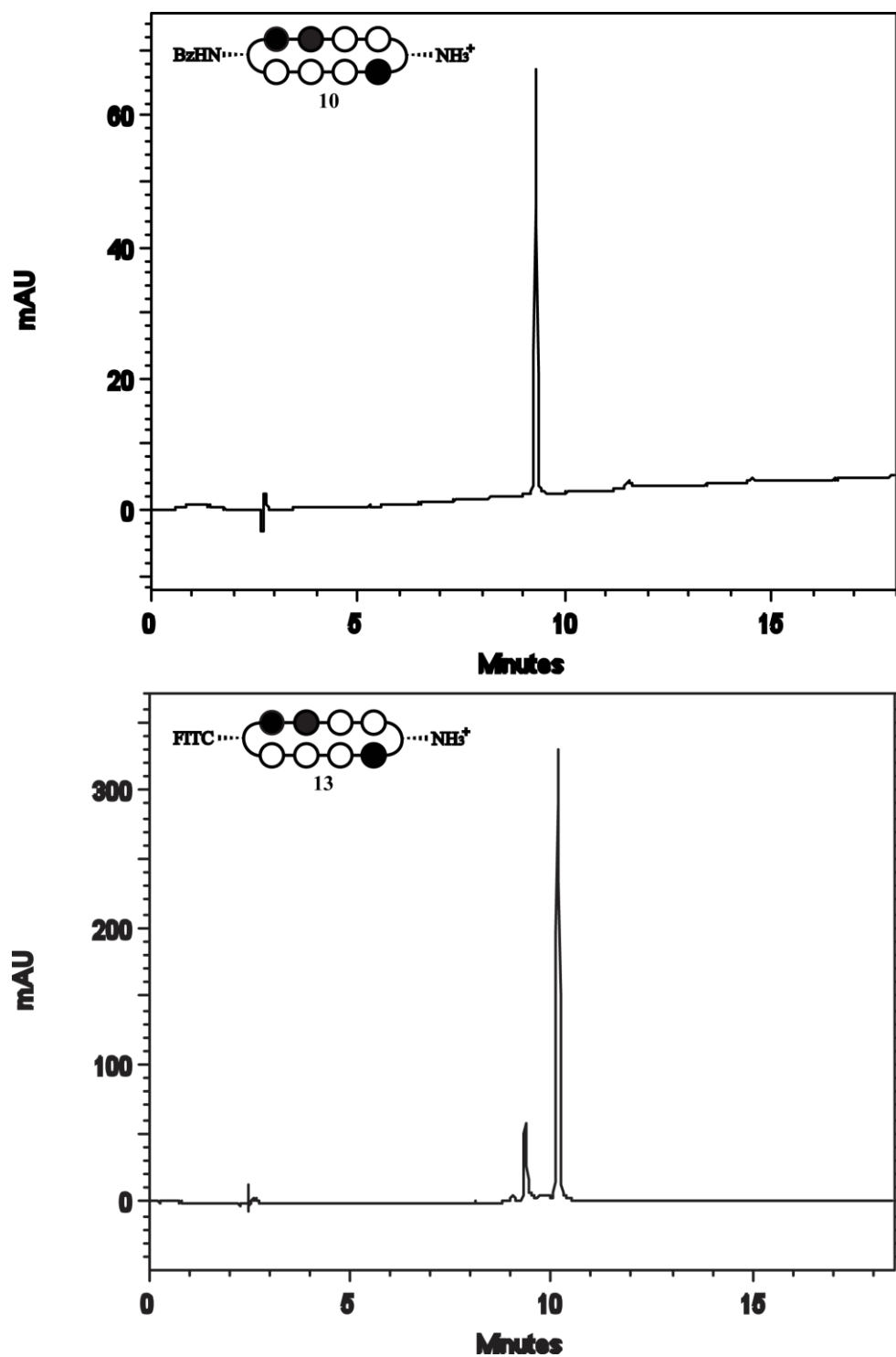


Figure 2.14 HPLC spectrum of **10** and **13**. Reverse-phase HPLC taken on Beckman Gold instrument equipped with a Phenomenex Gemini analytical column (250 × 4.6 mm, 5 μm) and a diode array detector, and the mobile phase consisted of a gradient of acetonitrile (MeCN) in 0.1% (v/v) aqueous TFA [10% MeCN, t = 0 → 30 s; 10% → 80% MeCN, t = 30 s → 18 min].

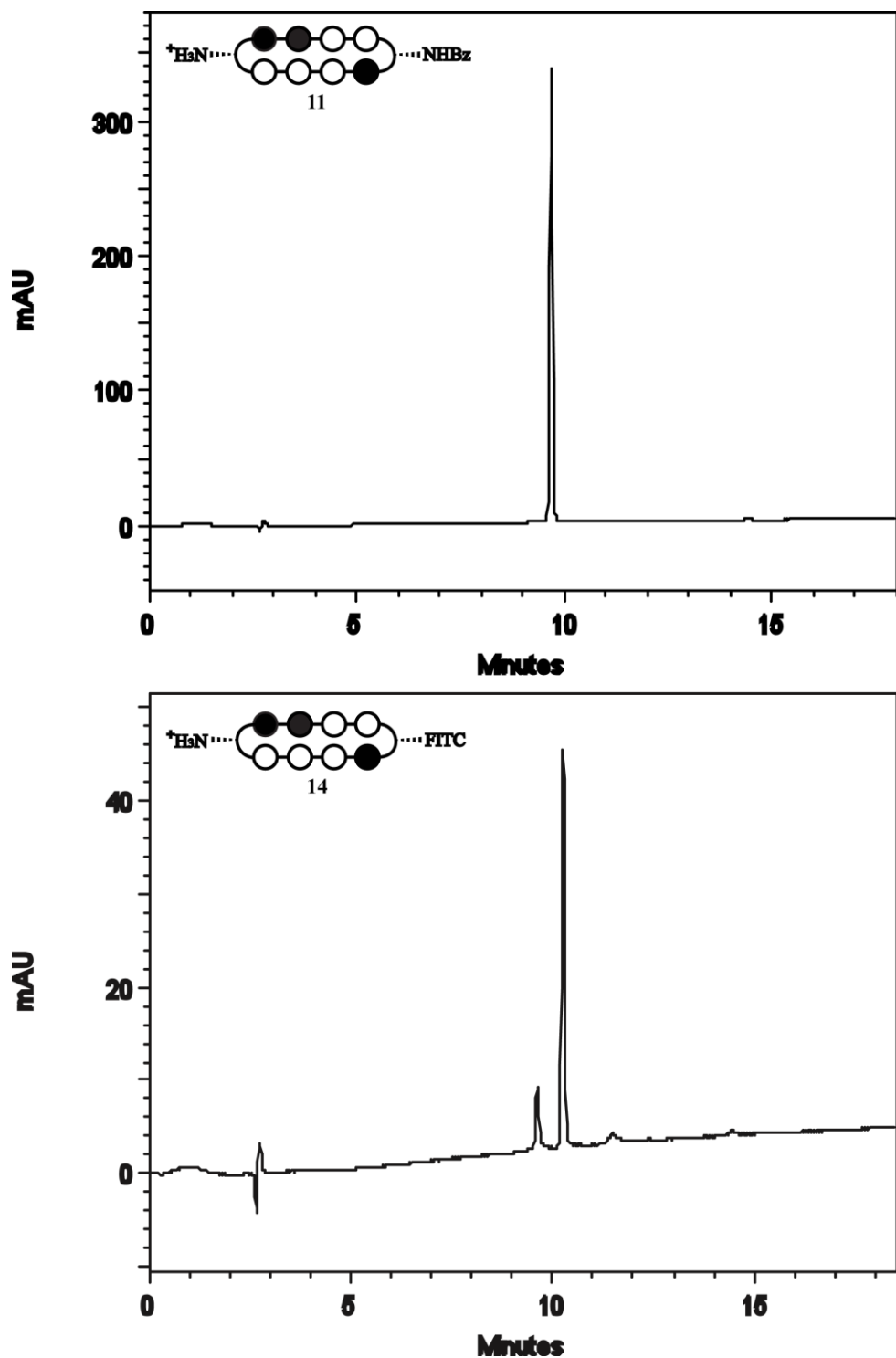


Figure 2.15 HPLC spectrum of 11 and 14. Reverse-phase HPLC taken on Beckman Gold instrument equipped with a Phenomenex Gemini analytical column (250 × 4.6 mm, 5 μm) and a diode array detector, and the mobile phase consisted of a gradient of acetonitrile (MeCN) in 0.1% (v/v) aqueous TFA [10% MeCN, t = 0 → 30 s; 10% → 80% MeCN, t = 30 s → 18 min].

Figure 2.16 HPLC spectrum of **15** and **16**. Reverse-phase HPLC taken on Beckman Gold instrument equipped with a Phenomenex Gemini analytical column (250 × 4.6 mm, 5 μm) and a diode array detector, and the mobile phase consisted of a gradient of acetonitrile (MeCN) in 0.1% (v/v) aqueous TFA [10% MeCN, t = 0 → 30 s; 10% → 80% MeCN, t = 30 s → 18 min].

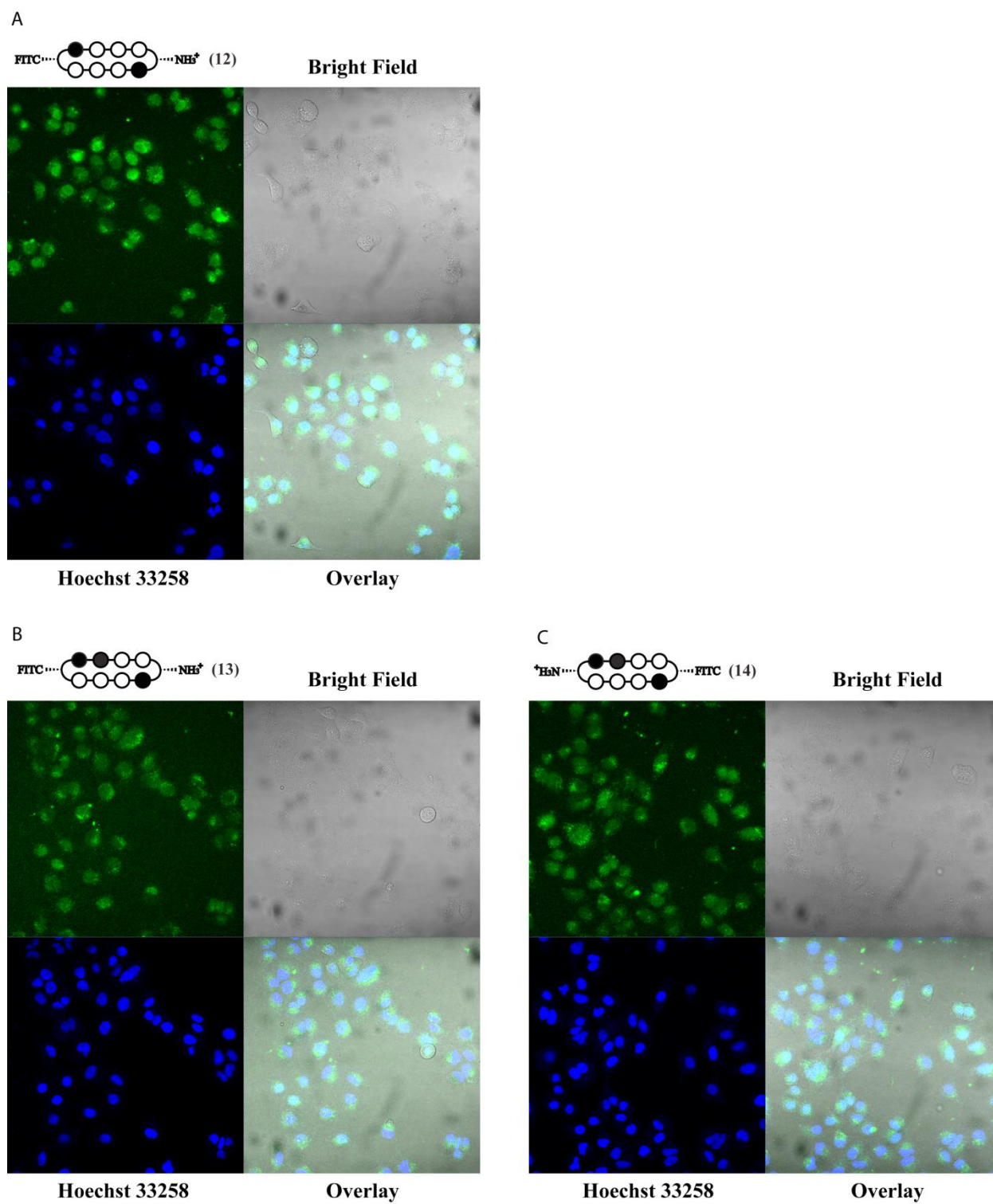


Figure 2.17 Confocal microscopy analysis of **12–14** in A549 cells.

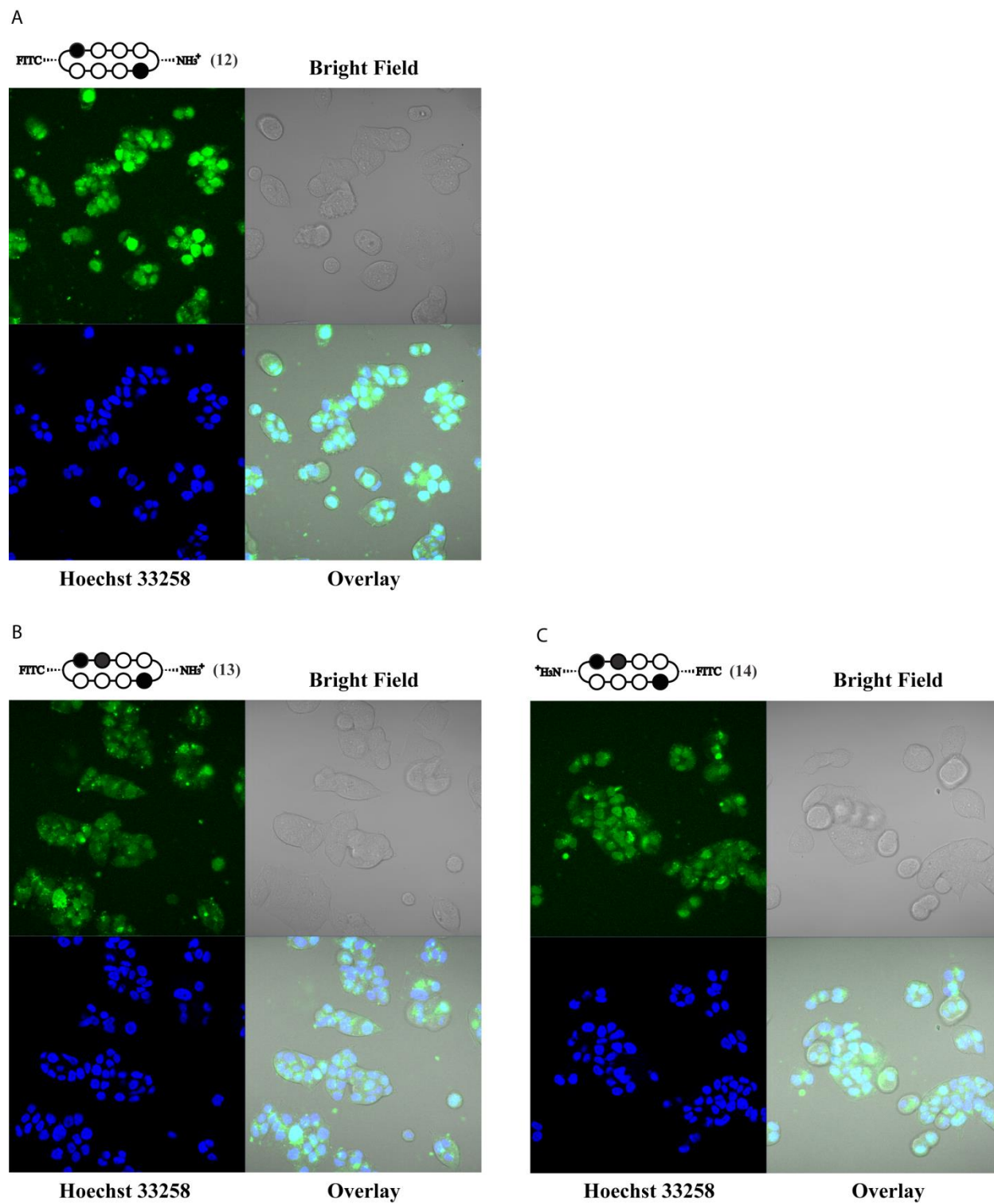
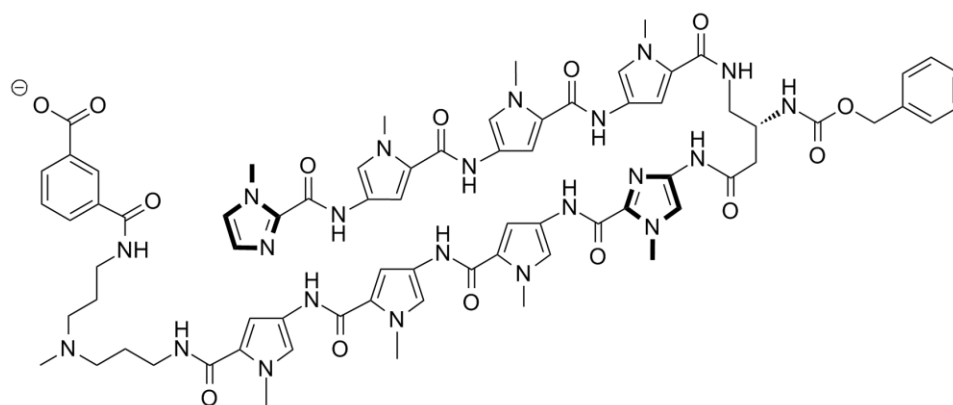


Figure 2.18 Confocal microscopy analysis of **12–14** in T47D cells.



S1

Chapter 3

DNA Sequence Selectivity of Hairpin Polyamide Turn Units

The text of this chapter was taken in part from a manuscript co-authored with Michelle E. Farkas, Christian Dose, and Peter B. Dervan (California Institute of Technology).

Farkas, M.E.; Li, B.C.; Dose, D.; Dervan, P.B. "DNA Sequence Selectivity of Hairpin Polyamide Turn Units" *Bioorg. Med. Chem. Lett.* **2009**, 19, 3919–3923.

Abstract

A class of hairpin polyamides linked by 3,4-diaminobutyric acid, resulting in a β -amine residue at the turn unit, showed improved binding affinities relative to their α -amino- γ -turn analogs for particular sequences. We incorporated β -amino- γ -turns in six-ring polyamides and determined whether there are any sequence preferences under the turn unit by quantitative footprinting titrations. Although there was an energetic penalty for G•C and C•G base pairs, we found little preference for T•A over A•T at the β -amino- γ -turn position. Fluorine and hydroxyl substituted α -amino- γ -turns were synthesized for comparison. Their binding affinities and specificities in the context of six-ring polyamides demonstrated overall diminished affinity and no additional specificity at the turn position. We anticipate that this study will be a baseline for further investigation of the turn subunit as a recognition element for the DNA minor groove.

3.1 Introduction

Hairpin pyrrole-imidazole (Py-Im) polyamides are a class of programmable synthetic ligands able to bind a broad repertoire of DNA sequences with affinities and specificities comparable to those of DNA-binding proteins.^{1,2} They have been shown to localize to the nuclei of living cells^{3, 4} and regulate endogenous gene expression by interfering with transcription factor/DNA interfaces.^{5–10} Discrimination of the four Watson-Crick base pairs is dependent upon Py-Im ring pairings in the minor groove. Pairing rules have been established whereby *N*-methyl imidazole/*N*-methylpyrrole (Im/Py) pairs target G•C, the reverse (Py/Im) target C•G, and Py/Py pairs target A•T and T•A.^{11–13}

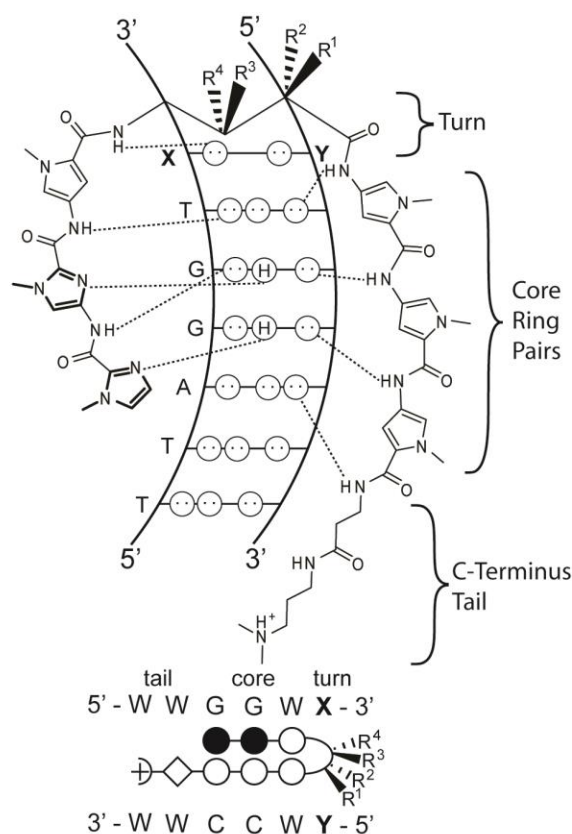


Figure 3.1 Schematic diagram of six-ring hairpin polyamide (ImImPy-turn-PyPyPy) targeting the DNA sequence 5'-WWGGWW-3'. Dashed lines indicate hydrogen bonds between the polyamide and DNA base pairs.

The turn unit in the hairpin is a recognition element, favoring T•A / A•T over G•C / C•G.¹⁴ There is an energetic penalty for unfavorable steric interaction with the exocyclic amine present at the edge of the G•C base pair (Fig. 1). The question arises whether discrimination between T•A and A•T with the turn unit can be achieved. Previous efforts toward the improvement of hairpin binding affinity have involved modifications of the turn unit. Early studies showed the optimal length of the turn element to be three methylene units, resulting in the use of γ -aminobutyric acid (γ -turn).¹⁵ Modification of the α -position of the parent γ -turn with (*R*)-2,4-diaminobutyric acid (α -amino- γ -turn) results in an approximately fifteen-fold increase in DNA-binding affinity.¹⁶ In contrast, hairpins containing the opposite enantiomer, (*S*)- α -amino- γ -turn, bind DNA with diminished affinities likely due to a steric clash of the amine with the wall of the minor groove. Polyamides containing α -hydroxy- γ -turns¹⁷ and α -diaminobutyric acid¹⁸ turns have been reported to impart additional elements of specificity, but with the cost of diminished binding affinities.

In a formal sense, a DNA minor groove binding hairpin Py-Im polyamide is an early example of a class of oligomers encoded by the order of monomer units that fold to a desired shape with a specific function, referred to as “foldamers.”^{19–21} The ring order of Py-Im polyamides codes in a programmable manner for a specific, contiguous sequence of Watson-Crick base pairs. The turn unit is both a shape element as well as a DNA recognition element, allowing the molecule to fold in a U-conformation. The turn unit deserves more attention and this paper represents an effort to create a baseline for the field.

Recently, we introduced a new class of hairpin polyamides linked by 3,4-diaminobutyric acid, resulting in a β -amino- γ -turn.²² These molecules showed improved binding affinities relative to their α -amino- γ -turn analogs for A/T-rich sequences. Additionally, polyamides containing the β -amino- γ -turn were found to have improved tolerance for synthetic modification at the amine position presumably due to their more central location on the floor of the minor groove. Due to limitations of quantitative

DNase I footprinting titrations^{23–25} for compounds where $K_a \geq 10^{10} \text{ M}^{-1}$, relative binding affinities for high affinity molecules are compared by using their thermal stabilization of DNA duplexes. It has been shown previously that increases in melting temperatures (ΔT_m) of DNA duplexes bound by hairpin polyamides correlate with DNA-binding affinity.^{26, 27}

We report herein a comparison of the sequence specificities of hairpin Py-Im polyamides containing the α -amino- γ -turn and the β -amino- γ -turn. Additionally, we have synthesized both hydroxyl and fluoro-substituted α -amino- γ -turns and determined their affinities and specificities in polyamides with analogous core ring pairs. By employing six-ring polyamides, which have lower binding affinities compared to eight-ring polyamides,²⁸ we are able to determine reliable equilibrium association constants (K_a) via quantitative DNase I footprinting titrations, and compare them with DNA duplex thermal stabilizations.

3.2 Results and Discussion

I. Polyamide synthesis

Six-ring hairpin polyamides (ImImPy-turn-PyPyPy) targeting the DNA sequence 5'-WWGGWW-3' were synthesized by solid-phase methods on PAM resin (Fig. 3.2).^{22, 29} In addition to the parent molecule containing an unsubstituted γ -aminobutyric acid hairpin (**1**), oligomers containing an amine moiety in the α and β turn positions (**2R**, **4R**, **4S**) and two polyamides with acetylated amines (**3R**, **5R**) were also synthesized. The acetylated, or capped, molecules were used to determine tolerance for modifications at the turn. Acetylated turn units have been shown to improve nuclear uptake of polyamides.⁴

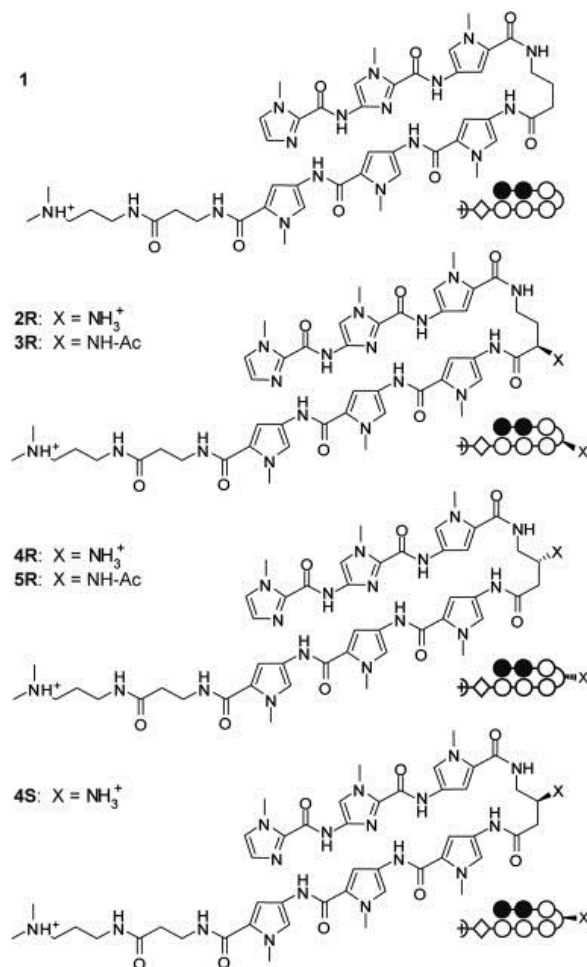


Figure 3.2 Chemical and ball-and-stick structures of polyamides containing free and acetylated amines. Ball-and-stick symbols are defined as follows: pyrrole is denoted by an open circle, imidazole is denoted by a filled circle, and β -alanine is denoted by a diamond shape.

II. Thermal stabilization of DNA duplexes.

Spectroscopic analyses were performed on the 11mer DNA duplex shown in Table 3.1.²² All hairpins analyzed provided an increase in melting temperature, confirming the formation of DNA/polyamide complexes. The ΔT_m values obtained for polyamides containing a free amine were within error of each other. However, acetylated polyamide **3R** (α -amino turn) showed a greater decrease in affinity than **5R** (β -amino- γ -turn). As had been demonstrated with eight-ring hairpin molecules,²² improvements in binding affinities for β - over α -amino- γ -turn six-ring polyamides are more pronounced with decreasing imidazole content (Fig. S3.10, Table 3.7).



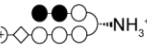


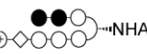
DNA = 5'-CTA TGGTA GAC-3'			
Polyamides	$T_m / ^\circ\text{C}$	$\Delta T_m / ^\circ\text{C}$	
—	45.1 (± 0.1)	—	
1 	54.3 (± 0.2)	9.2	
2R 	59.8 (± 0.3)	14.7	
4R 	60.0 (± 0.2)	14.9	
4S 	59.8 (± 0.2)	14.7	
3R 	54.9 (± 0.1)	10.1	
5R 	57.0 (± 0.2)	12.2	

Table 3.1 Melting temperatures of DNA/polyamide complexes for **1**, **2R**, **4R**, **4S**, **3R**, and **5R**. All values are derived from at least three melting temperature experiments, with standard deviations indicated in parentheses. ΔT_m values are given as T_m (DNA/polyamide) – T_m (DNA).

III. DNA binding affinity and sequence selectivity

The plasmid pCDMF6 was prepared to characterize polyamides targeting the sequence 5'-WGGWW-3' (Fig. 3.3). The designed insert contains four binding sites, varying the nucleotide base pair present under the turn unit.

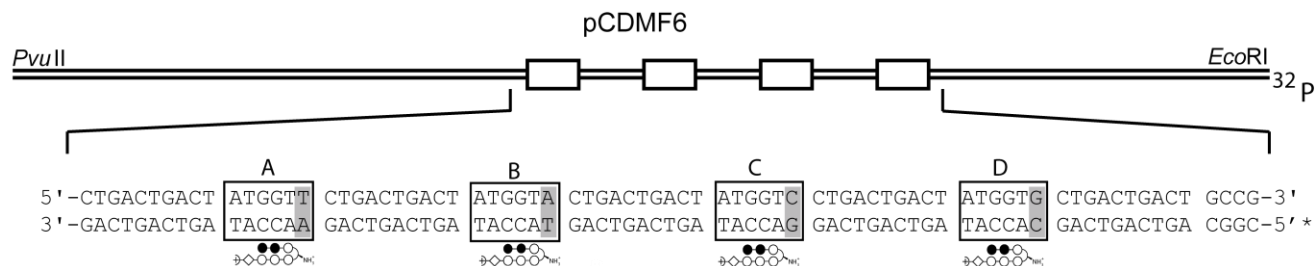


Figure 3.3 Illustration of the EcoRI/PvuII restriction fragment derived from plasmid pCDMF6, used to characterize polyamides. The designed polyamide binding sites are indicated by boxes; single base-pair mismatches are indicated by shaded regions.

Quantitative DNase I footprinting titrations were performed with the polyamides in order to measure their binding site affinities and specificities, as previously described.²⁵ As expected, the parent hairpin containing the γ -turn retained the lowest binding affinity, while experiments for **2R**, **4R**, and **4S** (Fig. 3.4, Table 3.2) corroborated the similar ΔT_m values obtained for duplex stabilization. None of these molecules bound the G•C base pair, and binding to C•G was greatly diminished. Polyamide **4R** revealed only a two-fold specificity for T•A over A•T (Table 3.3). Study of an additional polyamide series revealed similar trends (Fig. 3.5, Table 3.8). Analysis of polyamides **3R** and **5R** (Fig. 3.5, Table 3.2) revealed a greater decrease in binding affinities for the α -amino- γ -turn molecule than the β . Between **2R** and **3R** there is a five-fold decrease over T•A, and an eight-fold decrease over A•T. For β -amino- γ -turn polyamides **4R** and **5R**, there are 1.7- and 3.2- fold decreases for T•A and A•T, respectively. **5R** shows three-fold preference for binding T•A versus A•T (Table 3.3).

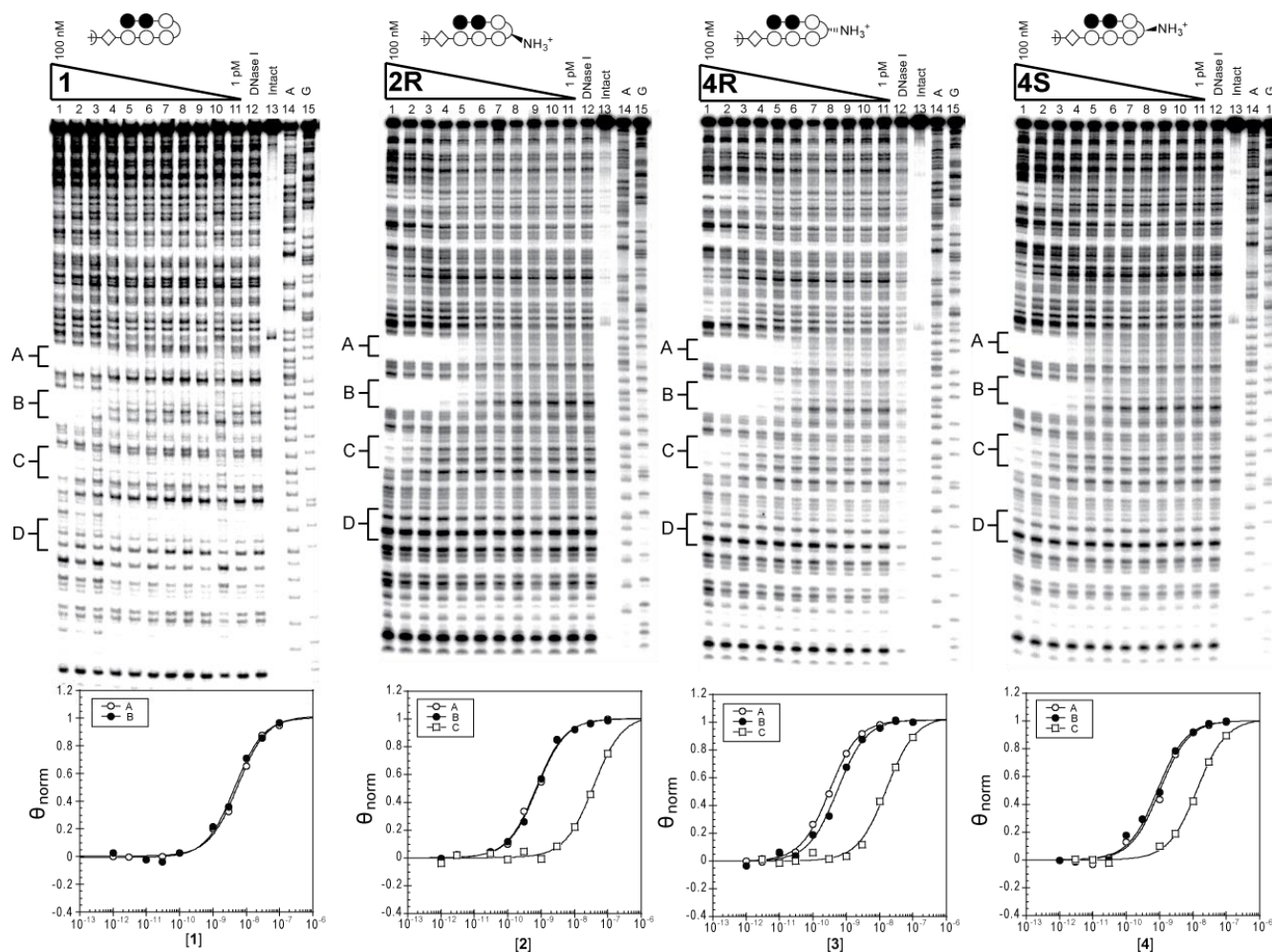


Figure 3.4 Quantitative DNase I footprinting titration experiments for polyamides **1**, **2R**, **4R**, and **4S** (left to right) on the 5' end labeled PCR product of plasmid pCDMF6: lanes 1–11, 100 nM, 30 nM, 10 nM, 3 nM, 1 nM, 300 pM, 100 pM, 30 pM, 10 pM, 3 pM, and 1 pM polyamide, respectively; lane 12, DNase I standard; lane 13, intact DNA; lane 14, A reaction; lane 15, G reaction. Respective isotherms are shown below.

	5'-ATGGTT-3'	5'-ATGGTA-3'	5'-ATGGTC-3'
1	$2.1 (\pm 0.6) \times 10^8$	$2.0 (\pm 0.5) \times 10^8$	$< 10^7$
2R	$1.6 (\pm 0.7) \times 10^9$	$1.7 (\pm 0.9) \times 10^9$	$3.9 (\pm 2.0) \times 10^7$
4R	$3.3 (\pm 0.1) \times 10^9$	$1.8 (\pm 0.2) \times 10^9$	$5.0 (\pm 1.1) \times 10^7$
4S	$1.1 (\pm 0.1) \times 10^9$	$1.3 (\pm 0.2) \times 10^9$	$6.0 (\pm 0.4) \times 10^7$
3R	$3.2 (\pm 0.4) \times 10^8$	$2.1 (\pm 0.3) \times 10^8$	$< 10^7$
5R	$2.0 (\pm 0.4) \times 10^9$	$5.2 (\pm 1.6) \times 10^8$	$8.9 (\pm 2.8) \times 10^7$

Table 3.2 Binding affinities (M^{-1}) for polyamides for **1**, **2R**, **4R**, **4S**, **3R**, and **5R**. Equilibrium association constants are reported as mean values from three DNase I footprinting titration experiments. Standard deviations are shown in parentheses.

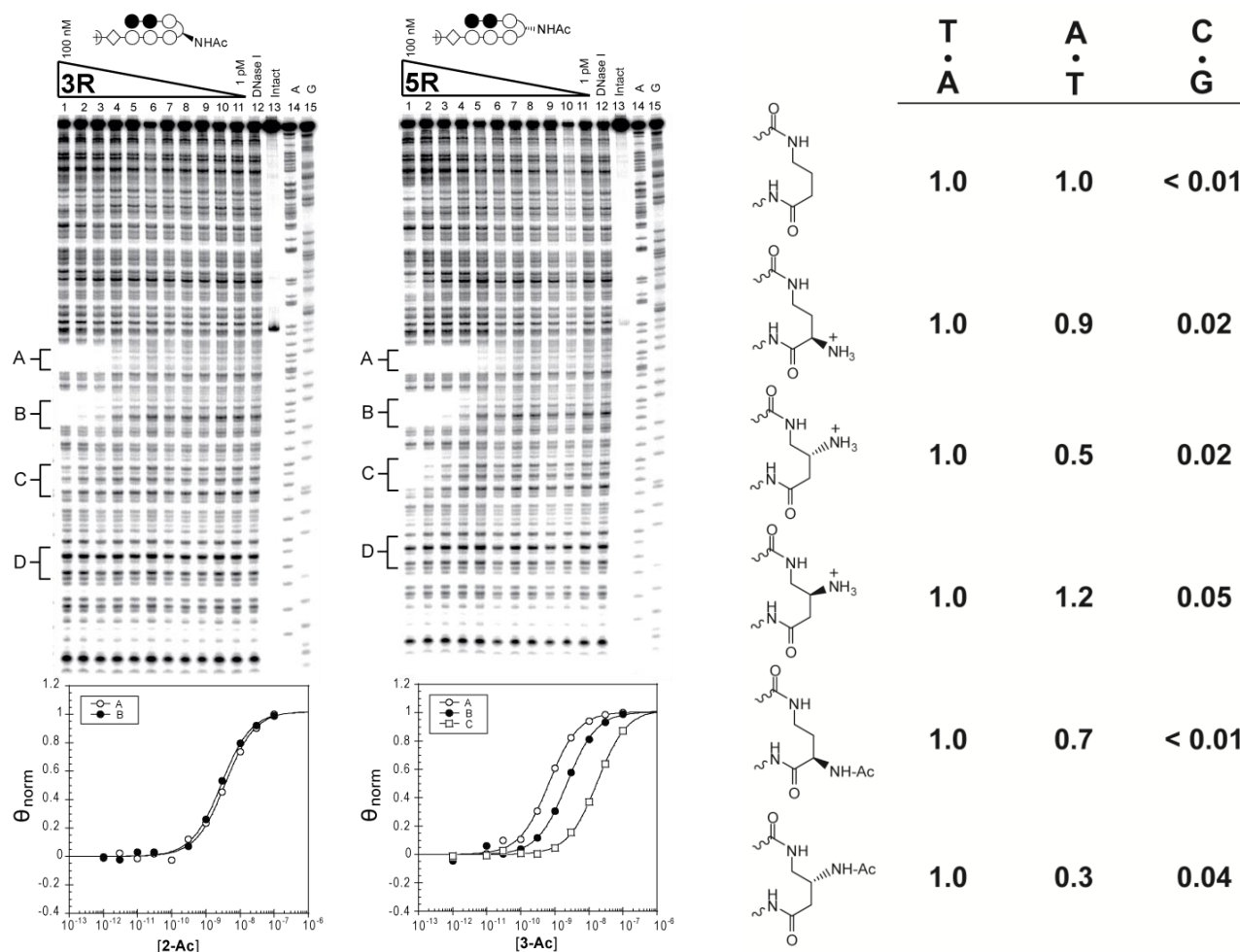


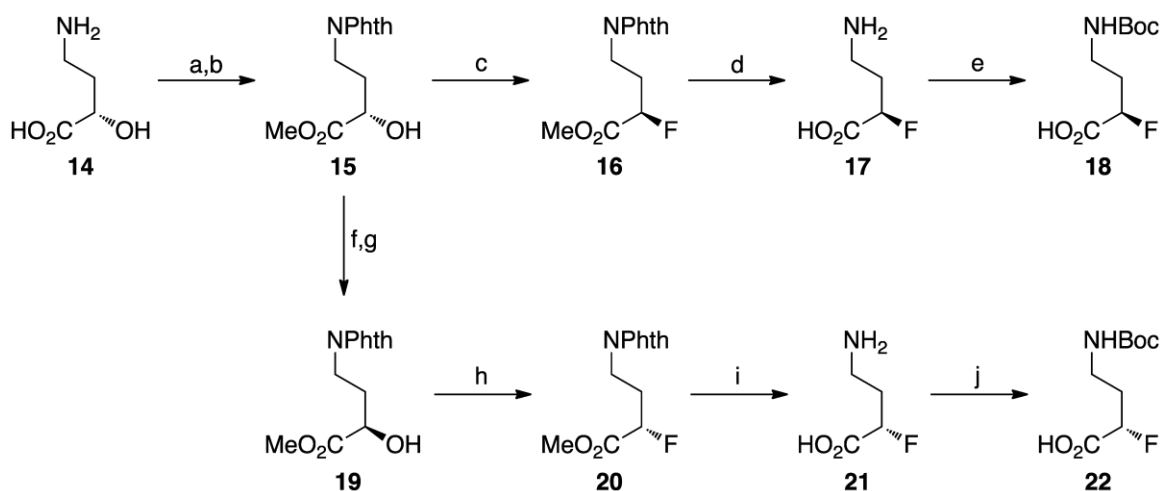
Figure 3.5 (left) Quantitative DNase I footprinting titration experiments for polyamides **3R** (left) and **5R** (right) on the 5' end labeled PCR product of plasmid pCDMF6: lanes 1–11, 100 nM, 30 nM, 10 nM, 3 nM, 1 nM, 300 pM, 100 pM, 30 pM, 10 pM, 3 pM, and 1 pM polyamide, respectively; lane 12, DNase I standard; lane 13, intact DNA; lane 14, A reaction; lane 15, G reaction. Respective isotherms are shown below.

Table 3.3 (right) Relative binding affinities for polyamides **1**, **2R**, **4R**, **4S**, **3R**, and **5R**. Relative binding affinities are reported as ratios of binding affinities (K_a) as determined by DNase I footprinting titration experiments for polyamides targeting 5'-WGGWW-3'. Sites containing G•C at the hairpin position have relative affinities < 0.01 (not shown).

IV. Fluoro and Hydroxyl Substituted Turn Units

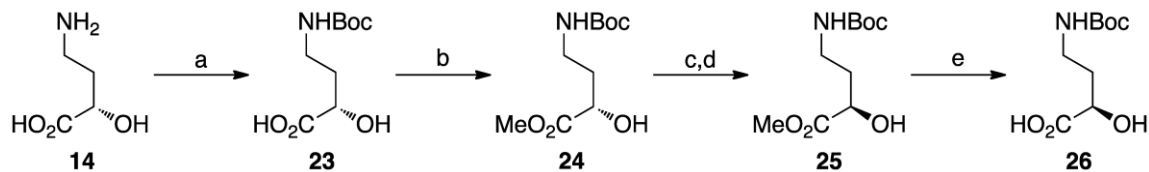
Fluorine and hydroxyl substituted hairpin turns were synthesized (Scheme 3.1 and 3.2) and incorporated in six-ring hairpin polyamides targeting the DNA sequence 5'-WWGGWW-3' (Fig. 3.6).^{30, 31} Polyamides were synthesized on PAM resin using standard solid-phase methods.

Scheme 3.1 Synthesis of α -fluoro GABA turns **18** and **22**

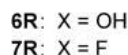


¹Reagents and conditions: (a) phthalic anhydride, 140 °C; (b) 2M HCl in Et₂O, MeOH; (c) DAST, pyridine, DCM; (d) 6M HCl (aq); (e) Boc₂O, NaHCO₃, THF, H₂O; (f) *p*-NO₂-PhCO₂H, PPh₃, DIAD, THF; (g) Et₃N, MeOH; (h) DAST, pyridine, DCM; (i) 6M HCl (aq); (j) Boc₂O, NaHCO₃, THF, H₂O.

Scheme 3.2 Synthesis of α -hydroxyl GABA turns **23** and **26**



¹Reagents and conditions: (a) Boc₂O, NaHCO₃, dioxane, H₂O; (b) CH₃I, K₂CO₃, DMF; (c) *p*-NO₂-PhCO₂H, PPh₃, DIAD, THF; (d) Et₃N, MeOH; (e) NaOH (aq), MeOH.



6S: X = OH
7S: X = F

DNA = 5'-CTA**TGGTA**GAC-3'

6R

Thermal stabilization analysis of the polyamides on an 11mer DNA duplex revealed that fluoro and hydroxyl substituted hairpins resulted in lower stabilizations than the corresponding amine-substituted and acetylated polyamides (Table 3.4). DNase I footprinting titrations on the plasmid

pCDMF6 (Fig. 3.3, Fig. 3.7) showed that both enantiomers of the hydroxyl and fluoro-hairpin turns resulted in decreased polyamide binding affinities relative to their amine substituted counterparts (Table 3.5). Additionally, none of these subunits resulted in increased elements of specificity at the turn position of the molecule (Table 3.6).

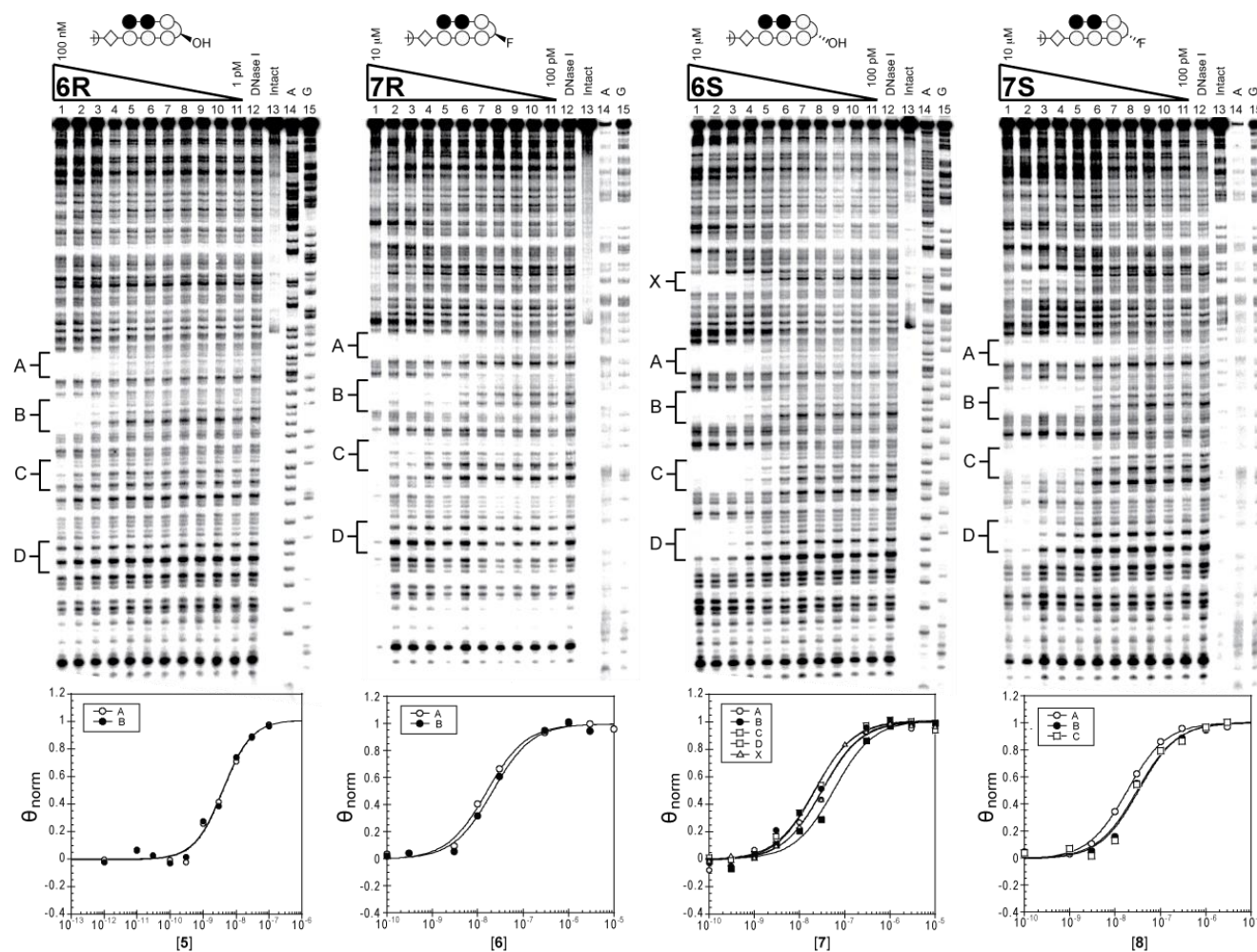


Figure 3.7 Quantitative DNase I footprinting titration experiments for polyamides **6R**, **7R**, **6S**, and **7S** (left to right) on the 5' end labeled PCR product of plasmid pCDMF6. For **6R**: lanes 1–11, 100 nM, 30 nM, 10 nM, 3 nM, 1 nM, 300 pM, 100 pM, 30 pM, 10 pM, 3 pM, and 1 pM polyamide, respectively; lane 12, DNase I standard; lane 13, intact DNA; lane 14, A reaction; lane 15, G reaction. Polyamides **7R**, **6S**, and **7S**: lanes 1–11, 10 μM, 3 μM, 1 μM, 300 nM, 100 nM, 30 nM, 10 nM, 3 nM, 1 nM, 300 pM, and 100 pM polyamide, respectively; lane 12, DNase I standard; lane 13, intact DNA; lane 14, A reaction; lane 15, G reaction. Respective isotherms are shown below.

	5'-ATGGTT-3'	5'-ATGGTA-3'	5'-ATGGTC-3'	5'-ATGGTG-3'
6R	$2.1 (\pm 0.4) \times 10^8$	$2.0 (\pm 0.5) \times 10^8$	$< 10^7$	$< 10^7$
7R	$5.3 (\pm 1.1) \times 10^7$	$4.5 (\pm 0.6) \times 10^7$	$< 10^7$	$< 10^7$
6S	$2.6 (\pm 0.6) \times 10^7$	$3.4 (\pm 1.2) \times 10^7$	$3.6 (\pm 1.1) \times 10^7$	$2.0 (\pm 0.7) \times 10^7$
7S	$6.1 (\pm 2.3) \times 10^7$	$3.9 (\pm 1.3) \times 10^7$	$3.5 (\pm 1.2) \times 10^7$	$< 10^7$

Table 3.5 Binding affinities (M^{-1}) for polyamides **6R**, **7R**, **6S**, and **7S**. Equilibrium association constants are reported as mean values from three DNase I footprinting titration experiments. Standard deviations are shown in parentheses.

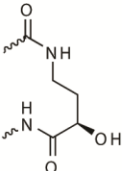
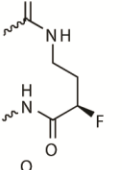
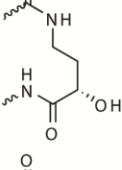
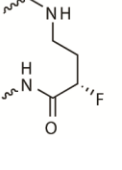
	T A	A T	C G	G C
	1.0	1.0	< 0.01	< 0.01
	1.0	0.8	< 0.01	< 0.01
	1.0	1.3	1.4	0.8
	1.0	0.6	0.6	< 0.01

Table 3.6 Relative binding affinities for polyamides **6R**, **7R**, **6S**, and **7S**. Relative binding affinities are reported as ratios of binding affinities (K_a) as determined by DNase I footprinting titration experiments for polyamides targeting 5'-WGGWW-3'.

3.3 Conclusions

By utilizing six-ring hairpin polyamides, we were able to combine DNase I footprinting titration and duplex stabilization analyses in order to fully characterize the binding preferences of various hairpin turn subunits. Although the hairpin turns investigated herein show modest DNA binding specificities, we anticipate that further study will yield moieties enabling discrimination amongst all four Watson-Crick base pairs and add an additional recognition element for DNA recognition.

3.4 Materials and Methods

Materials

(S)-(-)-4-amino-2-hydroxybutyric acid, phthalic anhydride, solid sodium hydrogensulfonate (NaHSO_4), 2M HCl in diethyl ether (Et_2O), pyridine, diethylaminosulfur trifluoride (DAST), di-*tert*-butyldicarbonate (Boc_2O), triphenyl phosphine (PPh_3), 4-nitrobenzoic acid, diisopropyl azodicarboxylate (DIAD), triethylamine, methyl iodide (CH_3I), 1 M aqueous HCl, anhydrous N,N-dimethylformamide (DMF) and tryptamine were purchased from Sigma-Aldrich. 1M aqueous NaOH, concentrated HCl, solid sodium sulfate (Na_2SO_4), and solid sodium bicarbonate (NaHCO_3) were purchased from EMD Chemicals. PyBOP and Boc-4-Abu-OH were purchased from NovaBioChem. Solid citric acid hexahydrate was purchased from Mallinckrodt Chemicals. (*R*)-2,4-Fmoc-Dbu(Boc)-OH was purchased from Bachem. (*R*)-3,4-Cbz-Dbu(Boc)-OH and (*S*)-3,4-Cbz-Dbu(Boc)-OH were purchased from Senn Chemicals AG.

Methods

Enantiopurities of precursors were probed via analytical chiral HPLC assays of their tryptamide derivatives (Fig. 3.11 and 3.12). All DNA oligomers were purchased from Integrated DNA Technologies. Polyamides were purified via preparative HPLC on an Agilent Technologies 1200 Series system using a Phenomenex Gemini column. Matrix-assisted, LASER desorption/ionization time-of-flight mass spectrometry (MALDI-TOF MS) was performed on an Applied Biosystems Voyager DR Pro spectrometer. NMR spectroscopy data was obtained on a Varian instrument operating at 500 MHz. HRMS were acquired using an Agilent 6200 Series TOF with an Agilent G1978A Multimode source in electrospray ionization (ESI), atmospheric pressure chemical ionization (APCI) or mixed (MM) ionization mode. Optical rotation measurements were measured on a Jasco P-1010 polarimeter at 589 nm in spectrophotometric grade solvents.

I. Polyamide Synthesis

Polyamides were synthesized with Boc- β -Ala-PAM resin (Peptides International) according to published synthesis protocols.^{22, 29}

Polyamide **1**: MALDI-TOF $[M+H]^+$ calcd for $C_{46}H_{60}N_{17}O_8^+ = 979.1$, observed = 978.8.

Polyamide **2R**: MALDI-TOF $[M+H]^+$ calcd for $C_{46}H_{62}N_{18}O_8^+ = 994.1$, observed = 993.9.

Polyamide **3R**: MALDI-TOF $[M+H]^+$ calcd for $C_{48}H_{63}N_{18}O_9^+ = 1036.1$, observed = 1036.0.

Polyamide **4R**: MALDI-TOF $[M+H]^+$ calcd for $C_{46}H_{62}N_{18}O_8^+ = 994.1$, observed = 994.0.

Polyamide **5R**: MALDI-TOF $[M+H]^+$ calcd for $C_{48}H_{63}N_{18}O_9^+ = 1036.1$, observed = 1035.9.

Polyamide **4S**: MALDI-TOF $[M+H]^+$ calcd for $C_{46}H_{62}N_{18}O_8^+ = 994.1$, observed = 993.9.

Polyamide **6R**: MALDI-TOF $[M+H]^+$ calcd for $C_{46}H_{60}N_{17}O_9^+ = 995.1$, observed = 995.0.

Polyamide **7R**: MALDI-TOF $[M+H]^+$ calcd for $C_{46}H_{59}FN_{17}O_8^+ = 996.5$, observed = 996.7.

Polyamide **6S**: MALDI-TOF $[M+H]^+$ calcd for $C_{46}H_{60}N_{17}O_9^+ = 995.1$, observed = 995.1.

Polyamide **7S**: MALDI-TOF $[M+H]^+$ calcd for $C_{46}H_{59}FN_{17}O_8^+ = 996.5$, observed = 996.6.

II. Synthesis of Fluoro and Hydroxyl Turn Precursors

(S)-methyl 4-(1,3-dioxoisindolin-2-yl)-2-hydroxy-butanoate (**15**). *(S)*-(-)-4-amino-2-hydroxybutyric acid (4.00 g, 33.6 mmol) **14** was combined with phthalic anhydride (4.97 g, 33.6 mmol). The solids were ground, mixed, and heated to 140°C, at which point the phthalic anhydride melted and dissolved **14**. After 30 min, the reaction mixture was cooled to room temperature and re-dissolved in EtOAc (300 mL). The solution was extracted with 1 M NaHSO₄ (100 mL, pH 3), washed with water (3 x 100 mL), and brine (100 mL). The organic layer was dried over Na₂SO₄, filtered, and concentrated in vacuo. To the crude mixture (8.3 g) dissolved in anhydrous methanol (250 mL) was slowly added 2 M HCl in Et₂O (250 mL). The reaction was stirred at room temperature; TLC indicated completion after 3 h. The

mixture was concentrated on rotovap and purified on a short silica gel column (9:1 DCM:EtOAc). The desired fractions were combined, concentrated and dried to give product **15** as a fine white powder (6.68 g, 76% yield). ^1H NMR [499.8 MHz, DMSO- d_6]: δ 7.83 (m, 4 H), 5.57 (d, $J = 5.5$ Hz, 1 H), 4.11 (m, 1 H), 3.68 (t, $J = 7.25$ Hz, 2 H), 3.59 (s, 3 H), 2.01 (m, 1 H), 1.84 (m, 1 H); ^{13}C NMR [125.7 MHz, DMSO- d_6]: δ 173.9, 167.8, 134.3, 131.7, 122.9, 68.0, 51.5, 34.3, 32.2; HRMS (MM: ESI–APCI) calcd for $\text{C}_{13}\text{H}_{13}\text{NO}_5$ $[\text{M}+\text{Na}]^+$ 286.0686, found 286.0684; $[\alpha]_{\text{D}}^{22} +10.40$ ($c = 0.5$, CHCl_3).

(R)-methyl 4-(1,3-dioxoisindolin-2-yl)-2-fluorobutanoate (16). To hydroxyl ester **15** (5.00 g, 19.0 mmol) in DCM (50 mL) was added pyridine (1.923 mL, 23.7 mmol) at 0°C . The solution was purged with argon and DAST (3.11 mL, 23.7 mmol) was added dropwise under argon pressure. The reaction was stirred at room temperature for 18 h and poured slowly into a cold saturated NaHCO_3 solution. The organic layer was extracted, washed with water (50 mL), 0.1 M HCl (50 mL), water (50 mL) and brine (50 mL), and dried (Na_2SO_4), filtered, and concentrated in vacuo. The product was purified via silica gel column chromatography (DCM to 9:1 DCM:EtOAc). The desired fractions were combined, concentrated and dried to yield compound **16** as a pale yellow solid (2.21 g, 44% yield). ^1H NMR [499.8 MHz, DMSO- d_6]: δ 7.85 (m, 4 H), 5.24 (ddd, $J_{\text{H-H}} = 3.5$ Hz, $J_{\text{H-H}} = 8.5$ Hz, $J_{\text{H-F}} = 48$ Hz, 2 H), 3.72 (m, 2 H), 3.65 (s, 3 H), 2.09-2.29 (brm, 2 H); ^{13}C NMR [125.7 MHz, DMSO- d_6]: δ 169.3 ($^2J_{\text{C-F}} = 23.5$ Hz), 167.7, 134.3, 131.7, 123.0, 86.7 ($^1J_{\text{C-F}} = 181.0$ Hz), 52.2, 33.1 ($^3J_{\text{C-F}} = 3.3$ Hz), 30.3 ($^2J_{\text{C-F}} = 20.7$ Hz); HRMS (MM: ESI–APCI) calcd for $\text{C}_{13}\text{H}_{12}\text{FNO}_4$ $[\text{M}+\text{H}]^+$ 266.0823, found 266.0830; $[\alpha]_{\text{D}}^{22} -2.64$ ($c = 0.5$, CHCl_3).

(R)-4-amino-2-fluorobutanoic acid (17). Ester **16** (300 mg, 1.13 mmol) was suspended in 6M HCl (3.0 mL) and refluxed for 16 h under argon pressure. The mixture was cooled to room temperature, the phthalic acid precipitate was removed by filtration. The filtrate was concentrated in vacuo, and the product was purified by recrystallization in iPrOH and Et₂O to afford **17** as white crystals (124 mg, 91% yield). ¹H NMR [499.8 MHz, D₂O]: δ 5.08 (ddd, $J_{\text{H-H}} = 4.0$ Hz, $J_{\text{H-H}} = 8.0$ Hz, $J_{\text{H-F}} = 49.0$ Hz, 2 H), 3.10 (m, 2 H), 2.09-2.32 (brm, 2 H); ¹³C NMR [125.7 MHz, D₂O]: δ 173.4 ($^2J_{\text{C-F}} = 23.0$ Hz), 87.6 ($^1J_{\text{C-F}} = 180.0$ Hz), 36.0 ($^3J_{\text{C-F}} = 3.8$ Hz), 29.6 ($^2J_{\text{C-F}} = 20.7$ Hz); HRMS (MM: ESI–APCI) calc'd for C₄H₈FNO₄ [M+H]⁺ 122.0612, found 122.061; [α]_D²² +10.64 (c = 0.5, H₂O).

(R)-4-(tert-butoxycarbonylamino)-2-fluorobutanoic acid (18). To a solution of amino acid **17** (40 mg, 0.33 mmol) in THF (1 mL) and water (1 mL), solid NaHCO₃ (83 mg, 0.99 mmol) and Boc₂O (87 mg, 0.40 mmol) was added at 0 °C. After 30 min, the solution was slowly warmed to room temperature and stirred for 16 h, followed by extraction with Et₂O (2 x 1.5 mL) to remove generated *tert*-butanol and unreacted Boc₂O. The aqueous layer was carefully acidified to pH 2.5 with half-saturated citric acid at 0°C, and extracted with DCM (3x1.5mL). The combined organic phase was dried (Na₂SO₄), filtered, concentrated and dried to give product **18** as a colorless oil (52 mg, 71% yield). ¹H NMR [499.8 MHz, DMSO-d₆]: δ 13.4 (brs, 1 H), 6.91 (t, $J = 5.5$ Hz, 1 H), 4.95 (ddd, $J_{\text{H-H}} = 3.5$ Hz, $J_{\text{H-H}} = 8.5$ Hz, $J_{\text{H-F}} = 49.0$ Hz, 2 H), 3.04 (m, 2 H), 1.75-2.01 (brm, 2 H), 1.37 (s, 9 H); ¹³C NMR [125.7 MHz, DMSO-d₆]: δ 170.9 ($^2J_{\text{C-F}} = 23.0$ Hz), 155.6, 86.6 ($^1J_{\text{C-F}} = 180.5$ Hz), 77.7, 35.7, 32.4 ($^2J_{\text{C-F}} = 20.2$ Hz), 28.2; HRMS (MM: ESI–APCI) calc'd for C₉H₁₆FNO₄ [M-H][−] 220.0991, found 220.1018; [α]_D²² +5.32 (c = 0.5, MeOH).

(R)-methyl 4-(1,3-dioxoisindolin-2-yl)-2-hydroxy-butanoate (19). To a solution of **15** (5.00 g, 19.0 mmol) in THF (125 mL) was added PPh₃ (5.485 g, 20.9 mmol) followed by 4-nitrobenzoic acid (9.53 g, 57.0 mmol). DIAD (4.06 mL, 20.9 mmol) was added dropwise to the solution at 0 °C, and the reaction was stirred at room temperature. TLC showed reaction completion after 4 h, and the solution was concentrated *in vacuo*. The product was isolated via silica gel column chromatography (100% DCM), and the combined fractions were concentrated and dried *in vacuo* to afford the Mitsunobu intermediate (R)-4-(1,3-dioxoisindolin-2-yl)-1-methoxy-1-oxobutan-2-yl 4-nitrobenzoate as a pale yellow powder (7.3 g, 93% yield). ¹H NMR [499.8 MHz, DMSO-d₆]: δ 8.30 (dd, *J* = 2.5 Hz, *J* = 9 Hz, 2 H), 8.17 (dd, *J* = 2.5 Hz, *J* = 9 Hz, 2 H), 7.78 (m, 4 H), 5.33 (dd, *J* = 5 Hz, *J* = 7.5 Hz, 1 H), 3.84 (m, 2 H), 3.65 (s, 3 H), 2.33 (m, 2 H); ¹³C NMR [125.7 MHz, DMSO-d₆]: δ 169.4, 167.9, 163.6, 150.4, 134.3, 134.0, 131.6, 130.7, 123.9, 123.0, 71.2, 52.5, 33.9, 30.0; HRMS (MM: ESI-APCI) calc'd for C₂₀H₁₆N₂O₈ [M+H]⁺ 413.0979, found 413.0975; [α]_D²² +28.6 (c = 0.5, CHCl₃).

To obtain the desired product **19**, triethylamine (9.93 mL, 77.5 mmol) was added to the intermediate (6.4 g, 15.5 mmol) in anhydrous methanol (480 mL). The reaction was monitored by TLC and was complete after 4 h. The solution was then concentrated and purified via column chromatography (DCM to 9:1 DCM:EtOAc). The desired fractions were combined, concentrated and dried to afford compound **19** as a fine white powder (3.86 g, 95% yield). ¹H NMR [499.8 MHz, DMSO-d₆]: δ 7.84 (m, 4 H), 5.57 (d, *J* = 5.5 Hz, 1 H), 4.12 (m, 1 H), 3.68 (t, *J* = 7.5 Hz, 2 H), 3.59 (s, 3 H), 2.02 (m, 1 H), 1.84 (m, 1 H); ¹³C NMR [125.7 MHz, DMSO-d₆]: δ 173.9, 167.8, 134.3, 131.7, 122.9, 67.9, 51.5, 34.3, 32.1; HRMS (MM: ESI-APCI) calc'd for C₁₃H₁₃NO₅ [M+Na]⁺ 286.0686, found 286.0688; [α]_D²² -10.28 (c = 0.5, CHCl₃).

(S)-methyl 4-(1,3-dioxoisindolin-2-yl)-2-fluorobutanoate (20). Synthesis was performed using R-enantiomer **19** (3.85 g, 14.6 mmol) in conjunction with the method for the synthesis of fluoroester **16**.

The product **20** was synthesized and isolated as a pale yellow solid (1.60 g, 41% yield). ^1H NMR [499.8 MHz, DMSO- d_6]: δ 7.85 (m, 4 H), 5.24 (ddd, $J_{\text{H-H}} = 3.5$ Hz, $J_{\text{H-H}} = 8.5$ Hz, $J_{\text{H-F}} = 48.0$ Hz, 2 H), 3.72 (m, 2 H), 3.65 (s, 3 H), 2.09-2.29 (brm, 2 H); ^{13}C NMR [125.7 MHz, DMSO- d_6]: δ 169.3 ($^2J_{\text{C-F}} = 23.5$ Hz), 167.7, 134.3, 131.7, 123.0, 86.7 ($^1J_{\text{C-F}} = 181.3$ Hz), 52.2, 33.1 ($^3J_{\text{C-F}} = 3.8$ Hz), 30.3 ($^2J_{\text{C-F}} = 20.2$ Hz); HRMS (MM: ESI-APCI) calc'd for $\text{C}_{13}\text{H}_{12}\text{FNO}_4$ $[\text{M}+\text{H}]^+$ 266.0823, found 266.0828; $[\alpha]_{\text{D}}^{22} +2.4$ ($c = 0.5$, CHCl_3).

(S)-4-amino-2-fluorobutanoic acid (21). This compound was synthesized by following the method used for the synthesis of amino acid **17**, but using the S-enantiomer **20** (1.60 g, 6.03 mmol) as starting material. The product was synthesized and isolated as fluffy white crystals (725 mg, 99% yield). ^1H NMR [499.8 MHz, D_2O]: δ 5.08 (ddd, $J_{\text{H-H}} = 4.0$ Hz, $J_{\text{H-H}} = 8.0$ Hz, $J_{\text{H-F}} = 49.0$ Hz, 2 H), 3.09 (m, 2 H), 2.08-2.32 (brm, 2 H); ^{13}C NMR [125.7 MHz, D_2O]: δ 173.4 ($^2J_{\text{C-F}} = 23.0$ Hz), 87.7 ($^1J_{\text{C-F}} = 180.0$ Hz), 36.0 ($^3J_{\text{C-F}} = 3.3$ Hz), 29.6 ($^2J_{\text{C-F}} = 20.7$ Hz); HRMS (MM: ESI-APCI) calc'd for $\text{C}_4\text{H}_8\text{FNO}_4$ $[\text{M}+\text{H}]^+$ 122.0612, found 122.0613; $[\alpha]_{\text{D}}^{22} -11.2$ ($c = 0.5$, H_2O).

(S)-4-(tert-butoxycarbonylamino)-2-fluorobutanoic acid (22). This compound was synthesized by following the method used for the synthesis of amino acid **18**, but using the S-enantiomer **21** (40 mg, 0.33 mmol) as starting material. The product **22** was synthesized and isolated as a colorless oil (51 mg, 70% yield). ^1H NMR [499.8 MHz, DMSO- d_6]: δ 13.3 (brs, 1 H), 6.91 (t, $J = 5.5$ Hz, 1 H), 4.95 (ddd, $J_{\text{H-H}} = 3.5$ Hz, $J_{\text{H-H}} = 8.5$ Hz, $J_{\text{H-F}} = 49.0$ Hz, 2 H), 3.04 (m, 2 H), 1.75-2.01 (brm, 2 H), 1.37 (s, 9 H); ^{13}C NMR [125.7 MHz, DMSO- d_6]: δ 170.8 ($^2J_{\text{C-F}} = 23.5$ Hz), 155.4, 86.4 ($^1J_{\text{C-F}} = 180.5$ Hz), 77.6, 35.6, 32.3 ($^2J_{\text{C-F}} = 19.9$ Hz), 28.1; HRMS (MM: ESI-APCI) calc'd for $\text{C}_9\text{H}_{16}\text{FNO}_4$ $[\text{M}-\text{H}]^-$ 220.0991, found 220.1017; $[\alpha]_{\text{D}}^{22} -5.04$ ($c = 0.5$, MeOH).

(S)-4-(tert-butoxycarbonylamino)-2-hydroxybutanoic acid (23). To a solution of (S)-(-)-4-amino-2-hydroxybutyric acid **14** (2.00 g, 16.8 mmol) dissolved in water (50 mL) and 1,4-dioxane (50 mL), NaHCO₃ (1.55 g, 18.5 mmol) and added Boc₂O (4.04 g, 18.5 mmol) was added at 0 °C. After 15 min, the turbid solution was slowly warmed to room temperature and stirred for 16 h. The solution was extracted with Et₂O (2 x 50mL) to rid of the generated *tert*-butanol and unreacted di-*tert*-butyldicarbonate. The aqueous layer was carefully acidified to pH 2.5 with 1 M HCl (~20 mL) at 0 °C, and extracted with DCM (3 x 50mL). The combined organic phase was dried (Na₂SO₄), filtered, concentrated and dried to give product **23** as a colorless oil (3.03 g, 82% yield). ¹H NMR [499.8 MHz, DMSO-d₆]: δ 6.75 (t, *J* = 5.0 Hz, 1 H), 3.93 (dd, *J* = 4.0 Hz, *J* = 8.5 Hz, 1 H), 3.00 (m, 2 H), 1.77 (m, 1 H), 1.57 (m, 1 H), 1.36 (s, 9 H); ¹³C NMR [125.7 MHz, DMSO-d₆]: δ 175.6, 155.5, 77.5, 67.7, 36.7, 34.1, 28.2; HRMS (MM: ESI–APCI) calc'd for C₉H₁₇NO₅ [M+Na]⁺ 242.0999, found 242.0997; [α]_D²² -3.96 (c = 0.5, MeOH).

(S)-methyl 4-(tert-butoxycarbonylamino)-2-hydroxybutanoate (24). To a solution of Boc-protected amino acid **23** (2.00 g, 9.1 mmol) dissolved in DMF (20 mL) was added K₂CO₃ (1.32 g, 9.54 mmol) at 0 °C. After 15 min, CH₃I (4.13 g, 29.12 mmol) was added slowly and the solution was stirred for 44 h at room temperature. The solution was then partitioned between H₂O (100 mL) and ethyl acetate (4 x 50 mL). The organic fractions were combined, dried (Na₂SO₄), filtered, concentrated and dried to give product **24** as a pale yellow oil (1.20 g, 57% yield). ¹H NMR [499.8 MHz, DMSO-d₆]: δ 6.76 (t, *J* = 5.0 Hz, 1 H), 5.39 (d, *J* = 6.0 Hz, 1 H), 4.04 (m, 1 H), 3.62 (s, 3 H), 2.99 (m, 2 H), 1.75 (m, 1 H), 1.59 (m, 1 H), 1.36 (s, 9 H); ¹³C NMR [125.7 MHz, DMSO-d₆]: δ 174.4, 155.5, 77.5, 67.8, 51.4, 36.4, 34.1, 28.2; HRMS (MM: ESI–APCI) calc'd for C₁₀H₁₉NO₅ [M+Na]⁺ 256.1155, found 256.1159; [α]_D²² +4.56 (c = 0.5, MeOH).

(R)-methyl 4-(tert-butoxycarbonylamino)-2-hydroxybutanoate (25). To a solution of ester **24** (650 mg, 2.75 mmol) in THF (13 mL) was added PPh₃ (795 g, 3.02 mmol) followed by 4-nitrobenzoic acid (1.38 g, 8.26 mmol). DIAD (589 μ L, 3.03 mmol) was added dropwise to the solution at 0 °C, and the reaction was stirred at room temperature. TLC showed a completed reaction after 8 h, and the solution was concentrated in vacuo. The product was isolated via silica gel column chromatography (95:5 DCM:EtOAc to 9:1 DCM:EtOAc), and the combined fractions were concentrated and dried in vacuo to afford the Mitsunobu intermediate *(R)*-4-(tert-butoxycarbonylamino)-1-methoxy-1-oxobutan-2-yl 4-nitrobenzoate as a colorless oil (890 mg, 84% yield). ¹H NMR [499.8 MHz, DMSO-d₆]: δ 8.38 (dd, J = 2.0 Hz, J = 9.0 Hz, 2 H), 8.24 (dd, J = 2.0 Hz, J = 9.0 Hz, 2 H), 6.99 (t, 5.5 Hz, 1 H), 5.20 (m, 1 H), 3.70 (s, 3 H), 3.16 (m, 2 H), 2.05 (m, 2 H), 1.34 (s, 9 H); ¹³C NMR [125.7 MHz, DMSO-d₆]: δ 169.9, 163.8, 155.6, 150.5, 134.3, 130.8, 124.0, 77.7, 70.9, 52.4, 35.8, 30.8, 28.1; HRMS (MM: ESI–APCI) calc'd for C₁₇H₂N₂O₈ [M-Boc+2H]⁺ 283.0925, found 283.0934; [α]_D²² +16.64 (c = 0.5, MeOH).

To obtain the desired product **25**, triethylamine (750 μ L, 5.38 mmol) was added to the intermediate (410 mg, 1.07 mmol) in anhydrous methanol (30 mL). The reaction was monitored by TLC and was complete after 1.5 h. The solution was then concentrated and run through a silica plug. DCM was run till the eluent was no longer UV active, at which point EtOAc was used to flush out the product. The EtOAc fractions were combined, concentrated and dried to afford compound **25** as a pale yellow oil (250 mg, 99% yield). ¹H NMR [499.8 MHz, DMSO-d₆]: δ 6.76 (t, J = 5.0 Hz, 1 H), 5.39 (d, J = 6.0 Hz, 1 H), 4.04 (m, 1 H), 3.62 (s, 3 H), 2.99 (m, 2 H), 1.76 (m, 1 H), 1.60 (m, 1 H), 1.36 (s, 9 H); ¹³C NMR [125.7 MHz, DMSO-d₆]: δ 174.4, 155.5, 77.5, 67.8, 51.4, 36.5, 34.1, 28.2; HRMS (MM: ESI–APCI) calc'd for C₁₀H₁₉NO₅ [M+Na]⁺ 256.1155, found 256.1158; [α]_D²² -4.28 (c = 0.5, MeOH).

(R)-4-(tert-butoxycarbonylamino)-2-hydroxybutanoic acid (26). To a solution of Boc-protected amino acid **25** in MeOH (2.5 mL) was added dropwise 1M NaOH (2.5 mL) at 0°C. The reaction mixture was warmed to room temperature and TLC showed a completed reaction after 30 min. The solution was cooled to 0 °C and re-acidified to pH2 by dropwise addition of 1 M HCl (2.5 mL), and extracted with EtOAc (3 x 2.5 mL). The organic fractions were then combined, dried (Na₂SO₄), filtered, concentrated and dried to give product **26** as a colorless oil (108 mg, 93% yield). ¹H NMR [499.8 MHz, DMSO-d₆]: δ 6.75 (t, *J* = 5.0 Hz, 1 H), 3.92 (dd, *J* = 4.0 Hz, *J* = 8.5 Hz, 1 H), 3.00 (m, 2 H), 1.77 (m, 1 H), 1.56 (m, 1 H), 1.36 (s, 9 H); ¹³C NMR [125.7 MHz, DMSO-d₆]: δ 175.6, 155.5, 77.4, 67.8, 36.7, 34.1, 28.2; HRMS (MM: ESI–APCI) calc'd for C₉H₁₇NO₅ [M+Na]⁺ 242.0999, found 242.0998; [α]_D²² +4.12 (c = 0.5, MeOH).

(R)-tert-butyl 4-(2-(1H-indol-3-yl)ethylamino)-3-fluoro-4-oxobutylcarbamate (27). To a solution of Boc-protected amino acid **18** (25 mg, 0.11 mmol) in anhydrous DMF (1.0 mL) was added tryptamine (91 mg, 0.55 mmol), followed by PyBOP (65 mg, 0.12 mmol). The reaction was stirred at room temperature for 1.5 h, and subsequently partitioned between H₂O (1 mL) and EtOAc (3 x 1 mL). The organic layers were then combined, washed with 10% citric acid (3 x 1 mL), saturated NaHCO₃ (3 x 1 mL), brine, dried (Na₂SO₄), filtered, and concentrated. The product was purified on a silica gel column (9:1 Et₂O:EtOAc), and the desired fractions were combined, concentrated and dried to afford the desired product **27** as a pale yellow oil (28 mg, 68%). ¹H NMR [499.8 MHz, DMSO-d₆]: δ 10.80 (s, 1 H), 8.26 (t, *J* = 5.5 Hz, 1 H), 7.53 (d, *J* = 8.0 Hz, 1 H), 7.32 (app dt, *J* = 1.0 Hz, *J* = 8.0 Hz, 1 H), 7.14 (d, *J* = 2.5 Hz, 1 H), 7.05 (ddd, *J* = 1.0 Hz, *J* = 7.0 Hz, *J* = 7.0 Hz, 1 H), 6.97 (ddd, *J* = 1.0 Hz, *J* = 7.0 Hz, *J* = 7.0 Hz, 1 H), 6.87 (t, *J* = 5.5 Hz, 1 H), 4.88 (ddd, *J* = 3.5 Hz, *J* = 8.5 Hz, *J* = 49.5 Hz, 1 H), 3.38 (m, 2 H), 3.03 (m, 2 H), 2.84 (t, 7.5 Hz, 2 H), 1.76-1.95 (m, 2 H), 1.37 (s, 9 H); ¹³C NMR [125.7 MHz, DMSO-d₆]: δ 168.7 (²*J*_{C-F} = 19.9 Hz), 155.3, 136.2, 127.2, 122.6, 120.9, 118.3, 118.2, 111.6,

111.3, 89.3 ($^1J_{\text{C-F}} = 181.9$ Hz), 77.6, 35.7, 32.7 ($^2J_{\text{C-F}} = 20.7$ Hz), 28.2, 25.0; HRMS (MM: ESI-APCI) calc'd for $\text{C}_{19}\text{H}_{26}\text{FN}_3\text{O}_3$ $[\text{M}+\text{Na}]^+$ 386.1850, found 386.1855; $[\alpha]_{\text{D}}^{22} +17.1$ ($c = 0.5$, MeOH).

(S)-tert-butyl 4-(2-(1H-indol-3-yl)ethylamino)-3-fluoro-4-oxobutylcarbamate (28). This compound was synthesized by following the method used for the synthesis of amide **27**, but instead using the S-enantiomer **23** (23 mg, 0.10 mmol) as starting material. The product **28** was synthesized and isolated as a pale yellow oil (25 mg, 66% yield). ^1H NMR [499.8 MHz, DMSO- d_6]: δ 10.80 (s, 1 H), 8.26 (t, $J = 5.5$ Hz, 1 H), 7.54 (d, $J = 8.0$ Hz, 1 H), 7.32 (app dt, $J = 1.0$ Hz, $J = 8.0$ Hz, 1 H), 7.14 (d, $J = 2.0$ Hz, 1 H), 7.05 (ddd, $J = 1.0$ Hz, $J = 7.0$ Hz, $J = 7.0$ Hz, 1 H), 6.97 (ddd, $J = 1.0$ Hz, $J = 7.0$ Hz, $J = 7.0$ Hz, 1 H), 6.87 (t, $J = 5.5$ Hz, 1 H), 4.88 (ddd, $J = 3.5$ Hz, $J = 8.5$ Hz, $J = 49.5$ Hz, 1 H), 3.38 (m, 2 H), 3.03 (m, 2 H), 2.84 (t, 7.5 Hz, 2 H), 1.76-1.95 (m, 2 H), 1.37 (s, 9 H); ^{13}C NMR [125.7 MHz, DMSO- d_6]: δ 168.8 ($^2J_{\text{C-F}} = 19.7$ Hz), 155.6, 136.2, 127.2, 122.6, 120.9, 118.3, 118.2, 111.6, 111.4, 89.3 ($^1J_{\text{C-F}} = 182.8$ Hz), 77.7, 35.7, 32.7 ($^2J_{\text{C-F}} = 19.9$ Hz), 28.2, 25.0; HRMS (MM: ESI-APCI) calc'd for $\text{C}_{19}\text{H}_{26}\text{FN}_3\text{O}_3$ $[\text{M}+\text{Na}]^+$ 386.1850, found 386.1855; $[\alpha]_{\text{D}}^{22} -16.6$ ($c = 0.5$, MeOH).

(S)-tert-butyl 4-(2-(1H-indol-3-yl)ethylamino)-3-hydroxy-4-oxobutylcarbamate (29). To a solution of Boc-protected amino acid **23** (24 mg, 0.11 mmol) in anhydrous DMF (1.0 mL) was added tryptamine (89 mg, 0.55 mmol), followed by PyBOP (64 mg, 0.12 mmol). The reaction was stirred at room temperature for 1.5 h, and subsequently partitioned between H_2O (1 mL) and EtOAc (3 x 1 mL). The organic layers were then combined, washed with 10% citric acid (3 x 1 mL), saturated NaHCO_3 (3 x 1 mL), brine, dried (Na_2SO_4), filtered, and concentrated. The product was purified on a silica gel column (9:1 Et_2O :EtOAc), and the desired fractions were combined, concentrated and dried to afford the desired product **29** as a pale yellow oil (25 mg, 62%). ^1H NMR [499.8 MHz, DMSO- d_6]: δ 10.8 (s, 1 H), 7.80 (t, $J = 6.0$ Hz, 1 H), 7.56 (d, $J = 8.0$ Hz, 1 H), 7.32 (app dt, $J = 1\text{Hz}$, $J = 8.0\text{Hz}$, 1 H), 7.14 (d,

$J = 2.5$ Hz, 1 H), 7.05 (ddd, $J = 1.0$ Hz, $J = 7.0$ Hz, $J = 7.0$ Hz, 1 H), 6.97 (ddd, $J = 1.0$ Hz, $J = 7.0$ Hz, $J = 7.0$ Hz, 1 H), 6.71 (t, $J = 5.5$ Hz, 1 H), 3.84 (m, 1 H), 3.36 (m, 2 H), 3.00 (m, 2 H), 2.82 (t, $J = 8.0$ Hz, 2 H), 1.78 (m, 1 H), 1.52 (m, 1 H), 1.37 (s, 9 H); ^{13}C NMR [125.7 MHz, DMSO- d_6]: δ 173.5, 155.6, 136.3, 127.2, 122.6, 120.9, 118.3, 118.2, 111.7, 111.3, 77.5, 69.2, 36.8, 34.7, 28.3, 25.3; HRMS (MM: ESI–APCI) calc'd for $\text{C}_{19}\text{H}_{27}\text{N}_3\text{O}_4$ $[\text{M}+\text{Na}]^+$ 384.1894, found 384.1894; $[\alpha]_D^{22}$ -14.4 ($c = 0.5$, MeOH).

(R)-tert-butyl 4-(2-(1H-indol-3-yl)ethylamino)-3-hydroxy-4-oxobutylcarbamate (30). This compound was synthesized by following the method used for the synthesis of amide **29**, but instead using the R-enantiomer **25** (10 mg, 0.05 mmol) as starting material. The product **30** was synthesized and isolated as a pale yellow oil (11 mg, 66% yield). ^1H NMR [499.8 MHz, DMSO- d_6]: δ 10.8 (s, 1 H), 7.80 (t, $J = 6.0$ Hz, 1H), 7.56 (d, $J = 8.0$ Hz, 1 H), 7.32 (app dt, $J = 1$ Hz, $J = 8.0$ Hz, 1 H), 7.14 (d, $J = 2.5$ Hz, 1 H), 7.05 (ddd, $J = 1.0$ Hz, $J = 7.0$ Hz, $J = 7.0$ Hz, 1 H), 6.97 (ddd, $J = 1.0$ Hz, $J = 7.0$ Hz, $J = 7.0$ Hz, 1 H), 6.71 (t, $J = 5.5$ Hz, 1 H), 3.84 (m, 1 H), 3.36 (m, 2 H), 3.00 (m, 2 H), 2.82 (t, $J = 8.0$ Hz, 2 H), 1.78 (m, 1 H), 1.52 (m, 1 H), 1.37 (s, 9 H); [125.7 MHz, DMSO- d_6]: δ 173.5, 155.6, 136.2, 127.2, 122.6, 120.9, 118.3, 118.2, 111.7, 111.3, 77.5, 69.2, 36.8, 34.7, 28.3, 25.3; HRMS (MM: ESI–APCI) calc'd for $\text{C}_{19}\text{H}_{27}\text{N}_3\text{O}_4$ $[\text{M}+\text{Na}]^+$ 384.1894, found 384.1897; $[\alpha]_D^{22}$ +15.0 ($c = 0.5$, MeOH)

III. Analytical Chiral HPLC Assays for 28–31.

The enantiopurity of compounds **18**, **22**, **23** and **26** were determined by chiral HPLC assays performed on the UV active tryptamide derivatives **27–30** (Fig. 3.11 and 3.12). The assays were taken on an Agilent 1100 Series HPLC utilizing a Chiralpak AD column (4.6 mm x 25 cm) obtained from Daicel Chemical Industries, Ltd.

IV. DNA Thermal Denaturation Assays

Melting temperature analysis was performed as previously described²² on a Varian Cary 100 spectrophotometer equipped with a thermo-controlled cell holder, using 10 mM sodium cacodylate buffer.

V. DNase I Footprinting Assays

Plasmids were constructed as previously described¹⁸ by annealing the following oligonucleotide pair: 5'-AGCTGCTGACTGACTATGGTTCTGACTGACTATGGTACTGACTGACTATGGTCCTGAC-TGACTATGGTGCTGACTGACTGCCGC-3' and 5'-GATCGCGGCAGTCAGTCAGCACCATAGTCAGTCAGGACCATAGTCAGTCAG-TACCATAGTCAGTCAGAACCATAGTCAGTCAGC-3'. 5' labeling of primers with ³²P and subsequent DNase I footprinting titrations were performed as previously described.^{18, 25}

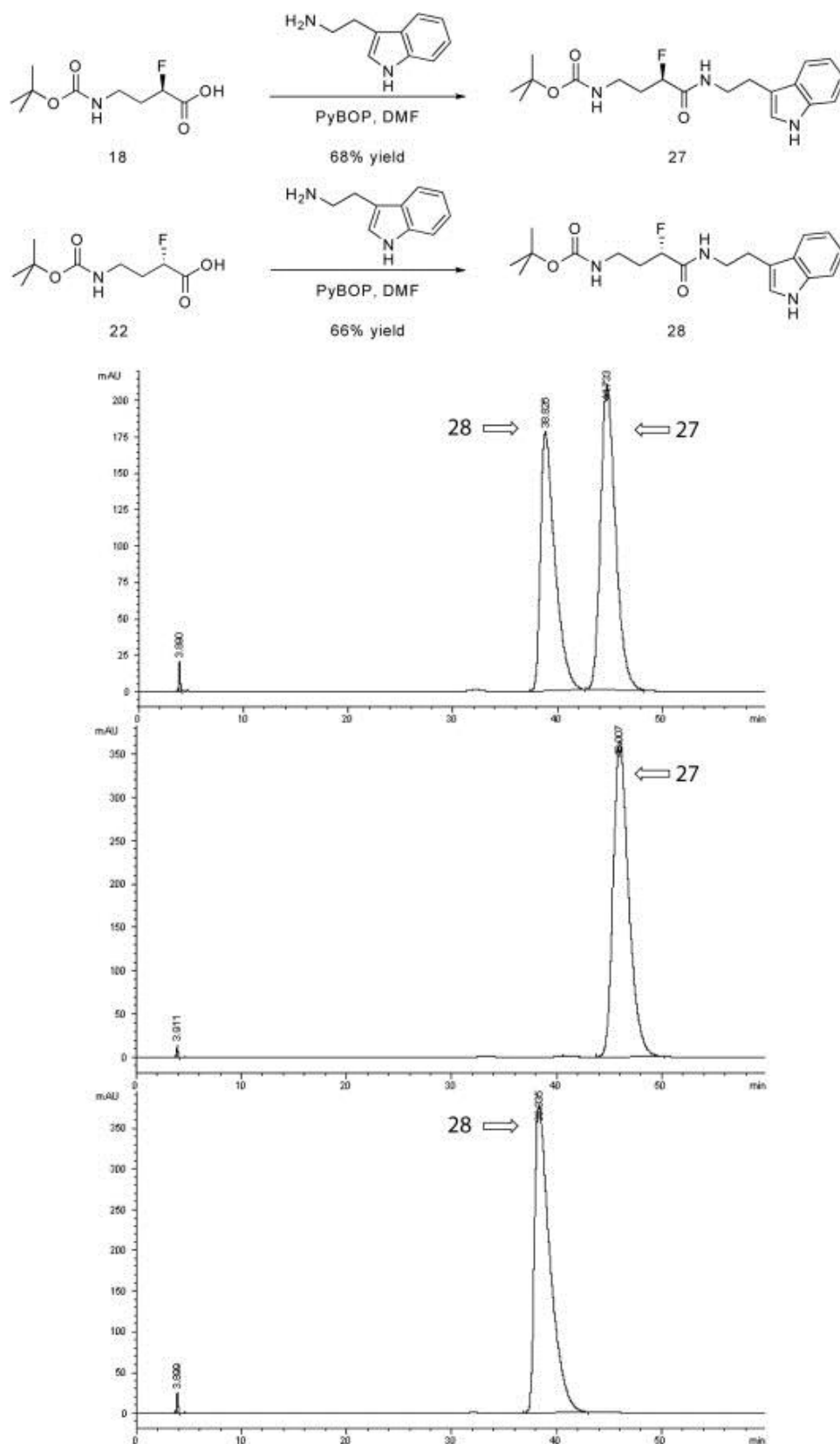


Figure 3.8 Analytical chiral HPLC assays for fluoro turn tryptamide derivatives **27** and **28**. (Top) Racemic mixture of **27** and **28**; (middle) R-enantiomer **27**; (bottom) S-enantiomer **28**.

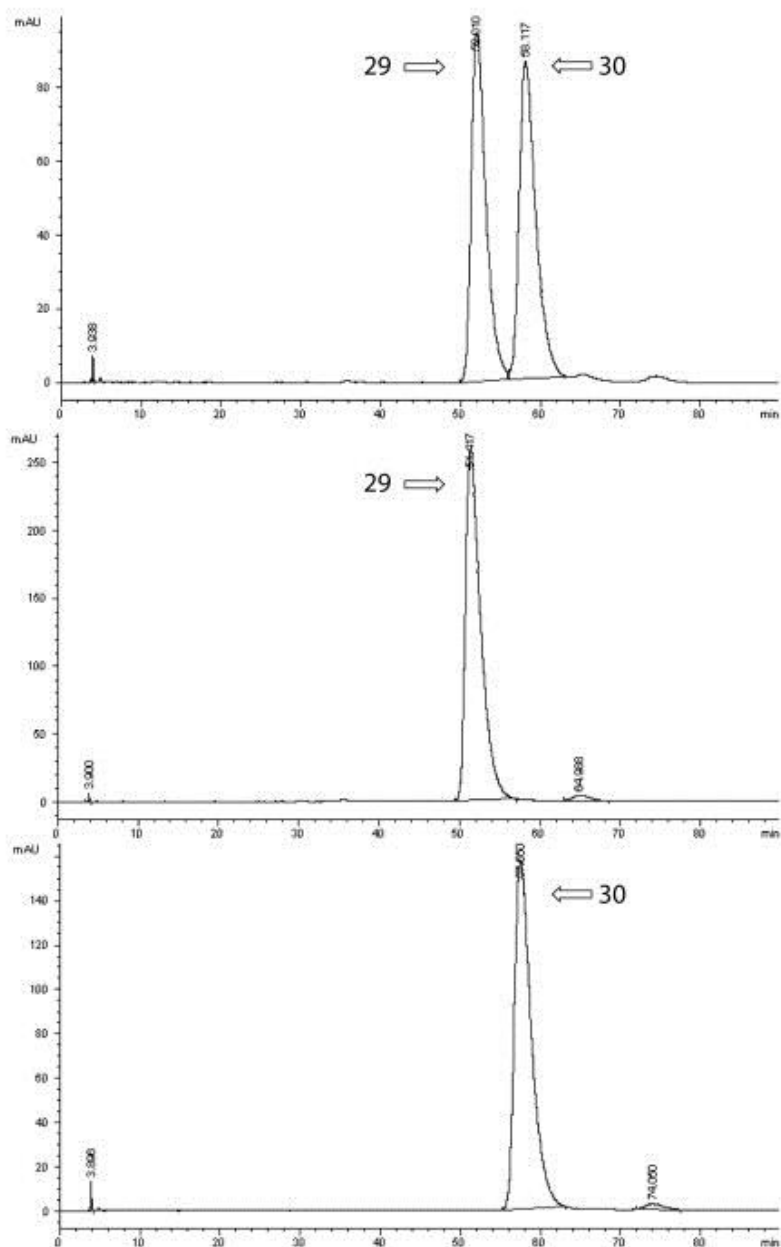
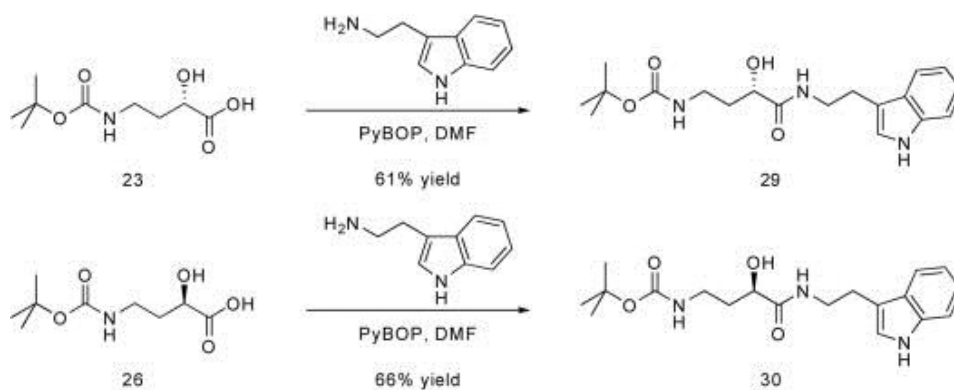


Figure 3.9 Analytical chiral HPLC assays for hydroxyl turn tryptamide derivatives **29** and **30**. (Top) Racemic mixture of **29** and **30**; (middle) *S*-enantiomer **29**; (bottom) *R*-enantiomer **30**.

3.5 Acknowledgements

We are grateful to the National Institutes of Health for research support. We thank David M. Chenoweth for helpful discussions. Mass spectrometry analyses were performed in the Mass Spectrometry Facility of the Division of Chemistry and Chemical Engineering at the California Institute of Technology.

3.6 References

- (1) Dervan, P. B. *Bioorg. Med. Chem.* **2001**. 9, 2215–2235.
- (2) Dervan, P. B.; Edelson, B. S. *Curr. Opin. Struct. Biol.* **2003**. 13, 284–299.
- (3) Best, T. P.; Edelson, B. S.; Nickols, N. G.; Dervan, P. B. *Proc. Natl. Acad. Sci. U. S. A.* **2003**. 100, 12063–12068.
- (4) Edelson, B. S.; Best, T. P.; Olenyuk, B.; Nickols, N. G.; Doss, R. M.; Foister, S.; Heckel, A.; Dervan, P. B. *Nucleic Acids Res.* **2004**. 32, 2802–2818.
- (5) Olenyuk, B. Z.; Zhang, G. J.; Klco, J. M.; Nickols, N. G.; Kaelin, W. G.; Dervan, P. B. *Proc. Natl. Acad. Sci. U. S. A.* **2004**. 101, 16768–16773.
- (6) Kageyama, Y.; Sugiyama, H.; Ayame, H.; Iwai, A.; Fujii, Y.; Huang, L. E.; Kizaka-Kondoh, S.; Hiraoka, M.; Kihara, K. *Acta Oncol.* **2006**. 45, 317–324.
- (7) Fukuda, N.; Ueno, T.; Tahira, Y.; Ayame, H.; Zhang, W.; Bando, T.; Sugiyama, H.; Saito, S.; Matsumoto, K.; Mugishima, H.; Serie, K. *J. Am. Soc. Nephrol.* **2006**. 17, 422–432.
- (8) Nickols, N. G.; Dervan, P. B. *Proc. Natl. Acad. Sci. U. S. A.* **2007**. 104, 10418–10423.
- (9) Nickols, N. G.; Jacobs, C. S.; Farkas, M. E.; Dervan, P. B. *ACS Chem. Biol.* **2007**. 2, 561–571.
- (10) Matsuda, H.; Fukuda, N.; Yao, E. H.; Ueno, T.; Sugiyama, H.; Matsumoto, K. *J. Hypertens.* **2008**. 26, S197–S197.
- (11) Kielkopf, C. L.; Baird, E. E.; Dervan, P. D.; Rees, D. C. *Nat. Struct. Biol.* **1998**. 5, 104–109.
- (12) White, S.; Szewczyk, J. W.; Turner, J. M.; Baird, E. E.; Dervan, P. B. *Nature*. **1998**. 391, 468–471.
- (13) Pelton, J. G.; Wemmer, D. E. *Proc. Natl. Acad. Sci. U. S. A.* **1989**. 86, 5723–5727.
- (14) Hsu, C. F.; Phillips, J. W.; Trauger, J. W.; Farkas, M. E.; Belitsky, J. M.; Heckel, A.; Olenyuk, B. Z.; Puckett, J. W.; Wang, C. C. C.; Dervan, P. B. *Tetrahedron*. **2007**. 63, 6146–6151.
- (15) Mrksich, M.; Parks, M. E.; Dervan, P. B. *J. Am. Chem. Soc.* **1994**. 116, 7983–7988.

- (16) Herman, D. M.; Baird, E. E.; Dervan, P. B. *J. Am. Chem. Soc.* **1998**. *120*, 1382–1391.
- (17) Zhang, W.; Minoshima, M.; Sugiyama, H. *J. Am. Chem. Soc.* **2006**. *128*, 14905–14912.
- (18) Farkas, M. E.; Tsai, S. M.; Dervan, P. B. *Bioorg. Med. Chem.* **2007**. *15*, 6927–6936.
- (19) Gellman, S. H.; Adams, B. R.; Dado, G. P. *J. Am. Chem. Soc.* **1990**. *112*, 460–461.
- (20) Appella, D. H.; Christianson, L. A.; Klein, D. A.; Powell, D. R.; Huang, X. L.; Barchi, J. J.; Gellman, S. H. *Nature*. **1997**. *387*, 381–384.
- (21) Gellman, S. H. *Accounts Chem. Res.* **1998**. *31*, 173–180.
- (22) Dose, C.; Farkas, M. E.; Chenoweth, D. M.; Dervan, P. B. *J. Am. Chem. Soc.* **2008**. *130*, 6859–6866.
- (23) Brenowitz, M.; Senear, D. F.; Shea, M. A.; Ackers, G. K. *Method Enzymol.* **1986**. *130*, 132–181.
- (24) Senear, D. F.; Dalmawiszhausz, D. D.; Brenowitz, M. *Electrophoresis*. **1993**. *14*, 704–712.
- (25) Trauger, J. W.; Dervan, P. B. *Meth. Enzymol.* **2001**. *340*, 450–466.
- (26) Pilch, D. S.; Poklar, N.; Gelfand, C. A.; Law, S. M.; Breslauer, K. J.; Baird, E. E.; Dervan, P. B. *Proc. Natl. Acad. Sci. U. S. A.* **1996**. *93*, 8306–8311.
- (27) Pilch, D. S.; Poklar, N.; Baird, E. E.; Dervan, P. B.; Breslauer, K. J. *Biochemistry*. **1999**. *38*, 2143–2151.
- (28) Trauger, J. W.; Baird, E. E.; Dervan, P. B. *Nature*. **1996**. *382*, 559–561.
- (29) Baird, E. E.; Dervan, P. B. *J. Am. Chem. Soc.* **1996**. *118*, 6141–6146.
- (30) Busby, G. W. *Ph.D. Thesis, Harvard University*. **1974**. 48–54.
- (31) Hoshi, H.; Aburaki, S.; Iimura, S.; Yamasaki, T.; Naito, T.; Kawaguchi, H. *J. Antibiot.* **1990**. *43*, 858–872.

3.7 Experimental Data

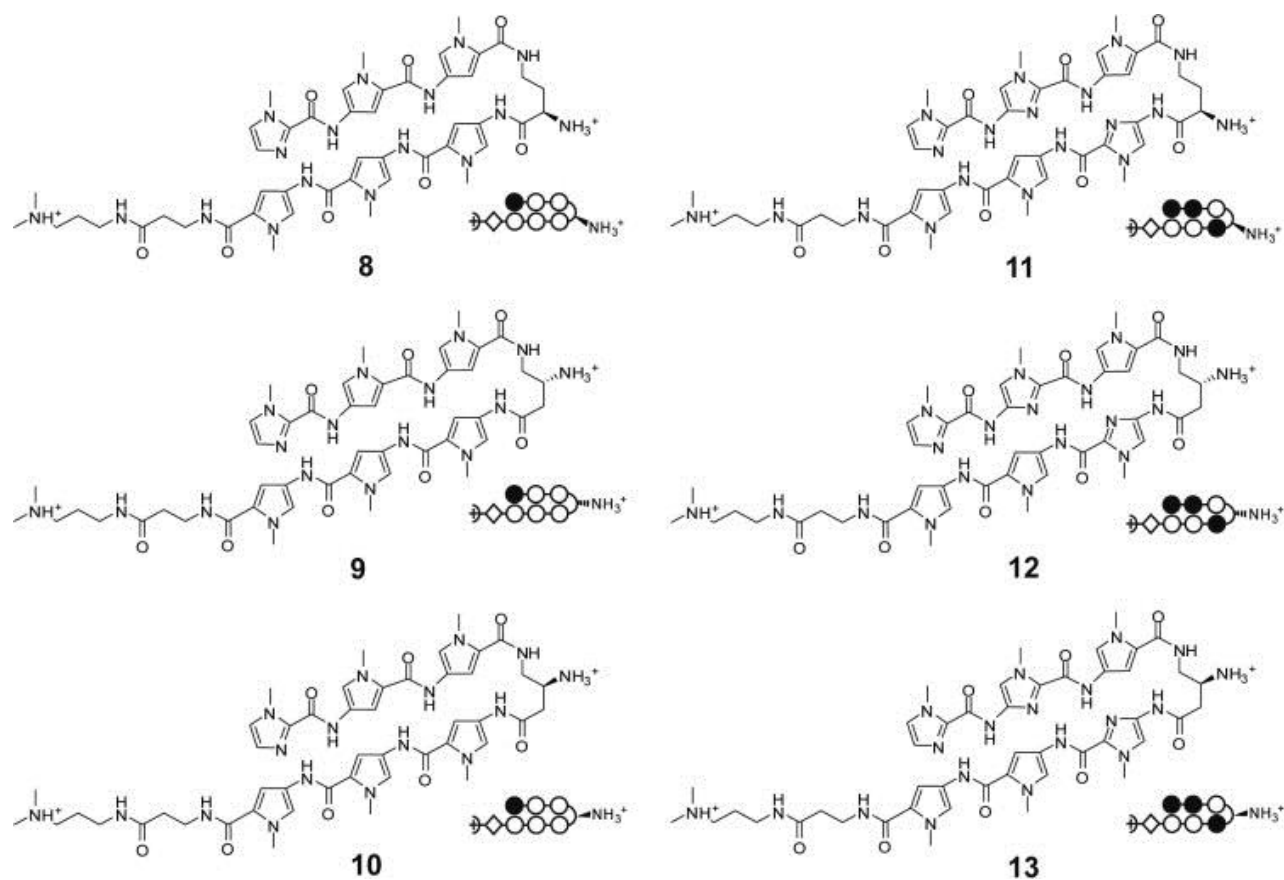


Figure 3.10 Chemical and ball-and-stick structures of polyamides targeted to 5'-WGWWW-3' (**8–10**) and 5'-WGGCW-3' (**11–13**) sequences. Ball and stick symbols are defined as follows: pyrrole is denoted by an open circle, imidazole is denoted by a filled circle, and β -alanine is denoted by a diamond shape.

DNA = 5'-CTC TGTTA CCA-3'			DNA = 5'-CTA TGTTA CCA-3'		DNA = 5'-CTC TGGCA CAC-3'		
Polyamides	$T_m / ^\circ\text{C}$	$\Delta T_m / ^\circ\text{C}$	$T_m / ^\circ\text{C}$	$\Delta T_m / ^\circ\text{C}$	Polyamides	$T_m / ^\circ\text{C}$	$\Delta T_m / ^\circ\text{C}$
—	47.3 (± 0.3)	—	44.0 (± 0.1)	—	—	56.0 (± 0.2)	—
8	58.2 (± 0.4)	10.9	59.9 (± 0.3)	15.9	11	64.3 (± 0.3)	8.3
9	60.3 (± 0.3)	13.0	62.0 (± 0.1)	18.0	12	62.7 (± 0.3)	6.7
10	58.9 (± 0.2)	11.6	61.0 (± 0.2)	17.0	13	62.0 (± 0.3)	6.0

Table 3.7 Melting temperatures of DNA/polyamide complexes **8–13**. All values are derived from at least three melting temperature experiments, with standard deviations indicated in parentheses. ΔT_m values are given as T_m (DNA/polyamide) - T_m (DNA).

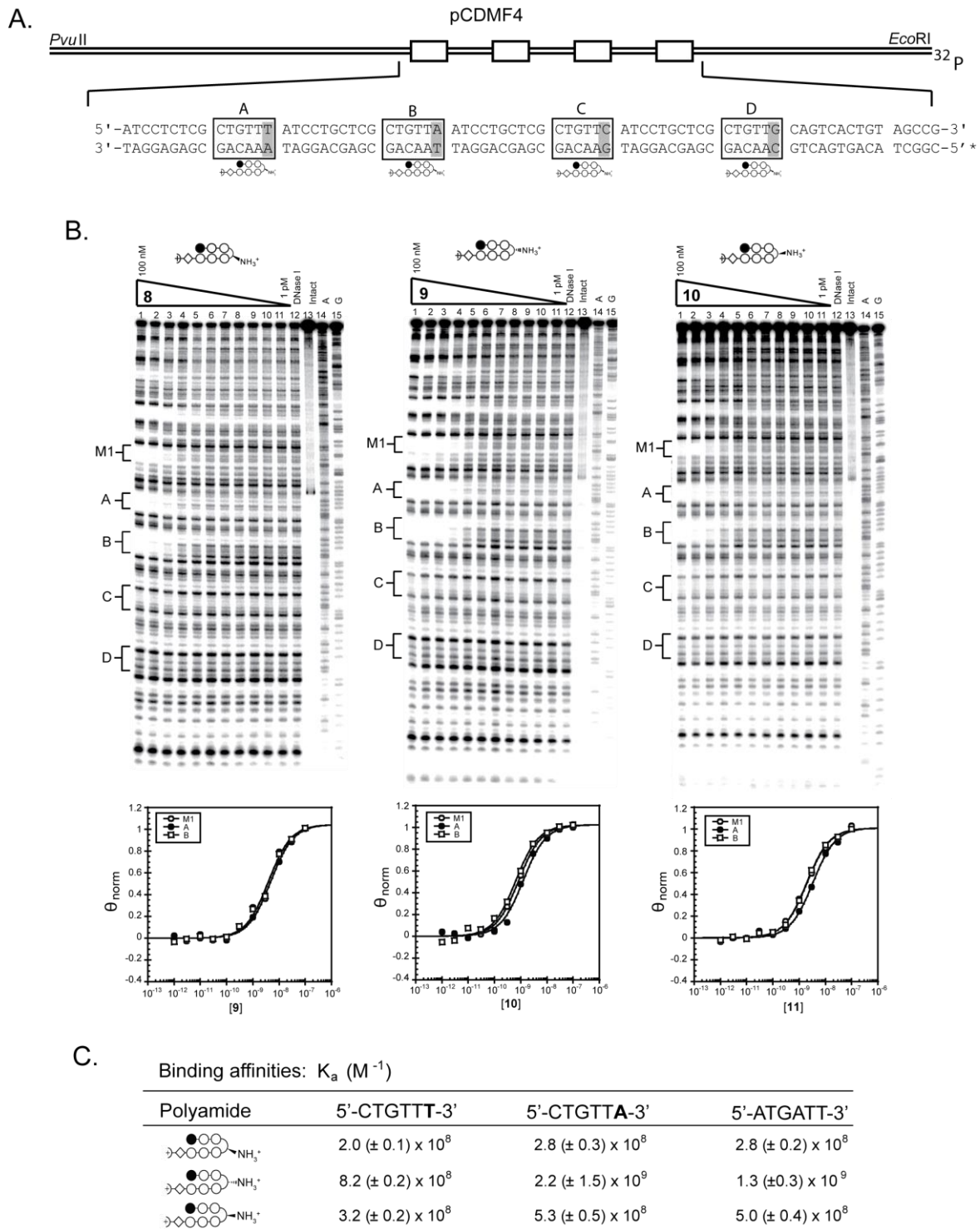


Figure 3.11 Quantitative DNase I footprinting titration experiments on (a) plasmid pCDMF4 for polyamides (b) 8–10. Lanes 1–11, 100 nM, 30 nM, 10 nM, 3 nM, 1 nM, 300 pM, 100 pM, 30 pM, 10 pM, 3 pM, and 1 pM, respectively; lane 12, DNase I standard; lane 13, intact DNA; lane 14, A reaction; lane 15, G reaction. Respective binding isotherms are shown below. (c) Table of equilibrium associations constants, reported as mean values from three DNase I footprinting titration experiments. Standard deviations are shown in parentheses.

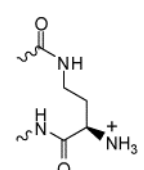
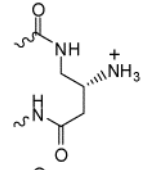
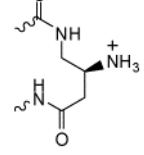
	$\frac{T}{A}$	$\frac{A}{T}$
	1.0	1.4
	1.0	2.7
	1.0	1.6

Table 3.8 Relative binding affinities for polyamides **8–10**. (a) Relative binding affinities are reported as ratios of binding affinities (K_a) as determined by DNase I footprinting titration experiments for polyamides targeting 5'-WGWW-3'. Sites containing G•C and C•G at the hairpin position have relative affinities < 0.01 (not shown).

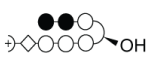
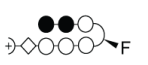
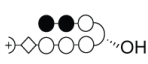

DNA = 5'-CTATGGTTGAC-3'			
	Polyamides	$T_m / ^\circ\text{C}$	$\Delta T_m / ^\circ\text{C}$
	—	46.7 (± 0.4)	—
6R		57.4 (± 0.4)	10.7
7R		55.1 (± 0.1)	8.4
6S		52.3 (± 0.2)	5.6
7S		55.4 (± 0.2)	8.7

Table 3.9 Melting temperatures of DNA/polyamide complexes for **6R**, **7R**, **6S**, and **7S**. All values are derived from at least three melting temperature experiments, with standard deviations indicated in parentheses. ΔT_m values are given as T_m (DNA/polyamide) – T_m (DNA).

Chapter 4

Synthetic Advances Underpinning the Biological Studies of Hairpin Polyamides

The text of this chapter was taken in part from the manuscripts cited below (California Institute of Technology).

1. Synold, T. W.; Xi, B.; Wu, J.; Yen, Y.; Li, B.C.; Yang, F.; Phillips, J.W.; Nickols, N.G.; Dervan, P.B. “Single-dose pharmacokinetic and toxicity analysis of pyrrole-imidazole polyamides in mice” *Cancer Chemother. Pharmacol.* **2012**, 70, 617–625.
2. Yang, F.; Nickols, N.G.; Li, B.C.; Marinov, G.; Wold, B. J.; Dervan, P.B. “Antitumor activity of a DNA minor groove binding Py-Im polyamide” *Proc. Natl. Acad. Sci. U.S.A.* **2013**, 110, 1863–1868.
3. Nickols, N.G.; Szablowski, J.; Hargrove, A.E.; Li, B.C.; Raskatov, J.A.; Dervan, P.B. “Activity of a Py-Im polyamide targeted to the estrogen response element” *Mol. Cancer Ther.* accepted **2013**.

Abstract

Py-Im polyamides targeted to the sequence 5'-WGWWCW-3', found in the consensus androgen response element (ARE), have been used to modulate AR-mediated gene transcription in LNCaP prostate cancer cell lines. To study these biological effects in an animal model, hairpin polyamides **1** and **2** have been administered to mice for pharmacokinetic characterization. The antitumor activity of **1** was further analyzed in a prostate tumor xenograft model, and the mice treated with **1** had smaller tumors and lower serum prostate-specific antigen (PSA) compared to untreated controls. In an effort to expand the scope of biological targets, polyamide **3** targeted to the estrogen response element (ERE) has also been synthesized and displayed favorable gene regulatory effects in T47D-KBLUC breast cancer cells and xenograft models.

4.1. Introduction

The androgen receptor (AR) is a member of the nuclear hormone receptor family of transcription factors.¹ Upon ligand binding, AR is released from the cytoplasm and translocated to the nucleus, where AR dimers can bind to the androgen response elements (ARE) of target genes and activate transcription.² AR-mediated gene expression is essential to normal prostate development and contributes to the progression of prostate cancer.³ While anti-androgen therapies are initially successful in slowing prostate cancer growth, nearly all patients eventually develop hormone refractory disease.⁴⁻⁶ Rather than targeting the AR ligand-binding domain, direct perturbation of the AR–ARE interactions may disrupt AR-induced transcriptional activity even in hormone-refractory conditions. Py-Im polyamide **1**, designed to bind the 5'-WGWWCW-3' sequence found in the consensus ARE, was previously shown to downregulate the expression of AR-driven genes in LNCaP prostate cancer cells.⁷

To further investigate the antitumor activity of ARE-targeted polyamides in animal models, hairpin polyamides **1** and **2** have been administered to both normal and LNCaP-engrafted mice. Compared to cell culture assays, animal studies often require significantly larger quantities of polyamide substrates. By combining solution-phase tetramer synthesis methods and microwave-assisted solid-phase techniques,^{8,9} **1** and **2** have been regularly synthesized on a 50-mg scale in an efficient and reliable manner. The pharmacokinetic profiles of **1** and **2** were then analyzed by intravenous (IV) tail vein injection into normal mice. While the biodistribution and toxicity profiles were significantly different, the plasma concentrations of both compounds were measured at levels higher than required for gene regulation in cell culture. Since it was less toxic to the animal host, **1** was administered subcutaneously (SC) to mice engrafted with LNCaP cells. Compared to vehicle controls, the mice treated with three injections of **1** had smaller tumors and decreased serum PSA levels.

While this *in vivo* toxicity is consistent with the perturbation of AR-mediated transcription by **1**, there has also been mounting evidence in support of two alternate mechanisms. Genome-wide mapping of RNA polymerase II (RNAP2) occupancy using ChIP-seq showed preferential perturbation by **1** at transcription start sites (TSS). Along with an observed decrease in RNAP2 large subunit RPB1 levels following polyamide treatment, this suggests that the tumor reduction effects may result from inhibition of RNAP2 activity. The proapoptotic activity of **1** in AR-negative DU145 cells supports an AR- independent mechanism. Cell cycle analysis revealed polyamide-induced S-phase accumulation caused by inhibition of replicative helicase and subsequent stalling of replication forks. Although it is unclear how each of these pathways contributes toward tumor toxicity, it has been shown that the antitumor activity of **1** is not a result of DNA damage.

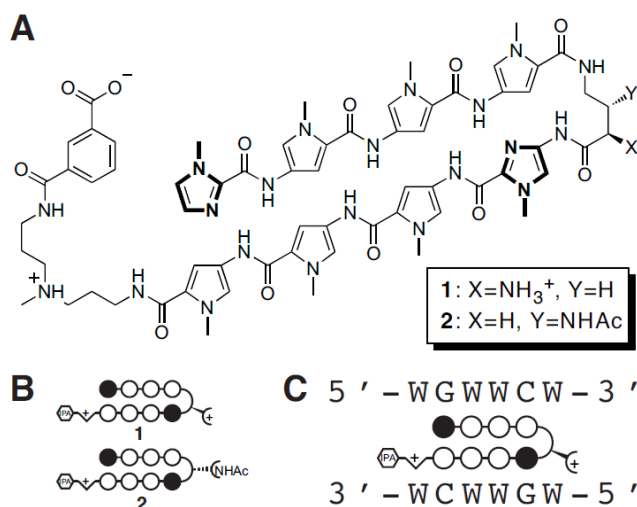


Figure 4.1 Chemical structure and binding preferences of the Py-Im polyamides **1** and **2**. (A) Chemical structure showing the two different turn functionalities. (B) Ball-and-stick representation of the polyamides. Open circles represent N-methylpyrrole residues, filled circles represent N-methylimidazoles. The hexagon represents the isophthalic acid moiety. (C) Hairpins **1** and **2** bind the same 5'-WGWWCW-3' DNA sequence, where W = A or T.

In a parallel effort to expand the scope of biological targets, polyamide **3** targeted to the 5'-WGGWCW-3' sequence found in the estrogen response element (ERE) was used to modulate estrogen receptor (ER)-mediated transcription in T47D-KBLUC breast cancer cells. Upon treatment with **3**, the expression of E2-activated genes such as *TFF1* and *WT1* were downregulated, whereas E2-suppressed expression of *TGFB2* was de-repressed. Furthermore, **3** was administered into mice engrafted with T47D-KBLUC, and the luciferase output in polyamide-treated mice were significantly lower compared to untreated controls. Unlike treatment with **1**, however, the tumor sizes remained largely unaffected by **3**, even under an extended 9-dose regimen.

4.2 Results and Discussion

I. Microwave-Assisted Synthesis of Hairpin Polyamides

As our biological research has progressed from cell culture to mice models, the reliable and efficient synthesis of hairpin polyamides has become crucial. With the recent development in microwave-assisted methods, the solid-phase synthesis of an 8-ring polyamide core can now be completed within days at dramatically improved yields of up to 56% recovery.⁹ In order to further improve and expedite the synthetic process to meet increasing demands for biological assays, the synthesis of polyamides **1–3** have been further streamlined by combining the use of tetramers **6** and **7** under microwave-assisted conditions (Fig. 4.2). In this retrosynthetic approach, the polyamide cores **15–17** were quickly assembled from intermediate **12** by sequential couplings of turn **9** or **10** and tetramer **6** or **7**. Following amine cleavage of **15–17**, the isophthalate conjugation, turn deprotection and acetylation steps have all been optimized in a peak-to-peak fashion (Fig. S4.1–S4.3). The DNA binding properties of **1–3** to the corresponding match sequences have been assessed by thermal denaturation assays (Fig. S4.4–S4.6).

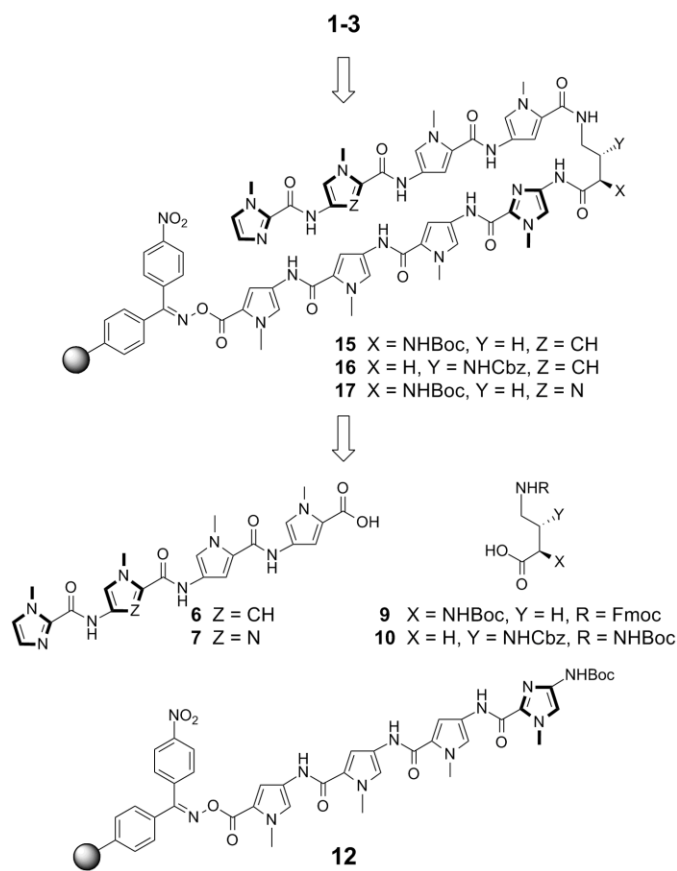
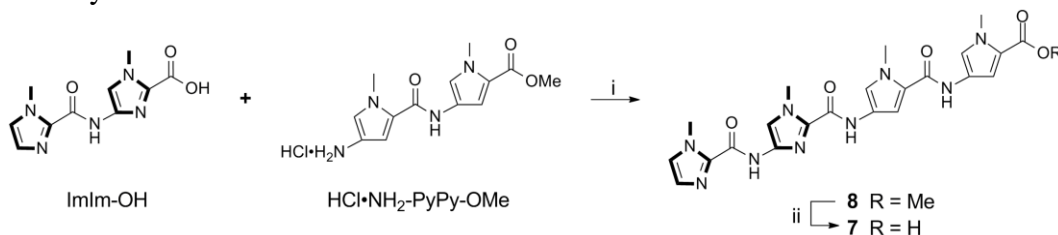


Figure 4.2 Retrosynthetic strategy towards hairpin polyamides **1-3**.

While the chiral turn units **9** and **10** are both commercially available and **6** has been obtained on a gram scale,⁸ the synthesis of **7** has not been previously reported. Starting with the ImIm-OH dimer, coupling with HCl•NH₂-PyPy-OMe under PyBOP-activated conditions afforded **8**, which was then saponified under basic conditions to afford tetramer **7** in 83% yield.

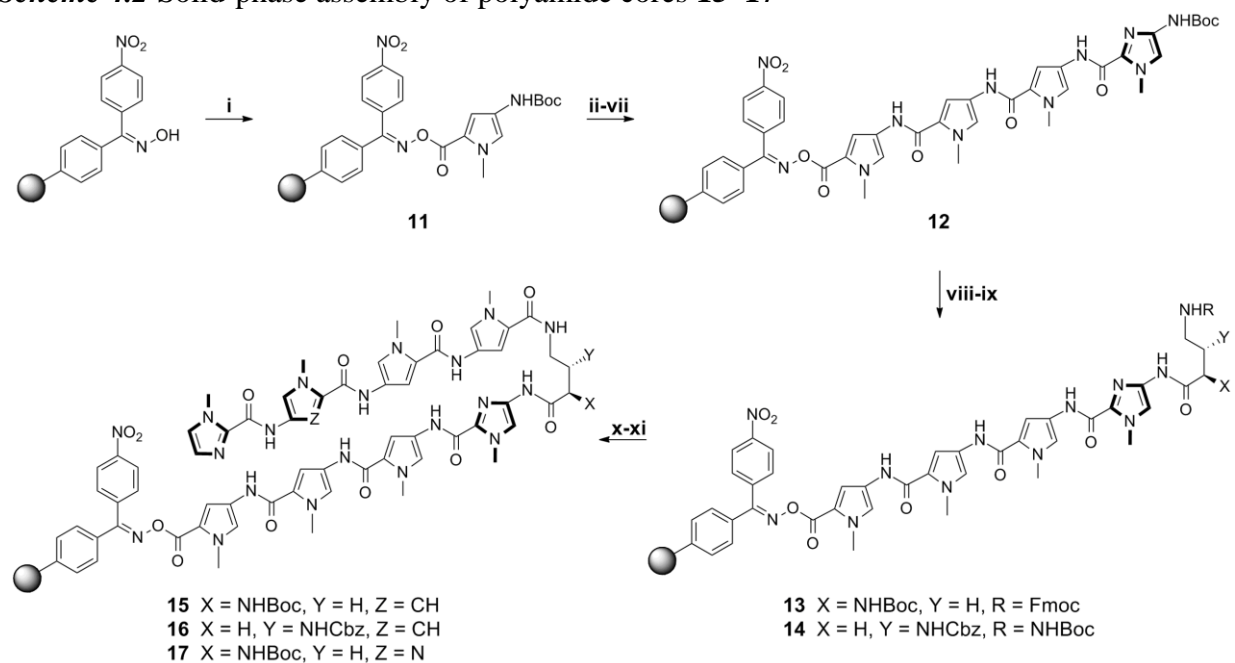
Scheme 4.1 Synthesis of tetramer intermediate **7**



¹Reagents and conditions: (i) PyBOP, DIEA, DMF; (ii) NaOH, MeOH.

The polyamide cores **15–17** were rapidly assembled on oxime resin via microwave-assisted conditions. Following the initial loading of BocPyOH to give **11**, three deprotection-coupling cycles with the corresponding monomers using the published protocols yielded intermediate **12**. The turn units **9** or **10** were then coupled under microwave irradiation to afford **13** or **14**. In particular, the protection group strategy on turn **9** and thereby **13** was reversed from the traditional Fmoc-D-Dab(Boc)-OH turn. This circumvented the need to deprotect the Fmoc turn and replace it with a Boc group following completion of the polyamide core, and was made possible only by using the tetramers **6** and **7**. Deprotection of the terminal Fmoc group in **13** using 20% piperidine, or the terminal Boc group in **14** using 80% trifluoroacetic acid (TFA), followed by microwave-assisted coupling of **6** or **7**, yielded polyamide core **15–17**.

Scheme 4.2 Solid-phase assembly of polyamide cores **15–17**

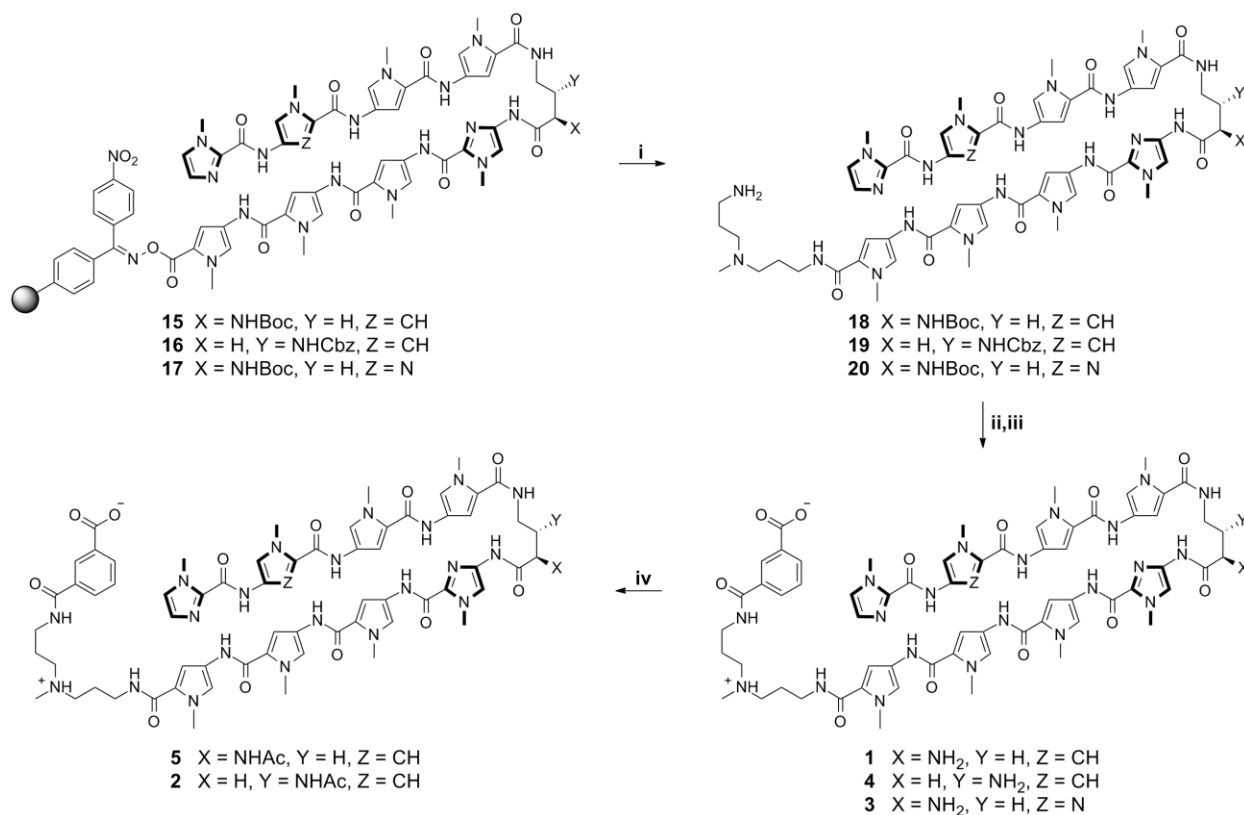


¹All PyBOP-mediated coupling conditions were performed under microwave-assisted conditions (Ref. 9)

²Reagents and conditions: (i) BocPyOH, PyBOP, DIEA, DMF; (ii) 80% TFA, DCM; (iii) BocPyOH, PyBOP, DIEA, DMF; (iv) 80% TFA, DCM; (v) BocPyOH, PyBOP, DIEA, DMF; (vi) 80% TFA, DCM; (vii) BocImOH, PyBOP, DIEA, DMF; (viii) 80% TFA, DCM; (ix) **9** (for **1**, **3** & **5**) or **10** (for **2** & **4**), PyBOP, DIEA, DMF; (x) 20% piperidine in DMF (for **1**, **3** & **5**) or 80% TFA in DCM (for **2** & **4**); (xi) **6** (for **1**, **2**, **4** & **5**) or **7** (for **3**), PyBOP, DIEA, DMF.

Starting from **15–17**, polyamides **1–5** were then obtained in several optimized steps in 24–37% yield overall. Cleavage of the resin-bound **15–17** with neat 3,3'-diamino-N-methyldipropylamine under microwave irradiation afforded triamine intermediates **18–20**, which were purified by HPLC and recovered in 36–52% yield. Previous concerns on the epimerization of the chiral turn amino group by these relatively harsh conditions were mitigated by reports from Puckett et al, which showed a retained stereochemistry of the Mosher amide derivatives using UPLC assays.⁹ Isophthalic acid conjugation onto the tail primary amine of **18–20**, followed by turn deprotection under acidic conditions, afforded polyamides **1**, **4** and **3**. Finally, **5** and **2** were obtained by acetylation of the amino turn in **1** and **4**, respectively.

Scheme 4.3 Synthesis of hairpin polyamides **1–5**



¹Reagents and conditions: (i) 3,3'-diamino-N-methyldipropylamine; (ii) Isophthalic acid, PyBOP, DIEA, DMF; (iii) TFA (for **1**, **3** & **5**) or 10% TFMSA in TFA (for **2** & **4**); (iv) Ac₂O, pyridine, DMF (for **2** & **5**).

II. Pharmacokinetic Studies of Polyamides **1** and **2**

Recently, polyamide **1** designed to bind a 5'-WGWWCW-3' sequence found in the consensus androgen response element (ARE), and thereby disrupt the androgen receptor (AR)-ARE interaction, was found to decrease the expression of AR-driven genes in LNCaP prostate cancer cells under dihydrotestosterone (DHT)-induced conditions.⁷ Polyamide derivative **2** has been developed and shown to exhibit the equivalent activity to **1** at ten-fold less concentration.¹⁰ In order to extend our research on the antitumor activity of polyamides *in vivo*, we have characterized the pharmacokinetic (PK) and toxicology profiles of **1** and **2** in mice models.

Following polyamide administration by a single intravenous tail injection, the blood plasma concentrations of **1** and **2** were monitored at various time points over a 24-hour time period using LC/MS/MS methods (Fig. 4.3A). Interestingly, despite an higher initial dose of 7.5 mg/kg for **1**, relative to 5 mg/kg for **2**, the area under the concentration curve (AUC) of **1** (67.5 µg/mL x hr) was twofold lower than **2** (144.8 µg/mL x hr). Tissue analysis further revealed a significantly higher concentration of **2** in liver, kidney and lung samples (301.3, 424.7 and 523.5 µg/mL x hr, respectively), as compared to **1** (157.7, 299.2 and 130.6 µg/mL x hr, respectively) (Fig. 4.3B). Additionally, weight curve experiments showed polyamide **2** to be more toxic than **1** (Fig. 4.3C). Animals treated with **1** only showed significant weight loss at the highest single injection of 10 mg/kg and otherwise displayed no signs of physical duress, whereas the mice administered with 4.5 mg/kg and 2.3 mg/kg doses of **2** not only lost more than 15% of body mass but also exhibited additional signs of physical duress. While the exact mechanisms behind these differences remain unclear, this nonetheless highlights the significant effects of minor structural modifications in mice models, and forms a valuable foundation for our future studies *in vivo*.

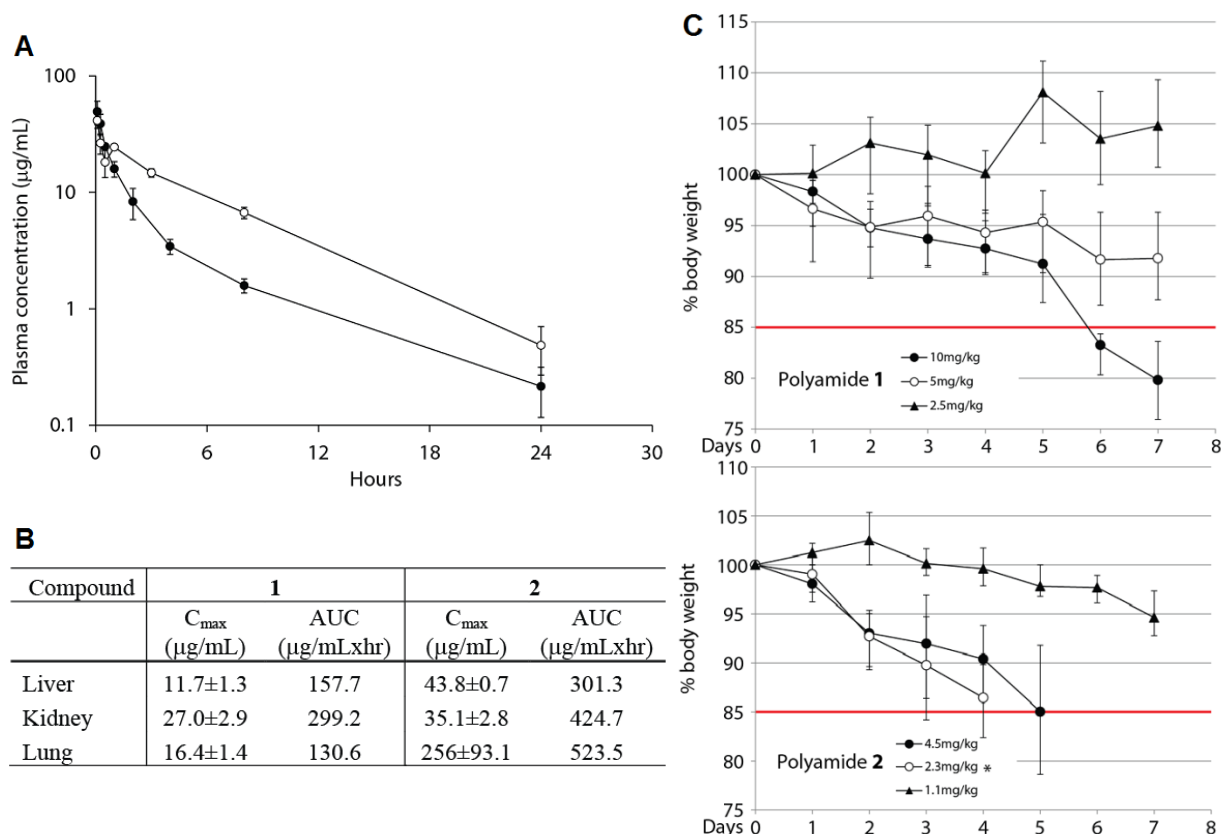


Figure 4.3 Biodistribution and toxicity profile of **1** and **2** in mice. (A) Plasma concentration versus time curves for **1** (closed circles) and **2** (open circles). Error bars indicate standard deviation. (B) Tissue pharmacokinetic parameters of **1** and **2** after a single IV injection. (C) Animal toxicity experiments for polyamides **1** and **2**. Animals were injected on day 0 and monitored for 7 days for weight loss and signs of duress. Error bars indicate standard deviation, $n = 4$ (* $n = 3$).

III. Antitumor Activity of Polyamide 1 in Prostate Tumor Xenografts

After establishing the PK and toxicity profiles of **1** in mice, we set forth to explore its antitumor activity in a prostate tumor xenograft model. Male immunocompromised NOD scid gamma (NSG) mice were engrafted with LNCaP cells (2.5 million cells) and the tumors were allowed to grow to $\sim 100 \text{ mm}^3$ prior to treatment. Vehicle control or 20 nmol ($\sim 1.4 \text{ mg/kg}$) polyamide **1** was then administered by subcutaneous (SC) injection once every 3 days. Following a cycle of three injections, the mice treated with **1** had noticeably smaller tumors (mean = 112

mg) compared to vehicle controls (mean = 310 mg) (Fig. 4.4A). Furthermore, serum PSA levels were measured by ELISA and found to be significantly lower in the polyamide-treated mice (Fig. 4.4B).

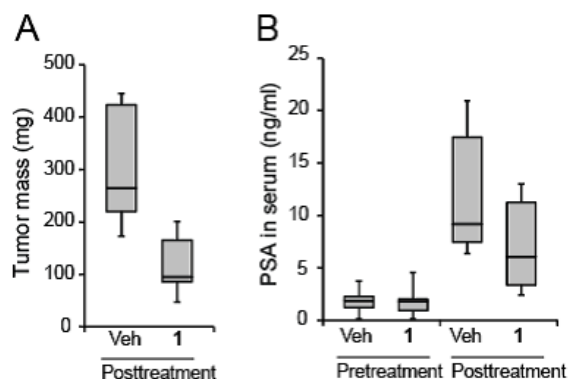


Figure 4.4 Polyamide **1** demonstrates anti-tumor activity in prostate cancer xenografts. (A) Male immunocompromised mice were engrafted with LNCaP cells and observed until tumors reached $\sim 100 \text{ mm}^3$. Tumor bearing mice were then treated with 20 nmol **1** ($n = 12$) or vehicle ($n = 13$) by SC injections into the flank distal to the tumor once every three days for a total of three injections. Mice were euthanized and tumors resected and weighed two days after final injection. Tumors from mice treated with **1** were smaller (mean: 112 mg, median: 94 mg; range: 47–201 mg) than those of vehicle treated mice (mean: 310 mg, median: 292 mg, range: 173–440 mg). Error bars represents max and min, boxes represents the upper and lower quartiles and median. $p = 1.6 \text{ E-}5$. (B) Serum PSA measured by ELISA pre- and post- treatment. Serum PSA is lower in the post-treatment serum of mice treated with **1** as compared to vehicle. $p = 0.024$.

Perhaps more importantly, tumor-free NSG mice treated with **1** under the same regimen showed no signs of physical duress or weight loss, whereas the LNCaP tumor-bearing NSG mice exhibited substantial weight loss by the experimental end point (Fig. 4.5). While this host toxicity may initially appear undesirable towards cancer therapeutic applications, the observed elevation in serum uric acid levels may be an indication of tumor lysis syndrome that is commonly associated with rapid tumor cell turnover.¹¹ In future studies, a key to overcoming this challenge will be finding the optimal polyamide concentration that yields maximum tumor reduction but causes minimal toxicity to the host.

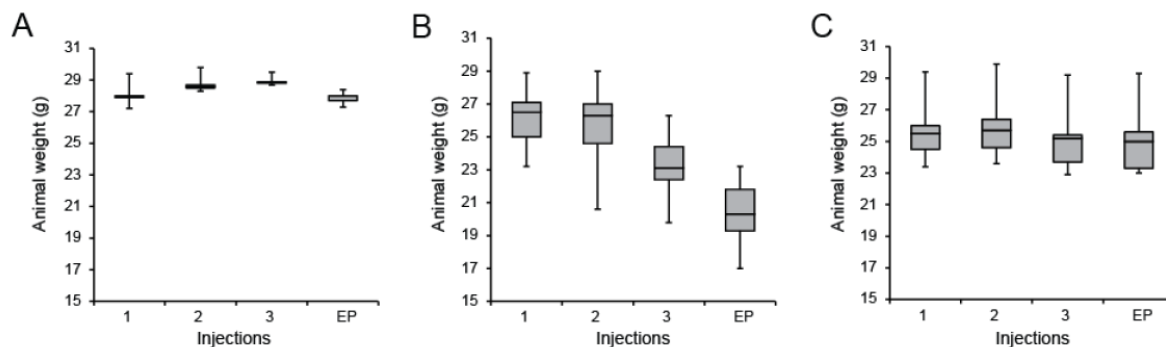


Figure 4.5 Animal weights were measured at each injection of **1** and at the experimental endpoint (EP). (A) Weight measurements of tumor free male immunocompromised mice treated with 20 nmol of **1** once every 3 days for 3 injections (n = 5). (B) Weight measurements of LNCaP tumor bearing male immunocompromised mice treated with 20 nmol of **1** once every 3 days for 3 injection (n = 12). (C) Weight measurements of LNCaP tumor bearing male immunocompromised mice treated with vehicle (5% DMSO in PBS) once every 3 days for 3 injections (n = 13). Experiments were end pointed 2 days after last injections. Error bars represents max and min, boxes represents the upper and lower quartiles and median.

IV. Transcription Regulation and in vivo Activity of ERE-Targeting Polyamide 3

In parallel to our efforts towards polyamide treatment of prostate cancer, Py-Im polyamide **3** targeted to the 5'-WGGWCW-3' sequence found in the estrogen response element (ERE) were synthesized and applied towards regulation of estrogen receptor (ER)-mediated transcription in T47D-KBLUC breast cancer cells (Fig. 4.6).

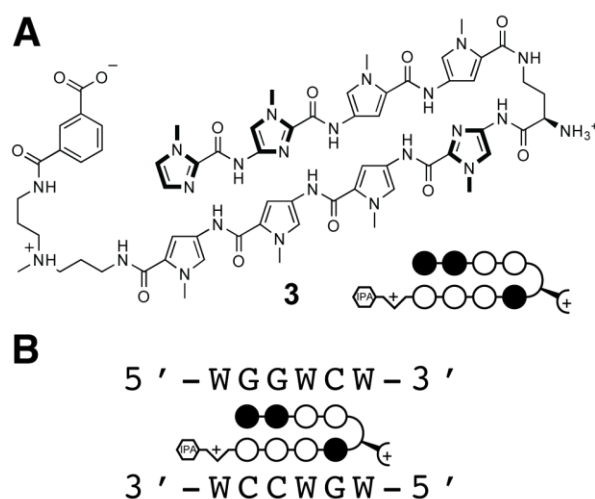


Figure 4.6 Chemical structure and binding preferences of **3**. (A) Chemical structure and ball-and-stick representation of **3**. (C) Polyamide **3** bound to its match 5'-WGGWCW-3' sequence.

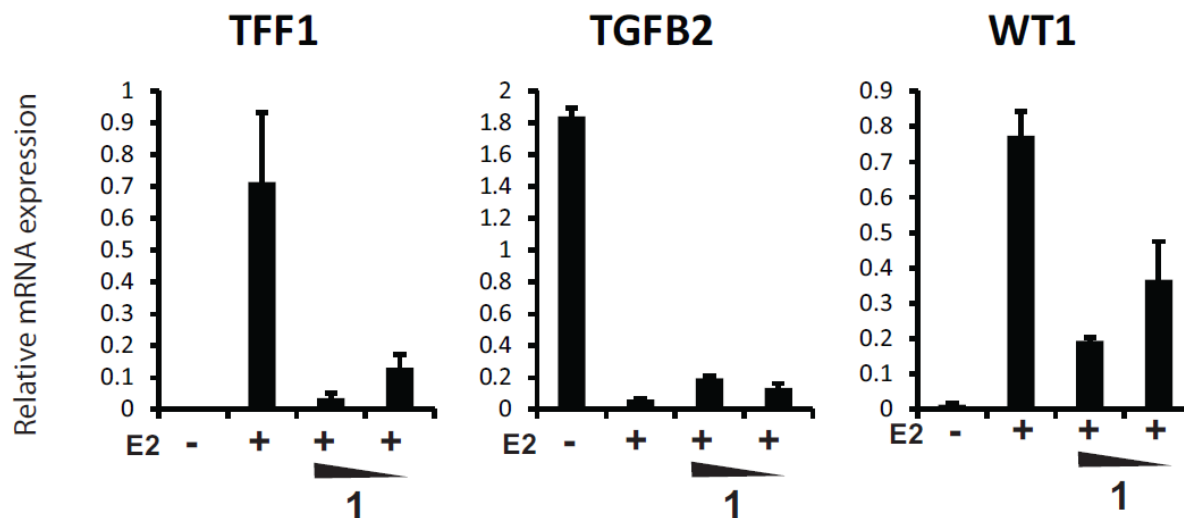


Figure 4.7 Relative mRNA levels of *TFF1*, *TGFB2* and *WT1* measured by qRT-PCR. Concentrations of **1** are 1.0 μ M and 0.3 μ M.

The genome-wide effects on 17- β -estradiol (E2)- induced gene expression upon treatment with 1 μ M **3** were analyzed by RNA-seq and confirmed by RT-qPCR (Fig. 4.7). Among the subset of E2-activated genes affected by **3**, many are important to tumor development and therapeutically relevant. In particular, Wilms Tumor 1 (*WT1*) expression is detectable in 90% of breast cancers and high levels of WT1 expression are correlated with poor survival rates,^{29,30} while *TFF1* is another predictor for breast cancer patient survival.³¹ On the other hand, the expression of transforming growth factor- β 2 (*TGF- β 2*) is strongly repressed by E2 and de-repressed three-fold by **3** at 1 μ M.³² While these genes most affected by E2 are counteracted by **3** in an anti-estrogenic manner, the majority of E2-regulated genes remain unresponsive to **3**. Furthermore, most of the gene expression changes by **3** are unrelated to E2 activity, suggesting an alternative mechanism of action.

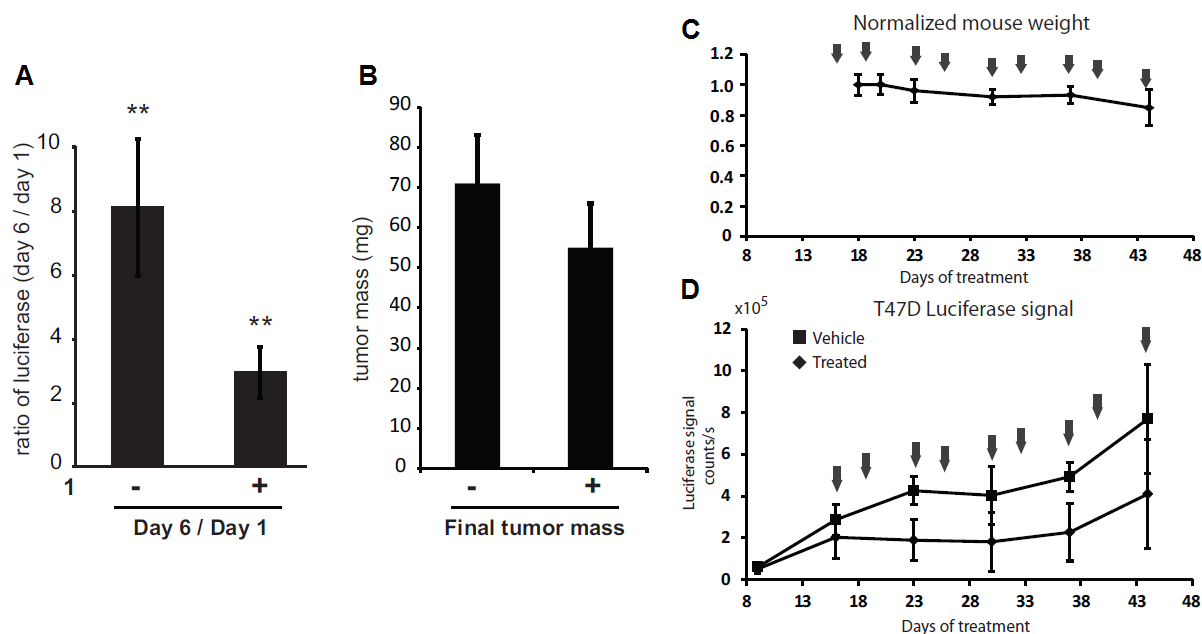


Figure 4.8 Xenograft studies. (A) Treatment of T47D-KBLUC bearing mice with **1** results in suppression of ER-driven luciferase. $**p < 0.01$. $n = 12$ mice per group. Errors are 95% CI. (B) Tumors masses at experimental endpoint were vehicle: 71 ± 12 mg (95% CI); **1**: 55 ± 11 mg (95% CI). (C) Treatment schedule for extended time-course experiments with normalized mouse weights over time. Arrows indicate treatment days. (D) Luciferase signal for polyamide **1** and vehicle treated groups. Error bars are standard deviations. Mean tumor masses at the endpoint for animals treated with vehicle is 165 ± 27 mg (95% CI) and for animals treated with **1** is 128 ± 54 mg (95% CI).

To further characterize the anti-estrogenic activity of **3** *in vivo*, T47D-KBLUC cells were engrafted into female NSG mice and supplemented with a slow-release subcutaneous E2 pellet in the right flank to facilitate E2-induced growth. After one week of growth, the mice were treated with either vehicle control or 25 nmol (~ 1.7 mg/kg) polyamide **3** via subcutaneous injection into the left flank every other day for a total of four injections. Following three injections, the luciferase output increased an average of three-fold for the mice treated with **3**, as compared to an eight-fold increase for the vehicle treated mice (Fig. 4.8A). The tumors were resected and weighed following the fourth injection, and the tumor masses of the mice treated with **1** (55 ± 11 mg) were found to be comparable to the vehicle controls (71 ± 12 mg) (Fig. 4.14B). To

investigate the effects of extended treatment with **3**, the same experiment setup was employed with a regimen of 9 injections over 25 days. Interestingly, the mice did not lose a significant amount of weight ($> 15\%$) until the final days of treatment (4.8C). Consistent with prior findings, the luciferase activity was consistently lower in the mice treatment with **3** (Fig. 4.8D).

4.3 Conclusions

In light of the regulation of AR-driven gene expression by **1** in LNCaP prostate cancer cells, the antitumor activity of **1** have been examined in mice models. The pharmacokinetic and toxicity profiles of **1** and **2** have been established in normal mice, and tumor growth inhibition was observed in LNCaP-engrafted immunocompromised mice administered with **1** relative to untreated controls. In addition to our studies on the biological effects of **1** in prostate cancer models, polyamide **3** designed to bind the ERE has also been shown to downregulate ER-driven luciferase signal in T47D-KBLUC breast cancer cell culture and mice xenografts.

A main challenge in future studies

Furthermore, preliminary *in vivo* studies have highlighted the significant changes in biological activity resulting from minor structural modifications in both hairpin and cyclic polyamides, so another priority will be testing for the right polyamide structure that offers the optimal therapeutic window. Finally, other polyamides that have been previously shown to modify the gene regulation of other transcription factors, such as HIF-1 α and glucocorticoid receptor (GR), shall also be examined for their *in vivo* effects.

4.4 Materials and Methods

Materials

All chemicals were purchased from Sigma-Aldrich, unless otherwise specified. Kaiser oxime resin and PyBOP were purchased from NovaBioChem. (*R*)-3,4-Cbz-Dbu(Boc)-OH was purchased from Peptides International. Fmoc-D-Dab(Boc)-OH was purchased from Bachem.

Methods

Polyamide monomers were obtained using previous protocols.³³ Microwave-assisted coupling reactions were conducted on a Biotage Initiator Eight synthesizer. Polyamides were purified via preparative HPLC on an Agilent Technologies 1200 Series system using a Phenomenex Gemini column. Matrix-assisted, LASER desorption/ionization time-of-flight mass spectrometry (MALDI-TOF MS) was performed on an Applied Biosystems Voyager DR Pro spectrometer. NMR spectroscopy data was obtained on a Varian instrument operating at 500 MHz. Polyamide concentrations were measured in 20% MeCN in 0.1% (v/v) aqueous TFA using an approximated extinction coefficient of $69\,200\text{ M}^{-1}\text{ cm}^{-1}$ at λ_{max} near 310 nm.³⁴

I. Microwave-Assisted Synthesis of Hairpin Polyamides

***ImImPyPyOH* (7).** A solution of ImImOH dimer (909 mg, 3.65 mmol) and PyBOP (2.3 g, 4.38 mmol, 1.2 eq.) in DIEA (1.9 mL, 11.0 mmol) and DMF (5 mL) was stirred for 10 min. The solution was then added to HCl•NH₂-PyPy-OMe (1.25 g, 3.83 mmol, 1.05 eq.) in DMF (10 mL) and stirred at 23 °C for 36 h. Upon confirmation of reaction completion by analytical HPLC, this solution was then added to dH₂O (80 mL) preacidified with aqueous HCl (1N, 11.0 mL, 11.0 mmol), yielding a precipitate that was isolated by centrifugation (~4200 rpm). The residual solid

was resuspended in dH₂O (80 mL), triturated, and collected by centrifugation (repeated 2×) to yield **8**. Without further purification or drying, this crude material was dissolved in a mixture of aqueous NaOH (1N, 40 mL, 40 mmol) and MeOH (40 mL), and stirred at 40°C for 16 hr. After analytical HPLC confirmed complete saponification, this solution was added to dH₂O (40 mL) preacidified with aqueous HCl (1 N, 40 mL, 40 mmol), yielding a precipitate that was isolated by centrifugation (4200 rpm). The residual solid was resuspended in dH₂O (80 mL) and collected by centrifugation (repeated 2×). The resultant solid, containing a small amount of residual H₂O, was frozen and lyophilized to dryness. The dried solid was then triturated with anhydrous Et₂O, filtered over a sintered glass funnel, washed with copious amounts of anhydrous Et₂O, and dried *in vacuo* to yield tetramer **7** as a tan solid (1.5 g, 3.04 mg, 83% yield). ¹H NMR [499.7 MHz, DMSO-d₆]: δ 12.15 (br s, 1 H), 10.36 (s, 1 H), 9.95 (s, 1 H), 9.73 (s, 1 H), 7.57 (s, 1 H), 7.46 (d, *J* = 1.0 Hz, 1 H), 7.43 (d *J* = 2.0 Hz, 1 H), 7.28 (d, *J* = 2.0 Hz, 1 H), 7.17 (d, *J* = 2.0 Hz, 1 H), 7.08 (d, *J* = 1.0 Hz, 1 H), 6.86 (d, *J* = 2.0 Hz, 1 H), 4.014 (s, 3 H), 4.011 (s, 3 H), 3.85 (s, 3 H), 3.82 (s, 3 H).

ImPyPyPy-(R)^{α-BocHN}-γ-ImPyPyPy-(+)-NH₂ (18). Starting with **12** (500 mg, 0.304 mmol), which was obtained using published microwave-assisted protocols, the N-terminal Boc group was removed by treatment with 80% TFA in DCM for 30 min. The resulting resin was washed with DCM (2x), DMF (2x), 20% DIEA in DMF (2x), DMF (2x), MeOH (2x), Et₂O (2x), and dried *in vacuo*. α-amino turn **9** (402 mg, 0.912 mmol, 3 eq.) was then activated with PyBOP (475 mg, 0.912 mmol, 3 eq.) and DIEA (320 μL, 1.824 mmol, 6 eq.) in DMF (3 mL), and added to the deprotected resin in a microwave synthesis vessel. The coupling reaction was set up in the microwave reactor at 60 °C for 30 min with constant stirring. The reaction mixture was filtered

into a peptide synthesis vessel, and the collected resin was washed with DMF (3x), MeOH (3x), Et₂O, and dried *in vacuo* to afford **13**. Selective deprotection of the γ -amino Fmoc group was achieved by treatment with 20% piperidine in DMF for 5 cycles x 4 min/cycle, and the resin was washed with DMF (2x), MeOH (2x) and Et₂O (2x). Tetramer **6** (299 mg, 0.608 mmol, 2.0 eq.) was then activated with PyBOP (349 mg, 0.671 mmol, 2.2 eq.) and DIEA (317 μ L, 1.824 mmol, 6.0 eq.) in DMF (3 mL), and added to the deprotected resin in a microwave synthesis vessel. The coupling reaction was set up in the microwave reactor at 60 °C for 5 min with constant stirring. The reaction mixture was filtered into a peptide synthesis vessel, and the collected resin was washed with DMF (3x), MeOH (3x), Et₂O, and dried *in vacuo* to afford **15** (720 mg). 3,3'-diamino-N-methyldipropylamine (2 mL) was then added to **15** (240 mg, 0.101 mmol), and the resin was cleaved under microwave irradiation at 60 °C for two 5-min cycles. The cleavage solutions were precipitated with cold Et₂O (~ 40 mL), centrifuged (4200 rpm), and the Et₂O supernatant was decanted to remove excess triamine. The remaining residue was dissolved in 6 mL 0.1% aqueous TFA at pH ~ 3, purified by reverse-phase HPLC, and lyophilized to dryness to afford **18** (41.3 mmol, 41% yield). MALDI-TOF $[M+H]^+$ calcd for C₆₂H₈₁N₂₂O₁₁⁺ = 1309.7, observed = 1309.9.

ImPyPyPy-(R) ^{β -CbzHN}- γ -ImPyPyPy-(+)-NH₂ (19). Starting with **12** (800 mg, 0.487 mmol), which was obtained using published microwave-assisted protocols, the N-terminal Boc group was removed by treatment with 80% TFA in DCM for 30 min. The resulting resin was washed with DCM (2x), DMF (2x), 20% DIEA in DMF (2x), DMF (2x), MeOH (2x), Et₂O (2x), and dried *in vacuo*. β -amino turn **10** (514 mg, 1.46 mmol, 3 eq.) was then activated with PyBOP (760 mg, 1.46 mmol, 3 eq.) and DIEA (509 μ L, 2.92 mmol, 6 eq.) in DMF (3.6 mL), and added to the

deprotected resin in a microwave synthesis vessel. The coupling reaction was set up in the microwave reactor at 60 °C for 30 min with constant stirring. The reaction mixture was filtered into a peptide synthesis vessel, and the collected resin was washed with DMF (3x), MeOH (3x), Et₂O, and dried *in vacuo* to afford **14** (970 mg). A fraction of resin **14** (300 mg, 0.151 mmol) was then treated with 80% TFA in DCM for 5 min, washed with DCM (2x), DMF (2x), 20% DIEA in DMF (2x), DMF (2x), MeOH (2x), Et₂O (2x), and dried *in vacuo*. Tetramer **6** (149 mg, 0.302 mmol, 2.0 eq.) was activated with PyBOP (236 mg, 0.453 mmol, 3.0 eq.) and DIEA (158 µL, 0.906 mmol, 6 eq.) in DMF (1.2 mL), and added to the deprotected resin in a microwave synthesis vessel. The coupling reaction was set up in the microwave reactor at 60 °C for 5 min with constant stirring. The reaction mixture was filtered into a peptide synthesis vessel, and the collected resin was washed with DMF (3x), MeOH (3x), Et₂O, and dried *in vacuo* to afford **16** (340 mg). 3,3'-diamino-N-methyldipropylamine (1.5 mL) was then added to **15** (170 mg, 0.076 mmol), and the resin was cleaved under microwave irradiation at 60 °C for two 5-min cycles. The cleavage solutions were precipitated with cold Et₂O (~ 40 mL), centrifuged (4200 rpm), and the Et₂O supernatant was decanted to remove excess triamine. The remaining residue was dissolved in 6 mL 0.1% aqueous TFA at pH ~ 3, purified by reverse-phase HPLC, and lyophilized to dryness to afford **19** (27.3 mmol, 36% yield). MALDI-TOF [M+H]⁺ calcd for C₆₅H₇₉N₂₂O₁₁⁺ = 1344.6, observed = 1344.8.

ImImPyPy-(R)^{α-BocHN}-γ-ImPyPyPy-(+)-NH₂ (20). Intermediate **13** (0.17 mmol) was prepared and deprotected with 20% piperidine in DMF under the same conditions as described for **18**. Tetramer **7** (168 mg, 0.340 mmol, 2.0 eq.) was then activated with PyBOP (177 mg, 0.340 mmol, 2.0 eq.) and DIEA (178 µL, 1.02 mmol, 6 eq.) in DMF (1.36 mL), and added to the deprotected

resin in a microwave synthesis vessel. The coupling reaction was set up in the microwave reactor at 60 °C for 5 min with constant stirring. The reaction mixture was filtered into a peptide synthesis vessel, and the collected resin was washed with DMF (3x), MeOH (3x), Et₂O, and dried *in vacuo* to afford **17** (400 mg). 3,3'-diamino-N-methyldipropylamine (1 mL) was then added to **17** (135 mg, 0.057 mmol), and the resin was cleaved under microwave irradiation at 60 °C for two 5-min cycles. The cleavage solutions were precipitated with cold Et₂O (~ 40 mL), centrifuged (4200 rpm), and the Et₂O supernatant was decanted to remove excess triamine. The remaining residue was dissolved in 6 mL 0.1% aqueous TFA at pH ~ 3, purified by reverse-phase HPLC, and lyophilized to dryness to afford **20** (29.4 mmol, 52% yield). MALDI-TOF [M+H]⁺ calcd for C₆₁H₈₀N₂₃O₁₁⁺ = 1310.6, observed = 1310.7.

ImPyPyPy-(R)^{α-H₂N}-γ-ImPyPyPy-(+)-IPA (1). Isophthalic acid (138 mg, 0.83 mmol, 20 eq.) was activated with PyBOP (54 mg, 0.103 mmol, 2.5 eq.) in DIEA (145 μL, 0.83 mmol, 20 eq.) and DMF (8.3 mL), and stirred for 10 min. The activated solution was then added dropwise to a solution of **18** (41.3 μmol) in DMF (2 mL) and stirred for 30 min. After confirmation of complete reaction by analytical HPLC, 40 mL cold Et₂O was added to the reaction mixture. The solution was then centrifuged at 4200 rpm, followed by removal of the supernatant, and the residual material was dried under steady air flow. Neat TFA (1 mL) was added to the oil residue and the solution was stirred for 30 min. Upon confirmation of complete deprotection by analytical HPLC, the solution was frozen in LN₂, diluted with 6 mL dH₂O, purified by reverse-phase HPLC and lyophilized to dryness to yield polyamide **1** (32 μmol, 78% yield). MALDI-TOF [M+H]⁺ calcd for C₆₅H₇₇N₂₂O₁₂⁺ = 1357.6, observed = 1357.9.

ImPyPyPy-(R) ^{β -H₂N}- γ -ImPyPyPy-(+)-IPA (4). Isophthalic acid (56 mg, 0.34 mmol, 20 eq.) was activated with PyBOP (22 mg, 0.043 mmol, 2.5 eq.) in DIEA (59 μ L, 0.34 mmol, 20 eq.) and DMF (3.2 mL), and stirred for 10 min. The activated solution was then added dropwise to a solution of **19** (17 μ mol) in DMF (1 mL) and stirred for 30 min. After confirmation of complete reaction by analytical HPLC, 40 mL cold Et₂O was added to the reaction mixture. The solution was then centrifuged at 4200 rpm, followed by removal of the supernatant, and the residual material was dried under steady air flow. The resulting oil residue was suspended in 900 μ L TFA, followed by dropwise addition of 100 μ L TFMSA, and the solution was stirred for 5 min. The solution was then frozen in LN₂, diluted with 6 mL dH₂O, purified by reverse-phase HPLC and lyophilized to dryness to yield polyamide **4** (13.4 μ mol, 79% yield). MALDI-TOF [M+H]⁺ calcd for C₆₅H₇₇N₂₂O₁₂⁺ = 1357.6, observed = 1358.1.

ImImPyPy-(R) ^{α -H₂N}- γ -ImPyPyPy-(+)-IPA (3). By following the reaction conditions described for the synthesis of **1**, and using **20** (12.6 μ mol) instead of **18** as starting material, polyamide **3** was obtained as an off-white powder (8.9 μ mol, 71% yield). MALDI-TOF [M+H]⁺ calcd for C₆₄H₇₆N₂₃O₁₂⁺ = 1358.6, observed = 1358.7.

ImPyPyPy-(R) ^{β -AcHN}- γ -ImPyPyPy-(+)-IPA (2). A solution of acetic anhydride (20 μ L) and pyridine (180 μ L) in DMF (1.8 mL) was added to **4** (12.3 μ mol), and stirred for 30 min. After confirmation of complete reaction by analytical HPLC, the solution was diluted with 6 mL dH₂O, purified by reverse-phase HPLC and lyophilized to dryness to afford polyamide **3** (11.4 μ mol, 88% yield). MALDI-TOF [M+H]⁺ calcd for C₆₇H₇₉N₂₂O₁₃⁺ = 1399.6, observed = 1400.0.

ImImPyPy-(R) ^{α -AcHN}- γ -ImPyPyPy-(+)-IPA (5). By following the reaction conditions described for the synthesis of **2**, and using **1** (15.0 μ mol) instead of **4** as starting material, polyamide **5** was obtained as an off-white powder (12.9 μ mol, 86% yield). MALDI-TOF $[M+H]^+$ calcd for $C_{67}H_{78}N_{22}O_{13}^+ = 1400.6$, observed = 1400.8.

II. Pharmacokinetic Studies of Polyamides 1 and 2

Pharmacokinetic studies were performed by Timothy W. Synold, Bixin Xi, Jun Wu and Yun Yen (City of Hope). Sample preparation was performed by Fei Yang (California Institute of Technology). Experimental details may be found in: Synold, T. W.; Xi, B.; Wu, J.; Yen, Y.; Li, B.C.; Yang, F.; Phillips, J.W.; Nickols, N.G.; Dervan, P.B. “Single-dose pharmacokinetic and toxicity analysis of pyrrole-imidazole polyamides in mice” *Cancer Chemother. Pharmacol.* **2012**, *70*, 617–625.

III. Antitumor Activity of Polyamide 1 in Prostate Tumor Xenografts

LNCaP tumor xenograft studies were performed by Fei Yang and Nicholas G. Nickols (California Institute of Technology). Experimental details may be found in: Yang, F.; Nickols, N.G.; Li, B.C.; Marinov, G.; Wold, B. J.; Dervan, P.B. “Antitumor activity of a DNA minor groove binding Py-Im polyamide” *Proc. Natl. Acad. Sci. U.S.A.* **2013**, *110*, 1863–1868.

IV. Transcription Regulation and in vivo Activity of ERE-Targeting Polyamide 3

qRT-PCR assays and T47D tumor xenograft studies were performed by Nicholas G. Nickols and Jerzy Szablowski (California Institute of Technology). Experimental details may be found in: Nickols, N.G.; Szablowski, J.; Hargrove, A.E.; Li, B.C.; Raskatov, J.A.; Dervan, P.B. “Activity of a Py-Im polyamide targeted to the estrogen response element” *Mol. Cancer Ther.* accepted (2013).

4.5 References

- (1) Tsai, M.J.; Omalley, B.W. *Annu. Rev. Biochem.* **1994**, *63*, 451–486.
- (2) Tyagi, R.K.; Lavrovsky, Y.; Ahn, S.C.; Song, C.S.; Chatterjee, B.; Roy, A.K. *Mol. Endocrinol.* **2000**, *14*, 1162–1174.
- (3) Scher, H.I. and Sawyers, C.L. *J. Clin. Oncol.* **2005**, *23*, 8253–8261.
- (4) Huggins, C. and Hodges, C.V. *Cancer Res.* **1941**, *1*, 293–297.
- (5) Huggins, C.; Stevens, R.E.; Hodges, C.V. *Arch. Surg. (Chicago)* **1941**, *43*, 209–223.
- (6) Oefelein, M.G.; Agarwal, P.K.; Resnick, M.I. *J. Urol.* **2004**, *171*, 1525–1528.
- (7) Nickols, N.G. and Dervan, P.B. *Proc. Natl. Acad. Sci. U.S.A.* **2007**, *104*, 10418–10423.
- (8) Chenoweth, D.M.; Harki, D.A.; Dervan P.B. *J. Am. Chem. Soc.* **2009**, *131*, 7175–7181.
- (9) Puckett, J.W.; Green, J.T.; Dervan, P.B. *Org. Lett.* **2012**, *14*, 2774–2777.
- (10) Chenoweth, D.M.; Harki, D.A.; Phillips, J.W.; Dose, C.; Dervan, P.B. *J. Am. Chem. Soc.* **2009**, *131*, 7181–7188.
- (11) Coiffer, B.; Altman, A.; Pui, C.H.; Younes, A.; Cairo, M.S. *J. Clin. Onc.* **2008**, *26*, 2767–2778.
- (12) Jung, Y. and Lippard, S.J. *J. Biol. Chem.* **2006**, *281*, 1361–1370
- (13) Ratner, J.N.; Balasubramanian, B.; Corden, J.; Warren, S.L.; Bregman, D.B. *J. Biol. Chem.* **1998**, *273*, 5184–5189.
- (14) El-Deiry, W.S. *Seminars in Cancer Biology* **1998**, *8*, 345–357.
- (15) Ljungman, M.; Zhang, F.F.; Chen, F.; Rainbow, A.J.; McKay, B.C. *Oncogene* **1999**, *18*, 583–592.
- (16) Arima, Y.; Nitta, M.; Kuninaka, S.; Zhang, D.; Fujiwara, T.; Taya, T.; Nakao, M.; Saya, H. *J. Biol. Chem.* **2005**, *280*, 19166–19176.

- (17) Derheimer, F.A.; O'Hagan, H.M.; Krueger, H.M.; Hanasoge, S.; Paulsen, M.T.; Ljungman, M. *Proc. Natl. Acad. Sci. U.S.A.* **2007**, *104*, 12778–12783.
- (18) Chen, C.D.; Welsbie, D.S.; Tran, C.; Baek, S.H.; Chen, R.; Vessella, R.; Rosenfeld, M.G.; Sawyers, C.L. *Nat. Med.* **2004**, *10*, 33–39.
- (19) Horoszewicz, J.S.; Leong, S.S.; Kawinski, E.; Karr, J.P.; Rosenthal, H.; Chu, T.M.; Mirand, E.A.; Murphy, G.P. *Cancer Res.* **1983**, *43*, 1809–1818.
- (20) Alimirah, F.; Chen, J.; Basrawala, Z.; Xin, H.; Choubey, D. *FEBS Lett.* **2006**, *580*, 2294–2300.
- (21) Tewari, M.; Quan, L.T.; O'Rourke, K.; Desnoyers, S.; Zeng, Z.; Beidler, D. R.; Poirier, G. G.; Salvesen, G.S.; Dixit, V.M. *Cell* **1995**, *81*, 801–809.
- (22) Aggarwal, M.; Sommers, J.A.; Shoemaker, R.H.; Brosh, R.M., Jr. *Proc. Natl. Acad. Sci. U.S.A.* **2011**, *108*, 1525–1530.
- (23) Sharma, S.; Otterlei, M.; Sommers, J.A.; Driscoll, H.C.; Dianov, G.L.; Kao, H.I.; Bambara, R.A.; Brosh, R.M., Jr. *Mol. Biol. Cell* **2004**, *15*, 734–750.
- (24) Dai, Y. and Grant, S. *Clin. Cancer Res.* **2010**, *16*, 376–383.
- (25) Olson, E.; Nievera, C.J.; Klimovich, V.; Fanning, E.; Wu, X. *J. Biol. Chem.* **2006**, *281*, 39517–39533.
- (26) Matsuoka, S.; Huang, M.; Elledge, S. J. *Science* **1998**, *282*, 1893–1897.
- (27) Rogakou, E. P.; Boon, C.; Redon, C.; Bonner, W. M. *J. Cell Biol.* **1998**, *146*, 905–916.
- (28) Sirbu, B.M.; Couch, F.B.; Feigerle, J.T.; Bhaskara, S.; Hiebert, S.W.; Cortez, D. *Genes Dev.* **2011**, *25*, 1320–1327.
- (29) Loeb, D.M.; Evron, E.; Patel, C.B.; Sharma, P.M.; Niranjana, B.; Buluwela, L.; Weitzman, S.A.; Korz, D.; Sukumar, S. *Cancer Res.* **2001**, *61*, 921–925.

- (30) Miyoshi, Y.; Ando, A.; Egawa, C.; Taguchi, T.; Tamaki, Y.; Tamaki, H.; Sugiyama, H.; Noguchi, S. *Clin. Cancer Res.* **2002**, *8*, 1167–1171.
- (31) Foekens, J.A.; Rio, M.C.; Seguin, P.; Vanputten, W.L.J.; Fauque, J.; Nap, M.; Klijn, J.G.M.; Chambon, P. *Cancer Res.* **1990**, *50*, 3832–3837.
- (32) Muller, V.; Jensen, E.V.; Knabbe, C. *Cancer Res.* **1998**, *58*, 263–267.
- (33) Baird, E.E. and Dervan, P.B. *J. Am. Chem. Soc.* **1996**, *118*, 6141–6146.
- (34) Trauger, J. W. and Dervan, P. B. *Methods Enzymol.* **2001**, *340*, 450–466.

4.6 Experimental Data

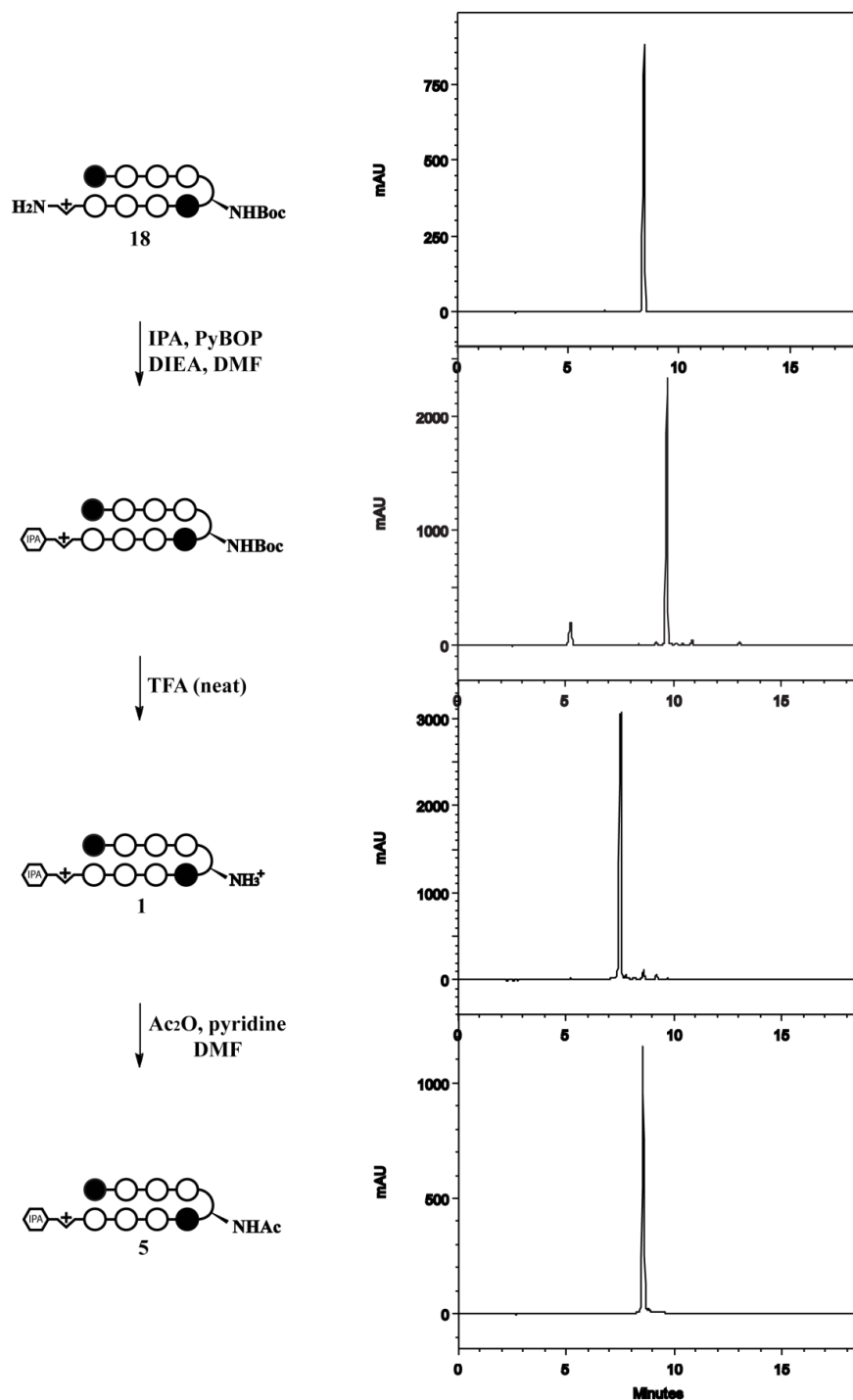


Figure 4.9 Crude HPLC spectra tracing the synthesis of **5** starting from **18**. Reverse-phase HPLC taken on Beckman Gold instrument equipped with a Phenomenex Gemini analytical column (250 \times 4.6 mm, 5 μm) and a diode array detector, and the mobile phase consisted of a gradient of acetonitrile (MeCN) in 0.1% (v/v) aqueous TFA [10% MeCN, $t = 0 \rightarrow 30$ s; 10% \rightarrow 80% MeCN, $t = 30$ s \rightarrow 18 min].

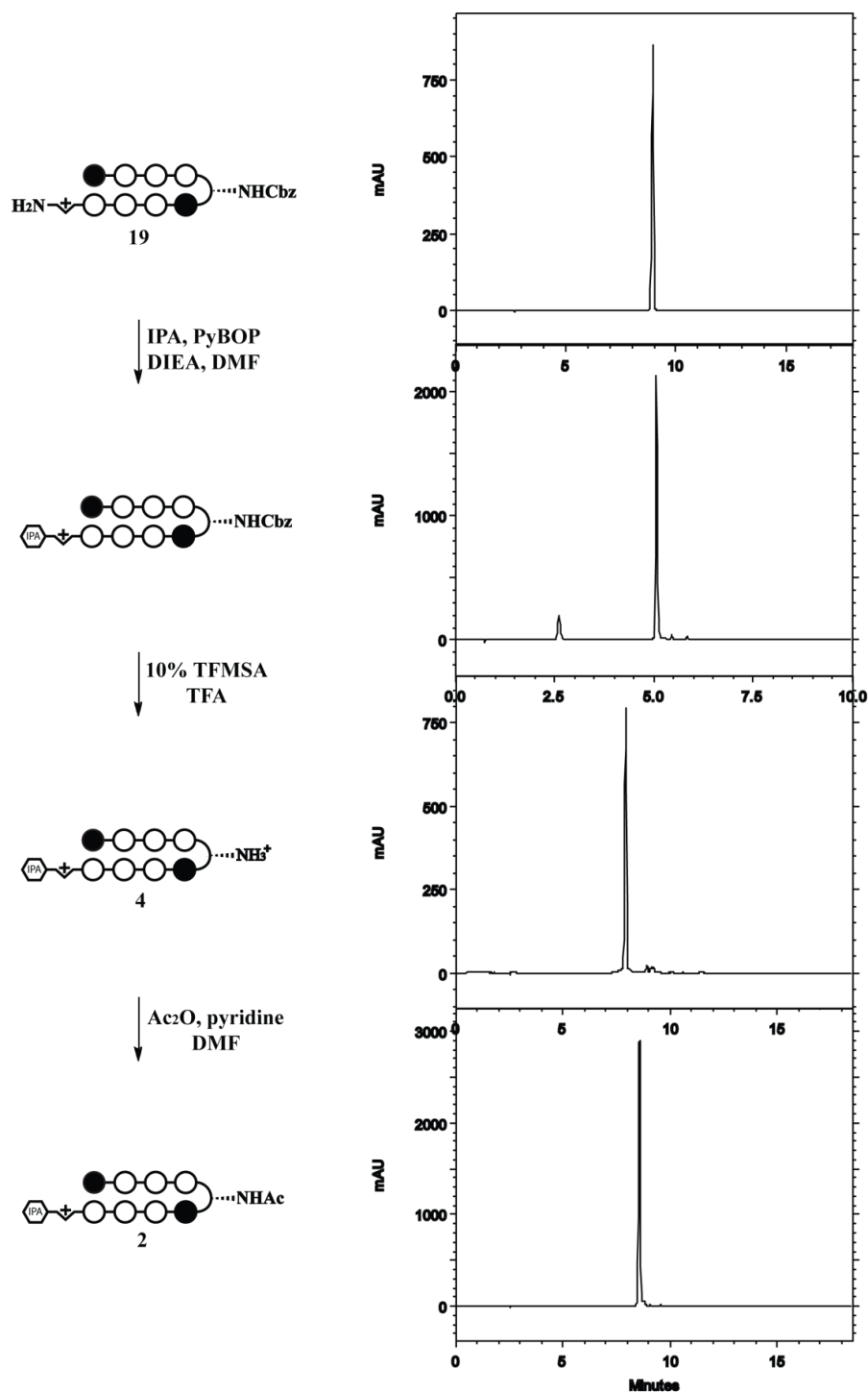


Figure 4.10 Crude HPLC spectra tracing the synthesis of **2** starting from **19**. Reverse-phase HPLC taken on Beckman Gold instrument equipped with a Phenomenex Gemini analytical column (250×4.6 mm, $5 \mu\text{m}$) and a diode array detector, and the mobile phase consisted of a gradient of acetonitrile (MeCN) in 0.1% (v/v) aqueous TFA [10% MeCN, $t = 0 \rightarrow 30$ s; 10% \rightarrow 80% MeCN, $t = 30$ s \rightarrow 18 min].

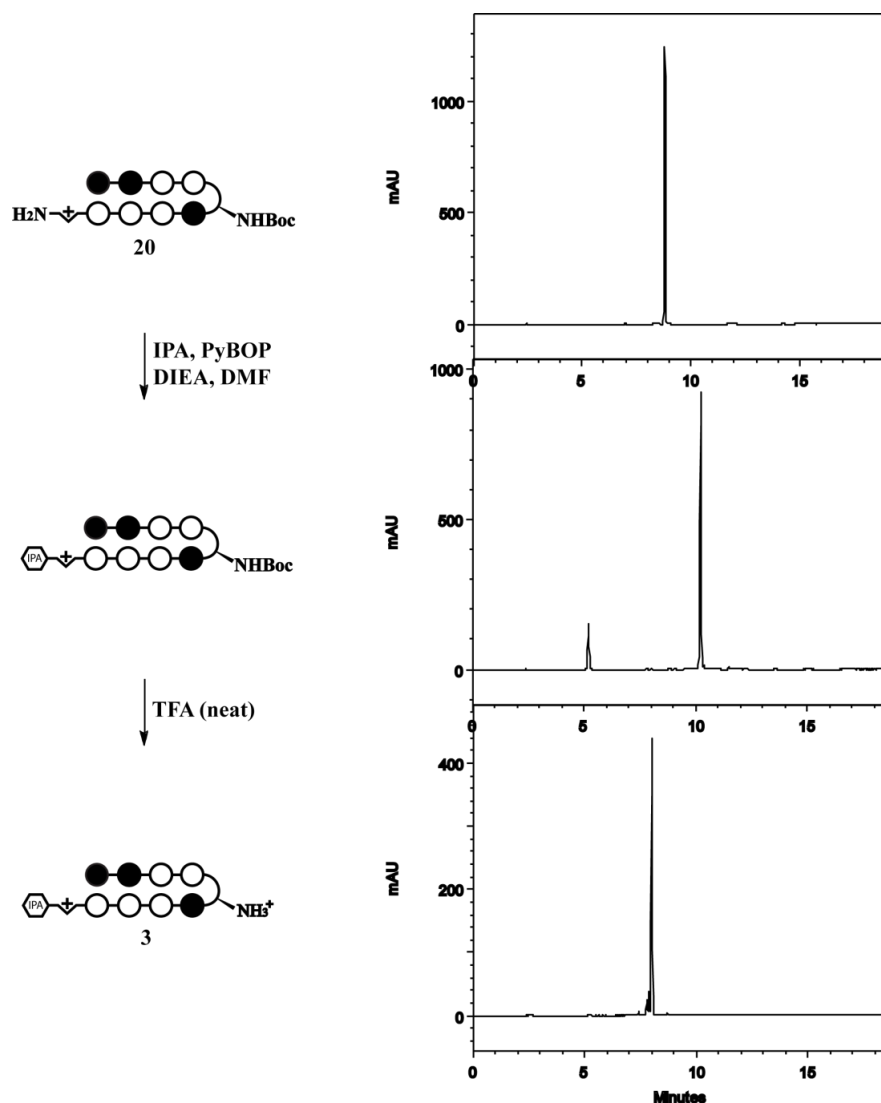


Figure 4.11 Crude HPLC spectra tracing the synthesis of **3** starting from **20**. Reverse-phase HPLC taken on Beckman Gold instrument equipped with a Phenomenex Gemini analytical column (250×4.6 mm, $5 \mu\text{m}$) and a diode array detector, and the mobile phase consisted of a gradient of acetonitrile (MeCN) in 0.1% (v/v) aqueous TFA [10% MeCN, $t = 0 \rightarrow 30$ s; 10% \rightarrow 80% MeCN, $t = 30$ s \rightarrow 18 min].

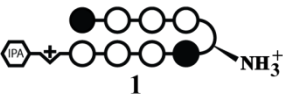

Polyamides	5'- TCGC AGAACA GCGA -3'	
	$T_m / ^\circ\text{C}$	$\Delta T_m / ^\circ\text{C}$
—	61.8 (± 0.4)	—
 1	76.8 (± 0.2)	15.0
 2	76.3 (± 0.3)	14.5

Table 4.1 Melting temperatures of DNA/polyamide complexes for **1** and **2**. All values are derived from at least three melting temperature experiments, with standard deviations indicated in parentheses. ΔT_m values are given as T_m (DNA/polyamide) – T_m (DNA).

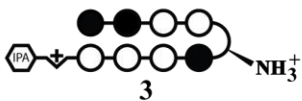
Polyamide	5'- CGA TGGTCA AGC -3'	
	$T_m / ^\circ\text{C}$	$\Delta T_m / ^\circ\text{C}$
—	54.0 (± 0.2)	—
 3	69.1 (± 0.3)	15.1

Table 4.2 Melting temperatures of DNA/polyamide complexes for **3**. All values are derived from at least three melting temperature experiments, with standard deviations indicated in parentheses. ΔT_m values are given as T_m (DNA/polyamide) – T_m (DNA).

Appendix A

Alternative Approaches towards Cyclic Polyamide Precursors

A.1 Introduction

Prior to the discovery of the optimal microwave-assisted conditions on 2-chlorotrityl resin, several approaches were explored towards the synthesis of cyclic polyamide **1**. Based on previously established DPPA-mediated macrocyclization procedures, the main focus was placed on effectively obtaining the amino acid precursor **2** (Fig. A.1).¹⁻³ Due to the polyaromatic nature of these intermediates, solubility remained an issue throughout these efforts, and limited the scope of reactions and purification methods that were applicable. The bigger problem, however, was the acid-labile C-terminal pyrrole carboxylic acid, which often resulted in decomposition products and proved detrimental in several of these attempts. Owing to these challenges, the alternative approaches were met with little success and never materialized to a convenient and reliable methodology, but nonetheless gave insight into facilitating the eventual development of the microwave-assisted solid-phase methods.⁴

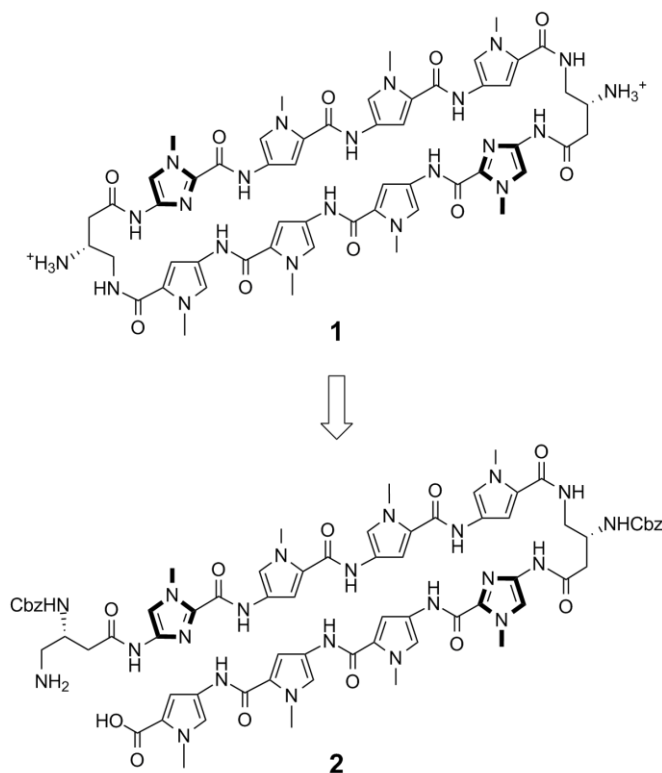


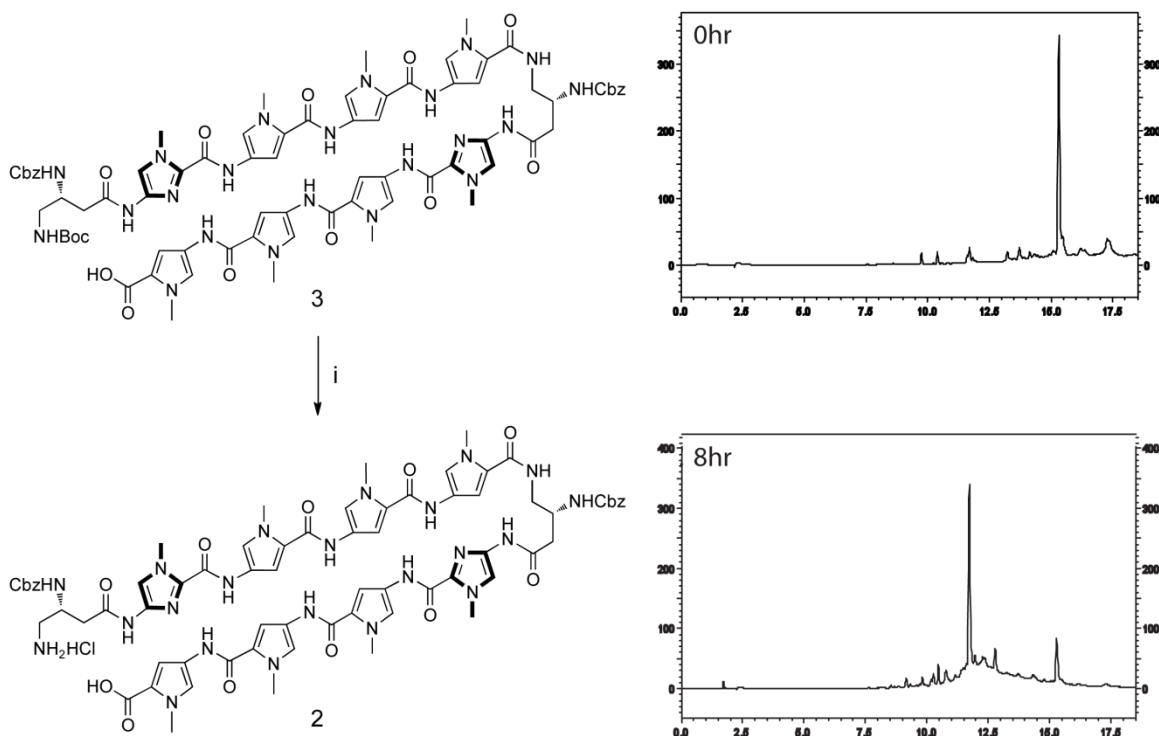
Figure A.1 Retrosynthesis of cyclic polyamide **1** from linear amino acid precursor **2**.

A.2 Results and Discussion

I. Direct Deprotection of Solution-Phase Intermediate

In the solution-phase synthesis reported by Chenoweth et al., **3** was rapidly assembled prior to activation of the pentafluorophenol ester for macrocyclization.⁵ While the initial synthesis proved effective, the cyclization yields were somewhat inconsistent and the substrate scope was limited, which created the need for a more reliable and divergent approach. As the DPPA-mediated macrocyclization procedure was proven to be an effective route towards synthesizing cyclic polyamides, the first attempt towards the amino acid precursor was made by directly deprotecting the N-terminal Boc group in **3** under acidic conditions (Scheme A.1).

Scheme A.1 Direct deprotection of **3** under acidic conditions



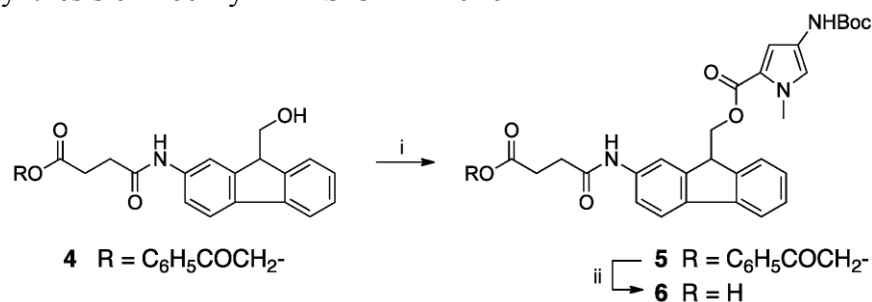
¹Reagents and conditions: (i) 3M HCl in EtOAc, -40°C, 8h, 31% yield.

Unfortunately, the C-terminal pyrrole carboxylic acid proved to be extremely labile under acidic conditions, often resulting in decomposition products at temperatures higher than -40°C (Fig. SA.1–3). This method was not only required constant temperature control, but the yields were also largely irreproducible. Further attempts to first protect the C-terminus as either a trimethylsilylethyl (TMSE) or fluorenylmethyl (Fm) ester resulted in decomposition as well.

II. Solid-Phase Synthesis on HFMS Resin

In light of the acid sensitivity of the pyrrole carboxylic acid, and in efforts to create a more time-efficient and divergent strategy, we began investigating solid-phase methods using the base-labile [9-hydroxymethyl-2-fluorenyl] succinamic acid (HMFS) resin.⁶ Prior to solid-phase assembly, HMFS phenacyl (Pac) ester was first synthesized using published conditions and pre-conjugated to the initial BocPyOH monomer to yield **5** (Scheme A.2).⁷

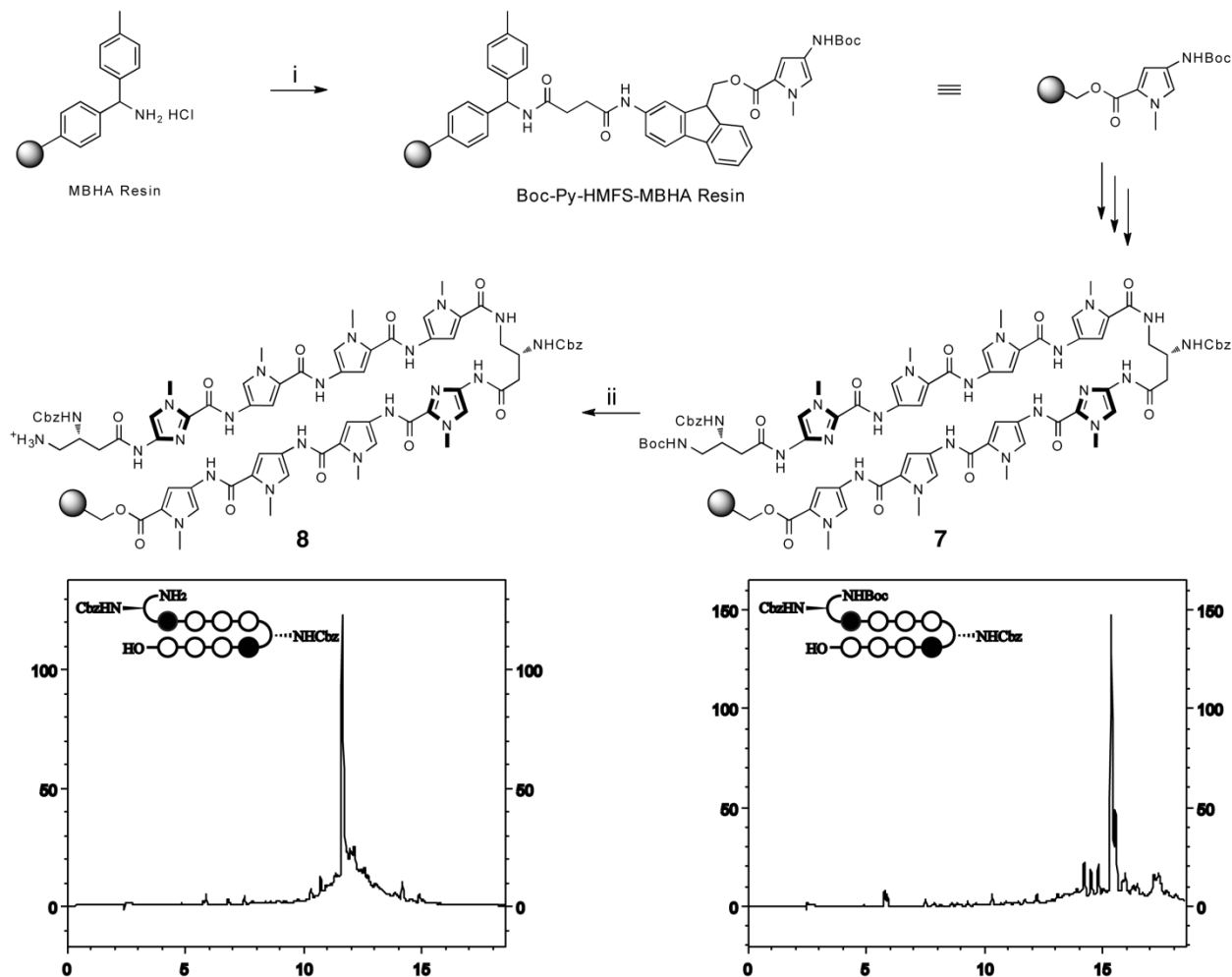
Scheme A.2 Synthesis of Boc-Py-HMFS-OH linker **6**



¹Reagents and conditions: (i) BocPyOH, EDC, DMAP, DCM; (ii) Zn(0), AcOH.

After removal of the Pac ester, **6** was then loaded onto MBHA resin for the polyamide core **7** was quickly assembled using oligomer intermediates under microwave-assisted conditions (Scheme A.3).⁸ While HPLC spectra of **7** indicated relative high purity, deprotection of the C-terminal Boc group with 80% TFA prior to final resin cleavage still resulted in decomposition.

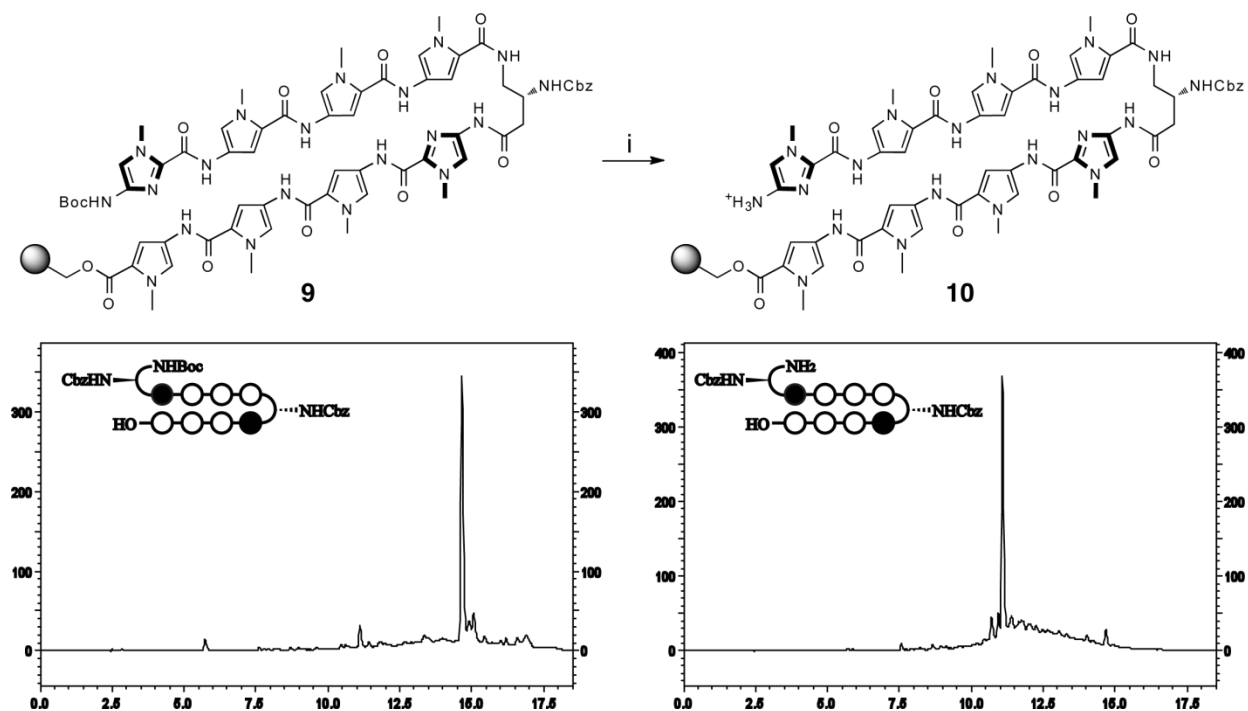
Scheme A.3 Microwave-assisted synthesis of **8** on HMFS resin



¹Reagents and conditions: (i) **6**, PyBOP, DIEA, NMP, m.w. 80 °C, 2 h; (ii) 80% TFA, DCM, 23 °C, 5 min.

Owing to this high sensitivity to acidic conditions, a subsequent attempt was made to protect the second turn unit with a terminal Fmoc group. Since the synthesis of N-Fmoc oligomers have not been established, this was performed in a monomer-by-monomer fashion. Unfortunately, deprotection of the second imidazole unit with TFA again resulted in decomposition (Scheme A.4). Overall, the decomposition observed in various conditions using HMFS resin, as well as the synthetic rigor required in the initial loading, rendered this approach impractical towards extensive scale-up for biological studies.

Scheme A.4 Microwave-assisted synthesis on HMFS resin

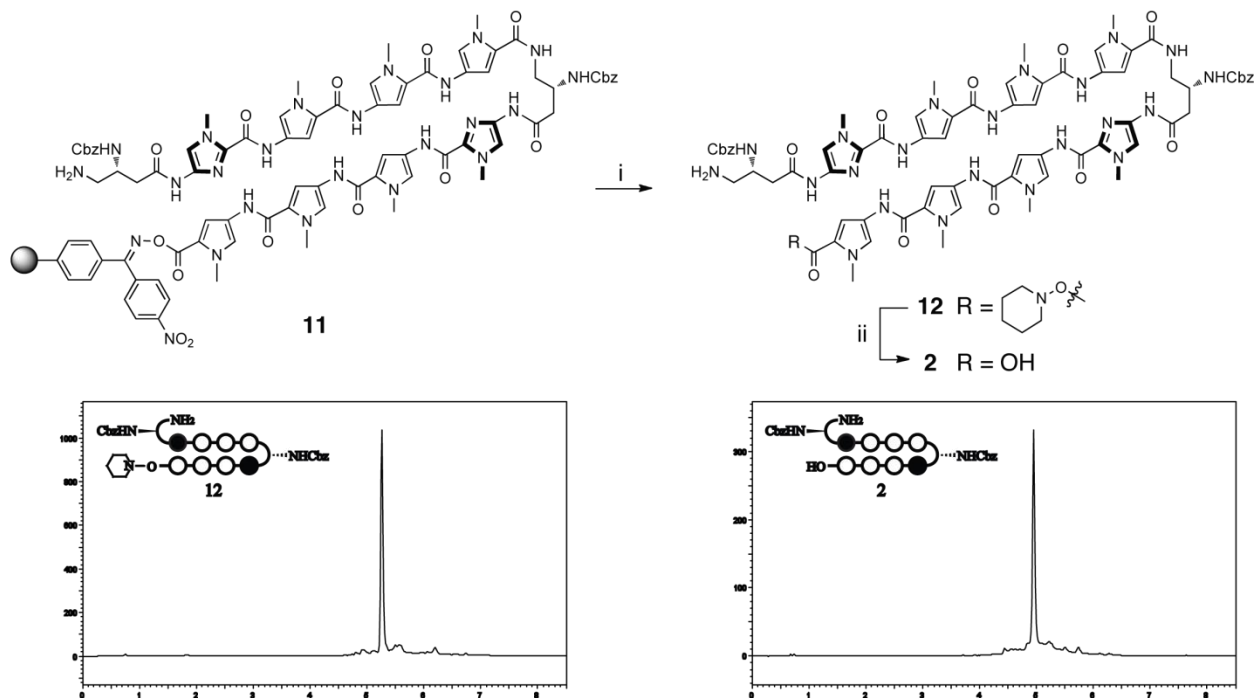


¹Reagents and conditions: (i) 80% TFA, DCM, 23 °C, 25 min.

III. Two-Step Cleavage off Oxime Resin

Given our extensive experience with oxime resin, an effective cleavage method to obtain a C-terminal carboxylic acid would allow us to take advantage of pre-existing solid-phase technologies towards cyclic polyamide precursors.^{8,9} Unfortunately, typical methods using aqueous 1,8-diazabicyclo[5.4.0]undec-7-ene (DBU) resulted in product decomposition and gave rise to concerns over epimerizing the α -amino stereocenters on the turn units.¹⁰ Alternatively, C-terminal carboxylic acids may be obtained from oxime resin using a two-step procedure involving initial cleavage with N-hydroxypiperidine (HOPip) and subsequent Zn-catalyzed removal of the HOPip ester.^{11–13} Using optimized microwave-assisted conditions, **11** was rapidly assembled and subjected to these conditions (Scheme A.5).

Scheme A.5 Two-step cleavage of **11** off Kaiser oxime resin



¹Reagents and conditions: (i) HOPIp, DMF, 23°C, 24 h; (ii) Zn(0), 90% AcOH, 16% yield overall.

The analytical HPLC spectra of both the intermediate **12** and precursor **2** were relatively clean, indicating a limited amount of decomposition. Due to technical difficulties in isolating **2**, however, the intermediate was only recovered in a modest 16% yield. Also, despite a deliberate filtration procedure, the generation of water-insoluble zinc products rendered this procedure undesirable for reverse-phase HPLC purification. While the recovery yields were less than ideal and the work-up was considerably labor intensive, this nonetheless set a firm baseline for the development of solid-phase techniques towards cyclic polyamide precursors, and may in itself be useful for small-scale divergent syntheses of hairpin and cyclic polyamides.

A.3 Conclusions

Multiple approaches were attempted towards the synthesis of cyclic polyamide precursor **2**. Direct deprotection of solution-phase intermediate **3** under acidic conditions resulted in decomposition, even at -40 °C. Due to this observed acid sensitivity of the C-terminal carboxylic acid, solid-phase synthesis of **2** on the base-labile HMFS resin was tried. Boc deprotection of the final resin intermediate **7** again led to decomposition, whereas efforts towards replacing the terminal Boc group with Fmoc was also unsuccessful. Using a two-step cleavage procedure, **2** was synthesized on Kaiser oxime resin under microwave-irradiation and isolated in 16% yield. While the recovery was modest, this was at the time an otherwise acceptable method, but the use of water-insoluble zinc during cleavage raised concerns regarding potential long-term damage to our reverse-phase HPLC systems. Ultimately, although none of these ventures directly resulted in success, these failed attempts highlighted some of the challenges towards synthesizing the zwitterionic polyaromatic intermediates. Perhaps most importantly, the more commonly used Boc protection scheme was proven infeasible, which led to the eventual development of microwave-assisted methods on 2-chlorotrityl resin using Fmoc chemistry.

A.4 Materials and Methods

Materials

All chemicals were purchased from Sigma-Aldrich, unless otherwise specified. Kaiser oxime resin and PyBOP were purchased from NovaBioChem. (*R*)-3,4-Cbz-Dbu(Boc)-OH was purchased from Peptides International. MBHA resin was purchased from Bachem.

Methods

Polyamide monomers were obtained using previous protocols.³³ Microwave-assisted coupling reactions were conducted on a Biotage Initiator Eight synthesizer. Polyamides were purified via preparative HPLC on an Agilent Technologies 1200 Series system using a Phenomenex Gemini column. Matrix-assisted, LASER desorption/ionization time-of-flight mass spectrometry (MALDI-TOF MS) was performed on an Applied Biosystems Voyager DR Pro spectrometer. NMR spectroscopy data was obtained on a Varian instrument operating at 500 MHz. Polyamide concentrations were measured in 20% MeCN in 0.1% (v/v) aqueous TFA using an approximated extinction coefficient of $69\,200\text{ M}^{-1}\text{ cm}^{-1}$ at λ_{max} near 310 nm.³⁴

I. Direct Deprotection of Solution-Phase Intermediate

Boc-protected intermediate **3** obtained from previous procedures⁵ was subjected to either 25% TFA in DCM or 4 M HCl in 1,4-dioxane at 23 °C, which resulted in rapid decomposition (Fig. SA.1 & SA.2). Similar conditions were then repeated at -40 °C with improved recovery, but required constant temperature control for extended periods of times (6 to 8 h) (Fig. SA.3). The best conditions were illustrated in Scheme A.1 and described as follows:

A solution of **2** (20 mg, 12.6 μmol) in EtOAc (1.8 mL) was first cooled to -40°C , followed by dropwise addition of 3M HCl in EtOAc (200 μL) at -40°C . The reaction mixture was then stirred at -40°C for 8 h. Upon confirmation of complete deprotection by analytical HPLC, the solution was frozen in LN₂, thawed in DMF, and the EtOAc was removed *in vacuo*. The remaining solution was then diluted in 6 mL 20% AcN in 0.1% aqueous TFA, purified by reverse-phase HPLC and lyophilized to dryness to afford precursor **2** (3.9 μmol , 31% yield). MALDI-TOF $[\text{M}+\text{H}]^{+}$ calcd for $\text{C}_{70}\text{H}_{77}\text{N}_{22}\text{O}_{15}^{+}$ = 1465.4, observed = 1465.7.

II. Solid-Phase Synthesis on HFMS Resin

Boc-Py-HMFS-OPac (5). A solution of BocPyOH (504 mg, 2.10 mmol, 6.0 eq.) and EDCI (201 mg, 1.05 mmol, 3.0 eq.) in DCM (720 μL) was stirred at 23°C for 1 h. The activated mixture was then added dropwise to a solution of **4** (150 mg, 0.350 mmol) in DCM (480 μL), followed by DMAP (43 mg, 0.350 mmol, 1.0 eq.), and stirred for 23°C for 40 h. The reaction mixture was then diluted with DCM (2 mL) and purified by silica gel chromatography (DCM to 4:1 DCM: EtOAc). The desired fractions were combined, concentrated and dried to afford **5** as a tan solid (173 mg, 0.266 mmol, 76% yield). ^1H NMR [499.8 MHz, DMSO- d_6]: δ 10.13 (s, 1 H), 9.04 (s, 1 H), 7.95 (m, 3 H), 7.80 (app d, $J = 7.5$ Hz, 2 H), 7.68 (app t, 1 H), 7.61 (m, 2 H), 7.55 (app t, $J = 7.5$ Hz, 2 H), 7.38 (app t, $J = 7.5$ Hz, 1 H), 7.26 (app t, $J = 7.5$ Hz, 1 H), 7.06 (s, 1 H), 6.59 (s, 1 H), 5.50 (s, 2 H), 4.71 (app dd, $J = 5$ Hz, $J = 10$ Hz, 1 H), 4.34 (m, 2 H), 3.56 (s, 3 H), 2.77 (t, 2 H), 2.69 (t, 2 H), 1.42 (s, 9 H).

Boc-Py-HMFS-OH (6). A solution of **5** (145 mg, 0.223 mmol) in AcOH (1 mL) was treated with zinc dust (291 mg, 4.45 mmol, 20 eq.) and stirred at 40 °C for 30 min. The solution was then filtered, and the filtrate was concentrated *in vacuo*. The residual oil was resuspended in EtOAc, washed with 1M HCl, dH₂O (3x), brine, dried (MgSO₄), filtered and concentrated to afford **6** as an off-white solid (118 mg, 0.223 mmol, 99% yield). ¹H NMR [499.8 MHz, DMSO-d₆]: δ 12.10 (s, 1 H), 10.12 (s, 1 H), 9.06 (s, 1 H), 7.94 (m, 1 H), 7.79 (app d, *J* = 8.0 Hz, 2 H), 7.61 (app t, *J* = 8.0 Hz, 2 H), 7.37 (t, *J* = 7.5 Hz, 1 H), 7.26 (app t, *J* = 7.5 Hz, 1 H), 7.07 (s, 1 H), 6.60 (s, 1 H), 4.68 (m, 1 H), 4.34 (m, 2 H), 3.57 (s, 3 H), 2.52-2.57 (m, 4 H), 1.42 (s, 9 H).

Boc-Py-HMFS-MBHA Resin. MBHA resin (100 mg, 0.076 mmol) was first washed with a 2:1 DMF:DIEA solution, MeOH (2x), and dried *in vacuo*. A solution of **6** (118 mg, 0.223 mmol, 2.9 eq.) and PyBOP (118 mg, 0.228 mmol, 3.0 eq.) in DIEA (79 μL, 0.456 mmol, 6.0 eq.) and NMP (550 μL) was stirred at 23 °C for 10 min, and then treated with the pre-washed MBHA resin. The reaction mixture was submitted to microwave irradiation at 80 °C for 2 h. The resin was then filtered and washed with NMP (2x), DCM (2x), NMP (2x), MeOH (2x), and dried *in vacuo*. Complete loading of the resin was confirmed by the Kaiser test.

Microwave-Assisted Solid-Phase Synthesis (7–10). Polyamide cores **7** and **9** were assembled on Boc-Py-HMFS-MBHA resin with the corresponding monomers using published microwave conditions.⁸ For **7**, the Im-turn unit was introduced as a dimer.^{5,14} As illustrated in Figures A.3 and A.4, TFA deprotection of the N-terminal Boc groups in **7** and **9** to yield **8** and **10** resulted in decomposition.

III. Two-Step Cleavage off Oxime Resin

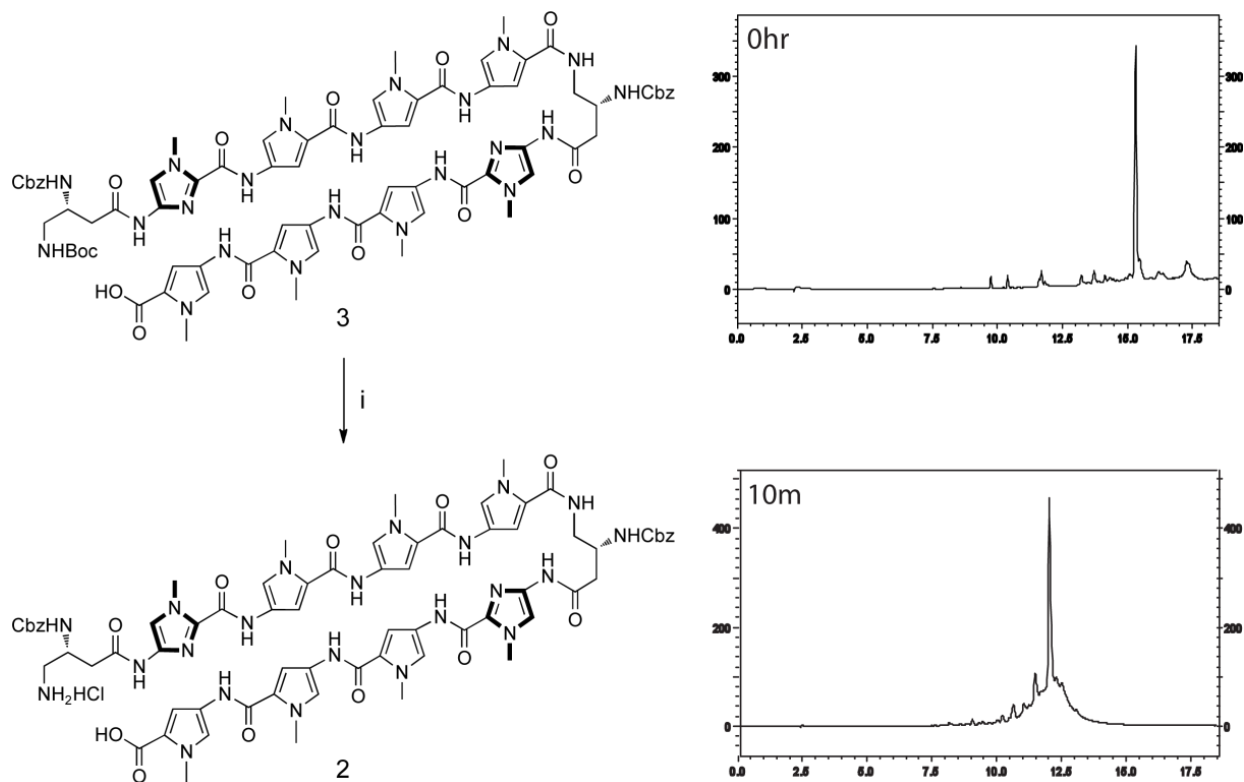
A solution of HOPip (22 mg, 0.21 mmol, 10 eq.) in DMF (200 μ L) was added to **11** (60 mg, 21 μ mol) and stirred at 23 °C for 24 h. The mixture was then filtered, and the resin was resubmitted to fresh solution of HOPip (22 mg, 0.21 mmol, 10 eq.) in DMF (200 μ L) and stirred for another 24 h. The mixture was again filtered and cold Et₂O was added to the combined filtrate, yielding a precipitate that was isolated by centrifugation. The crude 1-piperidyl ester **12** was then dissolved in 90% AcOH (5 mL) and stirred vigorously with Zn dust (100 mg) at 23 °C for 1 h. The mixture was then filtered and washed with 90% AcOH (5 mL). The combined filtrate was concentrated *in vacuo*, and the residue was redissolved in 6 mL 30% AcN in 0.1% aqueous TFA. Remaining Zn precipitate was then removed by centrifugation, and the supernatant was purified by reverse-phase HPLC and lyophilized to dryness to yield **2** as a light yellow solid (3.4 μ mol, 16% yield). MALDI-TOF $[M+Na]^+$ calcd for C₇₀H₇N₂₂NaO₁₅⁺ = 1487.6, observed = 1487.8.

A.5 References

- (1) Cho, J.; Parks, M.E.; Dervan, P.B. *Proc. Natl. Acad. Sci. U.S.A.* **1995**, *92*, 10389–10392.
- (2) Herman, D.M.; Turner, J.M.; Baird, E.E.; Dervan, P.B. *J. Am. Chem. Soc.* **1999**, *121*, 1121–1129.
- (3) Melander, C.; Herman, D.M.; Dervan, P.B. *Chem. Eur. J.*, **2000**, *6*, 4487–4497.
- (4) Li, B.C.; Montgomery, D.C.; Puckett, J.W.; Dervan, P.B. *J. Org. Chem.* **2013**, *78*, 124–133.
- (5) Chenoweth, D.M.; Harki, D.A.; Phillips, J.W.; Dose, C.; Dervan, P.B. *J. Am. Chem. Soc.* **2009**, *131*, 7182–7188.
- (6) Rabanal, F.; Giralt, E.; Albericio, F. *Tet. Lett.* **1992**, *33*, 1775–1779.
- (7) Nishiuchi, Y.; Nishio, H.; Inui, T.; Body, J.; Kimura, T. *J. Pept. Sci.* **2000**, *6*, 84–93.
- (8) Puckett, J.W.; Green, J.T.; Dervan, P.B. *Org. Lett.* **2012**, *14*, 2774–2777.
- (9) Belitsky, J.M.; Nguyen, D.H.; Wurtz, N.R.; Dervan, P.B. *Bioorg. Med. Chem.* **2002**, *10*, 2767–2774.
- (10) Pichette, A.; Voyer, N.; Larouche, R.; Meillon, J.-C. *Tetrahedron Lett.* **1997**, *38*, 1279–1282.
- (11) Nakagawa, S.H. and Kaiser, E.T. *J. Org. Chem.* **1983**, *48*, 678–685.
- (12) Sasaki, T.; Findeis, M.A.; Kaiser, E.T. *J. Org. Chem.* **1991**, *56*, 3159–3168.
- (13) Sewald, S. and Jakubke, H.-D. *Peptides: Chemistry and Biology* **2002**.
- (14) Chenoweth, D.M.; Harki, D.A.; Dervan, P.B. *J. Am. Chem. Soc.* **2009**, *131*, 7175–7181.

A.6 Experimental Data

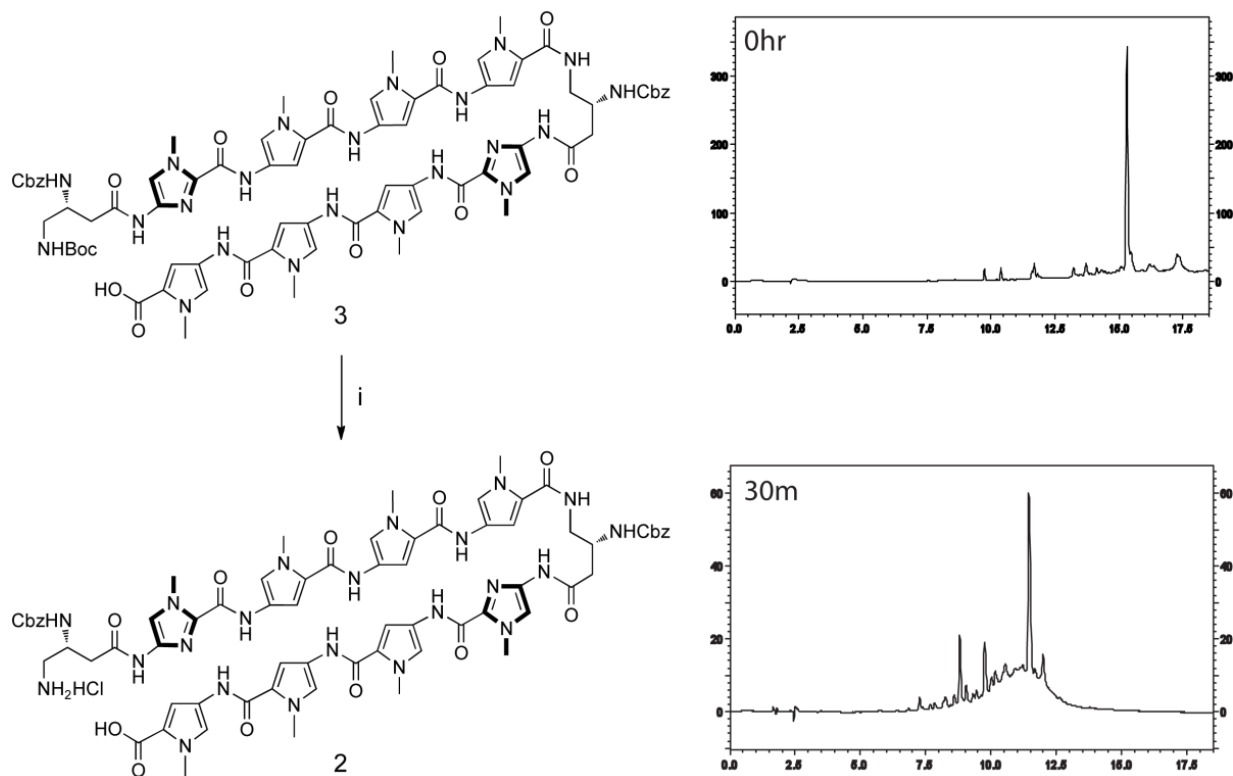
Scheme A.6 Direct deprotection of **3** with TFA at room temperature



¹Reagents and conditions: (i) 25% TFA, DCM, 23 °C, 10 min.

² Reverse-phase HPLC taken on Beckman Gold instrument equipped with a Phenomenex Gemini analytical column (250 × 4.6 mm, 5 μm) and a diode array detector, and the mobile phase consisted of a gradient of acetonitrile (MeCN) in 0.1% (v/v) aqueous TFA [10% MeCN, t = 0 → 30 s; 10% → 80% MeCN, t = 30 s → 18 min].

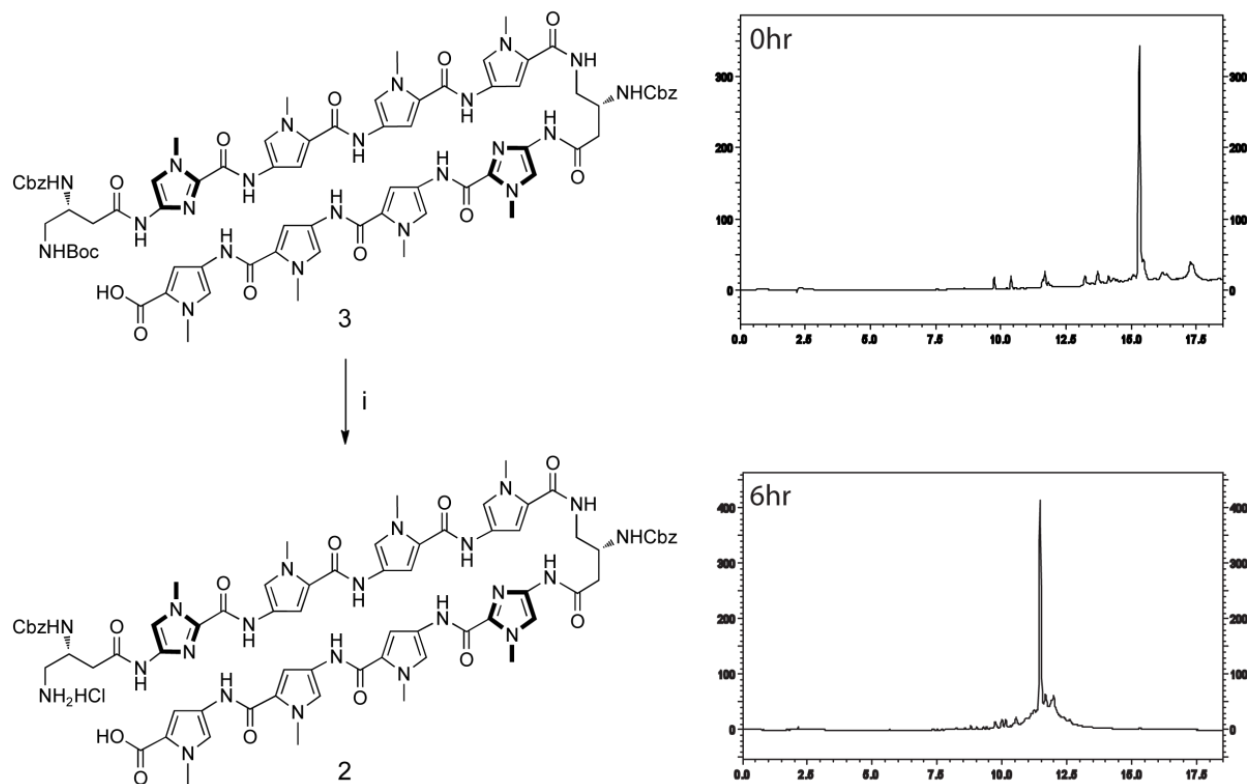
Scheme A.7 Direct deprotection of **3** with HCl at room temperature



¹Reagents and conditions: (i) 4M HCl in 1,4-dioxane, 23 °C, 30 min.

²Reverse-phase HPLC taken on Beckman Gold instrument equipped with a Phenomenex Gemini analytical column (250 × 4.6 mm, 5 μm) and a diode array detector, and the mobile phase consisted of a gradient of acetonitrile (MeCN) in 0.1% (v/v) aqueous TFA [10% MeCN, t = 0 → 30 s; 10% → 80% MeCN, t = 30 s → 18 min].

Scheme A.8 Direct deprotection of **3** with HCl at -40 °C



¹Reagents and conditions: (i) 25% TFA, DCM, -40 °C, 6 h.

² Reverse-phase HPLC taken on Beckman Gold instrument equipped with a Phenomenex Gemini analytical column (250 × 4.6 mm, 5 μm) and a diode array detector, and the mobile phase consisted of a gradient of acetonitrile (MeCN) in 0.1% (v/v) aqueous TFA [10% MeCN, t = 0 → 30 s; 10% → 80% MeCN, t = 30 s → 18 min].